THE STRUCTURAL ANALYSIS OF EARTHWORKS USING MATHEMATICAL MODELS AND BACK ANALYSES BASED ON THE BOUNDARY ELEMENT METHOD

by

GEORGE ANDERSON WATT, M.A., B.A.I.

A thesis submitted to the University of London
(Imperial College of Science and Technology)
for the Degree of
Doctor of Philosophy in the Faculty of Engineering

June 1983

ABSTRACT

This work deals with practical and theoretical aspects of investigating the structural behaviour of earthworks using mathematical models and back analyses based on the boundary element method. It comprises three principal topics. In the first, linearity and superposition, often with dimensional analysis, are used to obtain solutions for models for the response of inhomogeneous ground to surface loading. The models are of a half-space in which Poisson's ratio is constant and the shear modulus is proportional to the depth raised to a non-negative power. For the next, back analyses are made of load-deformation data from various parts of two quite different large sites using existing computer programs. The results obtained contributed to the understanding of their performance and are generally in agreement with those obtained by other workers using different methods. Finally, a new computer program AXSYM is described for the elastostatic analysis of axisymmetric problems using an auxiliary boundary. AXSYM is then used to obtain two comprehensive sets of stress and displacement values for a complete circular toric tunnel, and for a pair of equal spherical cavities, in infinite masses subject to radial and axial field stress.

ACKNOWLEDGEMENTS

The patient and dutiful supervision of John Bray is acknowledged first. The Author of this thesis also thanks John Watson for his advice and for the use of two of his computer programs. Also recognised is the contribution of staff and students at Imperial College in making memorable this period of his studies.

The granting of one year's unpaid leave following a sabbatical year in 1976 made it feasible to undertake the research work described in this thesis. The Author records his thanks for this opportunity to the Council and Senate of the The City University, London, and to his colleagues for their continued support. In particular, he is grateful to Dick Foster and Joe Capewell, former Head and Acting Head respectively of the Division of Geotechnical Engineering and to John Snell of the Department of Computer Science. The special interest shown in this work and the encouragement given by Peter Wolf, former Head of the Department of Civil Engineering, is also gratefully acknowledged.

The help and encouragement received from the Author's wife Elspeth throughout his research was vital. This included the exacting job of typing the manuscript at a time when demands for her time were steadily growing. The Author acknowledges her contribution with loving gratitude.

CONTENTS

		Page
	ABSTRACT	2
	ACKNOWLEDGEMENTS	3
	LIST OF FIGURES	7
	LIST OF TABLES	15
	NOTATION	19
	SIGN CONVENTIONS	22
CHAPTER 1	INTRODUCTION	
	1. Scope	23
	2. Direct formulation of the boundary element method	25
CHAPTER 2	SOME SPECIAL GROUND MODELS FOR GEOTECHNICAL ENGINEERING PROBLEMS	
	1. Introduction	29
	2. Expressions for surface settlement obtained by integral methods	31
	3. Dimensional analysis applied to ground models	40
	4. General solution for line and strip loads on an incompressible half-space	44
	5. Discussion	64
	6. Conclusion	67
CHAPTER 3	ELASTOSTATIC ANALYSIS OF LOAD-DEFORMATION BEHAVIOUR OF MIDDLE CHALK AT MUNDFORD	
	1. Introduction	68
	2. Site	70
	3. Tests and test results	71
	4. Previous analyses	79
	5. New analysis using BIEM	84
	6. The effect of the marl seams	102
	7. General conclusions	105

Page

CHAPTER 4 ELASTIC-PLASTIC ANALYSIS OF HORIZONTAL DISPLACEMENT AROUND A DEEP EXCAVATION IN OXFORD CLAY AT SAXON PIT

1. Introduction 107
2. Site 109
3. Tests and test results 112
4. Previous analyses 115
5. New analyses 118
6. General conclusions 135

CHAPTER 5 AXSYM: A COMPUTER PROGRAM FOR THE LINEAR ELASTOSTATIC ANALYSIS OF AXISYMMETRIC PROBLEMS USING THE INDIRECT BOUNDARY ELEMENT METHOD

1. Introduction 136
2. Analysis 138
3. AXSYM Procedure 151
4. Structure and operation of AXSYM 158
5. Discussion 171
6. Summary and conclusion 173

CHAPTER 6 CHARACTERISTICS, VALIDATION, TESTING AND PRACTICAL APPLICATION OF AXSYM

1. Introduction 174
2. Characteristics 176
3. Validation 180
4. Testing of AXSYM 191
5. Practical application of AXSYM 198
6. Summary and conclusions 208

CHAPTER 7 CONCLUSION

1. Review 209
2. Potential devlopments 211
3. Summary 212

Page

REFERENCES 213

APPENDICES

Appendix A.2 217
Appendix A.3 224
Appendix A.4 246
Appendix A.5 251
Appendix A.6 267

LIST OF FIGURES

Figure No.	Description
1.2.1	Problem body enclosed and defined by the surface S in an infinite mass
2.2.1	Vertical section through an area of uniform vertical loading on the surface of a semi-infinite mass
2.2.2	Plan on an element of uniform vertical loading on the surface of a semi-infinite mass
2.2.3	Isometric sketch of an area of arbitrary vertical loading on the surface of a semi-infinite mass
2.2.4	Plan on an infinite strip of uniform vertical loading on the surface of a semi-infinite mass
2.2.5	Plan on circular area of uniform vertical loading on the surface of a semi-infinite mass
2.2.6	Plan on a rectangular area of uniform vertical loading on the surface of a semi-infinite mass
2.2.7	Surface settlement profiles for square and rectangular areas of uniform vertical loading on the surface of a semi-infinite mass
2.3.1	Vertical section through an area of arbitrary vertical loading on the surface of a semi-infinite mass
2.4.1	Vertical sections through normal and tangential (a) line and (b) uniform strip loads on the surface of a semi-infinite mass
3.3.1	Vertical section through two lines of shafts and water level gauge positions at the tank (Ward et al. (1968))
3.3.2	(a) Section beneath tank showing Grades of chalk at various depths with values of Young's modulus E estimated from immediate vertical strains ε_o given by Ward et al. (1968) and shown in Table 3.4.1. (b) Comparison of Young's modulus E derived from the plate tests and laboratory tests with values derived from full scale tank test given by Burland and Lord (1969))

Figure No.	Description
3.3.3	Vertical section through the plate-loading test equipment (Ward et al. (1968))
3.3.4	Details of plate test equipment (Burland and Lord (1969))
3.3.5	Geological profile and grades of chalk alongside simplified pressure-settlement curves for plate test series T 4 (Ward et al. (1968))
3.4.1	Results of finite element analysis (a) Finite element results fitted to observed centre line settlements (b) Comparison between measured and deduced E values (c) Comparison between measured and predicted settlements down shafts at edge of tank (Burland et al. (1973))
3.4.2	Comparison of observed settlement profile of of the ground with Boussinesq prediction (shown dotted) and the finite element prediction. (Burland et al. (1973))
3.5.1.	Isometric sketch of the Mundford site stack model
3.5.2	Vertical section through the Mundford site stack model showing boundary element dimensions
3.5.3	Plan on the Mundford site stack model on the top surface of subregions 50 showing boundary element dimensions
3.5.4	Plan on the Mundford site stack model on the top surfaces of subregions 100 and 150 showing boundary element dimensions
3.5.5	Plan on the Mundford site stack model on the top surface of subregion 200 showing boundary element dimensions
3.5.6	(a) Section beneath tank showing Grades of chalk at various depths with values of immediate vertical strain ε for the tank test derived from the Mundford site stack model for the set of values of Young's modulus E and Poisson's ratio ν shown. (b) Comparison of average values of Young's modulus E_a for the tank test with associated average values for plate tests derived from the Mundford site stack model

Figure No.	Description
3.5.7	Example of computer output for tank test derived from the Mundford site stack model
3.5.8	Comparison between measured and predicted settlements for the tank test derived from the Mundford site stack model down shafts at (a) the centre and (b) the edge of the tank
3.5.9	Predicted settlement profiles of the ground for the tank test derived from the Mundford site stack model and comparison with observed values at the surface
3.5.10	Predicted lateral movement profiles for the tank test derived from the Mundford site stack model down shafts at the edge of tank assuming (a) uniform pressure and (b) no radial movement on the contact surface between tank and ground
3.5.11	Idealized pressure-settlement curve and typical plate-test results for Grade V, IV, and III chalk (after Burland and Lord (1969))
3.5.12	Typical plate-test results for Grade II chalk (Burland and Lord (1969)) and computational routine for δ_o described for Test T 4.5
3.6.1	Evolution of a pattern of stress distribution in rock elements (blocks) of the jointed medium depending on the angle of dip of the layers (Gaziev and Erlikhman (1971))
3.6.2	Elastic response of a model of regularly jointed rock to a line load. Polar diagram of $r\sigma_r$ (Bray (1981))
4.2.1	Plan showing successive faces of excavation, major joints in the Oxford Clay and layout of instrumentation (Burland et al. (1977))
4.2.2	Centre line section normal to the face showing position of successive faces and major joints, geology and instrumentation (Burland et al. (1977))
4.3.1	Vector movement of points on the centre line of the face showing relationship to face position (Burland et al. (1977))
4.3.2	Observed variation of (a) horizontal displacement, and (b) settlement of surface points on the centre line with distance from advancing face (Burland et al. (1977))

Figure No.	Description
4.3.3	Typical shear stress-displacement curves and strength envelope for direct drained shear tests on Lower Oxford Clay specimens sheared parallel to the bedding (Burland et al. (1977))
4.4.1	(a) Variation of total horizontal surface strain with distance from advancing face (derived from Fig. 4.3.2 (a)), (b) interpretation of the surface strain distribution derived from the observations on point 28 (after Burland et al. (1977))
4.5.1	Isometric sketch of Saxon pit model with infinitely remote boundaries for three-dimensional analysis
4.5.2	Plan on Saxon pit model with infinitely remote boundaries for three-dimensional analysis showing boundary elements
4.5.3	Saxon pit model with finitely remote boundaries for two-dimensional analysis
4.5.4	(a) Assumed distribution of traction on a nominal 20 m long gap FGH as shown in Fig. 4.5.3 and (b) equivalent distribution by superposition of triangular load systems
4.5.5	Distributions shown in (a),(b) and (c) of the normal component of loading per unit length for nominal 20, 30 and 40 m long gaps respectively as described in Figs. 4.5.3 and 4, for standard boundary conditions
4.5.6	Distributions shown in (a), (b) and (c) of the normal component of loading per unit length for nominal 20, 30 and 40 m long gaps respectively as described in Figs.4.5.3 and 4, for standard boundary conditions where the displacement amounts are reduced to 50%
4.5.7	Distributions shown in (a), (b) and (c) of the normal component of loading per unit length for nominal 20, 30 and 40 m long gaps respectively as described in Figs. 4.5.3 and 4, for standard boundary conditions where the displacement amounts are reduced to 10%
4.5.8	Horizontal displacements ΔU_1 induced by a 10 m advance in the face of excavation of the model shown by curve S for the conditions for Fig. 4.5.6 (b), and shown by curve T assuming no gap

Figure No.	Description
4.5.9	Saxon pit model with infinitely remote boundaries for two-dimensional analysis
4.5.10	Symmetric Saxon pit model with infinitely remote boundaries for two-dimensional analysis, and horizontal displacements ΔU_1 as described in Fig. 4.5.8 assuming a traction-free gap
5.2.1	(a) Radial and (b) axial ring load elements
5.3.1	General arrangement of a radial and an axial load element with a corresponding surface point
5.4.1	Segments of radial and axial load elements in the r-z plane showing notation used to specify the element end points
5.4.2	Segments of elements in the r-z plane used to define points showing notation used to specify the element end points
5.4.3	Example of input data for AXSYM (2)
5.4.4	Example of computer output for AXSYM (2)
6.2.1	Distributions of principal stresses induced in the r-z plane around a radial ring load element due to unit (a) radial and (b) axial intensities of loading
6.2.2	Distributions of principal stresses induced in the r-z plane around an axial ring load element due to unit (a) radial and (b) axial intensities of loading
6.3.1	Layouts of 4 and 30 load elements using mirror symmetry for a model of a spherical cavity in an infinite mass
6.3.2	Layouts A and B each of 16 load elements using mirror symmetry for a model of a spherical cavity in an infinite mass
6.4.1	Layout of 16 exterior load elements using mirror symmetry for a model of a sphere containing a spherical cavity of half its radius.

Figure No.	Description
6.4.2	Layout of 16 exterior load elements using mirror symmetry for a model of right circular cylinder of equal height and diameter containing a spherical cavity of half its radius
6.4.3	Layout of 20 load elements for a model of a right circular frustum of a cone
6.4.4	Infinite right circular cone of semi-angle α with a concentrated axial load P applied at the apex
6.5.1	Complete circular toric tunnel in an infinite mass subject to uniform radial and axial field stress
6.5.2	Two identical spherical cavities in an infinite mass subject to uniform radial and axial field stress

Figure No.	Description
A 2.2.1	(a) Infinite strip, (b) circular and (c) rectangular areas of integration for equation A 2.2.1
A 3.5.1	Isometric sketch of the Mundford site stack model (Fig. 3.5.1 bis)
A 3.5.2	Vertical section through the Mundford site stack model showing boundary element dimensions (Fig. 3.5.2 bis)
A 3.5.3	Plan on the Mundford site stack model on the top surface of subregion 50 showing boundary element dimensions (Fig. 3.5.3 bis)
A 3.5.4	Plan on the Mundford site stack model on the top surface of subregions 100 and 150 showing boundary element dimensions (Fig. 3.5.4 bis)
A 3.5.5	Plan on the Mundford site stack model on the top surface of subregion 200 showing boundary element dimensions (Fig 3.5.5 bis)
A 3.5.6	Vertical section through the Mundford site stack model showing assigned node identification numbers
A 3.5.7	Plan on the Mundford site stack model on the top surface of subregion 50 showing assigned node identification numbers
A 3.5.8	Plan on the Mundford site stack model on the top surface of subregion 100 showing assigned node identification numbers
A 3.5.9	Plan on the Mundford site stack model on the top surface of subregion 150 showing assigned node identification numbers
A 3.5.10	Plan on the Mundford site stack model on the top surface of subregion 200 showing assigned node identification numbers
A 3.5.11	Vertical section through the Mundford site stack model showing assigned element identification numbers
A 3.5.12	Plan on the Mundford site stack model on the top surface of subregion 50 showing assigned element identification numbers

Figure No.	Description
A 3.5.13	Plan on the Mundford site stack model on the top surface of subregion 100 showing assigned element identification numbers
A 3.5.14	Plan on the Mundford site stack model on the top surface of subregion 150 showing assigned element identification numbers
A 3.5.15	Plan on the Mundford site stack model on the top surface of subregion 200 showing assigned element identification numbers
A 3.5.16	Example of input data reproduced by the preprocessor in Watson's program for three-dimensional elastostatic analysis by the Boundary Integral Equation Method
A 4.5.1	Simplified Saxon pit model with infinitely remote boundaries for two-dimensional analysis
A 4.5.2	Simplified shear stress-displacement response curve
A 4.5.3	Variation of horizontal displacement with distance from the root of the crack in the simplified Saxon pit model with infinitely remote boundaries for two-dimensional analysis
A 6.5.1	Complete circular toric tunnel in an infinite mass subject to uniform radial and axial field stress (Fig. 6.5.1 bis)
A 6.5.2	Two identical spherical cavities in an infinite mass subject to uniform radial and axial field stress (Fig. 6.5.2 bis)

LIST OF TABLES

Table No.	Description
2.2.1	Value of $g(\theta)$
2.2.2	Notation and format for input cards for program GSETT
2.4.1	Value of c(n)
2.4.2	Values of $-r\sigma_r/P$
2.4.3	Values of $-r\sigma_r/Q$
2.5.1	Values of w'_o for a uniformly loaded square at points 1, 2 and 3, as shown in Fig. 2.2.7, and for an inscribed uniformly loaded circle at coincident points
2.5.2	Values of $w'_c - w'$ for a uniformly loaded square as shown in Fig. 2.2.7, and for an inscribed uniformly loaded circle at eight coincident points P,Q,R, etc., equally spaced from edge to centre C along a normal passing through C
3.3.1	Correlation between grades and the mechanical properties of the chalk at Mundford (Ward et al. (1968))
3.3.2	Mundford - Summary of tank test results (Burland (1977))
3.4.1	Values of Young's modulus E estimated from the immediate vertical strains measured beneath the centre of the tank at maximum load for two loading cycles (Poisson's ratio assumed equal to 0.1) (after Ward et al. (1968)) and similar values obtained by a reanalysis of the same data using Boussinesq's solution with Poisson's ratios of 0.1 and 0.25
3.5.1	Estimated values of Young's modulus E at various levels obtained by the stack model using plate test results as described in Section 5 where the parameters used below are also defined
5.2.1	Terms involving R and θ in the expressions for stress and displacement due to uniformly loaded ring elements

Table No.	Description
5.2.2	Limiting value as $k^2 \rightarrow 0$ of the integrals between the limits of 0 and π for θ of the terms in Table 5.2.1
5.4.1	Names and function of subprogram comprising AXSYM
5.4.2	Structure and operating modes of AXSYM
5.4.3	Number, function and spectification of input cards for AXSYM
5.4.4	Notation shceme and field lengths for input variables used in AXSYM
6.3.1	Identification numbers N and coordinates r, z of 30 points on the surface of a sphere of radius 100
6.3.2	Comparative values of stresses and displacements around a spherical cavity in an infinite mass subject to a unit uniaxial field stress for the four load element model of the spherical cavity as shown in Fig. 6.3.1 by dashed lines, where the coordinates of the points N are given in Table 6.3.1
6.3.3	Comparative values of fictitious load intensities q_r and q_z acting in the r and z directions respectively for the four element model of the spherical cavity in an infinite mass subject to unit uniaxial field stress shown in Fig. 6.3.1 by dashed lines, where the coordinates of the points N are given in Table 6.3.1
6.3.4	Values of tangential surface stress σ_m around a spherical cavity in an infinite mass subject to unit hydrostatic field stress for a 30 element model as shown in Fig. 6.3.1 by solid lines, where the coordinates of the points N are given in Table 6.3.1
6.3.5	Comparative values of tangential surface stresses σ_m around a spherical cavity in an infinite mass subject to unit hydrostatic stress for two 16-element models shown in Fig. 6.3.2 labelled A and B respectively where the coordinates of the points N are given in Table 6.3.1

Table No.	Description
6.3.6	Comparative values of the tangential surface stresses σ_m around a spherical cavity in an infinite mass subject to unit unixial field stress for two 16-element models, shown in Fig. 6.3.2 labelled A and B respectively, where the coordinates of the points N are given in Table 6.3.1
6.4.1	Comparative values of stresses and displacements along the r-axis of a spherical shell, with internal radius a and external radius 2a loaded by unit external pressure as shown in Fig. 6.3.2, where the coordinates of the points on the external surface indicated by dashed numbers are double those of the corresponding points on the interior surface
6.4.2	Comparative values of stresses and displacements along the axis of the frustum of a cone, as shown in Fig. 6.4.3 loaded according to the solution for an axial load P at the apex of an infinite cone with semi-angle a given in equation (6.4.1)
6.5.1	Comparative values of the stress components σ_r and σ_z at the surface of the tunnel shown in Fig. 6.5.1 when c/a = 10 at points N = 8, 14, and 20 given in Table A 6.5.1 for Poisson's ratio ν = 0, 0.25 and 0.49
6.5.2	Comparative values of the stress component σ_θ at the surface of the tunnel shown in Fig. 6.5.1 when c/a = 10 at points N = 8, 14, and 20 given in Table A 6.5.1 for Poisson's ratio ν = 0, 0.25 and 0.49
6.5.3	Values of the stress components σ_θ and σ_z at the surface of the tunnel shown in Fig. 6.5.1, when c/a = 10, 3, 1½ at points N = 8 and 20 given in Table A 6.5.1 for Poisson's ratio ν = 0.25
6.5.4	Comparative values of the stress components σ_θ and σ_z at the surfaces of the two identical spherical cavities shown in Fig. 6.5.2 when d/a = 2 at points N = 8, 14 & 20 given by Sternberg & Sadowsky (1952) and in Table A 6.5.2 when Poisson's ratio ν = 0.25

Table No.	Description
A 3.5.1	List of sectioned surfaces with assigned node identification numbers
A 3.5.2	List of sectioned surfaces with assigned element identification numbers
A 3.5.3	Error messages generated by preprocessor in Watson's computer program for three-dimensional elastic analysis
A 6.5.1	Total stresses and induced displacements associated with a complete circular toric tunnel in a homogeneous isotropic linear elastic infinite mass with uniform field stress (Fig. A 6.5.1)
A 6.5.2	Total stresses and induced displacements associated with two idential spherical cavities in a homogeneous isotropic linear elastic infinite mass with uniform field stress(Fig. A 6.5.2)

NOTATION

ENGLISH

Symbol	Entity
a	pure length, radius of body, radius of void in infinite mass
A	area of integration, constant
A^1	constant
$[a_{ij}]$	matrix of influence coefficients
c	cohesion component of shearing resistance, radius of load element
E	Young's modulus
E_a	average value of Young's modulus
E_1	complete elliptic integral of the second kind
f	normal component of line load intensity
$\{f\}$	column vector of normal components of line load intensities
F_1	complete elliptic integral of the first kind
G	shear modulus
l	shear band length
m	constant
n	non-negative real exponent
N	identificiation numbers of points in mass containing voids
p	normal stress, field stress
P	normal line load intensity
q	tangential stress, average pressure
Q	tangential line load intensity
s	axial distance
S	surface of area S
t	component of surface traction
T	component of traction induced by unit solution integrated over an element

Symbol	Entity
T'	component of traction induced by unit solution
u	component of displacement
U	component of displacement induced by unit solution integrated over an element
U'	component of displacement induced by unit solution
w	settlement
w_c	settlement at the point C
w'	settlement multiplied by special constants
w'_c	settlement at the point C multiplied by special constants
w_o	settlement at the point O outside the loaded area
w'_o	settlement at the point O outside the loaded area multiplied by special constants

GREEK

Symbol	Entity
α	semi-angle of a right circular cone
γ	unit weight of material, shear strain
δ	settlement
ε	normal strain
ν	Poisson's ratio
π	pi
σ	normal stress
Σ	summation
τ	shear stress
Φ	angle of shearing resistance, angle
ε_o	immediate vertical strain determined from field data

SIGN CONVENTIONS

Quantity	Type and Sign
(a) Force and displacement	Axial positive
(b) Stress	Compressive positive
(c) Strain	Contractive positive
(d) Stress	Compressive negative
(e) Strain	Contractive negative

Sign conventions (a),(b) and (c) are used throughout excepting Chapter 2.

Sign conventions (a),(d) and (e) are used in Chapter 2.

CHAPTER 1 INTRODUCTION

1. Scope

The structural behaviour of large earthworks is often both difficult to ascertain and intricate to model. The need to design such structures to very close tolerances in recent years has led to a dramatic increase in the amount and quality of the information from large scale site testing or in-service monitoring. There has been a similar advance in the variety and power of the mathematical procedures employed to analyse this information, especially in numerical methods using large computers. As a result of these developments, the design engineer's opportunity to exercise good judgement is significantly improved and the researcher's power to investigate their performance is greatly enhanced.

The Author's research, as presented herein, comprises three principal topics. The first is an extension and a generalisation of a mathematical model, described in Chapter 2, for the response of inhomogeneous ground to static surface loading. In Chapters 3 and 4, back analyses are made of load-deformation data from various parts of two different large sites using existing computer programs. Finally a new computer program called AXSYM, written by the Author, for the stress analysis of axisymmetric problems is presented in Chapter 5. Results for several test problems using AXSYM are given in Chapter 6. The program is also used to calculate a comprehensive set of stress and displacement values for two basic structures. Chapter 7 contains a summary of the work.

All of the above computer programs implement linear elastostatic stress analysis using the boundary element method. Indirect formulation of the boundary element method is used in the axisymmetric program and is described in the relevant chapter. On the other hand, direct formulation is used in the existing stress analysis programs and this version of the boundary element method is briefly described in the following section.

2. Direct formulation of the boundary element method

Consider an infinite space designated by a set of rectangular Cartesian coordinate axes x,y,z, as shown in Fig. 1.2.1, and suppose that the space is wholly occupied by a uniformly distributed linear elastic material. If the solution for a concentrated load applied at any point is known, then the induced stresses and displacements at any other point can be calculated. For a homogeneous isotropic material this is the Kelvin solution.

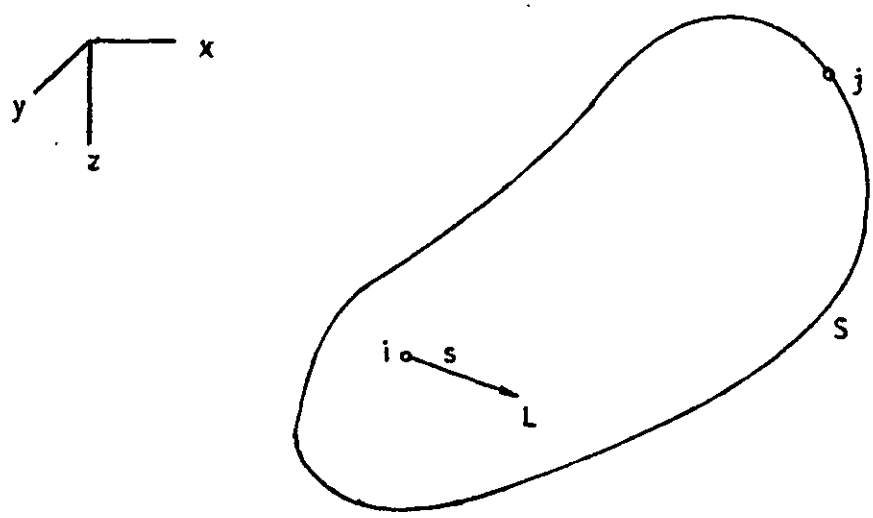


FIG. 1.2.1: PROBLEM BODY ENCLOSED AND DEFINED BY THE SURFACE S IN AN INFINITE MASS

Induced tractions can be calculated by use of the known solution at all points j on the trace of a surface S in the infinite space, as indicated in Fig. 1.2.1, due to a concentrated load L applied in an arbitrary direction s at any point i not on the surface . For a unit concentrated load, let the induced traction and relative displacements in x,y,z direction by denoted by T'_{sx} , T'_{sy} , T'_{sz} and U'_{sx} , U'_{sy} , U'_{sz} respectively.

If the specified loading of a problem body, enclosed and defined by the surface S, is represented by an appropriate selection from the set of all surface tractions and displacments in the x,y, z directions, denoted by t_x, t_y, t_z and u_x, u_y, u_z respectively,then Betti's reciprocal theorem gives

$$c_i(u_s)_i + \int (T'_{sx}\, u_x + T'_{sy}\, u_y + T'_{sz}\, u_z)dS = \int (U'_{sx}\, t_x + U'_{sy}\, t_y + U'_{sz} t_z)dS \qquad \ldots(1.2.1)$$

where $(u_s)_i$ is the component of displacement of the problem body in the arbitrary direction s at the point i, the value of the constant c_i is unity, and each integral is taken over the surface area S. By moving the point i to a locally smooth part of the surface , a boundary constraint equation is obtained for the problem body under the specified loading. In this equation the value of the constant c_i is reduced to ½ because the unit concentrated load is now equally shared between the volume coincident with the problem body and the complementary volume of the infinite space.

In many practical cases the surface S is approximately represented by n contiguous areal elements forming a completely facetted surface. The specified boundary loading is assumed constant over any element and, for a point j on it, comprises an appropriate selection from the set of surface traction and displacements denoted by $\{t_x, t_y, t_z\}_j$ and $\{u_x, u_y, u_z\}_j$ respectively. The boundary constraint equation is written at such a point on each element away from its edges, with the arbitrary direction s taken parallel to each of the coordinate axes. Denoting the integral, or the Cauchy Principal Value of the integral, where appropriate, of each dashed term in the boundary constraint equation by the removal of its dash, the complete set of 3n boundary

constraint equation may be written as the matrix equation (1.2.2), where the subscripts i, j refer to a point and an element respectively, and i, j = 1, 2, ..., n.

$$\left[\begin{bmatrix} T_{xx} & T_{xy} & T_{xz} \\ T_{yx} & T_{yy} & T_{yz} \\ T_{zx} & T_{zy} & T_{zz} \end{bmatrix}_{ij}\right]\left[\begin{bmatrix} u_x \\ u_y \\ u_z \end{bmatrix}_j\right] = \left[\begin{bmatrix} U_{xx} & U_{xy} & U_{xz} \\ U_{yx} & U_{yy} & U_{yz} \\ U_{zx} & U_{zy} & U_{zz} \end{bmatrix}_{ij}\right]\left[\begin{bmatrix} t_x \\ t_y \\ t_z \end{bmatrix}_j\right] \quad \ldots(1.2.2)$$

By interchanging relevant terms on both sides of the equation the vector on the r.h.s may be altered to contain only the specified boundary loading terms. The remaining boundary terms are obtained by the solution of the equation using either an inversion method or an iteration procedure.

The terms in the matrix equation may be scaled to aid the stability of the solving operation. In order to describe such a scaling procedure, assume that the boundary loading of the problem body has been specified completely in terms of surface tractions so that the equation to be solved is as shown in equation (1.2.2). In the scaling procedure the terms in the displacement vector are assumed to be divided by the greatest finite distance specified in the problem, the terms in the matrix of displacement are also divided by this distance and multiplied by Young's modulus and, finally, the terms in the traction vector are divided by Young's modulus.

Displacements at internal points are calculated by equation (1.2.1) with $c_i = 1$ and the associated strains by differentiating under the integral sign. The corresponding stresses are calculated using the elasticity equation.

It is possible to specify more complex problem bodies than that shown in Fig. 1.2.1 comprising several subregions with different mechanical constants. The interfaces within these bodies are treated in a similar way to that described previously for the simple problem body with a boundary surface S. The equality of the displacements and of the traction with signs reversed on either side of the interfaces is included in the construction of matrix equations similar to equation (1.2.2). Consequently they are larger than for a comparable simple problem body but are only partially populated.

Rizzo (1967) and Lachat and Watson (1975) used the direct formulation of the boundary element method for two- and three-dimensional elastostatic analysis respectively. The existing computer programs used by the Author in the back analyses in Chapter 3 and 4 were written by Watson.

CHAPTER 2 SOME SPECIAL GROUND MODELS FOR GEOTECHNICAL ENGINEERING PROBLEMS

1. Introduction

The mechanical properties of ground in some areas may vary so much with depth and direction that simple models, such as Boussinesq's, may be unable to adequately represent its short term response to loading for engineering purposes. Problems of this kind were discussed at length by Gibson (1974) in his Rankine Lecture. In particular, he described models for normally loaded ground with a horizontal surface, where the undrained Young's modulus increases approximately linearly with depth and any anisotrophy is ignored. For the extreme case in which the shear modulus is proportional to depth, closed form solutions were examined which had been obtained by Gibson (1967) and Awojobi and Gibson (1973). Notable use of the expression for subsurface settlement of a compressible material, due to a uniformly loaded circle, was made in the analysis of ground response test results for an important geotechnical engineering problem (Burland et al., (1973)).

Extensions to the range of these solutions have been made by the Author using two distinct analytical methods. Additionally some existing solutions are wholly or partially recovered. These results are described in the sections immediately following this introduction.

In a related paper dealing with incompressible materials, Calladine and Greenwood (1978) recovered Gibson's results for the special case where the shear modulus (G) is proportional to depth (z). Calladine and Greenwood stated in the summary to their paper that:

"The aim of this paper is to explain this well-known result (and others, concerning the stress field within the half-space) by tackling the basic cases in which normal line and point loads are applied to the surface."

In a later section they discussed the nature of the solution of this problem, adding the important observation that:

"Thus a radial stress field is to be expected when $G = mz$, or when $G = mz^{a}$, where a is a real exponent; but not when $G = C + mz$, nor when G is given by any two-term function of z."

(The symbols m, a and C represent constants in the above statement.)

This expectation is realized for both normal and tangential line loads in a later section below, where the general solution obtained by the Author is presented. By integrating the results, the corresponding cases for uniform strip loading are obtained.

For convenience, the notation and conventions of the work cited above are generally adhered to. In particular, tensile stresses are taken as positive, but the choice of such a scheme is strictly limited to the work treated in this chapter. Note, however, that the symbol used for the exponent of z is n and not a, and that both w and u_z are used to denote vertical settlement.

2. Expressions for surface settlement obtained by integral methods

A semi-infinite linear elastic body with a horizontal surface is shown in Fig. 2.2.1, where the shear modulus $G = mz$. A normal uniformly distributed surface load of intensity p acts on the body. For a circular loaded area of radius b, and the special value of $\frac{1}{3}$ for Poisson's ratio, Awojobi and Gibson (1973) proved that,

$$4\frac{m}{p}w(r,z) = \tfrac{1}{2}\log\left(\frac{(z^2-r^2+b^2)+\sqrt{((z^2+r^2-b^2)^2+4b^2z^2)}}{2z^2}\right) + \qquad \ldots(2.2.1)$$

$$+\frac{(r^2-b^2)^2+z^2(r^2+b^2)-(r^2-b^2)\sqrt{((z^2+r^2-b^2)^2+4b^2z^2)}}{(r^2-b^2)^2+2z^2(r^2+b^2)+z^4+(z^2-r^2+b^2)\sqrt{((z^2+r^2-b^2)^2+4b^2z^2)}}\,.$$

By superposing a downward load over a circle of radius b_1 and an upward load over a concentric circle of radius b_2 we obtain, for an annular load,

$$4\frac{m}{p}w_c = \frac{1}{2}\log\left(\frac{b_1^2}{b_2^2}\right) \qquad \ldots(2.2.2)$$

where w_c is the settlement at the point C. Based on an argument advanced by Awojobi and Gibson (1973), the equation may be generalised for an arbitrary constant value of Poisson's ratio (v) to give

$$4\frac{m}{p}w_c = \frac{1-2v}{1-v}\log\left(\frac{b_1^2}{b_2^2}\right). \qquad \ldots(2.2.3)$$

Writing r + dr and r for b_1 and b_2 respectively, and using symmetry and superposition, the surface settlement dw_c at the point C in Fig. 2.2.2 due to the elemental load pr.dr.dθ is seen to be given by

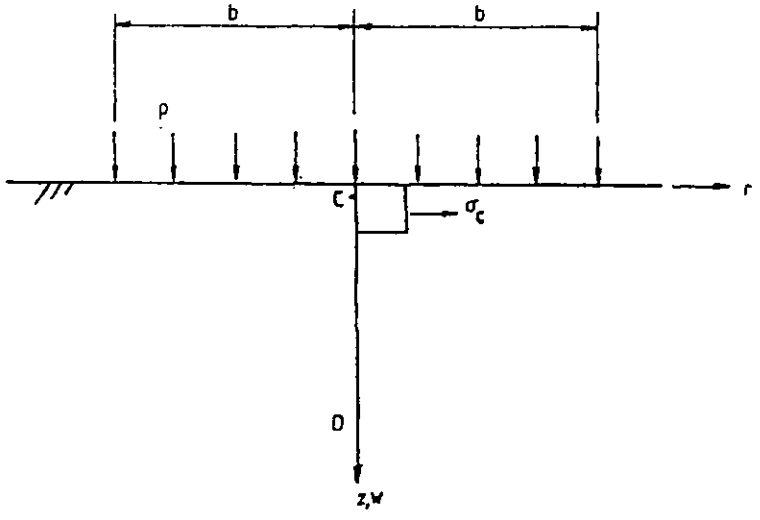


FIG. 2.2.1: VERTICAL SECTION THROUGH AN AREA OF UNIFORM VERTICAL LOADING ON THE SURFACE OF A SEMI-INFINITE MASS

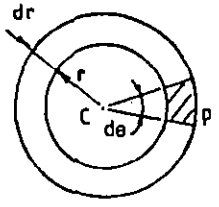


FIG. 2.2.2: PLAN ON AN ELEMENT OF UNIFORM VERTICAL LOADING ON THE SURFACE OF A SEMI-INFINITE MASS

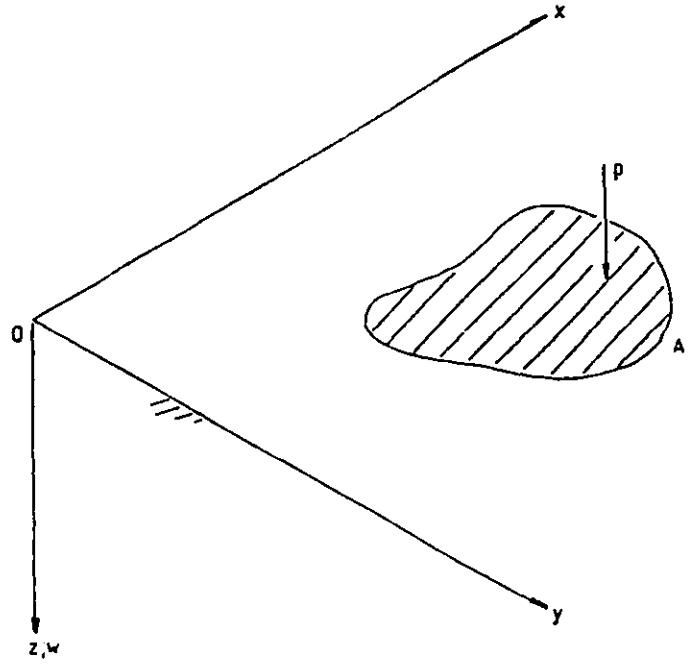


FIG.2.2.3: ISOMETRIC SKETCH OF AN AREA OF ARBITRARY VERTICAL LOADING ON THE SURFACE OF A SEMI-INFINITE MASS

$$dw_c = \frac{p}{4m} \quad \frac{1-2\nu}{1-\nu} \quad \frac{2dr}{r} \quad \frac{d\theta}{2\pi} \,. \qquad \ldots(2.2.4)$$

By integrating the differential equation over an arbitrary area A subject to a vertical load of intensity p(x,y), as shown in Fig. 2.2.3, we obtain the following equation for the vertical surface settlement w_o at a point 0 outside the loaded area A, when G = mz and ν=constant.

$$w_o = \frac{1}{4\pi} \quad \frac{1-2\nu}{1-\nu} \quad \frac{1}{m} \iint_A \frac{p\,dx\,dy}{x^2+y^2} \qquad \ldots(2.2.5)$$

Integration over specific area

For the point 0 outside the load area and for points 1 and 2 within it, the double integral has been evaluated, assuming p is constant, for the geometric arrangements shown in Fig. 2.2.4, Fig. 2.2.5 and Fig. 2.2.6. Note that the symbols a, b, a_1, b_1, ...,c_1, d_1, represent pure lengths between various points on the figures and are therefore always positive. Details of the methods used to perform the double integrals are given in Appendix A 2.2(a). Using these results, the following equations for the settlement w_o at the point 0, and the relative settlement $w_1 - w_2$ between the points 1 and 2, have been obtained. Awojobi and Gibson (1973) obtained similar results for the case shown in Fig.2.2.4 and Fig. 2.2.5.

For a uniformly distributed load on an infinitely long strip (Fig. 2.2.4):

$$w_o = \frac{1}{4} \quad \frac{1-2\nu}{1-\nu} \quad \frac{p}{m} \quad \log\left|\frac{a+b}{a-b}\right| \,, \qquad \ldots(2.2.6)$$

$$w_1 - w_2 = \frac{1}{4} \quad \frac{1-2\nu}{1-\nu} \quad \frac{p}{m} \quad \log\left|\frac{b^2-a_1^2}{b^2-a_2^2}\right| \,. \qquad \ldots(2.2.7)$$

For a uniformly distributed load on a circle (Fig. 2.2.5):

$$w_o = \frac{1}{4} \quad \frac{1-2\nu}{1-\nu} \quad \frac{p}{m} \quad \log\left|\frac{a^2}{a^2-b^2}\right| \,, \qquad \ldots(2.2.8)$$

$$w_1 - w_2 = \frac{1}{4} \frac{1-2\nu}{1-\nu} \frac{p}{m} \log \left| \frac{b^2 - a_1^2}{b^2 - a_2^2} \right| . \qquad \ldots(2.2.9)$$

For a uniformly distributed load on a rectangle (Fig. 2.2.6.):

$$w_o = \frac{1}{4\pi} \frac{1-2\nu}{1-\nu} \frac{p}{m} S\left(\frac{c}{b}, \frac{c}{a}\right) , \qquad \ldots(2.2.10)$$

$$w_1 - w_2 = \frac{1}{4\pi} \frac{1-2\nu}{1-\nu} \frac{p}{m} \left(S\left(\frac{c_1}{a_1}, \frac{c_2}{a_2}\right) + S\left(\frac{c_1}{b_1}, \frac{c_2}{b_2}\right) + S\left(\frac{d_1}{a_1}, \frac{d_2}{a_2}\right) + S\left(\frac{d_1}{b_1}, \frac{d_2}{b_2}\right) \right) , \qquad \ldots(2.2.11)$$

where

$$S\left(\frac{r}{p}, \frac{r}{q}\right) = \left[\theta\left(\log\left|\frac{\theta}{\tan\theta}\right| - 1\right) + \sum_{s=1}^{\infty} \frac{a_{2s}\theta^{2s+1}}{2s+1} \right]_{\tan^{-1}\left(\frac{r}{q}\right)}^{\tan^{-1}\left(\frac{r}{p}\right)} \qquad \ldots(2.2.12)$$

and

$$a_2 = \frac{1}{3}, \; a_{2s} = \frac{(-1)^{s+1} 2^{2s-1}}{s \times (2s+1)!} - \sum_{t=1}^{s-1} \frac{(-1)^t 2^{2t} \times (s-t)}{s \times (2t+1)!} a_{2s-2t}, \; s = 2,3,4\ldots, \qquad \ldots(2.2.13)$$

for $p, q, r > 0$.

It can also be shown that

$$S\left(\frac{r}{p}, \frac{r}{q}\right) = \left[g(\theta) \right]_{\tan^{-1}\left(\frac{r}{q}\right)}^{\tan^{-1}\left(\frac{r}{p}\right)} \qquad \ldots(2.2.14)$$

where

$$g(\theta) = \int_{\theta}^{\pi/4} \frac{2\phi \, d\phi}{\sin 2\phi} . \qquad \ldots(2.2.15)$$

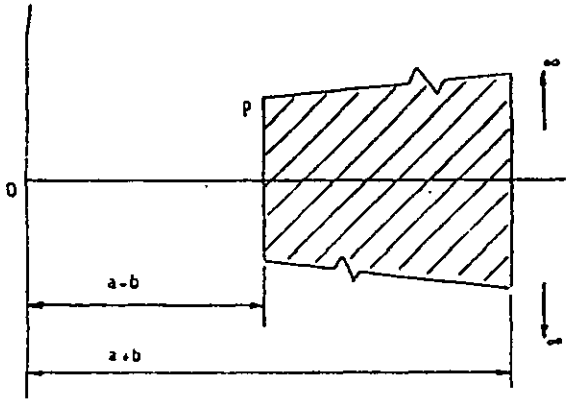


FIG. 2.2.4: PLAN ON AN INFINITE STRIP OF UNIFORM VERTICAL LOADING ON THE SURFACE OF A SEMI-INFINITE MASS

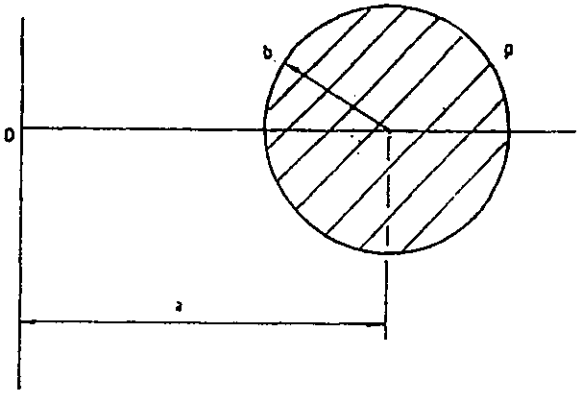


FIG. 2.2.5: PLAN ON CIRCULAR AREA OF UNIFORM VERTICAL LOADING ON THE SURFACE OF A SEMI-INFINITE MASS

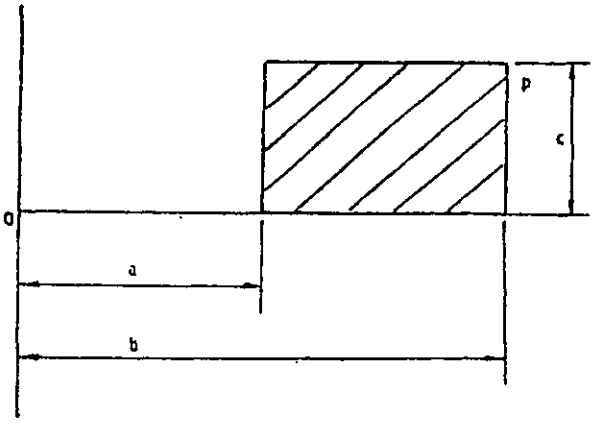


FIG. 2.2.6: PLAN ON A RECTANGULAR AREA OF UNIFORM VERTICAL LOADING ON THE SURFACE OF A SEMI-INFINITE MASS

The value of $\pi/4$ for the upper limit has been chosen for convenience. The singularity in the expression for $g(\theta)$ at $\theta = \frac{\pi}{2}$ can be isolated by writing it in the form,

$$g(\theta) = \int_{\theta}^{\pi/4} \left(\frac{2\phi}{\sin 2\phi} - \frac{\pi}{\pi - 2\phi} \right) d\phi + \frac{\pi}{2} \log \left| 2 - \frac{4\theta}{\pi} \right| \qquad \ldots(2.2.16)$$

Using Simpson's rule approximate values of $g(\theta)$ were obtained from equation (2.2.16). The values are tabulated with tan θ at 1° intervals of θ for the range 0° to 89° in Table 2.2.1.

By making the substitution

$$1 - 2\nu = \frac{-1}{\log \left| 2 - \frac{4\theta}{\pi} \right|} \qquad \ldots(2.2.17)$$

in equation (2.2.16) and noting that $\nu \to \frac{1}{2}$ as $\theta \to \frac{\pi}{2}$, both from below, it can be seen that the singularity is suppressed in the expression for w_o for a uniformly distributed load on a rectangle when the material is incompressible. It follows immediately that along any side of the rectangles shown in Fig. 2.2.6, $w_o = p/2m$, and that $w_o = w_1 - w_2 = 0$ elsewhere, when $\nu = \frac{1}{2}$. By the use of superpositions these results may be used for more general loading of incompressible material. A similar approach was described by Gibson (1967), Awojobi and Gibson (1973) and Gibson (1974).

In order to make the results contained in Table 2.2.1. more accessible, a small computer program GSETT has been written to calculate values of $S(r/p, r/q)$. The results are printed out under the heading DGTH, together with some associated quantities which are clearly labelled. The program incorporates the tabulated values mentioned above, and interpolates linearly between them where necessary. A listing of the program is given in Appendix A 2.2(b).

TABLE 2.2.1 VALUES OF g(θ)

θ°	tanθ	g(θ)	θ°	tanθ	g(θ)	θ°	tanθ	g(θ)
0	0.000	0.915966	30	0.577	0.357797	60	1.732	-0.505051
1	0.017	0.898511	31	0.601	0.336551	61	1.804	-0.548057
2	0.035	0.881050	32	0.625	0.315012	62	1.881	-0.592738
3	0.052	0.863574	33	0.649	0.293164	63	1.963	-0.639228
4	0.070	0.846077	34	0.675	0.270991	64	2.050	-0.687675
5	0.087	0.828551	35	0.700	0.248477	65	2.145	-0.738247
6	0.105	0.810990	36	0.727	0.225602	66	2.246	-0.791130
7	0.123	0.793386	37	0.754	0.202348	67	2.356	-0.846536
8	0.141	0.775731	38	0.781	0.178695	68	2.475	-0.904705
9	0.158	0.758019	39	0.810	0.154621	69	2.605	-0.965909
10	0.176	0.740241	40	0.839	0.130135	70	2.747	-1.030464
11	0.194	0.722390	41	0.869	0.105123	71	2.904	-1.098732
12	0.213	0.704459	42	0.900	0.079648	72	3.078	-1.171134
13	0.231	0.686439	43	0.933	0.053656	73	3.271	-1.248165
14	0.249	0.668322	44	0.966	0.027116	74	3.487	-1.330412
15	0.268	0.650101	45	1.000	0.000000	75	3.732	-1.418572
16	0.287	0.631765	46	1.036	-0.027726	76	4.011	-1.513492
17	0.306	0.613308	47	1.072	-0.056096	77	4.331	-1.616204
18	0.325	0.594720	48	1.111	-0.085147	78	4.705	-1.727993
19	0.344	0.575991	49	1.150	-0.114918	79	5.145	-1.850478
20	0.364	0.557113	50	1.192	-0.145454	80	5.671	-1.985743
21	0.384	0.538076	51	1.235	-0.176797	81	6.314	-2.136535
22	0.404	0.518869	52	1.280	-0.209000	82	7.115	-2.306575
23	0.424	0.499483	53	1.329	-0.242116	83	8.144	-2.501083
24	0.445	0.479907	54	1.376	-0.276202	84	9.514	-2.727704
25	0.466	0.460129	55	1.428	-0.311321	85	11.430	-2.998295
26	0.488	0.440138	56	1.483	-0.347543	86	14.301	-3.332722
27	0.510	0.419922	57	1.540	-0.384940	87	19.081	-3.768234
28	0.532	0.399469	58	1.600	-0.423957	88	28.636	-4.388459
29	0.554	0.378765	59	1.664	-0.463601	89	57.290	-5.460269

The input data is on punched cards. On the first card the total number of calculations of S(r/p, r/q) is specified. This quantity is entered in the variable NP. Succeeding cards specify the data for each calculation in turn, from which the values of the parameters r/p and r/q are obtained. Each data set comprises the four numbers hr, hp, kr, kq, where h and k are any non-zero real numbers. These data are entered in variables OPF, ADF, OPN, ADN in order.

The notation and format of the punched cards is given in Table 2.2.2. The field lengths for the variables NP and OPF, etc., are I2 and F10.0 respectively.

TABLE 2.2.2 NOTATION AND FORMAT FOR INPUT CARDS FOR PROGRAM GSETT

No. of cards	Column numbers						
	1	5	10	20	30	40	80
1		NP					
≥ 1			OPF	ADF	OPN	ADN	

The program GSETT was used to calculate the surface settlement w_o outside the loaded areas, and relative surface settlement $w_c - w$ within the loaded areas, for the square and rectangle shown in Fig. 2.2.7. The quantities w_o' and $w_c' - w'$ are plotted on Fig. 2.2.7, where

$$w_o' = 4\pi \frac{1-\nu}{1-2\nu} \frac{m}{p} w_o \qquad \ldots(2.2.18)$$

$$w_c' - w' = 4\pi \frac{1-\nu}{1-2\nu} \frac{m}{p} (w_c - w) \qquad \ldots(2.2.19)$$

The point C is positioned at the centre of the loaded area in each case. The settlements at the point C and at any other point within either loaded area are denoted by w_c and w respectively.

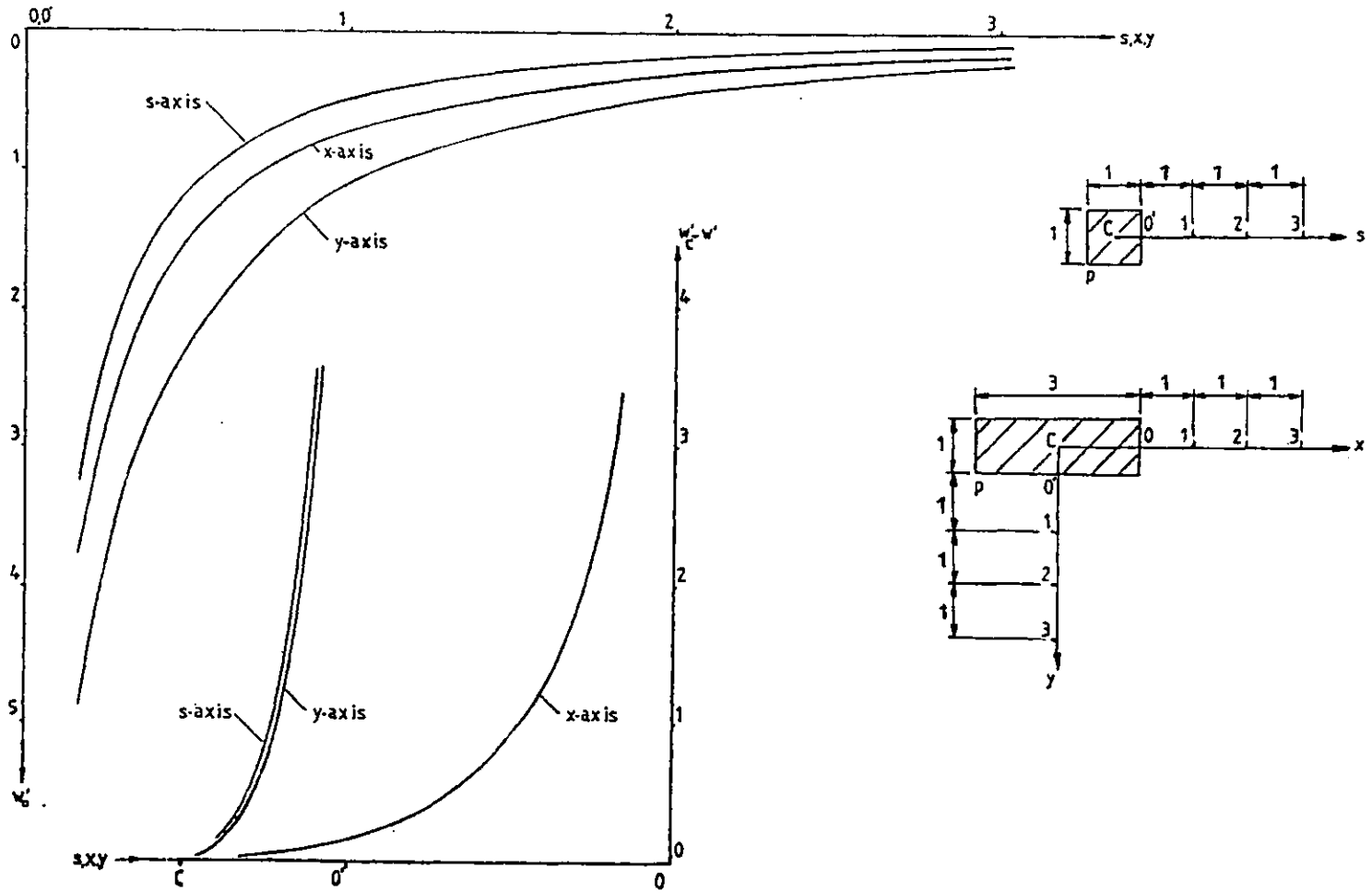


FIG. 2.2.7: SURFACE SETTLEMENT PROFILES FOR SQUARE AND RECTANGULAR AREAS OF UNIFORM VERTICAL LOADING ON THE SURFACE OF A SEMI-INFINITE MASS

3. Dimensional analysis applied to ground models

All physical equations are dimensionally homogeneous. The variables in any such equation can be regrouped and the equation rewritten in terms of dimensionless products and quotients of the variables. These groups can be regarded as new variables and represent a minimal set. The difference between the number of original and new variables equals the number of dimensions in the original equation.

It is possible to group variables of any formal physical equation in a similar way. Initially a set of variables is assembled which, it is assumed, adequately represent the governing physical influences on the occurrence. These variables are grouped according to the rules of the Theory of Dimensions and the equation rewritten in terms of fewer dimensionless variables. If other independent relationships are known between some of the original variables then one or more of the dimensionless groups may be eliminated.

Analysis based on this theory is characteristically simple in presentation but sometimes subtle in execution. Almost invariably it is equivalent to a much larger quantity of ordinary analysis. Using symmetry, superpostion and dimensional analysis some new expressions are obtained and some established results are partially recovered in surface settlement and stress due to the loading of a linear non-homogeneous elastic half-space.

Expressions for settlement

The settlement w_D of a point D on z-axis as shown in Fig. 2.2.1 may be assumed to be given by

$$w_D = f_1 \quad (p, b, z, m, \nu, n), \qquad \ldots(2.3.1)$$

where $G = mz^n$ and Poissons's ratio is an arbitrary constant.

Using dimensional analysis the equation may be rewritten as

$$\frac{w_D^n m}{p} = f_2 \left(\frac{p}{mb^n} , \frac{b}{z} , \nu , n \right). \qquad \ldots(2.3.2)$$

But because the system is linear $w_D \propto p$, and so $\frac{p}{mb^n}$ raised to the power n - 1 must appear as a factor and simultaneously vanish from the argument list, giving

$$\frac{w_D^n m}{p} = \left(\frac{p}{mb^n} \right)^{n-1} f_3 \left(\frac{b}{z} , \nu , n \right). \qquad \ldots(2.3.3)$$

This equation may be rewritten in the form

$$\frac{w_D mb^{n-1}}{p} = f \left(\frac{b}{z} , \nu , n \right). \qquad \ldots(2.3.4)$$

For $n = 0$, the equation is a partial solution for settlement at the centre of a uniformly loaded circular area on a homogeneous compressible material.

For $n = 1$, the case discussed in Section 2 above is represented. Alexander (1977) obtained an equation for w_D for incompressible material, giving

$$\frac{w_D m}{p} = f\left(\frac{b}{z}, \frac{1}{2}, 1\right) = \frac{1}{2}\left(1 - \frac{1}{\sqrt{(b^2/z^2 + 1)}}\right) . \qquad \ldots(2.3.5)$$

A partial solution similar to equation (2.3.4) may be obtained for an infinitely long strip load of width 2a, as shown in Fig. 2.2.1 when b and r are replaced by a and x respectively.

Expressions for surface stress

The horizontal normal stress σ_c at the point C as shown in Fig. 2.2.1 may be assumed to be given by

$$\sigma_c = f_1 \ (p, b, m, \nu, n). \qquad \ldots(2.3.6)$$

A similar expression applies to plane conditions shown in Fig. 2.2.1 when b and r are replaced by a and x respectively. Using dimensional analysis the equation may be rewritten as

$$\frac{\sigma_c}{p} = f_2 \left(\frac{p}{mb^n}, \nu, n\right). \qquad \ldots(2.3.7)$$

But because the system is linear and the boundary conditions are specified only in terms of boundary traction, $\sigma_c \propto p$. Therefore $\frac{p}{mb^n}$ must vanish from the argument list, giving

$$\frac{\sigma_c}{p} = f\ (\nu, n). \qquad \ldots(2.3.8)$$

By superposition a similar result is obtained for any axisymmetric load of intensity p(r) and where p = p(o), and in particular σ_c = o for any annular load.

Using symmetry and superposition in plane conditions, the following equations are obtained for the horizontal surface stress $\sigma_x(x)$ due to a vertical surface strip load p(x) as shown in Fig. 2.3.1.

$$\left.\begin{aligned} \frac{\sigma_x(x)}{p(x)} &= g\ (\nu\ ,\ n) \qquad a_1 < x < a_2 \\ \sigma_x(x) &= 0 \qquad\qquad\quad \text{elsewhere} \end{aligned}\right\} \qquad \ldots\ (2.3.9)$$

Lekhnitskii (1962), Gibson (1967), Alexander (1977), and Calladine and Greenwoood (1978) conclude variously that the stress distributions due to the above loading when n = 0 are unchanged when both n = 1 and $\nu = \frac{1}{2}$. Combining these results and the appropriate surface stress relations for homogeneous material given by Timoshenko and Goodier (1951), it follows that,

$$f\ (\tfrac{1}{2},1) = g\ (\tfrac{1}{2},1) = g\ (\tfrac{1}{2}.0) = g\ (\nu\ ,\ o) = -1 \qquad \ldots\ (2.3.10)$$

The Author's general solution for line and strip surface loads, given in the next section, includes expressions for g $(\frac{1}{2},n)$, where n $\geq$ o.

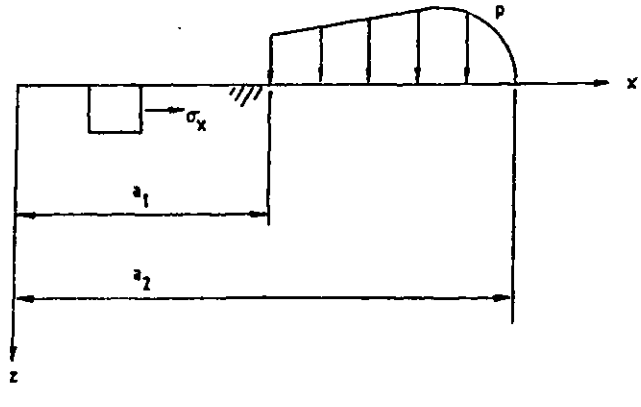


FIG. 2.3.1 VERTICAL SECTION THROUGH AN AREA OF ARBITRARY VERTICAL LOADING ON THE SURFACE OF A SEMI-INFINITE MASS

4. General solution for line and strip loads on an incompressible half-space

Consider either of the line loads of intensity P or Q applied normally and tangentially, respectively, to the plane surface of a linear elastic semi-infinite body, as shown in Fig. 2.4.1.(a). The material is incompressible and the shear modulus is given by $G = mz^n$, where $n \geq 0$.

In a similar way to that described in Section 3, dimensional analysis may be applied to the following formal stress equation for the line load P,

$$\sigma_r = f_1 \ (P, m, r, n, \theta) \qquad \ldots(2.4.1)$$

giving the revised form

$$\frac{r\sigma_r}{P} = f_2 \ \left(\frac{P}{mr^{n+1}}, n, \theta\right) . \qquad \ldots(2.4.2)$$

But since $\sigma_r \propto P$, we may write

$$\frac{r\sigma_r}{P} = f_3 \ (n, \theta). \qquad \ldots(2.4.3)$$

Thus for constant values of P and n, we have

$$r\sigma_r = F \ (\theta). \qquad \ldots(2.4.4)$$

In a similar way, we also have

$$r\sigma_\theta = F_1(\theta), \qquad \ldots(2.4.5)$$

$$r\tau_{r\theta} = F_2(\theta). \qquad \ldots(2.4.6)$$

The equilibrium equations for the element shown in Fig. 2.4.1 referred to polar coordinated are

$$\frac{\partial}{\partial r}(r\sigma_r) - \sigma_\theta + \frac{\partial \tau_{r\theta}}{\partial \theta} = 0 \ , \qquad \ldots(2.4.7)$$

$$\frac{\partial}{\partial r}(r^2 \tau_{r\theta}) + r\frac{\partial \sigma_\theta}{\partial \theta} = 0 \ .$$

Substitution of the above expressions for σ_r , σ_θ , and $\tau_{r\theta}$ gives

$$\frac{-1}{r} F_1 + \frac{1}{r} F_2' = 0 \ , \qquad \ldots(2.4.8)$$

$$F_2 + F_1' = 0 \ ,$$

where the primes denote differentiation w.r.t. θ. Since these equations must be true for the given loadings, it follows for each that $F_1 = F_2 = 0$ or $\sigma_\theta = \tau_{r\theta} = 0$. Hence we conclude that a radial stress field is produced around the line of application of either line load, and that the intensity of the field varies inversely with the radius.

The strain displacement equations and the elastic equations are:

$$\varepsilon_r = \frac{\partial u_r}{\partial r} \ ,$$

$$\varepsilon_\theta = \frac{u_r}{r} + \frac{1}{r}\frac{\partial u_\theta}{\partial \theta} \ , \qquad \ldots(2.4.9)$$

$$\gamma_{r\theta} = \frac{\partial u_\theta}{\partial r} - \frac{u_\theta}{r} + \frac{1}{r}\frac{\partial u_r}{\partial \theta} \ ;$$

$$\varepsilon_r = -\varepsilon_\theta = (\sigma_r - \sigma_\theta) / 4G \ ,$$

$$\gamma_{r\theta} = \tau_{r\theta}/G \quad , \qquad \ldots(2.4.10)$$

$$G = mr^n \cos^n\theta \ .$$

By eliminating ε_r, we obtain

$$\frac{\partial u_r}{\partial r} = \frac{f(\theta)}{r^{n+1}} \qquad \ldots(2.4.11)$$

where

$$f(\theta) = \frac{F(\theta)}{4m\cos^n\theta} \ . \qquad \ldots(2.4.12)$$

Hence, by integration,

$$\left.\begin{aligned} u_r &= \frac{-f(\theta)}{nr^n} + g(\theta) \quad , \quad n > 0 \\ u_r &= f(\theta).\log(r) + g(\theta) \quad , \quad n = 0 \end{aligned}\right\} \qquad \ldots(2.4.13)$$

It follows that:

$$r\sigma_r = 4m\,(\cos^n\theta)\quad f(\theta),\quad \sigma_\theta = \tau_{r\theta} = 0\quad ,\ n \geq 0$$

$$\left.\begin{aligned} u_r &= \frac{-f(\theta)}{nr^n} + g(\theta) \\ u_\theta &= \frac{-f'(\theta)}{n(n+1)r^n} + g'(\theta) + r\,h(\theta) \end{aligned}\right\},\ n > 0 \qquad \ldots(2.4.14)$$

$$\left.\begin{aligned} u_r &= f(\theta)\log(r) + g(\theta) \\ u_\theta &= (1 + \log(r))\,f'(\theta) + g'(\theta) + r\,h(\theta) \end{aligned}\right\},\ n = 0$$

where, by eliminating ε_θ

$$f(\theta) = D + E\theta\quad ,\quad n = 1$$

$$f(\theta) = H\cos(\theta\sqrt{(1-n^2)}) + I\sin(\theta\sqrt{(1-n^2)})\quad ,\quad n < 1$$

$$f(\theta) = J\exp(\theta\sqrt{(n^2-1)}) + K\exp(-\theta\sqrt{(n^2-1)})\quad ,\quad n > 1$$

$$g(\theta) = A\cos\theta + B\sin\theta$$

$$h(\theta) = C$$

and A, B, C, etc., are arbitrary constants.

For the P line load only, the components σ_r and u_r are even functions of θ, and u_θ is an odd function of θ. For the Q line load only, these relationships are interchanged. From the equilibrium of a semicircular region symmetrically underlying the line loads we also have,

$$P + \int_{-\pi/2}^{\pi/2} r\sigma_r \cos\theta\, d\theta = 0, \qquad \ldots(2.4.15)$$

$$Q + \int_{-\pi/2}^{\pi/2} r\sigma_r \sin\theta\, d\theta = 0 \qquad \ldots(2.4.16)$$

Using the above information, equations (2.4.17) and (2.4.18) are obtained for the radial stress and for the radial displacements, in which the arbitrary constants A,B,and C represent rigid body movements and C is small. Values of the constant c(n), which also appear in the equations, are given in Table 2.4.1 for n between 0 and 100. In Table 2.4.2 and Table 2.4.3 respectively, values of $-r\sigma_r/P$ and $-r\sigma_r/Q$ are given at 10° intervals of θ for a wide range of values of n.

TABLE 2.4.1 VALUES OF c(n)

n	c(n)	n	c(n)
0.0	0.63662	1.0	0.63662
0.1	0.64726	2.0	0.52436
0.2	0.65481	3.0	0.39927
0.3	0.65955	4.0	0.29181
0.4	0.66179	5.0	0.20803
0.5	0.66180	7.0	1.01028×10^{-1}
0.6	0.65983	10.0	3.20597×10^{-2}
0.7	0.65612	20.0	5.56905×10^{-4}
0.8	0.65089	50.0	1.67662×10^{-9}
0.9	0.64433	100.0	6.99862×10^{-19}

For $n = 0$

$$-r\sigma_r/P = c(0) \cos\theta$$

$$u_r = \left(- c(0) \frac{P}{4m} \log (r) + A\right) \cos\theta$$

$$u_\theta = \left(c(0) \frac{P}{4m} (1+ \log (r)) - A\right) \sin\theta$$

$$1/c\ (0) = 2\int_0^{\pi/2} \cos^2\theta\, d\theta = \pi/2$$

For $0 < n < 1$

$$-r\sigma_r/P = c(n) \cos^n\theta \cos (\theta \sqrt{(1-n^2)})$$

$$u_r = c(n) \frac{P}{4m} \frac{1}{n} \frac{1}{r^n} \cos (\theta \sqrt{(1-n^2)}) + A \cos\theta$$

$$u_\theta = -c(n) \frac{P}{4m} \frac{\sqrt{(1-n^2)}}{n(n+1)} \frac{1}{r^n} \sin (\theta \sqrt{(1-n^2)}) - A \sin\theta$$

$$1/c(n) = 2 \int_0^{\pi/2} \cos^{n+1}\theta \cos (\theta \sqrt{(1-n^2)})\, d\theta$$

For $n = 1$ ...(2.4.17)

$$-r\sigma_r/p = c(1) \cos\theta$$

$$u_r = c(1) \frac{P}{4m} \frac{1}{r} + A \cos\theta$$

$$u_\theta = - A \sin\theta$$

$$1/c(n) = 2 \int_0^{\pi/2} \cos^2\theta\, d\theta = \pi/2$$

For $n > 1$

$$-r\sigma_r/p = c(n) \cos^n\theta \cosh (\theta \sqrt{(n^2 - 1)})$$

$$u_r = c(n) \frac{P}{4m} \frac{1}{n} \frac{1}{r^n} \cosh (\theta \sqrt{(n^2 -1)}) + A \cos\theta$$

$$u_\theta = c(n) \frac{P}{4m} \frac{\sqrt{(n^2 - 1)}}{n(n + 1)} \frac{1}{r^n} \sinh (\theta \sqrt{(n^2 -1)}) - A \sin\theta$$

$$1/c(n) = 2\int_0^{\pi/2} \cos^{n+1}\theta \cosh (\theta \sqrt{(n^2 - 1)})\, d\theta$$

For $n = 0$

$$-r\sigma_r/Q = c(0) \sin\theta$$

$$u_r = (-c(0) \frac{Q}{4m} \log(r) + B) \sin\theta$$

$$u_\theta = (-c(0) \frac{Q}{4m} (1 + \log(r)) + B) \cos\theta + Cr$$

For $0 < n < 1$

$$-r\sigma_r/Q = c(n) \frac{1+n}{\sqrt{(1-n^2)}} \cos^n\theta \sin(\theta \sqrt{(1 - n^2)})$$

$$u_r = c(n) \frac{Q}{4m} \frac{1 + n}{n\sqrt{(1-n^2)}} \frac{1}{r^n} \sin(\theta \sqrt{(1 - n^2)}) + B \sin\theta$$

$$u_\theta = c(n) \frac{Q}{4m} \frac{1}{n} \frac{1}{r^n} \cos(\theta \sqrt{(1 - n^2)}) + B \cos\theta + Cr$$

For $n = 1$ ...(2.4.18)

$$-r\sigma_r/Q = 2\, c(1)\, \theta \cos\theta$$

$$u_r = 2\, c(1) \frac{Q}{4m} \frac{1}{r} \theta + B \sin\theta$$

$$u_\theta = c(1) \frac{Q}{4m} \frac{1}{r} + B \cos\theta + Cr$$

For $n < 1$

$$-r\sigma_r/Q = c(n) \frac{1 + n}{\sqrt{(n^2-1)}} \cos^n\theta \sinh(\theta \sqrt{(n^2 - 1)})$$

$$u_r = c(n) \frac{Q}{4m} \frac{1 + n}{n\sqrt{(n^2-1)}} \frac{1}{r^n} \sinh(\theta \sqrt{(n^2 - 1)}) + B \sin\theta$$

$$u_\theta = c(n) \frac{Q}{4m} \frac{1}{n} \frac{1}{r^n} \cosh(\theta \sqrt{(n^2 - 1)}) + B \cos\theta + Cr$$

TABLE 2.4.2 VALUES OF $-r\sigma_r/P$

	$\theta = 0^\circ$	10°	20°	30°	40°	50°	60°	70°	80°	90°
n = 0	0.637	0.627	0.598	0.551	0.488	0.409	0.318	0.218	0.111	0
0.1	0.647	0.637	0.605	0.553	0.484	0.400	0.305	0.202	0.098	0
0.5	0.662	0.649	0.612	0.554	0.477	0.386	0.288	0.190	0.098	0
1.0	0.637	0.627	0.598	0.551	0.488	0.409	0.318	0.218	0.111	0
2.0	0.524	0.532	0.550	0.566	0.561	0.515	0.413	0.258	0.089	0
3.0	0.399	0.429	0.506	0.600	0.659	0.630	0.484	0.253	0.054	0
7.0	0.101	0.166	0.370	0.695	0.986	0.967	0.559	0.131	0.004	0
10.0	0.032	0.081	0.278	0.696	1.159	1.139	0.525	0.067	0	0
100.0	0	0	0	0.011	1.938	1.771	0.001	0	0	0

TABLE 2.4.3 VALUES OF $-r\sigma_r/Q$

	$\theta =$ 0°	10°	20°	30°	40°	50°	60°	70°	80°	90°
n = 0.0	0	0.111	0.218	0.318	0.409	0.488	0.551	0.598	0.627	0.637
0.1	0	0.123	0.242	0.351	0.446	0.523	0.576	0.603	0.581	0
0.5	0	0.171	0.331	0.467	0.570	0.630	0.638	0.584	0.447	0
1.0	0	0.219	0.418	0.577	0.681	0.714	0.667	0.532	0.309	0
2.0	0	0.270	0.515	0.706	0.813	0.809	0.678	0.434	0.153	0
3.0	0	0.277	0.541	0.705	0.897	0.879	0.681	0.357	0.077	0
7.0	0	0.160	0.420	0.801	1.138	1.117	0.645	0.151	0.004	0
10.0	0	0.084	0.306	0.770	1.282	1.259	0.580	0.074	0	0
100.0	0	0	0	0.011	1.957	1.789	0.001	0	0	0

The equations for stress and displacement for strip loading may be obtained by use of equations (2.4.17) and (2.4.18). Assuming, for simplicity, that the constant C vanishes, the substitutions given below in equations (2.4.19) are made as appropriate in these equations.

$$\sigma_x = \sigma_r \sin^2 \theta$$

$$\sigma_z = \sigma_r \cos^2 \theta$$

$$\tau_{xz} = \sigma_r \sin \theta \cos \theta$$

$$u_x = u_r \sin \theta + u_\theta \cos \theta$$

$$u_z = u_r \cos \theta - u_\theta \sin \theta \qquad \ldots(2.4.19)$$

$$P = pdx$$

$$Q = qdx$$

$$\tan \theta = -x/z_o$$

$$r = \sqrt{(x^2 + z_o^2)}$$

where z_o is constant.

By integrating these equations between the limits denoted formally by the numbers 1 and 2, we obtain the general expressions for stresses and displacements due to the strip loading shown in Fig. 2.4.1.(b). The general expressions are in the form of integrals and may be evaluated by numerical techniques for specific points in the half-space. Most of the results for surface conditions, on the other hand, have been obtained either in the form of algebraic, trigonometric and hyperbolic expressions or as constants.

The expression for the vertical strip load of intensity p are given in equation (2.4.20), (2.4.21), (2.4.22), (2.4.23) for $n = o$, $o < n < 1$, $n = 1$, and $n > 1$ respectively. The corresponding expressions for the horizontal strip load of intensity q are given in equations (2.4.24), (2.4.25), (2.4.26) and (2.4.27) for the same n values. The arbitrary constants A^1 and B^1 in these equations represent rigid body movements. It is noted that $n = 0$ gives Boussinesq's solutions for incompressible material, and $n = 1$ includes Gibson's results (Gibson (1967)).

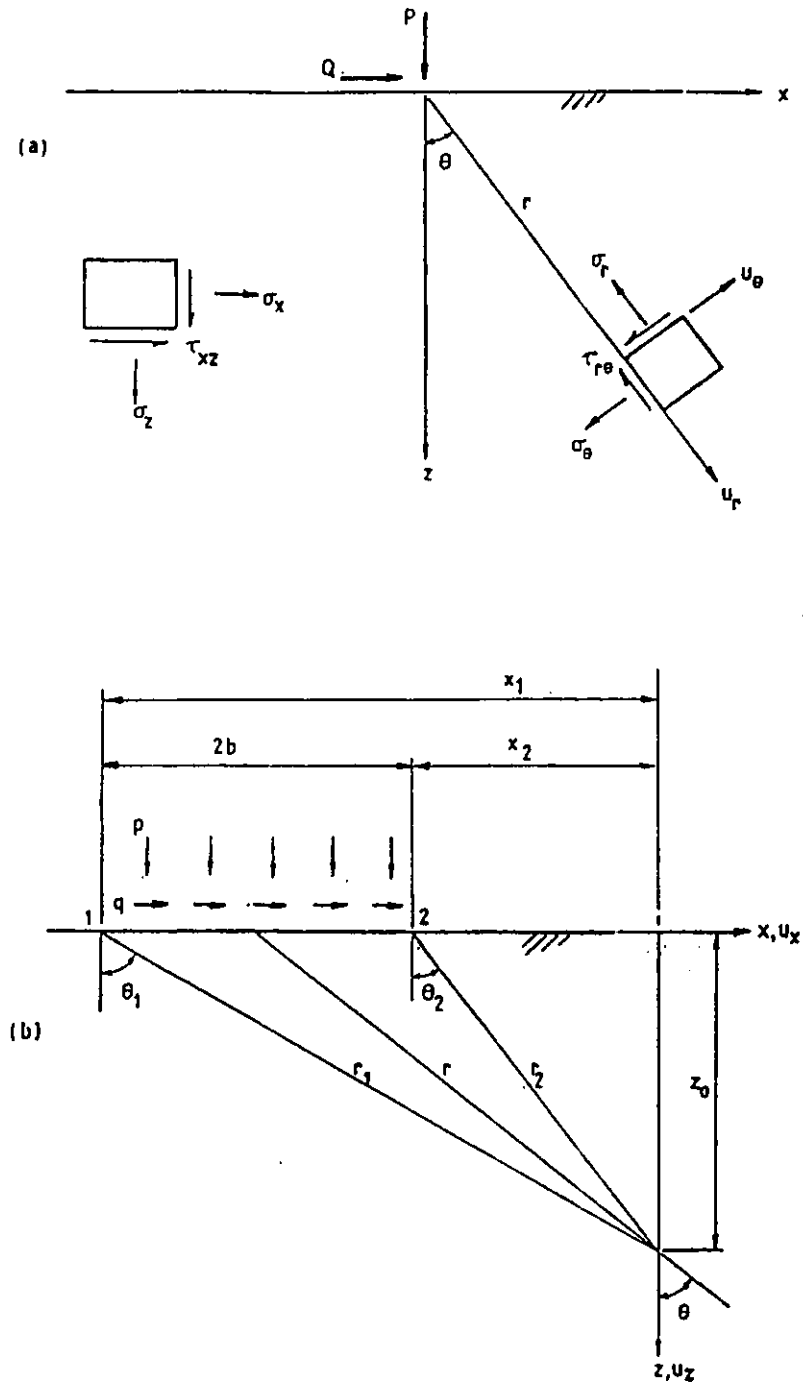


FIG. 2.4.1: VERTICAL SECTIONS THROUGH NORMAL AND TANGENTIAL (a) LINE AND (b) UNIFORM STRIP LOADS ON THE SURFACE OF A SEMI-INFINITE MASS

For $n = 0$ and $z_o > 0$:

$$\sigma_x/p = c(0)\int_1^2 \sin^2\theta \, d\theta = \frac{1}{\pi}(\theta - \sin\theta\cos\theta)_1^2$$

$$\sigma_z/p = c(0)\int_1^2 \cos^2\theta \, d\theta = \frac{1}{\pi}(\theta + \sin\theta\cos\theta)_1^2$$

$$\tau_{xz}/p = c(0)\int_1^2 \sin\theta\cos\theta \, d\theta = \frac{1}{\pi}(\sin^2\theta)_1^2$$

$$u_x = -c(0)\frac{p}{4m} z_o \int_1^2 \tan\theta \, d\theta = \frac{-p}{2\pi m} z_o (\log(\sec\theta))_1^2$$

$$u_z = c(o)\frac{p}{4m} z_o \int_1^2 (\sec^2\theta \log(z_o \sec\theta) + \tan^2\theta) \, d\theta + A^1$$

$$= \frac{p}{2\pi m} z_o (\tan\theta \log(z_o \sec\theta))_1^2 + A^1$$

For $n = 0$, $z_o = 0$ and both $|x_1|$ and $|x_2| < 2b$:

$$\sigma_x/p = -1$$
$$\sigma_z/p = -1 \qquad \ldots(2.4.20)$$
$$\tau_{xz} = 0$$

For $n = 0$, $z_o = 0$ and either $|x_1|$ or $|x_2| > 2b$:

$$\sigma_x = 0$$

$$\sigma_z = 0$$

$$\tau_{xz} = 0$$

For $n = 0$ and $z_o = 0$:

$$u_x = 0$$

$$u_z = \frac{-p}{2\pi m} (x \log |x|)_1^2 + A^1$$

For $0 < n < 1$ and $z_o > o$:

$$\sigma_x/p = c(n)\int_1^2 \cos^{n-1}\theta \sin^2\theta \cos(\theta\sqrt{(1-n^2)})\, d\theta$$

$$\sigma_z/p = c(n)\int_1^2 \cos^{n+1}\theta \cos(\theta\sqrt{(1-n^2)})\, d\theta$$

$$\tau_{xz}/p = c(n)\int_1^2 \cos^{n}\theta \sin\theta \cos(\theta\sqrt{(1-n^2)})\, d\theta$$

$$u_x = \frac{-c(n)}{n}\ \frac{p}{4m}\ \frac{1}{z_o^{n-1}}\int_1^2 \cos^{n-2}\theta\,(\sin\theta\cos(\theta\sqrt{(1-n^2)}) - $$

$$-(\sqrt{((1-n)/(1+n))})\cos\theta\sin(\theta\sqrt{(1-n^2)}))d\theta$$

$$u_z = \frac{-c(n)}{n}\ \frac{p}{4m}\ \frac{1}{z_o^{n-1}}\int_1^2 \cos^{n-2}\theta\,(\cos\theta\cos(\theta\sqrt{(1-n^2)}) +$$

$$+(\sqrt{((1-n)/(1+n))})\sin\theta\sin(\theta\sqrt{(1-n^2)}))\,d\theta + A^1$$

For $0 < n < 1$, $z_o = 0$, and both $|x_1|$ and $|x_2| < 2b$:

$$\sigma_x/p = -1$$

$$\sigma_z/p = -1 \qquad \ldots(2.4.21)$$

$$\tau_{xz} = 0$$

For $0 < n < 1$, $z_o = 0$, and either $|x_1|$ or $|x_2| > 2b$:

$$\sigma_x = 0$$

$$\sigma_z = 0$$

$$\tau_{xz} = 0$$

For $0 < n < 1$ and $z_o = 0$:

$$u_x = \frac{-c(n)}{n}\ \frac{p}{4m}\ \frac{1}{1-n}\cos(\tfrac{1}{2}\pi\sqrt{(1-n^2)})\,(|x|^{1-n})_1^2$$

$$u_z = \frac{c(n)}{n}\ \frac{p}{4m}\ \frac{1}{\sqrt{(1-n^2)}}\sin(\tfrac{1}{2}\pi\sqrt{(1-n^2)})\,(x|x|^{-n})_1^2 + A^1$$

For $n = 1$ and $z_o > 0$:

$\left.\begin{matrix}\sigma_x/p \\ \sigma_z/p \\ \tau_{xz}/p\end{matrix}\right\}$ same as equation (2.4.20)

$$u_x = -c(1) \frac{p}{4m} \int_1^2 \tan\theta \, d\theta = \frac{-p}{2\pi m} (\log(\sec\theta))_1^2$$

$$u_z = -c(1) \frac{p}{4m} \int_1^2 d\theta + A^1 = \frac{-p}{2\pi m} (\theta)_1^2 + A^1$$

For $n = 1$ and $z_o = 0$:

$\left.\begin{matrix}\sigma_x/p \\ \sigma_z/p \\ \tau_{xz}/p\end{matrix}\right\}$ same as equation (2.4.20)

$$u_x = \frac{-p}{2\pi m} (\log|x|)_1^2 \qquad \ldots(2.4.22)$$

For $n = 1$, $z_o = 0$ and both $|x_1|$ and $|x_2| < 2b$

$$u_z = \frac{p}{2m} + A^1$$

For $n = 1$, $z_o = 0$ and either $|x_1|$ or $|x_2| > 2b$

$$u_z = A^1$$

For $n > 1$ and $z_o > 0$:

$$\sigma_x/p = c(n) \int_1^2 \cos^{n-1}\theta \sin^2\theta \cosh(\theta\sqrt{(n^2-1)})\, d\theta$$

$$\sigma_z/p = c(n) \int_1^2 \cos^{n+1}\theta \cosh(\theta\sqrt{(n^2-1)})\, d\theta$$

$$\tau_{xz}/p = c(n) \int_1^2 \cos^{n}\theta \sin\theta \cosh(\theta\sqrt{(n^2-1)})\, d\theta$$

$$u_x = \frac{-c(n)}{n} \frac{p}{4m} \frac{1}{z_o^{n-1}} \int_1^2 \cos^{n-2}\theta(\sin\theta \cosh(\theta\sqrt{(n^2-1)}) + (\sqrt{((n-1)/(n+1))}) \cos\theta \sinh(\theta\sqrt{(n^2-1)}))\, d\theta$$

$$u_z = \frac{-c(n)}{n} \frac{p}{4m} \frac{1}{z_o^{n-1}} \int_1^2 \cos^{n-2}\theta (\cos\theta \cosh(\theta\sqrt{(n^2-1)}) - (\sqrt{((n-1)/(n+1))}) \sin\theta \sinh(\theta\sqrt{(n^2-1)}))\, d\theta + A^1$$

For $n > 1$, $z_o = 0$ and both $|x_1|$ and $|x_2| < 2b$:

$$\sigma_x/p = -1$$

$$\sigma_z/p = -1 \qquad \ldots(2.4.23)$$

$$\tau_{xz} = 0$$

For $n > 1$, $z_o = 0$, and either $|x_1|$ or $|x_2| > 2b$:

$$\sigma_x = 0$$

$$\sigma_z = 0$$

$$\tau_{xz} = 0$$

For $n > 1$ and $z_o = 0$:

$$u_x = \frac{c(n)}{n} \frac{p}{4m} \frac{1}{n-1} \cosh(\tfrac{1}{2}\pi\sqrt{(n^2-1)}) (|x|^{1-n})_1^2$$

$$u_z = \frac{c(n)}{n} \frac{p}{4m} \frac{1}{\sqrt{(n^2-1)}} \sinh(\tfrac{1}{2}\pi\sqrt{(n^2-1)}) (x|x|^{-n})_1^2 + A^1$$

For $n = 0$ and $z_o > 0$:

$$\sigma_x/q = c(0) \int_1^2 \frac{\sin^3\theta}{\cos\theta}\, d\theta = \frac{1}{\pi} \left(2 \log (\sec\theta) + \cos^2\theta\right)_1^2$$

$$\sigma_z/q = c(0) \int_1^2 \sin\theta \cos\theta\, d\theta = \frac{1}{\pi} (\sin^2\theta)_1^2$$

$$\tau_{xz}/q = c(0) \int_1^2 \sin^2\theta\, d\theta = \frac{1}{\pi} (\theta - \sin\theta \cos\theta)_1^2$$

$$u_x = c(0) \frac{q}{4m} z_o \int_1^2 (\sec^2\theta \log (z_o \sec\theta) + 1) d\theta + B^1$$

$$= \frac{q}{2\pi m} z_o (-\tan\theta + \tan\theta \log (z_o \sec\theta) + 2\theta)_1^2 + B^1$$

$$u_z = -c(0) \frac{q}{4m} z_o \int_1^2 \tan\theta\, d\theta = \frac{-q}{2\pi m} z_o (\log(\sec\theta))_1^2$$

For $n = 0$, $z_o = 0$ and both $|x_1|$ and $|x_2| < 2b$:

$$\sigma_x/q = \frac{2}{\pi} (\log |x|)_1^2$$

$$\sigma_z = 0 \qquad \ldots(2.4.24)$$

$$\tau_{xz}/q = -1$$

For $n = 0$, $z_o = o$ and either $|x_1|$ or $|x_2| > 2b$:

$$\sigma_x/q = \frac{2}{\pi} (\log |x|)_1^2$$

$$\sigma_z = 0$$

$$\tau_{xz} = 0$$

For $n = 0$ and $z_o = 0$:

$$u_x = \frac{-q}{2\pi m} (x \log |x|)_1^2 + \frac{qb}{\pi m} + B^1$$

$$u_z = 0$$

For $0 < n < 1$ and $z_o > o$:

$$\sigma_x/q = c(n)\ \sqrt{((1+n)/(1-n))}\int_1^2 \cos^{n-1}\theta \sin^2\theta \sin(\theta\sqrt{(1-n^2)})\, d\theta$$

$$\sigma_z/q = c(n)\ \sqrt{((1+n)/(1-n))}\int_1^2 \cos^{n+1}\theta \sin(\theta\sqrt{(1-n^2)})\, d\theta$$

$$\tau_{xz}/q = c(n)\ \sqrt{((1+n)/(1-n))}\int_1^2 \cos^{n}\theta \sin\theta \sin(\theta\sqrt{(1-n^2)})\, d\theta$$

$$u_x = \frac{-c(n)}{n}\ \frac{q}{4m}\ \frac{1}{z_o^{n-1}}\int_1^2 \cos^{n-2}\theta\ (\sqrt{((1+n)/(1-n))}\sin\theta \sin(\theta/(1-n^2)) + \cos\theta \cos(\theta\sqrt{(1-n^2)}))\, d\theta + B^1$$

$$u_z = \frac{-c(n)}{n}\ \frac{q}{4m}\ \frac{1}{z_o^{n-1}}\int_1^2 \cos^{n-2}\theta\ (\sqrt{((1+n)/(1-n))}\cos\theta \sin(\theta/(1-n^2)) - \sin\theta \cos(\theta\sqrt{(1-n^2)}))\, d\theta$$

For $0 < n < 1$, $z_o = 0$, and both $|x_1|$ and $|x_2| < 2b$:

$$\sigma_x = 0$$

$$\sigma_z = 0 \qquad \ldots(2.4.25)$$

$$\tau_{xz}/q = -1$$

For $0 < n < 1$, $z_o = 0$, and either $|x_1|$ or $|x_2| > 2b$:

$$\sigma_x = 0$$

$$\sigma_z = 0$$

$$\tau_{xz} = 0$$

For $o < n < 1$ and $z_o = 0$

$$u_x = \frac{c(n)}{n(1-n)}\ \frac{q}{4m}\ (\sqrt{((1+n)/(1-n))}\sin(\tfrac{1}{2}\pi\sqrt{(1-n^2)})\ (x\,|x|^{-n})_1^2 + B^1$$

$$u_z = \frac{c(n)}{n(1-n)}\ \frac{q}{4m}\ \cos(\tfrac{1}{2}\pi\sqrt{(1-n^2)})\ (|x|^{1-n})_1^2$$

For $n = 1$ and $z_o > 0$:

$$\sigma_x/q = 2\,c(1)\int_1^2 \theta \sin^2\theta\, d\theta = \frac{1}{\pi}\left(\theta^2 - \theta \sin 2\theta - \tfrac{1}{2}\cos 2\theta\right)_1^2$$

$$\sigma_z/q = 2\,c(1)\int_1^2 \theta \cos^2\theta\, d\theta = \frac{1}{\pi}\left(\theta^2 + \theta \sin 2\theta + \tfrac{1}{2}\cos 2\theta\right)_1^2$$

$$\tau_{xz}/q = 2\,c(1)\int_1^2 \theta \sin\theta \cos\theta\, d\theta = \frac{1}{\pi}\left(-\theta \cos 2\theta + \tfrac{1}{2}\sin 2\theta\right)_1^2$$

$$u_x = -c(1)\,\frac{q}{4m}\int_1^2 (2\theta \tan\theta + 1)\, d\theta + B^1$$

$$= \frac{-q}{2\pi m}\left(2\int_1^2 \theta \tan\theta\, d\theta + (\theta)_1^2\right) + B^1$$

$$u_z = -c(1)\,\frac{q}{4m}\int_1^2 (2\theta - \tan\theta)\, d\theta$$

$$= \frac{-q}{2\pi m}\left(\theta^2 - \log(\sec\theta)\right)_1^2$$

For $n = 1$, $z_o = 0$ and both $|x_1|$ and $|x_2| < 2b$:

$$\sigma_x = 0$$

$$\sigma_z = 0 \qquad \ldots(2.4.26)$$

$$\tau_{xz}/q = -1$$

$$u_x = \frac{q}{2m}\log|x_1 x_2| - \frac{q}{m}\log|x_p| + B^1, \text{ where } |x_p| \to 0$$

For $n = 1$, $z_o = o$ and either $|x_1|$ or $|x_2| > 2b$:

$$\sigma_x = 0$$

$$\sigma_z = 0$$

$$\tau_{xz} = 0$$

$$u_x = \pm\frac{q}{2m}(\log|x|)_1^2 \quad \begin{matrix} , x_1 > 0 \\ , x_2 < 0 \end{matrix}$$

For $n = 1$ and $z_o = 0$:

$$u_x = \frac{q}{2\pi m}(\log|x|)_1^2$$

For $n > 1$ and $z_o > o$:

$$\sigma_x/q = c(n) \sqrt{((n+1)/(n-1))} \int_1^2 \cos^{n-1}\theta \sin^2\theta \sinh(\theta \sqrt{(n^2-1)})\, d\theta$$

$$\sigma_z/q = c(n) \sqrt{((n+1)/(n-1))} \int_1^2 \cos^{n+1}\theta \sinh(\theta \sqrt{(n^2-1)})\, d\theta$$

$$\tau_{xz}/q = c(n) \sqrt{((n+1)/(n-1))} \int_1^2 \cos^{n}\theta \sin\theta \sinh(\theta \sqrt{(n^2-1)})\, d\theta$$

$$u_x = \frac{-c(n)}{n} \frac{q}{4m} \frac{1}{z_o^{n-1}} \int_1^2 \cos^{n-2}\theta \left(\sqrt{((n+1)/(n-1))} \sin\theta \sinh(\theta\sqrt{(n^2-1)}) + \right.$$

$$\left. + \cos\theta \cosh(\theta \sqrt{(n^2-1)}) \right) d\theta + B^1$$

$$u_z = \frac{-c(n)}{n} \frac{q}{4m} \frac{1}{z_o^{n-1}} \int_1^2 \cos^{n-2}\theta \left(\sqrt{((n+1)/(n-1))} \cos\theta \sinh(\theta\sqrt{(n^2-1)}) - \right.$$

$$\left. - \sin\theta \cosh(\theta \sqrt{(n^2-1)}) \right) d\theta$$

For $n > 1$, $z_o = 0$ and both $|x_1|$ and $|x_2| < 2b$:

$$\sigma_x = 0$$

$$\sigma_z = 0 \qquad \ldots(2.4.27)$$

$$\tau_{xz}/q = -1$$

For $n > 1$, $z_o = 0$ and either $|x_1|$ or $|x_2| > 2b$:

$$\sigma_x = 0$$

$$\sigma_z = 0$$

$$\tau_{xz} = 0$$

For $n > 1$ and $z_o = 0$:

$$u_x = \frac{-c(n)}{n(n-1)} \frac{q}{4m} \left(\sqrt{((n+1)/(n-1))} \right) \sinh(\tfrac{1}{2}\pi\sqrt{(n^2-1)}) \left(x\,|x|^{-n} \right)_1^2 + B^1$$

$$u_z = \frac{-c(n)}{n(n-1)} \frac{q}{4m} \cosh(\tfrac{1}{2}\pi\sqrt{(n^2-1)}) \left(|x|^{1-n} \right)_1^2$$

5. Discussion

To illustrate the advantage to be gained by use of the tabulated results for the surface settlement of a compressible half-space, consider the question of the difference in effect of square and circular loading. Using GSETT the settlements may be calculated at points 1,2 and 3 for a uniformly loaded square of unit side as shown in Fig. 2.2.7. The settlements for an inscribed uniformly loaded circle at coincident points is obtained from the closed form solution given in equation (2.2.8). Values of w_o' are given in Table 2.5.1 below for both figures. Assuming that the intensity of loading is the same, it is seen from Table 2.5.1 that the ratios of the settlements at the corresponding points are close to $4/\pi$ ($\doteq 1.273$), which is the ratio of the total load on the square and the circle respectively. Clearly the effect on settlement of the differences in shape of the areas is small at these points and the results of Saint-Venant's principle are evident.

TABLE 2.5.1. VALUES OF w_o' FOR A UNIFORMLY LOADED SQUARE AT POINTS 1,2 AND 3, AS SHOWN IN FIG. 2.2.7, AND FOR AN INSCRIBED UNIFORMLY LOADED CIRCLE AT COINCIDENT POINTS

	1	2	3
w_o' (square)	0.478	0.164	0.083
w_o' (circle)	0.370	0.128	0.065
(w_o' (square)/w_o'(circle))	1.292	1.281	1.278

Interior relative settlements for both of the above mentioned figures may be calculated in a similar way for the eight points P,Q,R etc., defined in Table 2.5.2 below. Values of $w_c' - w'$, given in Table 2.5.2, are proportional to the settlement at each of the eight points relative to that at the centre C. The results show that the circular load indents the surface of the half space more sharply than the square for equal load intensity.

TABLE 2.5.2 VALUES OF $w_c' - w'$ FOR A UNIFORMLY LOADED SQUARE, AS SHOWN IN FIG. 2.2.7, AND FOR AN INSCRIBED UNIFORMLY LOADED CIRCLE AT EIGHT COINCIDENT POINTS P,Q,R,ETC., EQUALLY SPACED FROM EDGE TO CENTRE C ALONG A NORMAL PASSING THROUGH C

	P	Q	R	S	T	U	V	W
$w_c' - w'$ (square)	4.498	2.595	1.604	0.989	0.581	0.308	0.131	0.032
$w_c' - w'$ (circle)	4.905	2.918	1.847	1.160	0.691	0.370	0.159	0.039

The laws of elastostatics are obeyed by the model on which GSETT is based, but because the shear modulus vanishes at the surface, some problems of interpretation are presented. Associated difficulties arise in relating its behaviour to the mechanical properties of ground. Some of these problems may be avoided at the expense of increased complexity by the modifications to the model described by Brown and Gibson (1979). Geotechnical models in which $G = mz^n$ with $n > 0$ fall, perhaps, into a different category to Boussinesq's because of the use made of them. The latter is often used to calculate stresses and displacements which are expected to occur in the ground. The former type, on the other hand, is usually better employed in the prediction

of patterns of behaviour. These categories are not conceived as being mutually exclusive however, and some models may be tolerably successful in both.

6. Conclusion

The interpretation of ground response test results, and the prediction of patterns of behaviour in geotechnical engineering may be considerably aided by the model in which $G = mz^n$ with $n \geq 0$. The extension to the range of the model made by the Author has significantly increased both the number and type of problems to which it can be applied. A further development for axisymmetric conditions is possible and there is also scope for its use with Boundary Element Methods.

CHAPTER 3 ELASTOSTATIC ANALYSIS OF THE LOAD-DEFORMATION BEHAVIOUR OF MIDDLE CHALK AT MUNDFORD

1. Introduction

In order to find out whether some of the site requirements, made by the European Organisation for Nuclear Research (CERN), for the support of a large proton accelerator could be met by a certain area at Mundford, Norfolk, England, a comprehensive investigation of its load-deformation properties was made during 1966-1967. A description of the investigation and a summary of the assessement of the properties of the ground were given by Ward et al. (1968). It should be added for completeness that, in the event, the site was not used, so that all the predictions made about its behaviour in service have necessarily remained untested.

A generally favourable view of its suitability was reached by Ward et al. (1968). In particular they concluded that the short-term load-deformation behaviour of the relevant parts of the site would meet CERN's requirements. The following quotation from their paper serves to illustrate the exacting nature of these stipulations:

> "More precisely to cover the latter requirement CERN adopted the criterion that the vertical displacement of the ground surface at a distance of 50m from a surface shielding load of 10,000 tonnes applied over a square area at a uniform load intensity of 4 kg/sq.cm should not exceed 0.5mm."

Ward et al. (1968) used a simple, isotropic elastic model for the ground in making their appraisal. In presenting some of their calculated values for Young's modulus using this model, one of the possible effects of its simplicity was acknowledged when they wrote:

> "A more refined analysis in which the varying stiffness with depth is taken into account might lead to different values."

Analytical solutions for a special case of varying stiffness with depth for a half space in plane conditions or in axisymmetric conditions have been obtained by Gibson (1967) and by Awojobi and Gibson (1973). This work was discussed in detail in Chapter 2.

Although the analytical model increases the number and variety of problems which can be tackled in this way, it is clear that for most practical purposes only numerical methods are sufficiently powerful and flexible. Because of the large amount of accurate and precise geotechnical information made available by Ward et al. (1968) and in later supplements by Burland and Lord (1969), Burland et al. (1973) and Burland (1977), (1978), it was decided to use the Boundary Integral Equation Method to make a comprehensive analysis of the short-term pre-yield deformation behaviour of the ground at Mundford. Similar earlier work by Burland et al. (1973) and Burland (1969) in which the Finite Element Method was directly involved provided a valuable comparison, as did the comparative study made by Burland and Lord (1969), of the different test results obtained from the Mundford investigation. Where there are significant differences between the results obtained by the two numerical methods used, attempts have been made to interpret the discrepancies constructively.

2. Site

The Mundford site was approximately 5 x 9 km in extent over which the ground elevation varied between 14 and 35 m O.D. It was set on the Middle Chalk in a zone of simple geological structure and significant lateral uniformity. The details and sequence of the ground materials shown in the geological profiles in Fig.3.3.1 and Fig.3.3.5 are typical for the area. The thickness of the Twin Marls seam was 6.4 cm. It was assumed that the Mount Ephraim Marl, occuring locally a further 14.5 m below the Twin Marls, was 10 cm thick. Both seams extended subhorizontally across the site. Ward et al. (1968) reported that for an area adjacent to that shown in Fig.3.3.1:

> "...the maximum recorded water levels vary from 8.0 to 10.8 m above O.D., the seasonal fluctuation varying from about 2.4 to 3.2 m."

3. Tests and test results

The site tests revealed important steady increases in the stiffness and strength of the chalk with depth. During the loading tests there was an initial, approximately linear elastic deflection response in the short term, and a strong localization of the surface deformation around the loading area for the full scale tank test. The yield values were well defined and generally considerably above those expected in service.

Ward et al. (1968) established a relatively simple but precise system of visual classification of the chalk, broadly related to its stiffness and strength. The terms used in the nomenclature were Grade I to Grade V inclusive. The qualities used to distinguish between the Grades included hardness of material, and joint spacing and tightness. The significance of joint orientation was emphasized in their general discussion. Progression from the smaller to the larger Grade numbers corresponded to a decrease in hardness, etc. (Table 3.3.1).

The full scale surface loading test consisted essentially of filling and emptying a large diameter steel tank with water and measuring the resulting ground movements in adjoining vertical shafts. The general arrangement is shown in Fig.3.3.1. The two lines of shafts etc. radiating from the centre line of the tank are at right angles to each other in plan. Values of the average vertical strains ε_o over specific thicknesses (e.g. Level 5 - 6) of the ground were given by Ward et al. (1968) and are shown in Fig.3.3.2.(a).

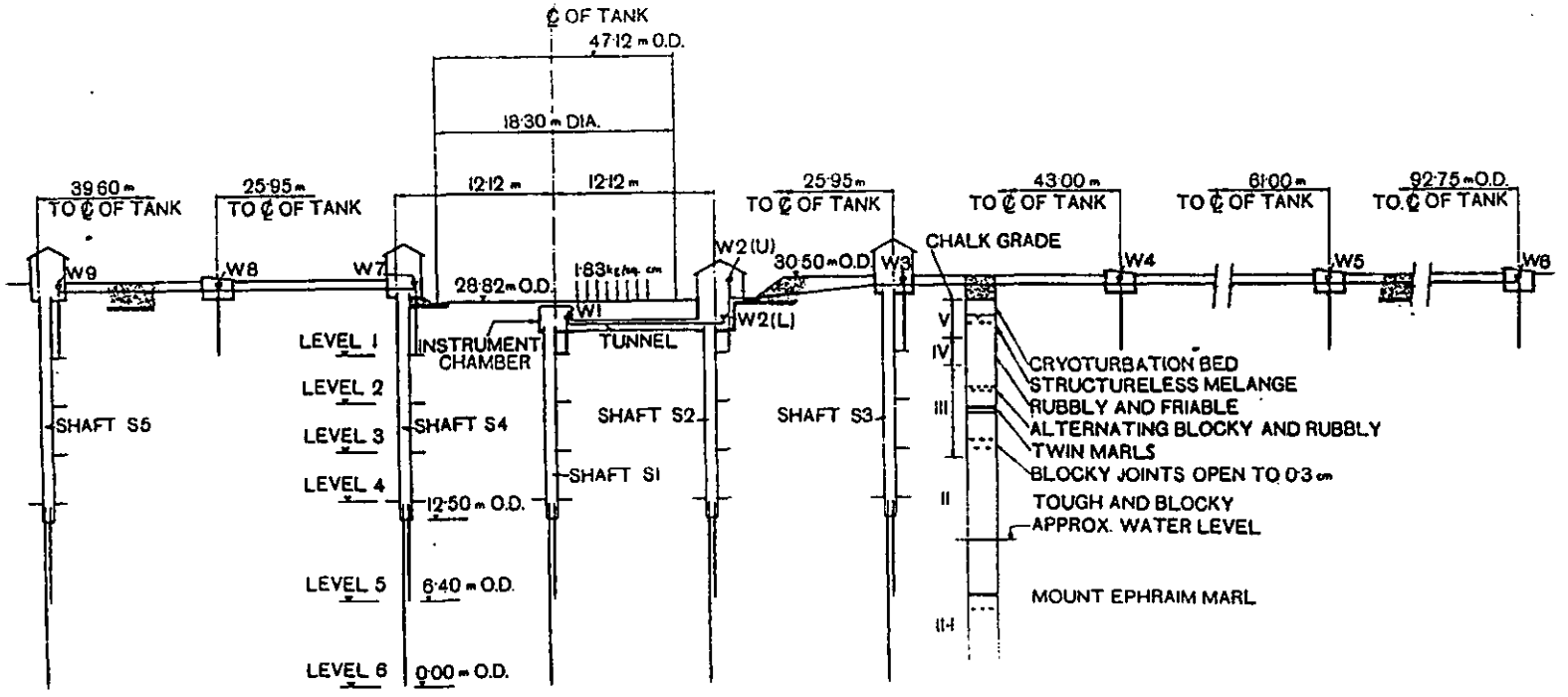
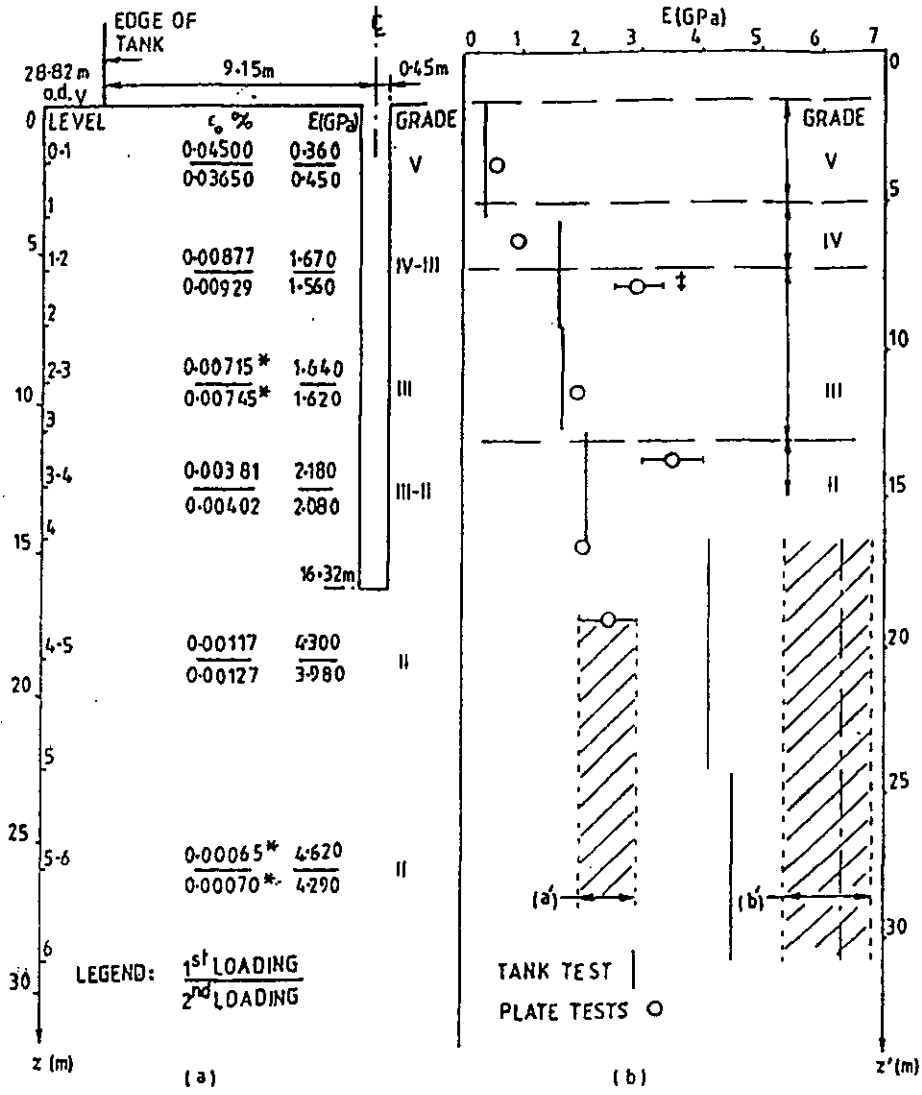


FIG. 3.3.1: VERTICAL SECTION THROUGH TWO LINES OF SHAFTS AND WATER LEVEL GAUGE POSITIONS AT THE TANK (WARD ET AL. (1968))



Notes:

* Adjusted to eliminate the influence of marl seam
‡ Carried out above tough bed
(a') Range of plate test results for Grade II chalk
(b') Range of laboratory values
z Average depth below tank
z' Depth below ground surface

FIG. 3.3.2: (a) SECTION BENEATH TANK SHOWING GRADES OF CHALK AT VARIOUS DEPTHS WITH VALUES OF YOUNG'S MODULUS E ESTIMATED FROM IMMEDIATE VERTICAL STRAINS ε_o GIVEN BY WARD ET AL. (1968) AND SHOWN IN TABLE 3.4.1. (b) COMPARISON OF YOUNG'S MODULUS E DERIVED FROM THE PLATE TESTS AND LABORATORY TESTS WITH VALUES DERIVED FROM FULL SCALE TANK TEST GIVEN BY BURLAND AND LORD (1969)

Table 3.3.2 is a reproduction of a summary due to Burland (1977) of the tank test results showing settlements at several elevations in the shafts adjoining the test tank. Burland et al. (1973) reported that the total [horizontal] inward movement of level 3 relative to the top was 0.134 mm in shaft S2 after complete emptying from full of the test tank shown in Fig.3.3.1. They added that this movement was accompanied simultaneously by a relative vertical movement between the same levels of 0.94 mm.

The general arrangement and details for the plate loading test are shown in Figs. 3.3.3 and 4. Four test series, T1 to T4, were run, of which series T1 was mainly preliminary. Ward et al. (1968) published results for the series T2, T3 and T4. Fig.3.3.5 refers to the last of them. Burland and Lord (1969) later gave important supplementary details for the early part of the load-deformation curves shown on Figs. 3.5.11 and 12.

Results from laboratory compression tests were also given by Burland and Lord (1969) for samples of Grade II chalk from the site of the tank test. In summarizing those on nine specimens, each 55 mm in diameter by 120 mm high, they reported that:

> "The values of E [Young's modulus] (which appear to be almost independent of cell pressure) lie between 5,400 MN/m^2 and 6,800 MN/m^2 ... with an average value of 6,300 MN/m^2 ... . Poisson's ratio lies between 0.18 and 0.27 with an average of 0.24."

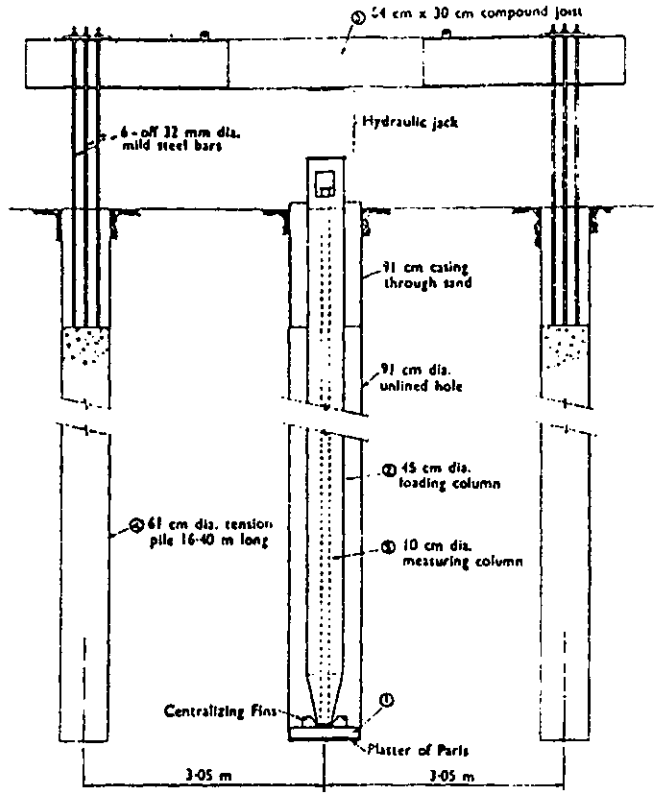


FIG. 3.3.3: VERTICAL SECTION THROUGH THE PLATE-LOADING TEST EQUIPMENT (WARD ET AL. (1968))

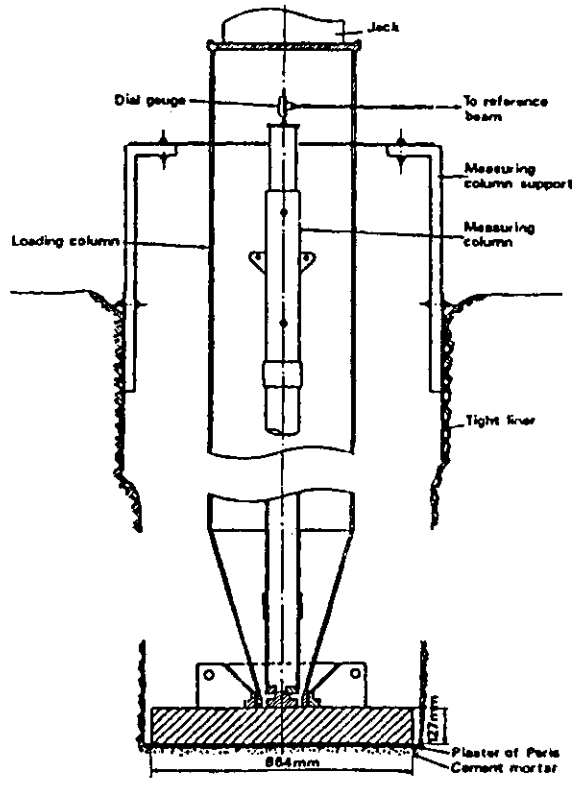


FIG. 3.3.4: DETAILS OF PLATE TEST EQUIPMENT (BURLAND AND LORD (1969))

TABLE 3.3.1 CORRELATION BETWEEN GRADES AND THE MECHANICAL PROPERTIES OF THE CHALK AT MUNDFORD (WARD ET AL. (1968))

Grade	Brief description	Approximate range of E (kg/sq. cm)	Bearing pressure causing 'yield' (kg/sq. cm)	Creep properties
V	Structureless remoulded chalk containing lumps of intact chalk	< 5000	< 2	Exhibits significant creep
IV	Friable to rubbly chalk with open joints often infilled with soft remoulded chalk	5000–10 000	2–4	Exhibits significant creep
III	Medium to hard rubbly to blocky chalk with closely spaced, slightly open joints	10 000–20 000	4–6	For pressures not exceeding 4 kg/sq. cm creep is small and terminates in a few months
II	Medium hard to hard chalk with widely-spaced, tight joints	20 000–50 000	> 10	Negligible creep for pressures of at least 4 kg/sq. cm
I	Hard brittle chalk with widely-spaced, tight joints	> 50 000	> 10	Negligible creep for pressures of at least 4 kg/sq. cm

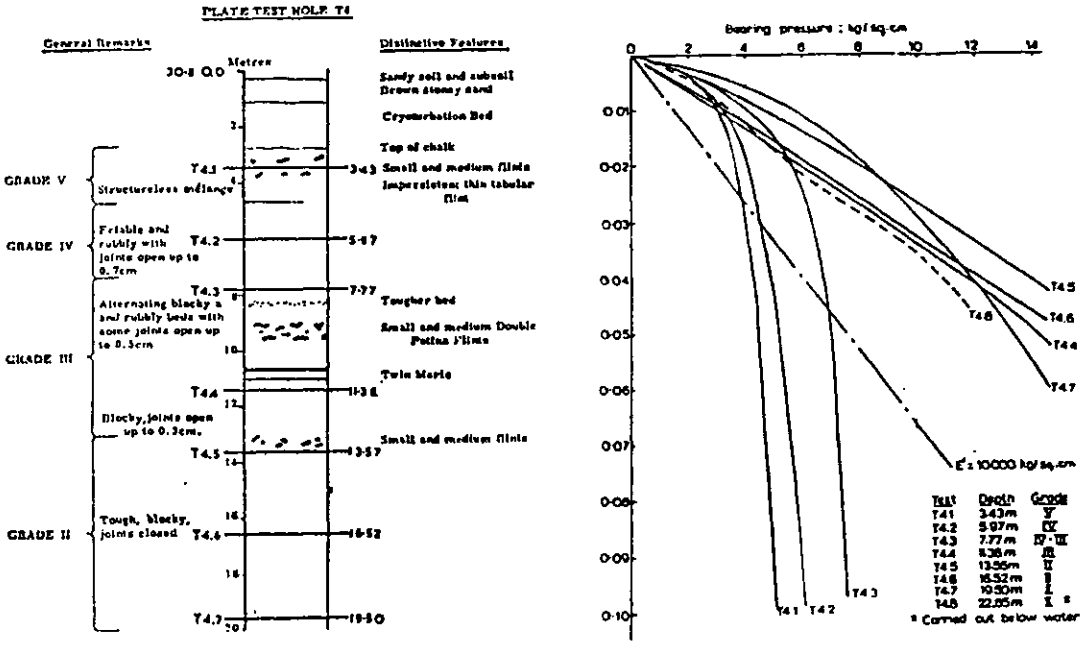


FIG. 3.3.5: GEOLOGICAL PROFILE AND GRADES OF CHALK ALONGSIDE SIMPLIFIED PRESSURE-SETTLEMENT CURVES FOR PLATE TEST SERIES T 4 (WARD ET AL. (1968))

TABLE 3.3.2 MUNDFORD - SUMMARY OF TANK TEST RESULTS (BURLAND (1977))

Radius of tank = 9.15 m

Pressure of water = 1.83 kg/cm^2

Level	Depth (m)	Settlement (mm)							
		shaft 1	shaft 2	shaft 4	shaft 3	shaft 5	shaft W8	shaft W 4	shaft W 5
0	0	2.58	-	-	-	-	-	-	-
1	3.81	1.188	0.280	0.282	0.069	0.038	0.071	0.025	-
2	7.32	0.879	0.256	0.272	0.071	0.048	-	-	-
3	10.93	0.521	0.211	0.188	0.071	0.051	-	-	-
4	14.59	0.381	0.170	0.178	0.074	0.056	-	-	-
5	22.57	0.302	0.109	0.125	0.066	0.033	-	-	-
6	28.97	0.160	0.084	0.084	0.061	0.033	-	-	-
Metres from C.L.		0.0	12.12	12.12	25.95	39.60	25.95	43.0	61.0

Average settlement of edge of tank is 0.813 mm

Marl seams at depths of 8.4 m and 22.9 m

Ward et al. (1968) gave the following mechanical properties obtained from undistrubed samples taken from the Twin Marls seam at the site of the tank test:

"Swelling pressure	1.87 kg/sq. cm
Coefficient of volume compressibility and swelling for a change of 1 kg/sq. cm at the swelling pressure, $m_{vc} = m_{vs}$	0.0043 sq.cm/kg "

In its original form the usefulness of the large amount of accurate information gathered from the field and the laboratory observations and tests was very limited. The results from the full-scale tank-test, for example, referred only to the immediate vicinity of the loaded area. Results from the plate loading tests were similarly confined.

A scheme was therefore evolved to predict economically the load-deformation properties of the ground over the whole site. It was based on the correlation of Grades of chalk with values of those mechanical properties which were thought to be relevant. Ward et al. (1968) developed the system shown in Table 3.3.1. In the part dealing with short term pre-yield behaviour, the values of Young's modulus E which are indexed against the Grades of chalk, were based mainly on a theoretical elastic analysis of the full-scale tank-test results and to a smaller extent on the plate bearing test results.

4. Previous Analyses

Values for the short-term deformation properties of the ground were obtained indirectly by back analysis of several different linear elastic mathematical models. In the matching procedure the geometric configuration and the boundary conditions were represented either as well as the model parameters would allow or as fully as was considered necessary. Generally the former situation applied for closed form solutions and the latter for finite element methods. Next the model parameters corresponding to deformation properties of different parts of the ground were adjusted until the load-deformation behaviour of the model and prototype coincided sufficiently closely. It was generally necessary to use this section of the procedure iteratively in all but the simplest models.

Table 3.4.1. shows the range of values of Young's modulus at several different depths beneath the centre of the test tank obtained by Ward et al. (1968) from an elastic analysis of a simple isotropic mathematical model. Results of a reanalysis by the Author of the same data using the elastic solution for a uniform vertical loading on a circular area with Poisson's ratios of 0.1 and 0.25 are also shown.

An analysis of the results of the full-scale tank-test was made by Burland et al. (1973) using the Finite Element Method. Several ranges of values for Young's modulus with depth were tried until the deformations in the ground under the centre of the tank were matched satisfactorily as shown in Fig. 3.4.1(a). A linear variation of Young's modulus was eventually selected as shown in Fig. 3.4.1(b) where the upper limit was based on the maximum value measured in laboratory compression tests

TABLE 3.4.1 VALUES OF YOUNG'S MODULUS E ESTIMATED FROM THE IMMEDIATE VERTICAL STRAINS MEASURED BENEATH THE CENTRE OF THE TANK AT MAXIMUM LOAD FOR TWO LOADING CYCLES (POISSON'S RATIO ASSUMED EQUAL TO 0.1)(AFTER WARD ET AL. (1968)) AND SIMILAR VALUES OBTAINED BY A REANALYSIS OF THE SAME DATE USING BOUSSINESQ'S SOLUTION WITH POISSON'S RATIOS OF 0.1 AND 0.25

Level	Average depth below tank (m)	Chalk grade	Loading	Immediate vertical strain ε_o(%)	Young's modulus E (kg/sq.cm)	$\frac{\sigma_v-0.2\sigma_h}{\varepsilon_o}$ (kg/sq.cm)	$\frac{\sigma_v-0.5\sigma_h}{\varepsilon_o}$ (kg/sq.cm)
0 - 1	1.91	V	1st	0.04500	3700	3723	3018
			2nd	0.03650	4600	4590	3720
1 - 2	5.57	IV-III	1st	0.00877	16900	17523	16286
			2nd	0.00929	15900	16542	15252
2 - 3	9.13	III	1st	0.00715*	16600	16579	16021
			2nd	0.00745*	16500	15911	15376
3 - 4	12.76	III-II	1st	0.00381	22200	22499	22193
			2nd	0.00402	21100	21324	21034
4 - 5	18.59	II	1st	0.00117	43700	44252	44257
			2nd	0.00127	40200	40768	40773
5 - 6	25.77	II	1st	0.00065*	47000	46954	47271
			2nd	0.00070*	43600	43600	43894

* Adjusted to eliminate influence of marl seam.

σ_v and σ_h are the vertical and horizontal stresses respectively.

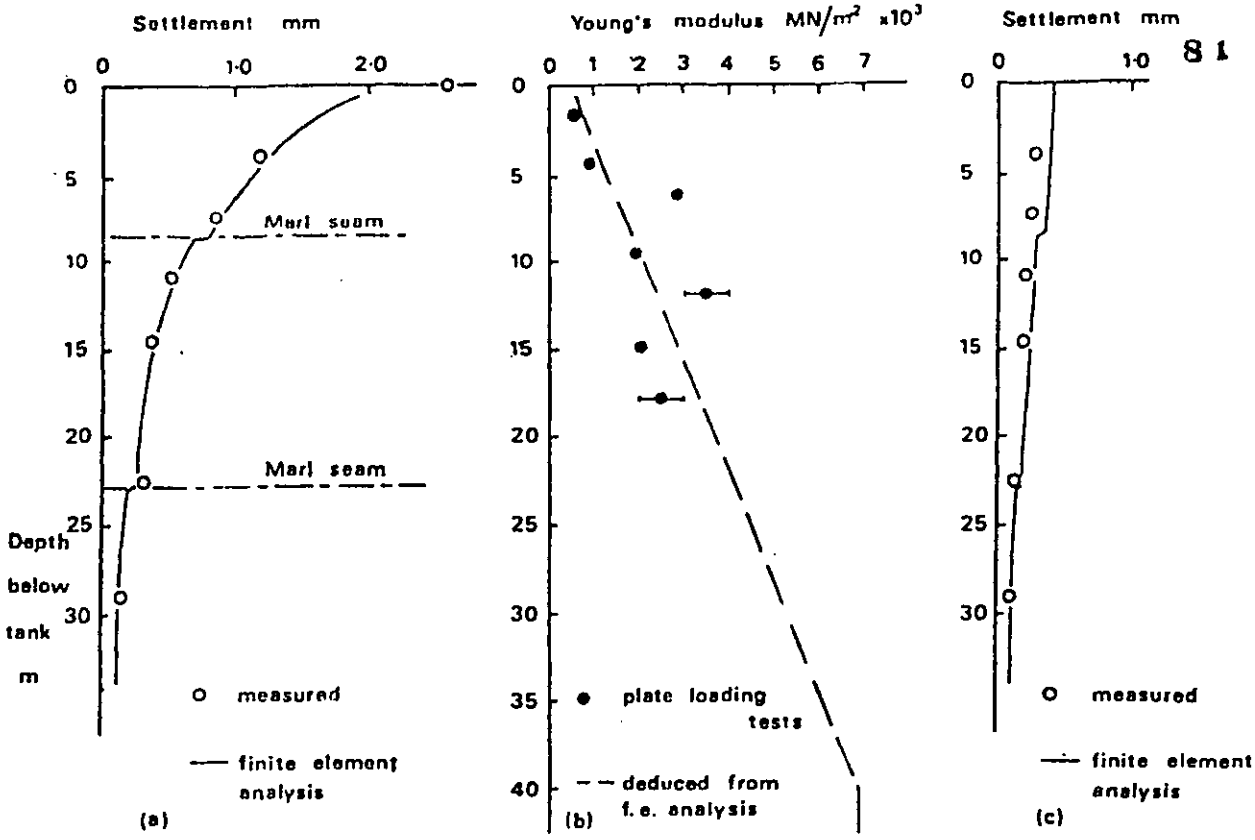


FIG. 3.4.1: RESULTS OF FINITE ELEMENT ANALYSIS (a) FINITE ELEMENT RESULTS FITTED TO OBSERVED CENTRE LINE SETTLEMENTS (b) COMPARISON BETWEEN MEASURED AND DEDUCED E VALUES (c) COMPARISON BETWEEN MEASURED AND PREDICTED SETTLEMENTS DOWN SHAFTS AT EDGE OF TANK (BURLAND ET AL. (1973))

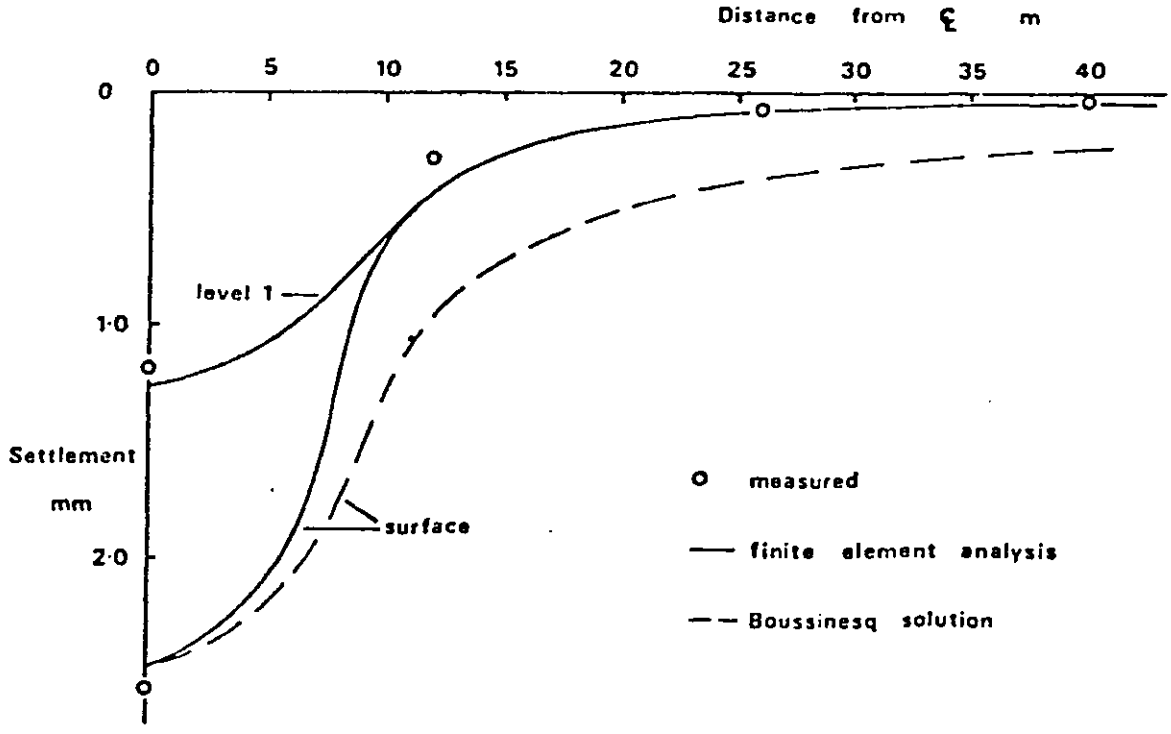


FIG. 3.4.2: COMPARISON OF OBSERVED SETTLEMENT PROFILE OF THE GROUND WITH BOUSSINESQ PREDICTION (SHOWN DOTTED) AND THE FINITE ELEMENT PREDICTION (BURLAND ET AL.(1973))

on intact specimens of Grade II chalk. Results from the compression tests also influenced the choice of 0.24 for Poisson's ratio.

Using this model Burland et al. (1973)also calculated horizontal displacements of the wall of a shaft at the edge of the tank. They obtained movements of 0.038 mm away from the tank at level 3 and 0.069 mm towards the tank at the top of the shaft.

An analysis of the data from the plate loading tests was made by Burland and Lord (1969). They used the classical equation relating Young's modulus for an elastic foundation to the surface deformation caused by a rigid punch. Rates of change of average load with settlement were taken from the plate-loading test curves. Poisson's ratio was assumed to be 0.24. The results are shown on Fig.3.3.2(b).

Burland and Lord (1969) drew attention to significant differences between the model and reality and attached important qualifications to their use of the classical equation. The reader is referred to Burland and Lord (1969) for the full account of their criticism. A depth correction factor for the classical equation was discussed in detail by Burland (1969) and (1978). He obtained values for the factor over a range of depth and Poisson's ratios from an elastic analysis based on the Finite Element Method. In a section dealing with the pressure settlement curves from all the plate loading tests at Mundford, Burland et al. (1973) declared how they had obtained their results as follows:

> " The value of Young's modulus E for each test was determined from the well known expression for a rigid punch of a diameter D:

$$E = \frac{q}{\rho} \frac{\pi}{4} D (1-\nu^2) \times I_D$$

Where q is the average pressure,

ρ is the settlement

and I_D is the depth correction factor."

Burland et al. (1973) considered that the different values for Young's modulus at the various depth shown in Fig.3.4.1(b) were comparable and consistent. In their view the choice of 0.24 for Poisson's ratio was sound because of the degree of agreement found between the model predictions and the displacements observed during the large scale tank test. The values of the coefficient of volume compressibility deduced from the model for the upper and lower marl seams were 0.0114 m^2/MN and 0.0183 m^2/MN respectively. Burland et al. (1973) also claimed excellent agreement with the observed settlements down shafts at the edge of the tank (Fig.3.4.1(c)) and between the deflected shapes of both the ground surface and level 1 underneath and around the test tank (Fig.3.4.2).

It is noted that in the analysis using Finite Element Methods made by Burland et al. (1973) over 800 relatively inefficient three-noded constant strain elements were employed. Their model also required the arbitrary specification of internal boundaries and boundary conditions.

5. New Analysis using BIEM

A similar approach to that of Burland et al. (1973) was made by the Author using Watson's program for three-dimensional elastostatic analysis by the Boundary Integral Equation Method. In this analysis, however, the model was developed to represent the results of both the tank test and the plate-loading test. The program allows connected, compatible, finite and infinite subregions of any reasonable shape to be specified which are composed of homogeneous, isotropic, linear elastic materials.

It was thought that a stack of four subregions, three of finite thickness and one of infinite thickness, would provide the necessary scope for an acceptable and economic representation of the ground. The identification numbers used for these subregions are 50, 100, 150 and 200, as shown in Fig. 3.5.1. The subregions were defined by four horizontal planes at and below the surface. Appropriate values of Young's modulus were specified for each subregion to represent an increasing stiffness with depth. This arrangement will be referred to as the stack model.

The network of surface elements shown on the plans and elevation on Figs. 3.5.2 to 3.5.5 inclusive is typical of that used in the stack models. The planes were defined by a combination of finite and infinite boundary elements generally arranged in a symmetric pattern around the centre lines of the test tank and the vertical shaft. The shaft itself was defined by cylindrical elements along its axes and by plane end elements. Parabolic variation in shape and traction over the elements can be represented by the program in the particular mode

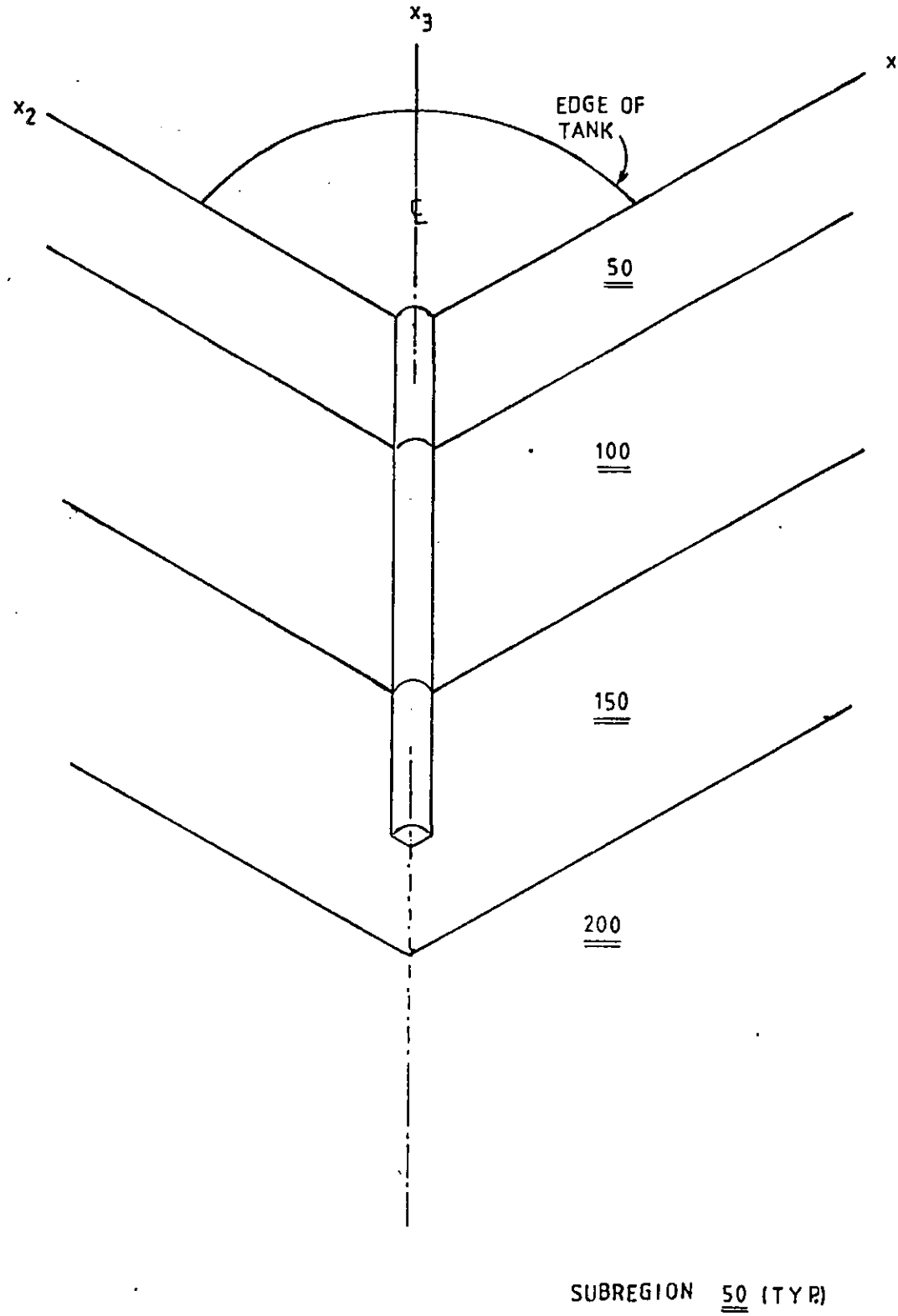


FIG. 3.5.1: ISOMETRIC SKETCH OF THE MUNDFORD SITE STACK MODEL

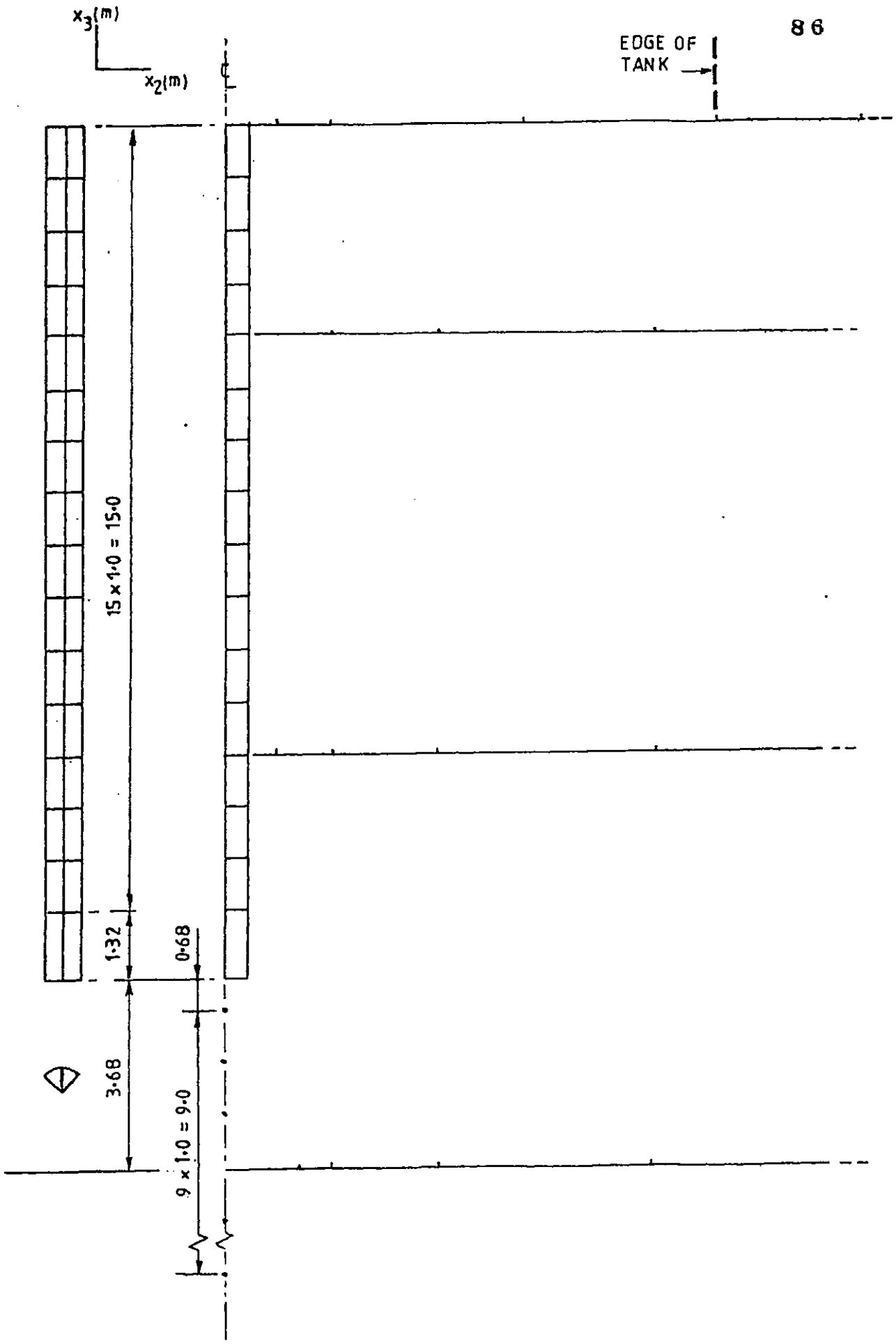


FIG. 3.5.2: VERTICAL SECTION THROUGH THE MUNDFORD SITE STACK MODEL SHOWING BOUNDARY ELEMENT DIMENSIONS

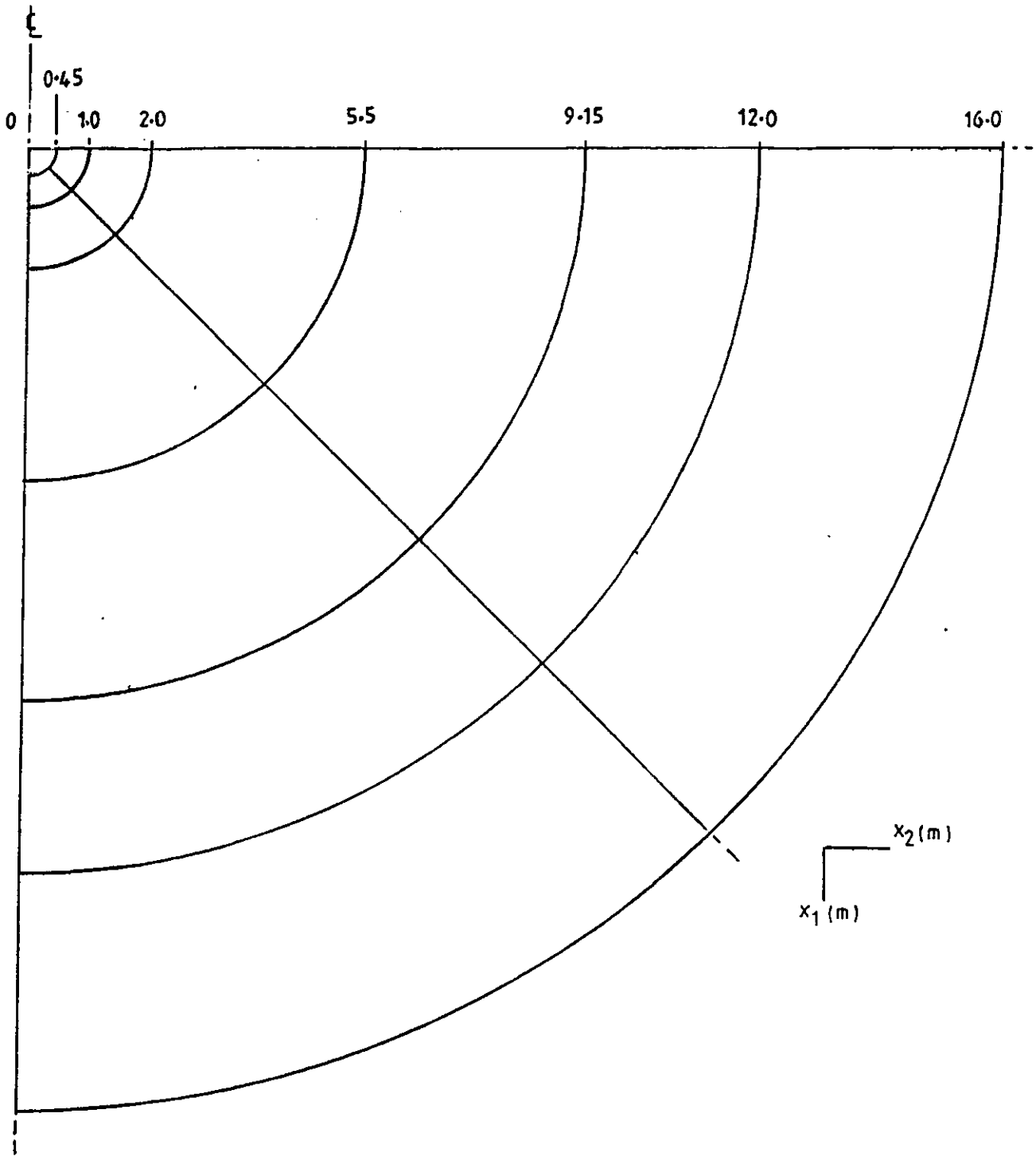


FIG. 3.5.3: PLAN ON THE MUNDFORD SITE STACK MODEL ON THE TOP SURFACE OF SUBREGION 50 SHOWING BOUNDARY ELEMENT DIMENSIONS

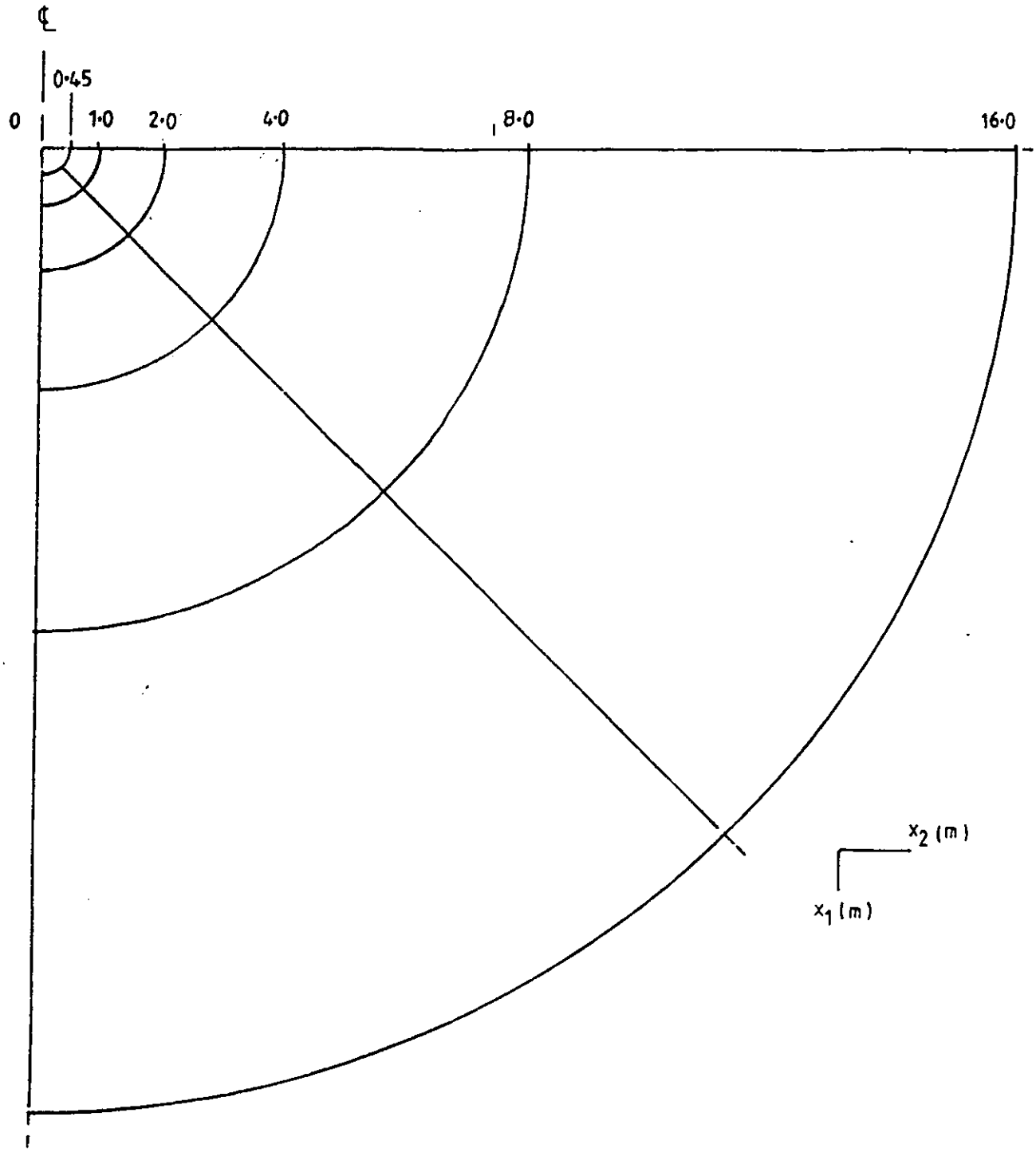


FIG. 3.5.4: PLAN ON THE MUNDFORD SITE STACK MODEL ON THE TOP SURFACES OF SUBREGIONS 100 AND 150 SHOWING BOUNDARY ELEMENT DIMENSIONS

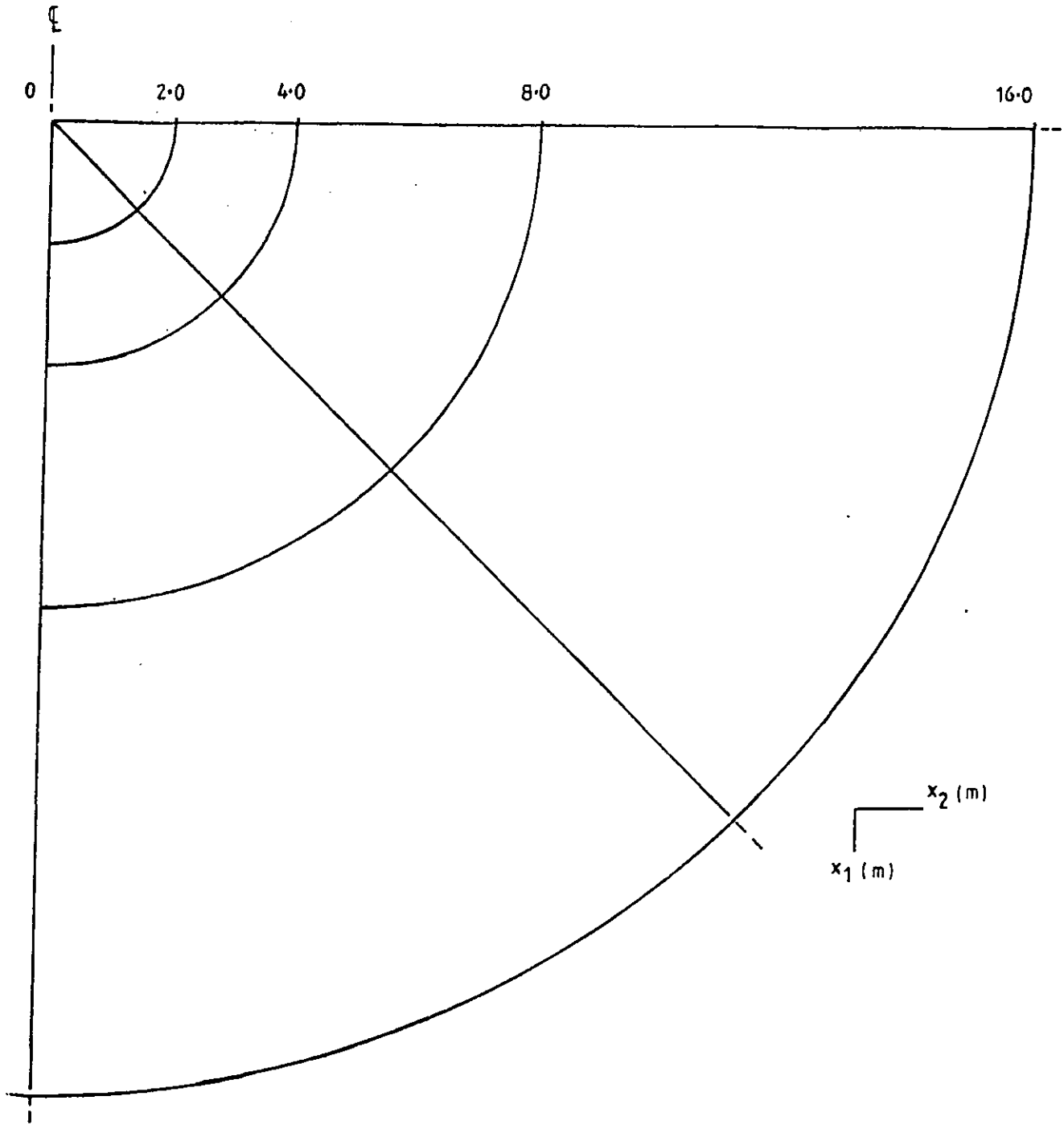


FIG. 3.5.5: PLAN ON THE MUNDFORD SITE STACK MODEL ON THE TOP SURFACE OF SUBREGION 200 SHOWING BOUNDARY ELEMENT DIMENSIONS

selected for this model. Consequently in the choice of the size, shape and distribution of the elements due consideration was given to their expected curvatures after loading. Convenience in the representation of the applied loading was also taken into account. Except where noted otherwise the applied loading was assumed to be uniform pressure.

As a working rule an upper limit of 90° for the angle subtended at any node of an element by any other element was adhered to. Observance of this rule helped to contain within acceptable limits any inaccuracies in the numerical integration calculations. Long thin finite elements were avoided for the same reason. The ratio of their extreme overall dimensions was usually kept well below 10.

Techniques for efficient numbering of nodes and elements and the related preparation and specification for such a network are described in Appendix A 3.5. The simple and easy way in which the levels of the planes defining subregions can be changed is also explained there. In this analysis, however, no variation was made in these levels because the match achieved with the observed behaviour and with the changes of material was sufficiently close.

Guided by the description of the ground profile given by Ward et al. (1968) and, for the first attempt, by their estimates for Young's modulus at the different levels (Fig. 3.3.2), a series of six sets of elastic constants were tried in the model. Each computer run took approximately 200 seconds to complete and consumed 60 units on the ULCC system using the CDC 7600 machine. The initial set of values of elastic constants used comprised basically the weighted averages of the values of

Young's modulus E and the depth Δz over which they obtained. A small reduction was made in certain cases for the discontinuity in modular values between successive zones, e.g. in computing the weighted average for the second zone the first term was reduced by 10%, i.e.(0.9 x 1.56), giving the following calculation for Young's modulus for the model:

$$(\Sigma E.\Delta z) / (\Sigma \Delta z)$$

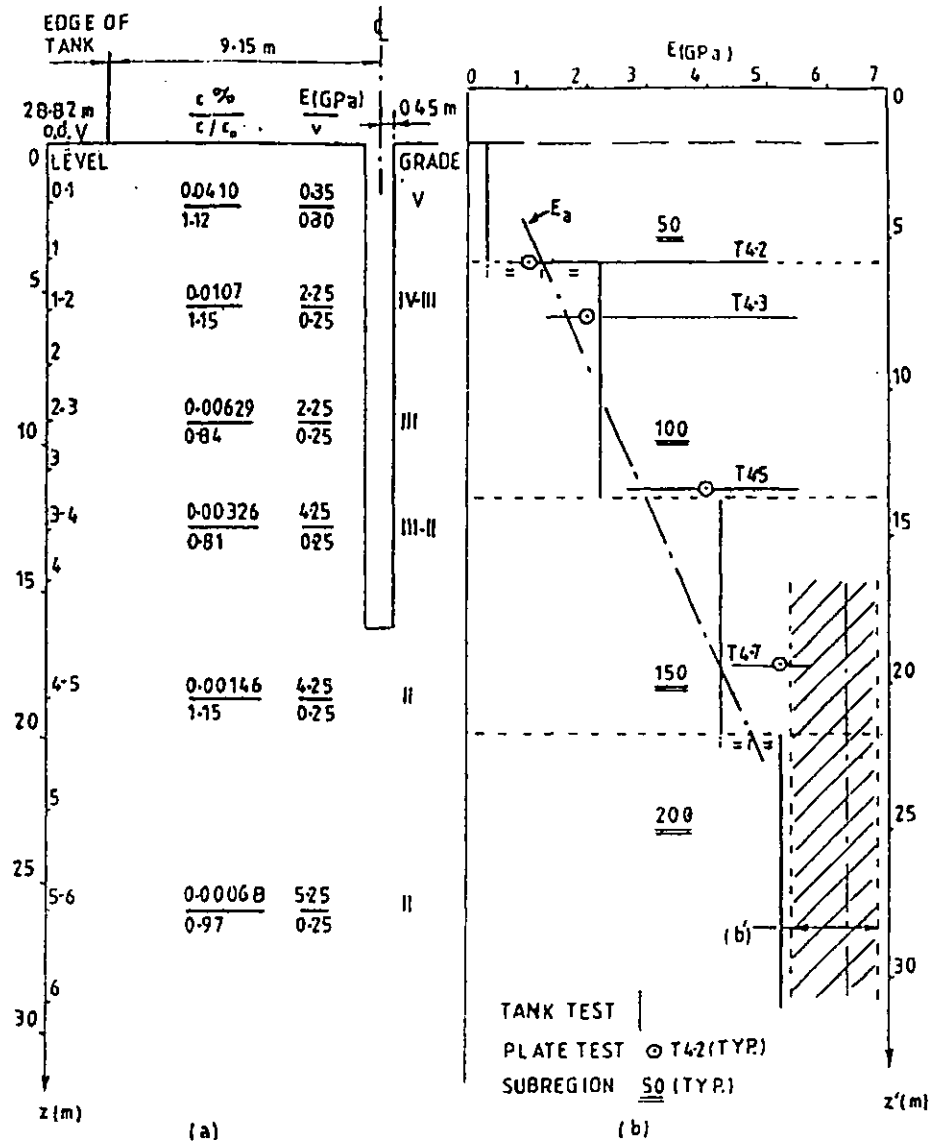
$$= \frac{(0.9 \times 1.56) \times 3.32 + 1.62 \times 3.61 + 2.08 \times 1.07}{3.32 + 3.61 + 1.07} \simeq 1.59 \text{ GPa}$$

Proceeding in this way the initial set of representative values of Young's modulus E for the model was obtained as given below.

Depth below tank (metres)	0 - 4	4 - 12	12 - 20	> 20
Young's modulus (GPa)	0.45	1.59	3.31	4.29

Successive values were chosen so as to progressively reduce the difference betweeen the vertical strains based on field observations given by Ward et al. (1968) and those obtained from the model . Mainly on precedent Poisson's ratio was fixed at 0.25 except for the upper subregion which in later trials was increased to 0.3. The increase was made to allow for the presence of pasty chalk near the ground surface. It is noted that these values did not deviate far from the average value of Poisson's ratio obtained by Burland and Lord (1969) for intact specimens of grade II chalk in laboratory compression tests.

The results for the best match which was obtained are shown in Fig. 3.5.6. In the column giving the ratios of model to field vertical strains $\varepsilon/\varepsilon_o$, it can be seen that all the model values are within $\pm$ 20% of those developed in the field at the end of the second loading cycle. A typical example of the computer output is shown in Fig.3.5.7.



Notes:

ε_0 2nd loading (see Fig. 3.3.2(a))
(b') Range of laboratory values
z Average depth below tank
z' Depth below ground surface

FIG. 3.5.6: (a) SECTION BENEATH TANK SHOWING GRADES OF CHALK AT VARIOUS DEPTHS WITH VALUES OF IMMEDIATE VERTICAL STRAIN ε FOR THE TANK TEST DERIVED FROM THE MUNDFORD SITE STACK MODEL FOR THE SET OF VALUES OF YOUNG'S MODULUS E AND POISSON'S RATIO ν SHOWN. (b) COMPARISON OF AVERAGE VALUES OF YOUNG'S MODULUS E_a FOR THE TANK TEST WITH ASSOCIATED AVERAGE VALUES FOR PLATE TESTS DERIVED FROM THE MUNDFORD SITE STACK MODEL

FULL-SCALE TEST-TANK AT MUNDFORD
TEST-TANK FULL OF WATER WITH NO RADIAL FORCE ON INTERFACE

DISPLACEMENT AND STRESS AT NODES SUBREGION 50 * INDICATES INTERIOR NODE

NODE	DISPLACEMENT U1 U2 U3	STRESS TENSOR 11 12 13 22 23 33	PRINCIPAL STRESSES, AND DIRECTION COSINES OF PRINCIPAL DIRECTIONS				VON MISES AND TRESCA CRITERIA	NODE
1	0.	-3.20E+02 0. 0.	4.11E+01	0.00	1.00	-.00	3.29E+02	1
	-2.592E-04	4.11E+01 -2.45E-03	-2.42E+02	0.00	.00	1.00	1.80E+02	
	-2.245E-03	-2.42E+02	-3.20E+02	1.00	0.00	0.00		
2	-9.927E-05	-2.68E+02 1.27E+02 2.97E-09	3.75E+01	.38	.92	.00	3.26E+02	2
	-2.397E-04	-1.50E+01 -1.23E-09	-2.42E+02	.00	-.00	1.00	1.79E+02	
	-2.245E-03	-2.42E+02	-3.21E+02	.92	-.38	-.00		
3	-1.833E-04	-1.39E+02 1.80E+02 -1.73E-03	4.11E+01	.71	.71	-.00	3.29E+02	3
	-1.833E-04	-1.39E+02 -1.73E-03	-2.42E+02	.00	.00	1.00	1.80E+02	
	-2.245E-03	-2.42E+02	-3.20E+02	.71	-.71	.00		
4	-2.397E-04	-1.50E+01 1.27E+02 -1.62E-09	3.75E+01	.92	.38	.00	3.26E+02	4
	-9.927E-05	-2.68E+02 3.92E-09	-2.42E+02	-.00	.00	1.00	1.79E+02	
	-2.245E-03	-2.42E+02	-3.21E+02	.38	-.92	.00		
5	-2.592E-04	4.11E+01 0. -2.45E-03	4.11E+01	1.00	0.00	-.00	3.29E+02	5
	0.	-3.20E+02 0.	-2.42E+02	.00	0.00	1.00	1.80E+02	
	-2.245E-03	-2.42E+02	-3.20E+02	0.00	-1.00	0.00		
6	0.	-2.31E+02 0. 0.	-4.56E-02	0.00	1.00	-.00	2.36E+02	6
	-1.515E-04	-4.56E-02 -2.73E-04	-2.31E+02	1.00	0.00	0.00	1.20E+02	
	-2.039E-03	-2.41E+02	-2.41E+02	0.00	-.00	-1.00		
8	-1.071E-04	-1.15E+02 1.15E+02 -1.93E-04	-4.56E-02	.71	.71	-.00	2.36E+02	8
	-1.071E-04	-1.15E+02 -1.93E-04	-2.31E+02	.71	-.71	-.00	1.20E+02	
	-2.039E-03	-2.41E+02	-2.41E+02	-.00	-.00	-1.00		
10	-1.515E-04	-4.56E-02 0. -2.73E-04	-4.56E-02	1.00	0.00	-.00	2.36E+02	10
	0.	-2.31E+02 0.	-2.31E+02	0.00	1.00	0.00	1.20E+02	
	-2.039E-03	-2.41E+02	-2.41E+02	.00	0.00	1.00		
11	0.	-2.00E+02 0. 0.	-3.97E-02	0.00	1.00	.00	2.02E+02	11
	-1.388E-04	-3.97E-02 2.92E-03	-2.00E+02	1.00	0.00	0.00	1.02E+02	
	-1.864E-03	-2.04E+02	-2.04E+02	0.00	.00	-1.00		

FIG. 3.5.7: EXAMPLE OF COMPUTER OUTPUT FOR TANK TEST DERIVED FROM THE MUNDFORD SITE STACK MODEL

The observed vertical settlements at shaft S1 given in Table 3.3.2 are well represented by the model as shown in Fig. 3.5.8(a) in which they are denoted by the letter w, when a simple correction is made for the compression of the two marl seams underlying the test area. The marl seams are about 6.4 cm and 10 cm thick and extend roughly horizontally at depths of 8.4 m and 22.9 m respectively below the tank. The amounts of compression have been calculated as follows:

At 8.4m : $0.0114 \times 6.4 \times 0.15 = 0.011$ cm

At 22.9m : $0.0183 \times 10.0 \times 0.4 = 0.007$ cm

where the magnitudes of the normal traction were obtained from the model and the values of the volume compressibility are the same as those used by Burland et al. (1973). No attempt has been made to eliminate the accumulated total correction of 0.018 cm from the measured value of 0.258 cm vertical settlement at the top of the shaft.

The observed values and the model values for vertical settlement w in Shaft S2 are plotted in Fig. 3.5.8(b). The model values are seen to be almost double those observed at the deepest point but the ratio reduces steadily to about 1.3 at a depth approximately 5 m below the ground surface. The compression of the marl seams at Shaft S2 was calculated in a similar way to that described above for Shaft S1. Variations in model settlements along several horizontals at different depths below the test tank are shown in Fig. 3.5.9. It has not been found possible to accommodate the field measurements reported by Burland et al. (1973) of a relative vertical movement of 0.94 mm in Shaft S2 between the top and level 3 during unloading. This value seems to imply an immediate surface movement considerably at variance with complete elastic recovery.

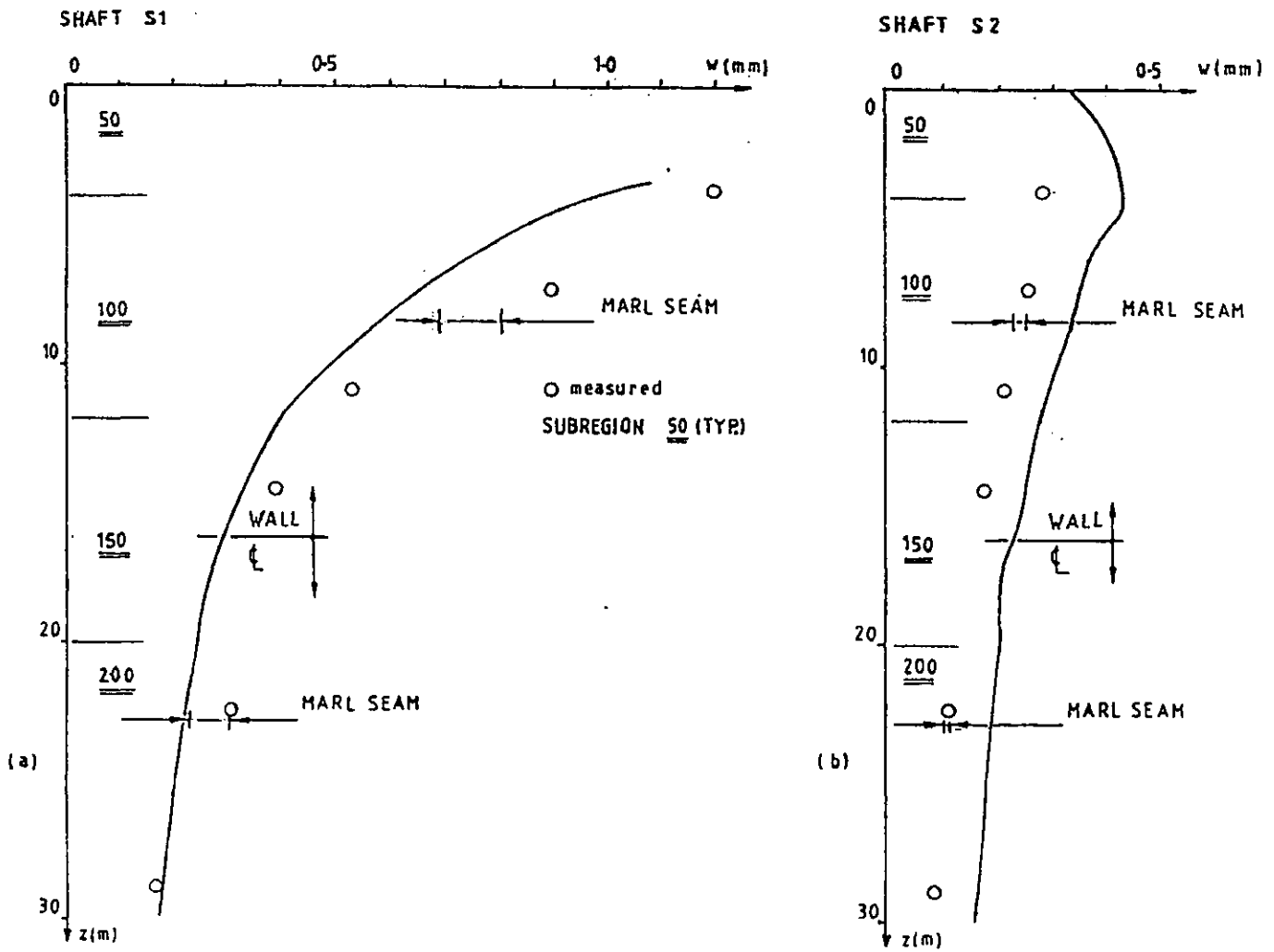


FIG. 3.5.8: COMPARISON BETWEEN MEASURED AND PREDICTED SETTLEMENTS FOR THE TANK TEST DERIVED FROM THE MUNDFORD SITE STACK MODEL DOWN SHAFTS AT (a) THE CENTRE AND (b) THE EDGE OF THE TANK

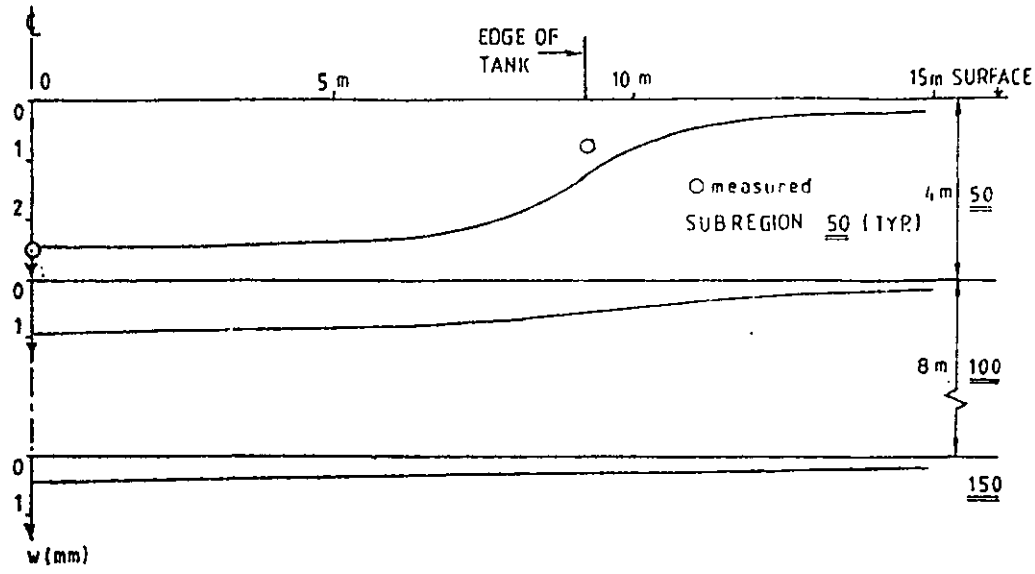


FIG. 3.5.9: PREDICTED SETTLEMENT PROFILES OF THE GROUND FOR THE TANK TEST DERIVED FROM THE MUNDFORD SITE STACK MODEL AND COMPARISON WITH OBSERVED VALUES AT THE SURFACE

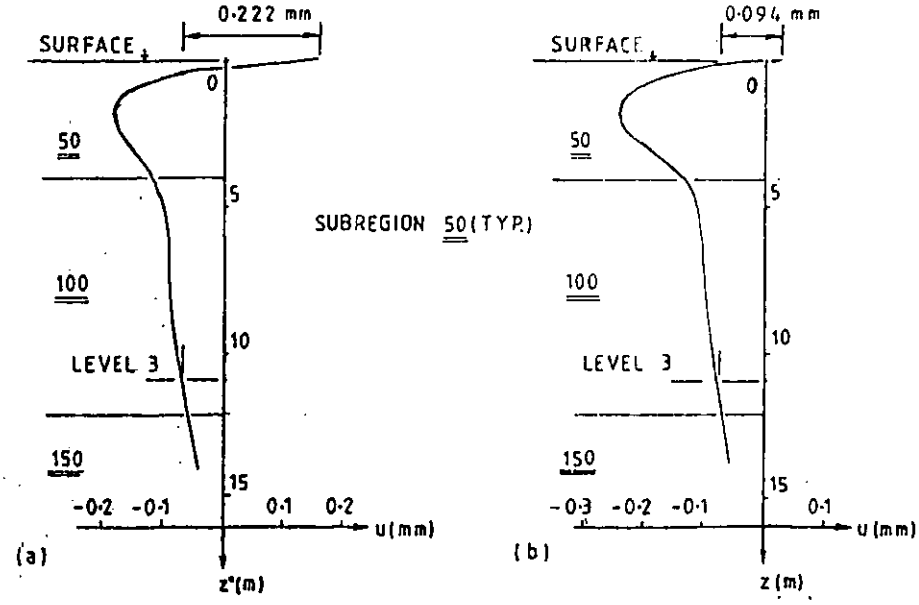


FIG. 3.5.10: PREDICTED LATERAL MOVEMENT PROFILES FOR THE TANK TEST DERIVED FROM THE MUNDFORD SITE STACK MODEL DOWN SHAFTS AT THE EDGE OF TANK ASSUMING (a) UNIFORM PRESSURE AND (b) NO RADIAL MOVEMENT ON THE CONTACT SURFACE BETWEEN TANK AND GROUND

In all the cases studied above it was assumed that in the model the tank loading was applied to the ground as a uniform pressure. An alternative tank loading was considered where in addition to uniform pressure all radial movements on the contact surface were prevented. The results for a uniform pressure only were found to differ very slightly from the alternative tank loading.

There was a large difference, however, between the horizontal deformations u of the wall of Shaft S2 near the surface due to the two different loading conditions. Values at points on a vertical line nearest the tank on the wall of the shaft are plotted on Figs. 3.5.10(a) and (b) respectively. The model values of 0.222mm and 0.094mm for relative horizontal movement between the top of the shaft and level 3 for the two loading conditions bracket the field value of 0.134mm. Whilst in the absence of further information the amount of horizontal restraint exerted on the chalk by the test tank must remain unknown it is thought that the two loading cases represent its extremes.

The adequacy of the particular stack model to represent the response of the ground during the plate tests was investigated in the following way. In Table 3.5.1 estimates are given of the vertical pressure p in the ground below the test tank at the same elevation as the plate tests assuming a unit weight density of 20 kN/m^3 for the chalk. The increases in pressure Δp induced during the tank test along its axis at these levels were taken from the previous computer analysis. These values were used to define chords to the relevant pressure settlement curves for the plate test shown in Figs. 3.5.11 and 12. The slope of each chord represents approximately the constant of proportionality over the pressure increment. Assuming a notional increment of 1000 kN/m^2 for

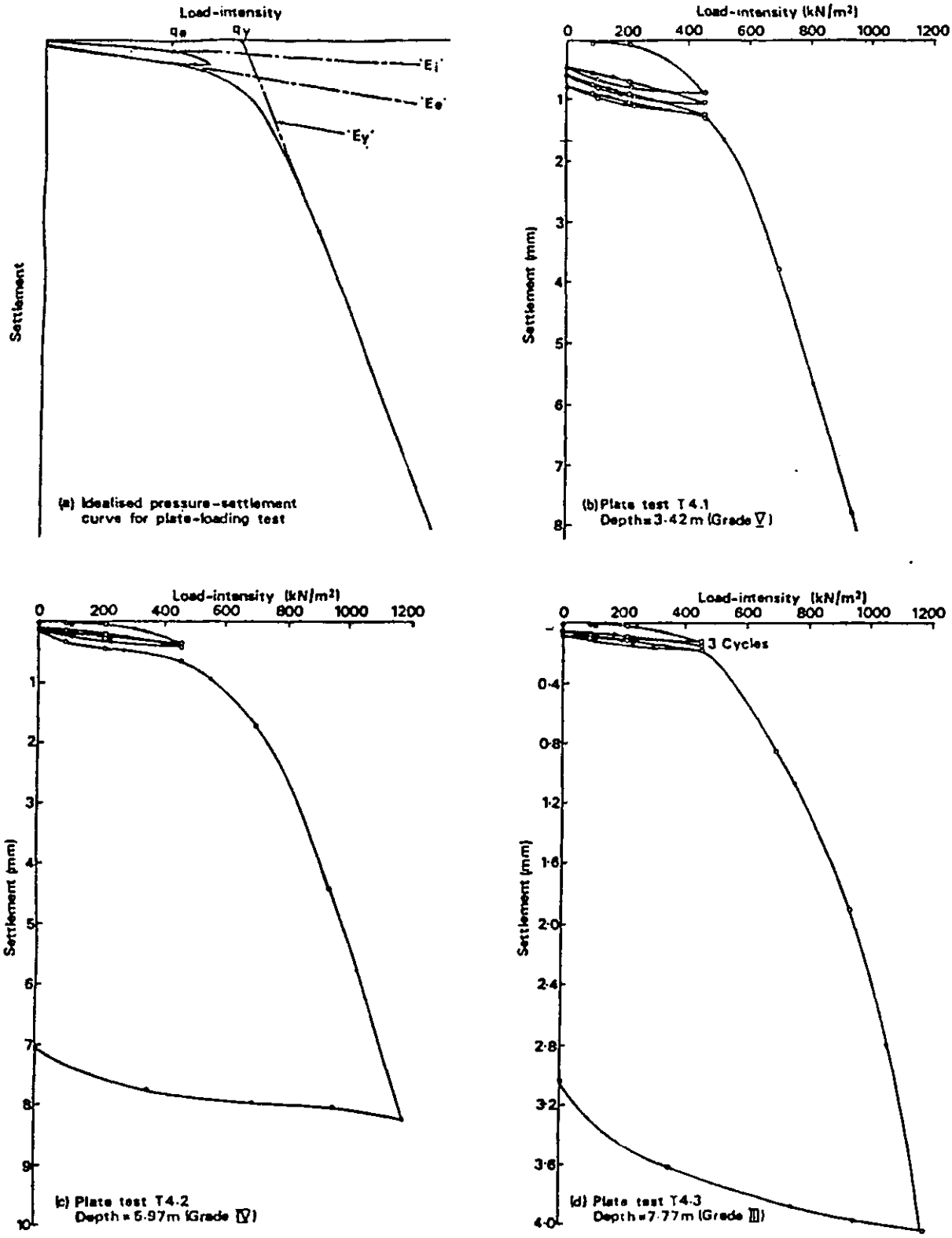


FIG. 3.5.11: IDEALIZED PRESSURE-SETTLEMENT CURVE AND TYPICAL PLATE-TEST RESULT FOR GRADE V, IV, AND III CHALK (AFTER BURLAND AND LORD (1969))

convenience, it was possible to calculate the settlement δ_o which would have occurred in the ground had its response remained constant. The corresponding settlement δ for the same configuration was obtained by new computer runs. The plate loading on the ground was assumed to be a uniform pressure and the settlement at its centre was quoted. Effects due to the tension piles and due to any other loads were ignored in addition to the influence of the marl seams.

A typical computational routine for δ_o is reproduced on Fig. 3.5.12 for Test T 4.5. The network of elements for the model used in evaluating δ at the same level is similar to that shown in Figs. 3.5.2 to 5. The esimated values of Young's modulus given in Table 3.5.1 at each of the four levels is the product of the average value of Young's modulus E_a shown in Fig. 3.5.6(b) and the corresponding value of δ/δ_o. A summary of the modular values obtained by use of the model is plotted on Fig. 3.5.6(b).

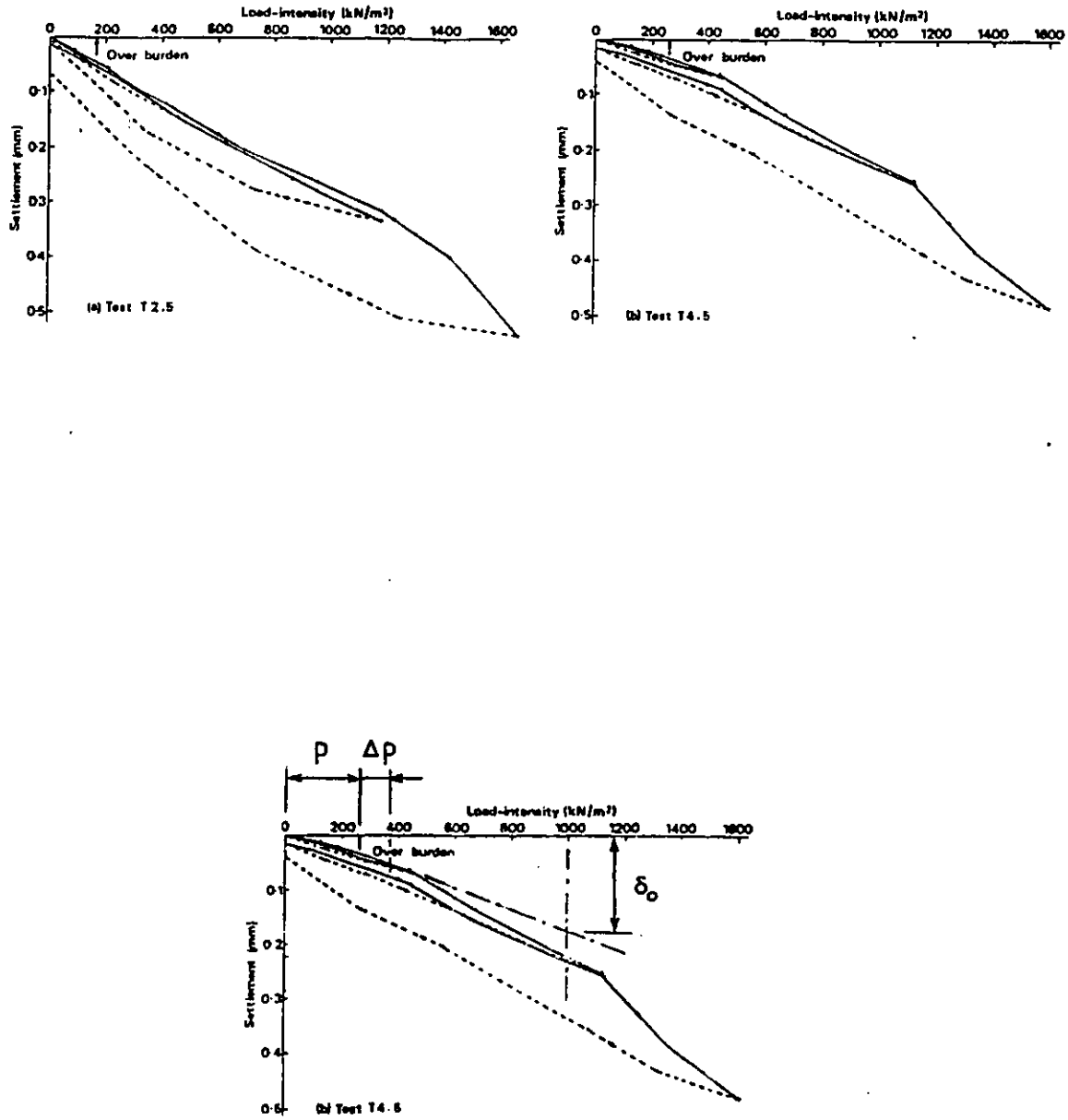


FIG. 3.5.12: TYPICAL PLATE-TEST RESULTS FOR GRADE II CHALK (BURLAND AND LORD (1969)) AND COMPUTATIONAL ROUTINE FOR δ_o DESCRIBED FOR TEST T. 4.5

TABLE 3.5.1 ESTIMATED VALUES OF YOUNG'S MODULUS E AT VARIOUS LEVELS OBTAINED BY THE STACK MODEL USING PLATE TEST RESULTS AS DESCRIBED IN SECTION 5 WHERE THE PARAMETERS USED BELOW ARE ALSO DEFINED

Plate test	Elevation o.d.(m)	p (kPa)	Δp (kPa)	δ_o (mm)	δ (mm)	Young's modulus E (GPa)
T 4.2	24.83	80	170	0.4	0.332	1.08
T 4.3	23.03	115	150	0.25	0.293	2.00
T 4.5	17.23	230	95	0.18	0.245	4.00
T 4.7	11.30	350	55	0.12*	0.148	5.23

* Estimated value

6. The effect of marl seams

The amount by which the marl seams compressed during the tank test was estimated by the simple, but adequate calculations given above. It is suggested, however, that the relatively low modulus of the marl had an additional important but less obvious effect on the deformation. Specifically it is thought that the seams contributed to the pattern of strongly local settlement and recovery in and around the area of the tank test.

In order to explain this idea suppose that a normal line load is applied to the horizontal surface of a homogeneous isotropic half-space. Consider a horizontal plane at some depth beneath the surface. The extent of the normal tractions along it depends upon the induction of shear stress in the space above it. If slip occurs and shear stress is thereby reduced then the extent of the distribution is thereby reduced. It follows that the resulting settlement along any adjacent horizontal plane is concentrated near the line load.

Experimental investigations by Gaziev and Erlikhman (1971) showed that departures of this kind did occur in the stress response of model jointed rock systems. In presenting their results for the case shown in Fig. 3.6.1 the authors added the following comment:

> "For the horizontally stratified foundation when the load is normal to the first set of joints the stress pattern is of a shape stretched in the direction of the loading."

In a theoretical investigation of the elastic response of regularly

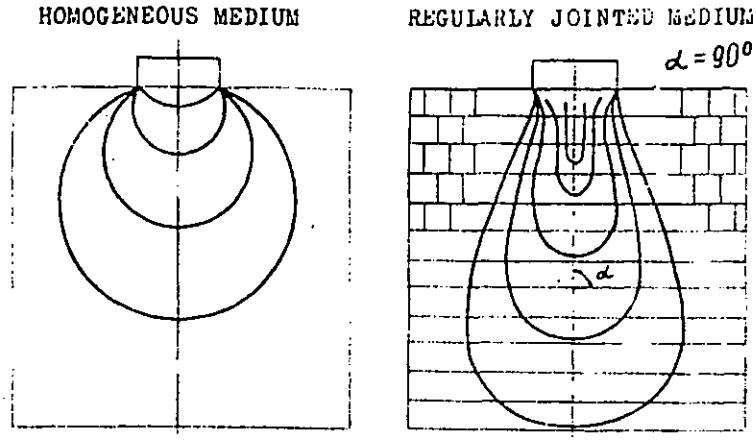


FIG. 3.6.1: EVOLUTION OF A PATTERN OF STRESS DISTRIBUTION IN ROCK ELEMENTS (BLOCKS) OF THE JOINTED MEDIUM DEPENDING ON THE ANGLE OF DIP OF THE LAYERS (GAZIEV AND ERLIKHMAN (1971))

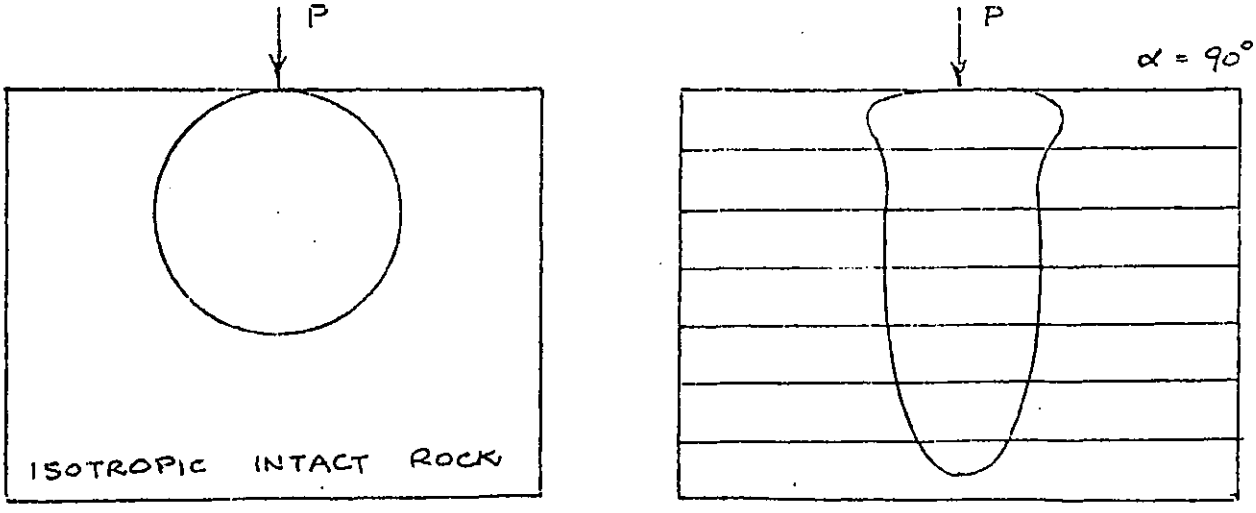


FIG. 3.6.2: ELASTIC RESPONSE OF A MODEL OF REGULARLY JOINTED ROCK TO A LINE LOAD. POLAR DIAGRAM OF $r\sigma_r$ (BRAY (1981))

jointed rock to a line load applied to its surface Bray (1981) found a similar anomalous stress distribution as shown in Fig.3.6.2.

If the Author's hypothesis concerning the concentrating effect of the marl seams is correct, and presupposing an otherwise perfect match of elastic properties, then the model settlements at points sufficiently far away from the centre line would be greater than those observed in the field, notwithstanding any effect due to an increase in Young's modulus with depth. Attention has already been drawn to examples of discrepancies of this kind in the settlements of points at various depths in shafts on the perimeter of the test tank. It should also be noted that, other things being equal, the results of such a mismatch between model and prototype would lead to an underestimate of the value of Young's modulus.

7. General Conclusions

Previous analyses by Ward et al. (1968), Burland and Lord (1969) and Burland et al. (1973) dealt with the large scale tank test and the plate loading test separately, using analytical and Finite Element methods and a range of different mathematical models. The new work is the first analysis using the Boundary Integral Equation Method in which a comprehensive approach has been made by attempting to interpret the tank and the plate tests by one and the same model.

The results obtained by the Author are consistent, reasonable, and comparable despite some unavoidable modelling difficulties. One such difficulty has led indirectly to the suggestion that the influence of the marl seams may have augmented the strong local vertical deformation under the tank. The resources of the three-dimensional elastostatic program have been employed judiciously although plainly uneconomically in the axisymmetric situations. Possible additional routines allowing extensive thin layers to be readily specified and gradual variations of the values of the elastic constants across subregions would be very useful.

In general the stack model performed adequately although incompletely. The degree to which it has been successful supports the choice for the extent and locations of the subregions and for the values of their elastic constants. These constants, of course, do not represent essential or basic properties of the various Grades of chalk, but may well be the best and perhaps the only means available of assessing the in place bulk reponse of the ground materials within the applied loading range. It is asserted that in any future cases significant improvements

in the economic evaluation and use of such constants could be made by the more comprehensive approach possibly using the Boundary Integral Equation Method.

CHAPTER 4 ELASTIC-PLASTIC ANALYSIS OF HORIZONTAL DISPLACEMENT AROUND A DEEP EXCAVATION IN OXFORD CLAY AT SAXON PIT

1. Introduction

A large number of field observations, including many accurate measurements of displacement, were made in the ground surrounding the face of excavation of a 29m deep brickpit, inclined at 72° to the horizontal, during its continual working over a period of three years. The survey was carried out continuously during 1969-71 at the London Brick Company's Saxon pit at Whittlesey near Peterborough, England.

A study of the ground displacement and progressive failure caused by the excavation was made by Burland et al. (1977). In it they observed that as a result of the excavation, the vertical and horizontal pressure was reduced in the surrounding ground and, in particular, this gave rise to inward and vertical movement. They also reported that the soil was overconsolidated, having previously remarked that in such a case the horizontal movements tend to dominate. The main purpose of their study was

> "...to measure the magnitude and extent of the ground movements at Saxon pit and to examine the relative influence of material properties and geological factors on deformation behaviour."

Following an analysis of the field observations, the specific problem emerged of proposing a structure, the behaviour of which would be consistent with the occurrence of certain displacements observed during

the advancing of the face of excavation. Burland et al. (1977) decided upon a structure containing a horizontal shear band positioned near the bottom of the face of excavation of approximately the same length as the depth of the face. Although their solution was not supported by any attempt to simulate the observations by means of rigorous analysis, Burland et al. (1977) strongly encouraged the commissioning of such work.

Apart from a simplified analysis which was not computer based, the Author employed existing computer programs exclusively in his analysis of the proposed structure using mathematical models. In the latter case the analysis was made in two distinct stages. Initially the capacity of the shear band within the structural model to exhibit elastic and plastic displacement was tested for different values of remote horizontal stress. Then the horizontal surface displacements which occurred when the face of excavation was advanced by a typical increment were calculated for a structure containing a shear band of certain critical length at a particular value of remote horizontal stress.

2. Site

Details of the successive faces of excavation at the east end of Saxon pit shown in Figs. 4.2.1 and 4.2.2 were given by Burland et al. (1977). A key plan of the brickpit is inserted in the former and the geological succession is included in the latter. The relationship of the coordinates and elevations to the survey control pillars is given in Burland et al. (1977). At the time of the excavation there was virgin ground to the east and the south. The ground is level towards the east but drops away to the south.

The callow referred to in Fig. 4.2.2 is inferior material overlying the area to a depth of 3 - 6m. It was removed from the site at the beginning of the work. The horizontally bedded clay exposed at the face of excavation is highly overconsolidated and fissured throughout. Near the edge, small angular blocks are formed of less than 10 mm across, increasing to 150 mm at a depth of 13 m. At the base, newly exposed clay shows fissures spaced at more than 300 mm. A residual covering of unworked clay at the base of the brickpit overlies a succession of relatively thin layers of sand, clay, and limestone.

The traces of two orthogonal sets of near vertical major joints are shown on Fig. 4.2.1 by dashed lines. Joints in the set intersecting the excavation face at a low angle were preferentially opened up by stress relief. Only the most prominent joints were seen to extend to the surface. No evidence of faulting was found.

Natural groundwater level is considerably above the bottom of the brick-pit, but continuous drainage has resulted in a drawdown locally.

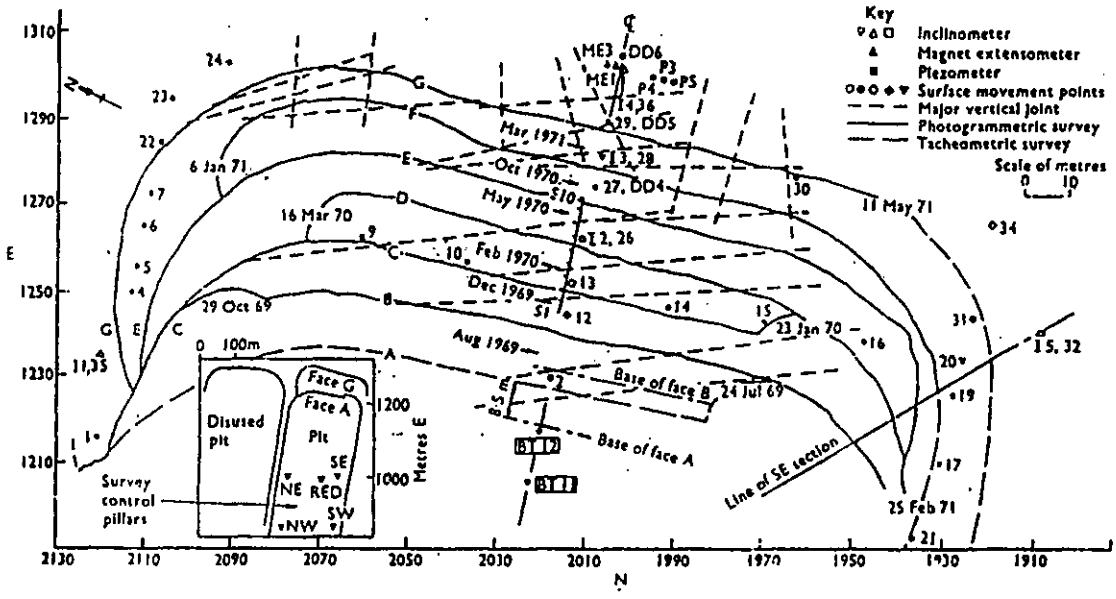


FIG. 4.2.1: PLAN SHOWING SUCCESSIVE FACES OF EXCAVATION, MAJOR JOINTS IN THE OXFORD CLAY AND LAYOUT OF INSTRUMENTATION (BURLAND ET AL. (1977))

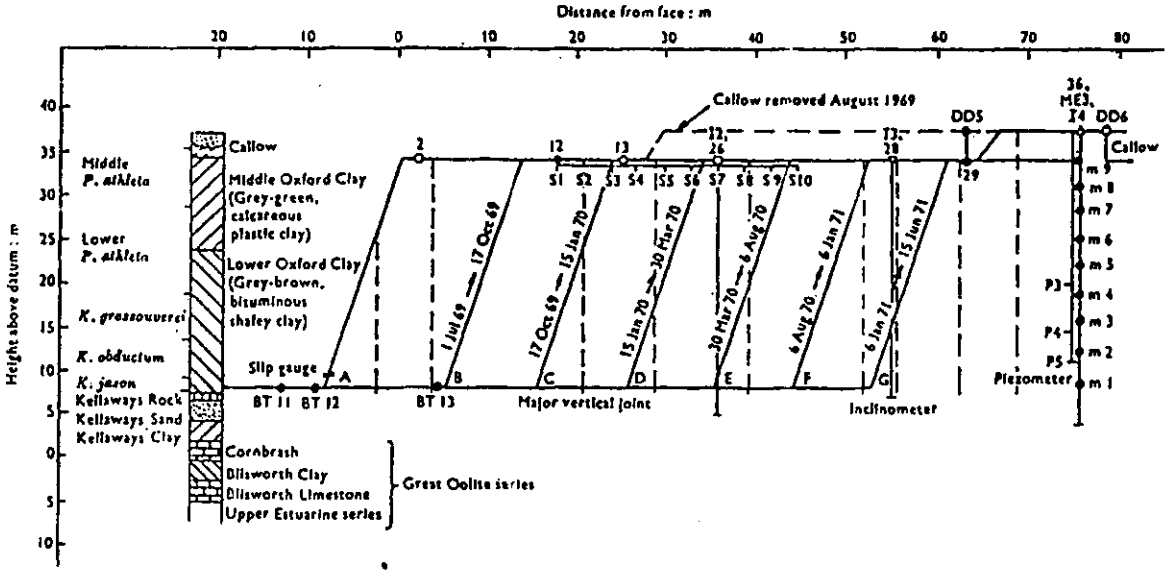


FIG. 4.2.2: CENTRE LINE SECTION NORMAL TO THE FACE SHOWING POSITION OF SUCCESSIVE FACES AND MAJOR JOINTS, GEOLOGY AND INSTRUMENTATION (BURLAND ET AL. (1977))

A steady hydraulic uplift of the base occurring during 1969-70 culminated in a local failure of the base of the brickpit in May 1970 when the accumulated water burst through to the surface appoximately 200 m west of the working face (Burland et al. (1977), Moore and Longworth (1979)).

3. Tests and test results

Field measurements were made of the ground displacements using a variety of instruments and methods. These are described in detail by Burland and Moore (1973) and by Burland et al. (1972). Piezometers were installed in an attempt to measure changes in groundwater pressure as the face of excavation was advanced. The layout of the instrumentation is shown in Fig. 4.2.1. An important composite record is contained in Fig. 4.3.1 of the vector movement of points on the centre line of the face of excavation showing their relationship to the face. Observed variations of the horizontal and vertical displacement of surface points on the centre line with distance from the advancing face are shown in Fig. 4.3.2.

Typical strength results are given in Fig. 4.3.3 for the Lower Oxford Clay sheared parallel to the bedding. The results are based on tests in standard 60 mm square shear boxes. The specimens were trimmed from block samples taken near the bottom of the face of excavation. The brittleness of the material is evidenced by the dramatic fall in strength from the peak values after a few millimetres relative displacement.

Undrained triaxial test results showed that the undrained shear strength and undrained Young's modulus progressively increase with depth. The rate is proportionally greater in the Lower Oxford Clay than in the Middle Oxford Clay. The undrained vertical Young's modulas E_v increases from 20 MN/m^2 to 150 MN/m^2 and the values for horizontally orientated specimens are approximately double. The maximum value of the corresponding factor for the undrained shear strength is 1.7.

The unit weight of the clay is approximately 19.9 kN/m^3.

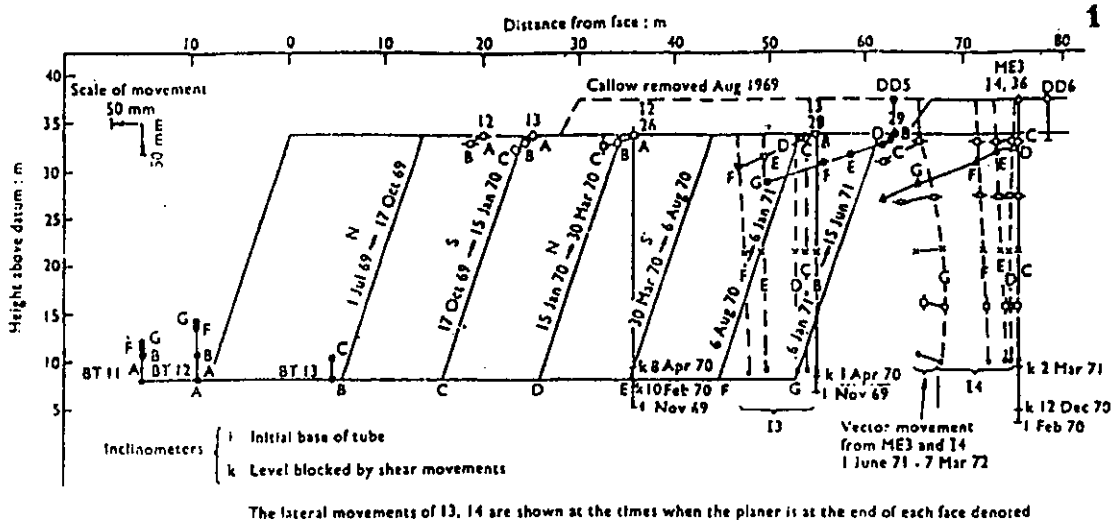


FIG. 4.3.1: VECTOR MOVEMENT OF POINTS ON THE CENTRE LINE OF THE FACE SHOWING RELATIONSHIP TO FACE POSITION (BURLAND ET AL. (1977))

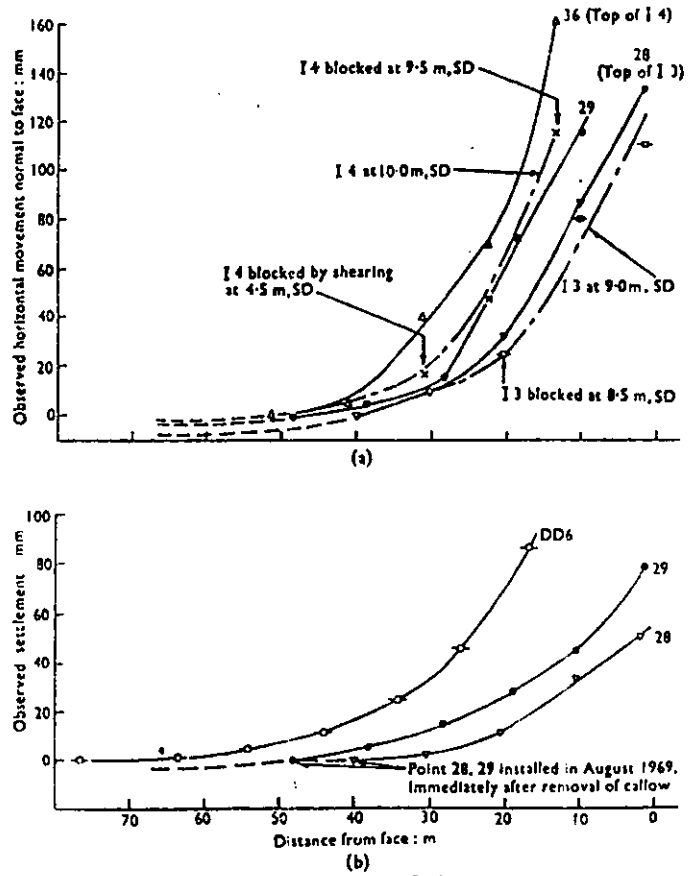


FIG. 4.3.2: OBSERVED VARIATION OF (a) HORIZONTAL DISPLACEMENT, AND (b) SETTLEMENT OF SURFACE POINTS ON THE CENTRE LINE WITH DISTANCE FROM ADVANCING FACE (BURLAND ET AL. (1977))

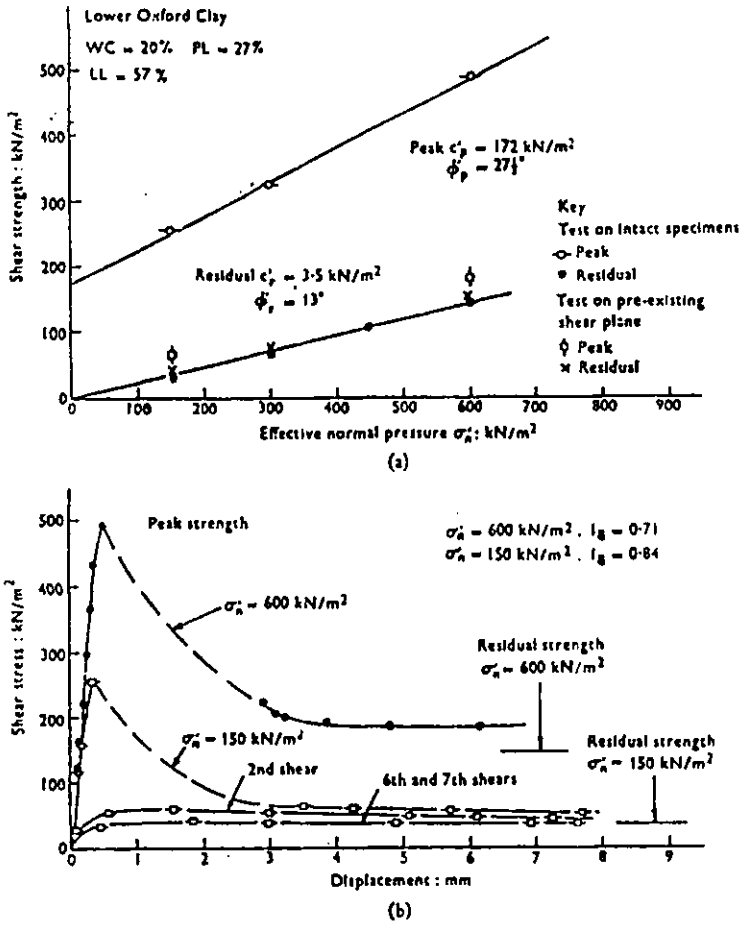


FIG. 4.3.3: TYPICAL SHEAR STRESS-DISPLACEMENT CURVES AND STRENGTH ENVELOPE FOR DIRECT DRAINED SHEAR TESTS ON LOWER OXFORD CLAY SPECIMENS SHEARED PARALLEL TO THE BEDDING (BURLAND ET AL. (1977))

4. Previous Analyses

The interpretation made by Burland et al. (1977) of the horizontal surface strain variation with distance from the advancing face is concisely illustrated in Fig. 4.4.1. The authors stated that the distribution of horizontal strain shown in this figure "is believed to reflect the existence and mode of propagation of a horizontal shear band near the base of the excavation". Burland et al. (1977) calculated that the change in the horizontal strain $\Delta\varepsilon_h$ along the shear band is within the range -0.03% and-0.125% by use of the following expression,

$$\Delta\varepsilon_h = - \frac{\gamma h \tan \phi_r}{E_h} \times \frac{1}{h} \qquad \ldots(4.4.1)$$

where h is the vertical height of the advancing face and l is the length of the shear band. The values of the horizontal Young's modulus E_h was assumed to be between 150 and 300 MN/m^2 and l between 20 and 30 m, with $\phi_r = 13^o$. The authors used the above results merely to confirm that for this case the extension can be expected to be small. It is noted that although Burland et al. (1977) did not state how equation (4.4.1) was established, it is effectively recovered in differential form in the course of the analyis described in Appendix A 4.5 as equation (A 4.5.5).

Estimates of the lengths of the shear band and end region are problematic, however, when based only on indirect and meagre evidence. Lengths of 5-7 m were estimated for the end region based on Fig. 4.4.1(a) and theoretical values of 1-3 m (Palmer and Rice (1973)) were quoted by Burland et al. (1977). The authors also stated that, as the excavation advances, the length of the fully developed shear band can vary significantly. Lengths of at least 30 m, 18 m, and 27 m were mentioned.

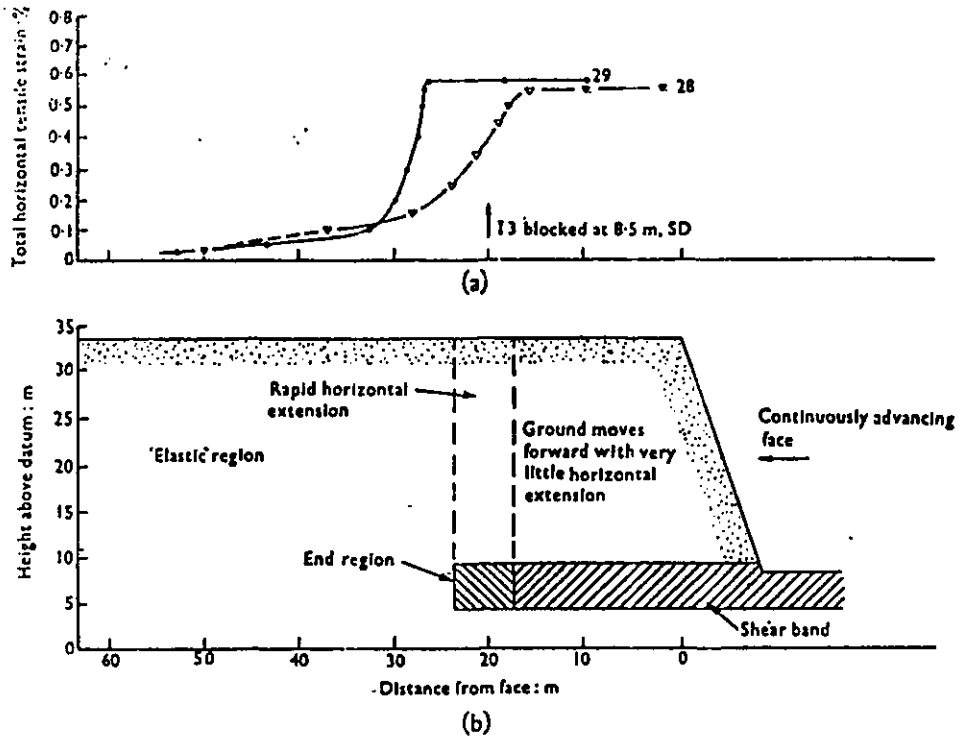


FIG. 4.4.1: (a) VARIATION OF TOTAL HORIZONTAL SURFACE STRAIN WITH DISTANCE FROM ADVANCING FACE (DERIVED FROM FIG. 4.3.2 (a)), (b) INTERPRETATION OF THE SURFACE STRAIN DISTRIBUTION DERIVED FROM THE OBSERVATIONS ON POINT 28 (AFTER BURLAND ET AL. (1977))

Some uncertainty is also acknowledged concerning the propagation of the shear band where, it is thought, movement along its length may be intermittent and variable. This uncertainty is increased by a lack of information about the rate and amount of variation of shear strength between peak and residual strength, the drainage conditions, the position of major joints, and the rate of advancement of the face of excavation.

In a retrospective analysis of the field observations, Moore and Longworth (1979) discussed the question of the contributions to the observed vertical movement of hydraulic uplift and of heave of the base of the brickpit which occurred as a direct response to the reduction of stress accompanying excavation. By a process of reconstruction and making assumption concerning the effect of the outburst they concluded that the non-hydraulic ground heave around the face of the excavation was approximately 30 - 60 mm. If this range of values is correct then it appears that the local hydraulic uplift was of the same order of magnitude immediately prior to the outburst.

5. New analyses

Analytical models requiring the use of computer programs were employed exclusively in the new work described in this section. An account of a simplified analysis which is not computer based is given in Appendix A 4.5 and is briefly discussed at the end of this section. It should be noted that differences in detail occur between the several models used in the various analyses of the problem.

Burland et al. (1977) pointed out that there was considerable scope for analytical modelling of this structure using rigorous analysis and that "Every effort has been made to present the observations in sufficient detail to make this possible". They acknowledged however, that it would have been of particular value to have been able to include "a direct measure of the initial in situ horizontal effective pressures, together with in situ determinations of the horizontal Young's modulus". To overcome the first of these deficiencies the Author assumed a range of remote horizontal pressures and used it in a computer based analysis of the influence of shear bands of various lengths on the behaviour of the structure. The consistency of the behaviour of Burland et al.'s (1977) proposed structure with the field observations of horizontal displacement was tested for a particular value of remote horizontal stress and a shear band of a certain critical length. Vertical movements were not investigated because of the complications introduced by the effects of hydraulic uplift.

Three-dimensional model analysis

A three-dimensional model was initially tried with the corner of the working face and the long plain areas at its base and crest represented as shown in Fig. 4.5.1. The associated computational work was done using Watson's program for three-dimensional elastostatic analysis by the Boundary Integral Equation Method. Two subregions were employed, one for the bank of Oxford Clay and one for the supporting material. The layout of the horizontal elements of the model is shown in Fig. 4.5.2, with the position of the steeply inclined elements indicated by a dashed line. Two rows of rectangular elements of equal depth were used to define the inclined face. The non-horizontal edges of the inclined elements continued the patterns of the adjoining horizontal elements. Provision was made in the element layout for the specification of various horizontal cracks at the bottom of the inclined face. The model is symmetrical about both axes.

The results of preliminary trials showed that each complete computer run would use about 100 units. But since only the loading of the structure was to be changed and not the geometry nor the mechanical properties of the materials, it was planned that the results of the calculations for the unchanging part of the problem would be stored on magnetic tape and reused in the way provided for in Watson's program. The saving possible by this method would be considerably more than half that for complete runs and would have made this approach economically viable. Unfortunately the operation also required an equivalent amount of temporary disk storage which was found to be unavailable on the system at ULCC and so this attempt was abandoned.

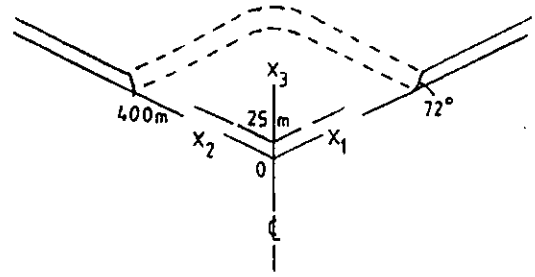


FIG. 4.5.1: ISOMETRIC SKETCH OF SAXON PIT MODEL WITH INFINITELY REMOTE BOUNDARIES FOR THREE-DIMENSIONAL ANALYSIS

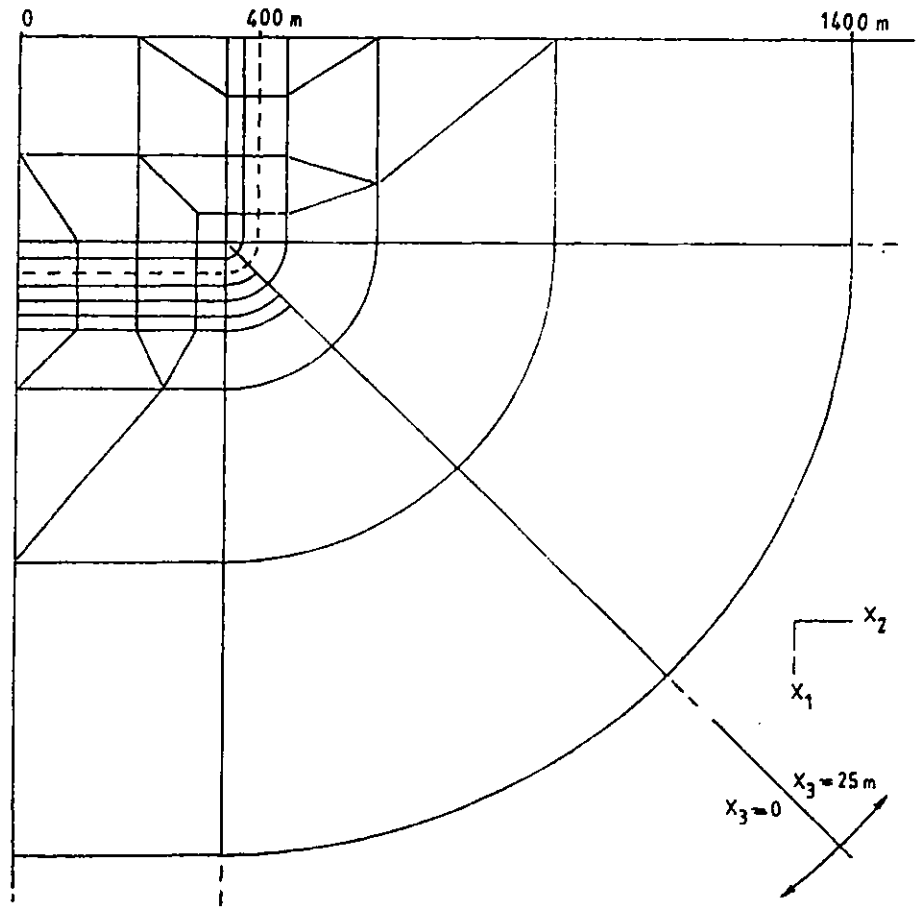


FIG. 4.5.2: PLAN ON SAXON PIT MODEL WITH INFINITELY REMOTE BOUNDARIES FOR THREE-DIMENSIONAL ANALYSIS SHOWING BOUNDARY ELEMENTS

Two-dimensional model analysis

In order to pursue the investigation attention was transferred to the centre section normal to excavation face shown in Fig. 4.3.1 and, assuming plane conditions, an alternative approach was made using a new program written by Watson for two-dimensional elastostatic analysis by the Boundary Integral Equation Method. The program is in most other respects similar to Watson's three-dimensional program, and further general descriptive details are omitted. But the new program, although operative, was not then complete and special analytical methods had to be used to meet the following deficiencies: more than one subregion, field stresses, infinite elements, and infinitely thin cracks could not be specified, and internal stresses and internal displacments could not be calculated.

Following a number of trials, the model shown in Fig. 4.5.3 was chosen in which no normal displacements are permitted along the boundary ABC. The value of Young's modulus is 100 MN/m^2 and Poisson's ratio is 0.25. The unit weight of the material is 19.6 kN/m^3. A normal uniform compressive displacement of 4.8 m is applied to the boundary CD and a linearly varying displacment, of equal magnitude at the point C and vanishing at the point B, is applied to the boundary BC in the direction C to B. This set of boundary conditions is called the standard set of boundary conditions for the particular model. It is assumed to represent the special effect of relatively stiff rock at the base of the structure coupled with a horizontal field stress of a particular magnitude.

The action of the shear band and end region within the structure is modelled by normal and tangential traction, applied to the surface of the gap FGH. In order to keep its width constant, equal and opposite normal loads are applied at certain zones along the gap. The associated tangential loads are determined by assuming that the material exhibits either residual shear strength with $\phi' = 13^{o}$ and $c' = 0$ or peak shear strength with $\phi' = 27\frac{1}{2}^{o}$ and $c' = 172\ kN/m^{2}$. Any effect due to water on the development of shear strength is ignored. The assumed direction of the applied shear tractions on the faces of the gap is such as to oppose overthrusting of the excavated face EF into the brickpit.

Three models with nominal gap lengths 20, 30 and 40 m were tested using the set of standard boundary conditions previously described. These models were also tested with two similar sets of boundary conditions, in which the magnitude of the displacements are reduced separately to 50% and to 10% of those in the set of standard boundary conditions.

By inspecting the values of the resulting horizontal displacements of points on the horizontal faces of the gap, it can be fairly readily assessed whether or not significant relative horizontal displacments occur along it for the particular gap length and assumed set of boundary conditions. The results of this assessment may be interpreted as determining whether or not horizontal plastic shear failure occurs in a structure containing a shear band and end region of a certain length, when the structure is subjected to a horizontal field stress of a particular intensity.

The same analytical method was used for each of the nine calculations made for the different models and sets of boundary conditions. Details of one of these calculations are given below in outline. Two equal enlargements are shown in Fig. 4.5.4(a) and (b) of the area around the nominal 20 m long gap FGH in Fig. 4.5.3 and equally spaced nodes $F, A'_1, A'_2, \ldots, A'_5$ and $H, A_1, A_2, \ldots, A_5$ are sited on the upper and lower faces as shown. Considering only self weight of the structure and the standard boundary conditions applied to the outer boundary, let u_i denote the vertical displacement between A'_i and A_i, where $i = 1, 2, \ldots, 5$. In the real situation, there will be a distribution of traction on the surface of the gap. For simplicity, it is assumed that residual shear strength is exhibited on the upper and lower faces and that the distribution of surface traction is linear between the nodes, as shown in Fig. 4.5.4 (a), where the corresponding normal nodal loadings per unit length are denoted by $f_1, f_2, \ldots, f_5$. The linear distribution is treated as the superposition of simple triangular load systems as illustrated in Fig. 4.5.4 (b). Let $a_{ij}f_j$ be the vertical displacement between A'_i and A_i due to the influence of two equal and opposite triangular loads of maximum intensity f_j, centred over A'_j and A_j respectively, where $j = 1, 2, \ldots, 5$. The resulting vertical displacement between A'_i and A_i due to all the loads is given by the expression

$$a_{i1}f_1 + a_{i2}f_2 + \ldots + a_{i5}f_5 + u_i .$$

Assuming no vertical separation between A'_i and A_i, the above expression equals zero, so that

$$a_{i1}f_1 + a_{i2}f_2 + \ldots + a_{i5}f_5 = - u_i .$$

Considering the displacement of all the nodes, the complete set of equations can be written as the matrix equation

$$[a_{ij}] \{f_j\} = - \{u_i\} .$$

The values of a_{ij} and u_i were determined for all i, j using Watson's two-dimensional boundary element program.

Using the geometry of Fig. 4.5.4 (b), with self weight of the structure and standard boundary conditions applied to the outside boundary shown in Fig. 4.5.3, the following results were obtained, where lengths are in metres and loadings per unit length in MN/m.

$$\begin{bmatrix} 0.508 & 0.354 & 0.249 & 0.158 & 0.057 \\ 0.396 & 0.368 & 0.226 & 0.153 & 0.055 \\ 0.266 & 0.255 & 0.274 & 0.160 & 0.054 \\ 0.182 & 0.169 & 0.174 & 0.194 & 0.064 \\ 0.079 & 0.077 & 0.073 & 0.075 & 0.080 \end{bmatrix} \begin{Bmatrix} f_1 \\ f_2 \\ f_3 \\ f_4 \\ f_5 \end{Bmatrix} = - \begin{Bmatrix} -1.1443 \\ -0.9854 \\ -0.8148 \\ -0.6093 \\ -0.2783 \end{Bmatrix}$$

The solution to this equation is: $f_1 = 1.263$, $f_2 = 0.459$, $f_3 = 0.861$, $f_4 = 0.657$, and $f_5 = 0.384$ MN/m.

When peak strength is assumed to occur on the faces of the gap, additional constant and linearly distributed tangential traction are introduced when calculating the amount of horizontal displacement induced at the nodes. Some degree of error, thought to be small, is therefore incurred by using the values of a_{ij} relevant to the assumption of residual shear strength. On the other hand, when residual strength is exhibited on the faces of the gap, no moment is generated by the simple triangular load systems if the opposing resultant vertical components are staggered by an amount $w \tan 13^\circ$, where w is the width of the gap. By mistake only half this value was specified in the model and, in addition, extra unbalanced moments are introduced when peak strength is assumed to occur. The size of the error introduced by the unbalanced moments is not known, but in the critical calculations it is thought to be tolerable. Arbitrary slight adjustments of the standard loading had to be made immediately adjacent to the roots of the gaps because of their lengths and curved ends. Any error incurred by these changes is probably small.

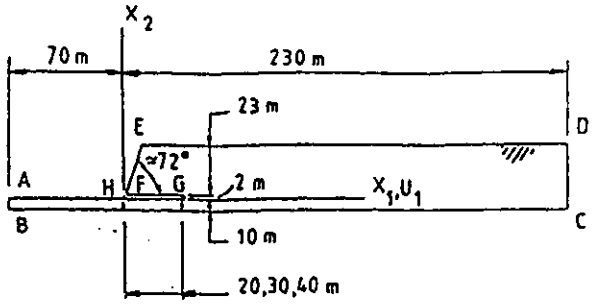


FIG. 4.5.3: SAXON PIT MODEL WITH FINITELY REMOTE BOUNDARIES FOR TWO-DIMENSIONAL ANALYSIS

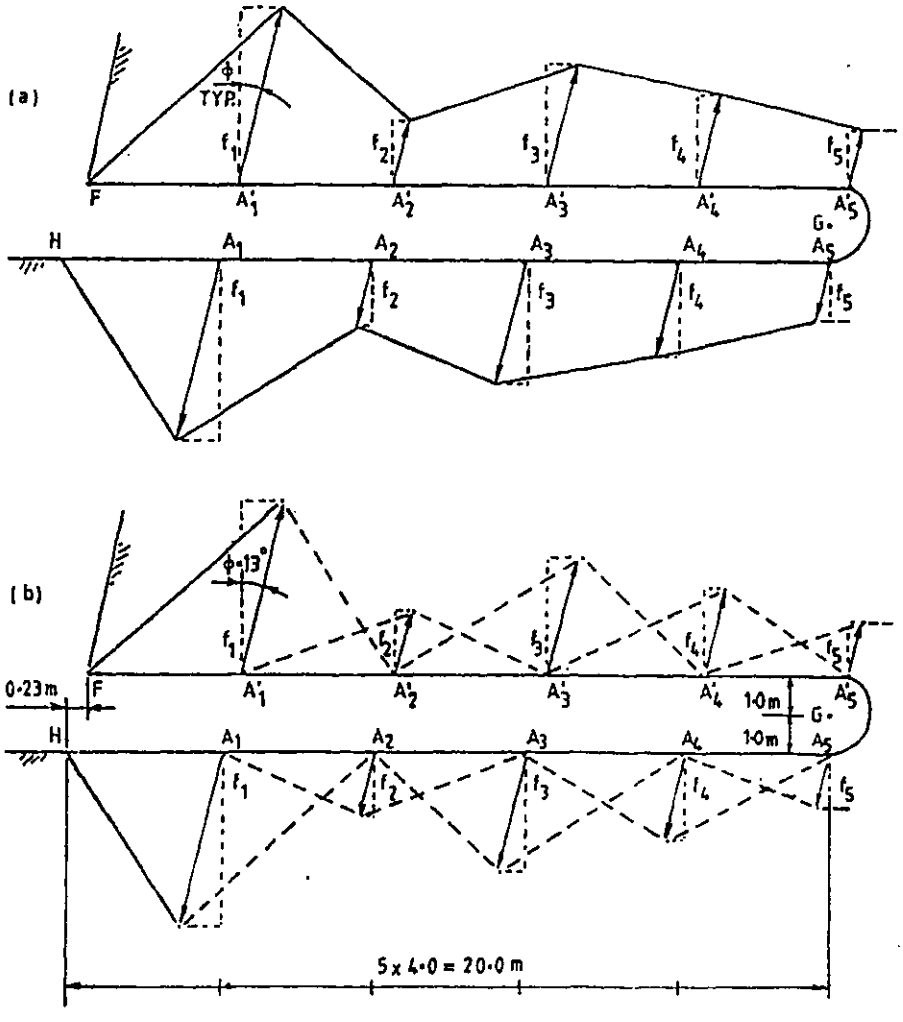


FIG. 4.5.4: (a) ASSUMED DISTRIBUTION OF TRACTION ON A NOMINAL 20 m LONG GAP FGH AS SHOWN IN FIG. 4.5.3 AND (b) EQUIVALENT DISTRIBUTION BY SUPERPOSITION OF TRIANGULAR LOAD SYSTEMS

Distributions of the normal component of loading per unit length, denoted by the letter f and expressed in MN/m, are shown in Fig. 4.5.5 (a),(b),(c) on the faces of the nominal 20, 30, and 40 m long gaps, respectively, for the standard boundary conditions. Fig. 4.5.6 (a),(b),(c) and Fig. 4.5.7 (a),(b),(c) show similar distributions when the displacement amounts specified for the standard boundary conditions are reduced to 50% and 10% respectively. In all of these figures the position of the point H corresponds to that shown in Fig. 4.5.3 as does that of the X_1-axis. Either residual or peak shear strength is assumed to occur on the faces of the gap: the hatched portions in the figures indicate where peak strength prevails. Tables giving the horizontal displacements U'_1, U_1 in metres in the direction X_1, on the upper and lower faces of the gap respectively are also shown in these figures at the specified points. The values of the relative horizontal displacement at each of these points can be obtained by subtraction and a judgement made of their significance. In particular, it may be possible to decide whether or not plastic movement occurs.

The figures suggest that when the gap length is 40 m and the amounts of displacement are less than some value between 50% and 100% of that specified in the standard boundary conditions, no large average horizontal relative displacement is induced along the length of the gap. Subsequent large displacements along the gap are implied , however, when its length is later reduced to 20 m. At a length of approximately 30 m it appears that a transition stage may have been reached.

The amount of horizontal relative displacement between the faces may be arbitrarily distinguished by an order of magnitude. The smaller order of magnitude, it is suggested, may be associated with an overall elastic response and the larger order of magnitude with plastic behaviour.

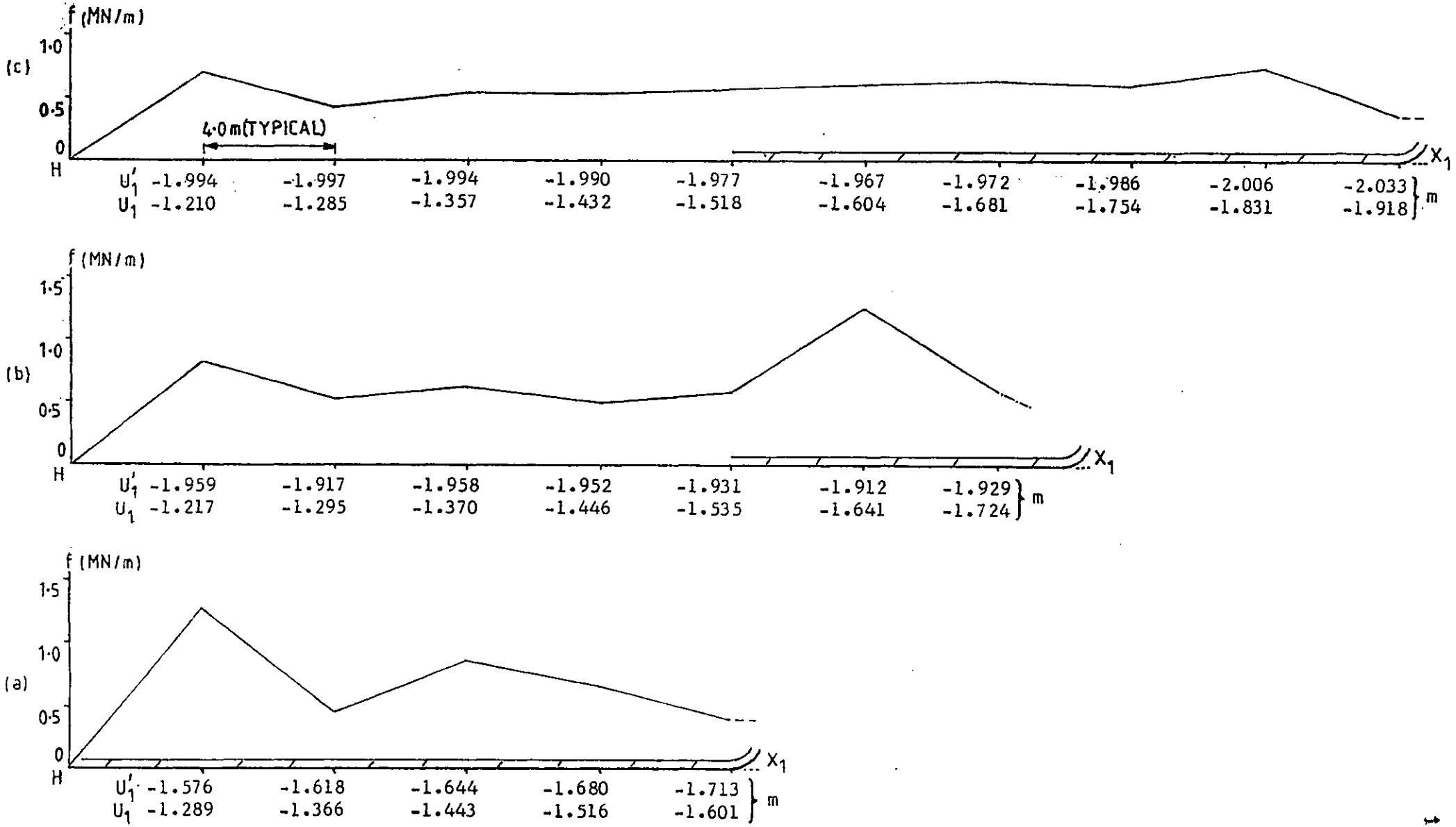


FIG. 4.5.5: DISTRIBUTIONS SHOWN IN (a), (b) AND (c) OF THE NORMAL COMPONENT OF LOADING PER UNIT LENGTH FOR NOMINAL 20, 30 AND 40 m LONG GAPS RESPECTIVELY AS DESCRIBED IN FIGS. 4.5.3 AND 4, FOR STANDARD BOUNDARY CONDITIONS

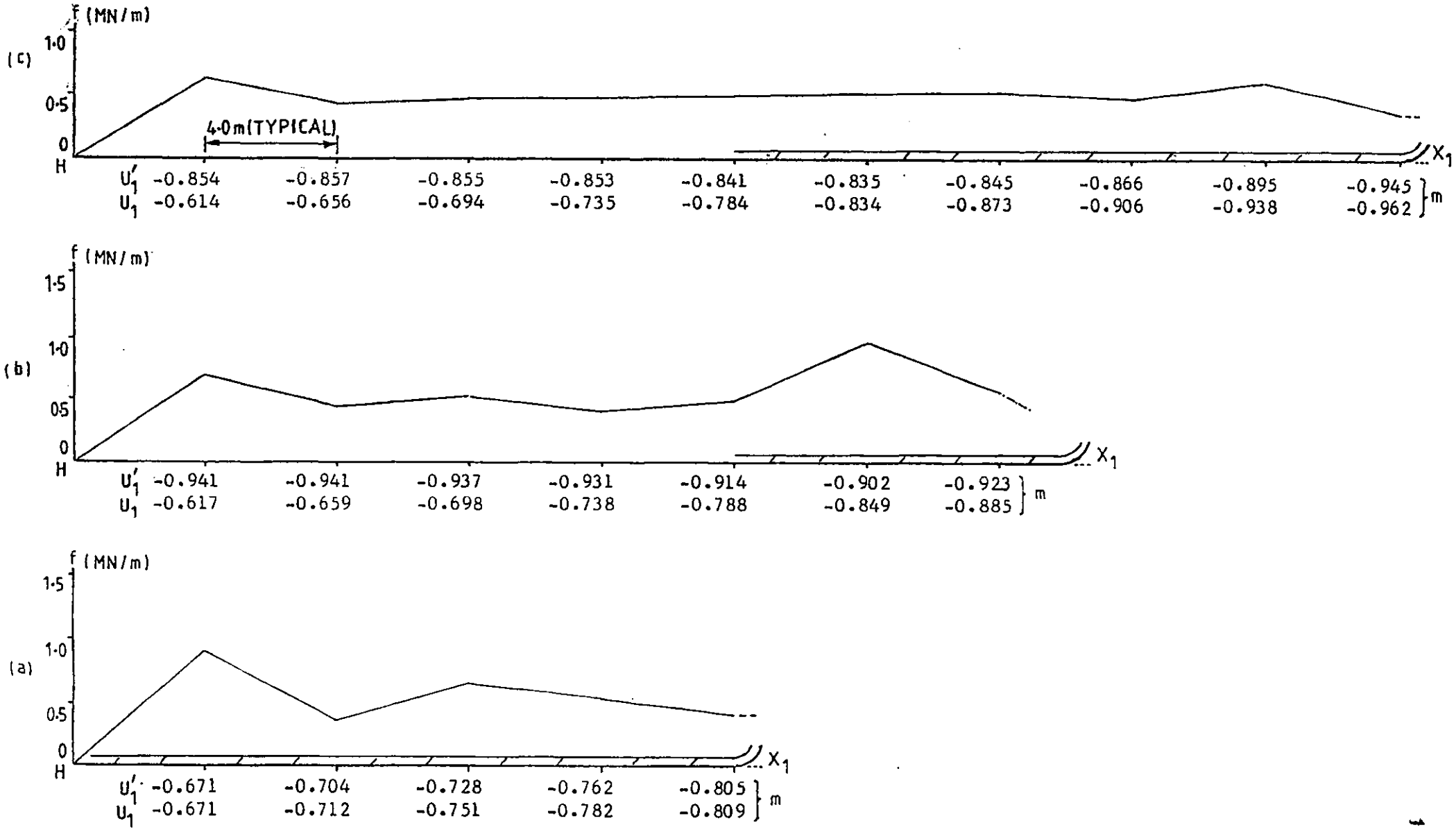


FIG. 4.5.6: DISTRIBUTIONS SHOWN IN (a), (b) AND (c) OF THE NORMAL COMPONENT OF LOADING PER UNIT LENGTH FOR NOMINAL 20, 30 AND 40 m LONG GAPS RESPECTIVELY AS DESCRIBED IN FIGS. 4.5.3 AND 4, FOR STANDARD BOUNDARY CONDITIONS WHERE THE DISPLACEMENT AMOUNTS ARE REDUCED TO 50%

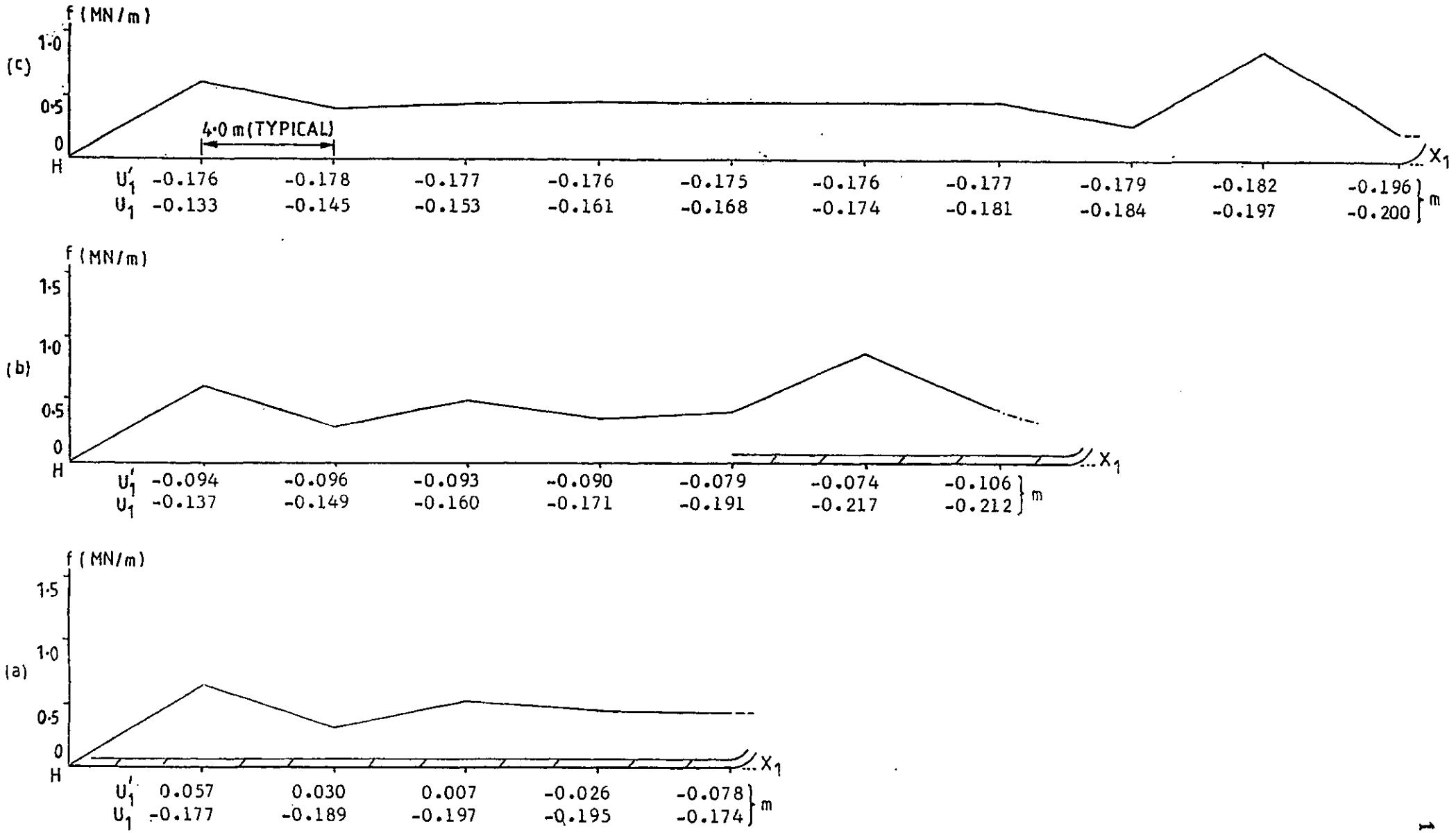


FIG. 4.5.7: DISTRIBUTIONS SHOWN IN (a), (b) AND (c) OF THE NORMAL COMPONENT OF LOADING PER UNIT LENGTH FOR NOMINAL 20, 30 AND 40 m LONG GAPS RESPECTIVELY AS DESCRIBED IN FIGS. 4.5.3 AND 4, FOR STANDARD BOUNDARY CONDITIONS WHERE THE DISPLACEMENTS ARE REDUCED TO 10%

If the effect of the gap is interpreted in terms of a coincident shear band and end region, as suggested earlier, then depending on its length, either one or the other response predominates at the same particular value of horizontal field stress.

In order to calculate the horizontal displacements induced by advancing the excavation face by 10 m, two similar structures were considered, each containing a 30 m long gap. The first structure is as shown in Fig. 4.5.3. The second structure has the same overall length but the distance AH is 80 m and its complement is 220 m. The field stresses were represented by the standard boundary conditions where the displacement amounts were reduced by 50%. The assumed shear strength along the gap is indicated in Fig. 4.5.6(b). The horizontal displacements were calculated using Watson's two-dimensional program. The induced horizontal displacements ΔU_1 along the surface behind the edge of the face of the excavation due to the 10 m advance were obtained by subtracting corresponding displacements. These values are given by Curve S in Fig. 4.5.8 where the two structures are shown superposed. Corresponding values for structures containing no gap were also obtained and are given by Curve T in Fig. 4.5.8. It is seen that Curve S shows a general flattening off of the relative surface displacements directly above the gap and that this characteristic is absent from Curve T.

An alternative two-dimensional model analysis

The introduction of artificial boundaries remote from the area of interest, with an assumed set of boundary conditions, as used in the previous two-dimensional model, brings with it the possibility of gross error in the estimated values of displacements, even when the stress values are approximately correct. An alternative model is described below in which artifical boundaries are not required.

Consider a semi-infinite body with a horizontal surface passing through A'EE'D as shown in Fig. 4.5.9. Plane stress conditions are assumed with the principal stresses normal and parallel to the surface. In the section shown, the horizontal stress is equal to the vertical stress multiplied by a constant K. The vertical stress is given by the product of the unit weight of material and the depth below the surface. The long-dashed lines AH and HE on Fig. 4.5.9 trace the surface shape of the horizontal base and the inclined face of excavation of the brick-pit respectively for any one of the stages of excavation shown in Fig. 4.3.1. This shape is assumed to be reflected in the line AA'. The distance chosen for AH is relatively large to avoid any significant mirror image interaction in the area of the face of excavation. The tractions induced along the long-dashed lines are easily obtained by use of the appropriate stress transformation equation or by inspection. By applying equal and opposite tractions the total displacements caused by excavating the brickpit to the stage shown may be calculated using a suitable computer program.

Repeating the whole procedure described above for the surface shape AHH'E'D in Fig. 4.5.9 and subtracting the two sets of results

gives the displacements induced by advancing the excavation face from HE to H'E' . In both cases infinite vertical displacements of the area of interest w.r.t. a point at infinity can be avoided by placing the excavated material elsewhere so that it does not create any significant non-uniform effects at the pit.

As stated earlier, infinite elements were not available in Watson's two-dimensional program at the time of this analysis, so that part of the model described above had to be altered. The modified model is shown in Fig. 4.5.10 and is assumed to be symmetrical about the lines A''C and A''A. The model of the brickpit had to be inverted because of a computer program requirement that the body be described only in the first quadrant for any problem using the double symmetry specification. In order to represent the shear band and end region, a gap FGH was introduced along which tractions could be applied as before to represent shearing resistance. Self weight of the material was ignored. Therefore some significant error may be introduced by the local unbalanced moments due to couples generated by the tangential tractions on the faces of the gap.

Traction applied to the surface AH and FE shown in Fig. 4.5.10 simulated the excavation of the pit AHFE as before. A shear zone and end region was included coincident with the gap FGH. The resulting displacements were calculated using Watson's two-dimensional program. The whole procedure described above was repeated for the pit AH'F'E' and gap F'G'H'. By subtraction the relative displacments were obtained for advancing the excavation face from FE to F'E'. In particular the relative horizontal displacements ΔU_1 along the surface E'D are given by the graph shown in Fig. 4.5.10 , assuming that Young's modulus is

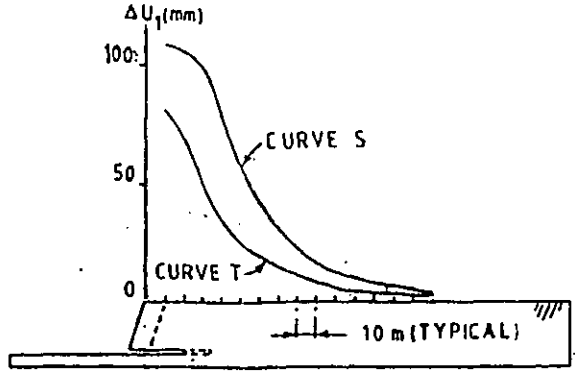


FIG. 4.5.8: HORIZONTAL DISPLACEMENT ΔU_1 INDUCED BY A 10 m ADVANCE IN THE FACE OF EXCAVATION OF THE MODEL SHOWN BY CURVE S FOR THE CONDITIONS FOR FIG. 4.5.6 (b), AND SHOWN BY CURVE T ASSUMING NO GAP

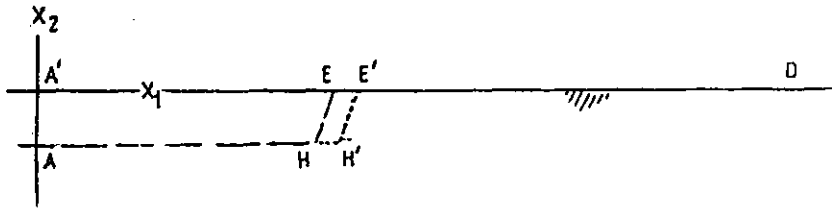


FIG. 4.5.9: SAXON PIT MODEL WITH INFINITELY REMOTE BOUNDARIES FOR TWO-DIMENSIONAL ANALYSIS

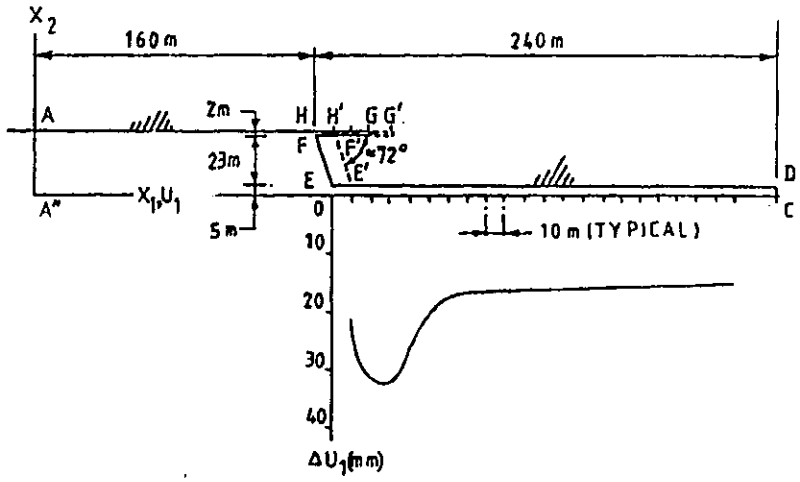


FIG. 4.5.10: SYMMETRIC SAXON PIT MODEL WITH INFINITELY REMOTE BOUNDARIES FOR TWO-DIMENSIONAL ANALYSIS, AND HORIZONTAL DISPLACEMENTS ΔU_1 AS DESCRIBED IN FIG. 4.5.8 ASSUMING A TRACTION-FREE GAP

100 MN/m^2, Poisson's ratio of 0.25 and value of the constant K is approximately 0.3. The tractions are assumed to vanish on the faces of the gap coincident with the shear band and end region. This was a trial problem and the results are obviously at variance with the results of the previous analysis. Shortage of time did not permit further work along this line of investigation.

In the case of the simplified analysis described in Appendix A 4.5, the calculated horizontal displacement variation is plotted on Fig. A 4.5.3. The observed variation shown in Fig. 4.3.2 (a) is drawn to the same scale and it can readily be seen that the curve representing the analytical values is markedly flatter. It is suggested that the difference can be attributed to the following:

(1) inelastic behaviour of the clay bank, including the opening of tension cracks

(2) the action of water pressure

(3) the variation of vertical pressure over the plane of the shear band

(4) variations in the horizontal displacement, strain, and stress with depth over the shear band.

Notwithstanding this difference it is clear the response of the model is comparable with the field observations of horizontal displacement.

6. General conclusions

Burland et al. (1977) concluded that a horizontal shear band existed near the bottom of the face of excavation of Saxon pit and greatly influenced the deformations which occurred in the surrounding ground. The results of the simplified analysis described in Appendix A 4.5 narrowly support this interpretation. In the computer based analysis, attention was concentrated on the horizontal components of the displacement associated with advancing the excavation face by about 40% of its vertical height and the Author found that a mathematical model of the structure,containing an element simulating the action of the shear band, exhibited similar behaviour. Although somewhat crude and limited in scope, the models used to carry out this analysis were devised to make the best use of the computer programs and computer systems then available. Deficiencies present in Watson's program for two-dimensional elastostatic analysis using the Boundary Integral Equation Method, which prompted the creation of some of the unusual analytical methods employed above, have now been remedied.

CHAPTER 5 AXSYM: A COMPUTER PROGRAM FOR THE LINEAR ELASTOSTATIC ANALYSIS OF AXISYMMETRIC PROBLEMS USING THE INDIRECT BOUNDARY ELEMENT METHOD

1. Introduction

Many geotechnical problems such as vertical shafts and ring tunnels are axisymmetric or nearly so. But analysis of these problems in two dimensions may be restrictive, inappropriate, and misleading. For example, in an infinite mass subject to hydrostatic field stress, two dimensional elastostatic analysis gives the maximum direct stress around a circular cavity one third larger than that generated around a spherical cavity. On the other hand, even with the saving possible using the boundary element method, a general three dimensional computer analysis usually requires relatively large amounts of input data, memory space, and machine time. Axisymmetric analysis, therefore, is of considerable interest because it contains many of the desirable features of the other two.

A new boundary element program AXSYM has been written by the Author to treat axisymmetric elastostatic problems in linear isotropic material. The indirect method is used in which radial and axial ring elements form an auxiliary boundary outside the body, and uniform normal and tangential fictitious loads are applied at the elements. The loads are adjusted to generate prescribed tractions at the boundary of the body. This set of fictitious loads is also used to calculate displacements and internal stresses.

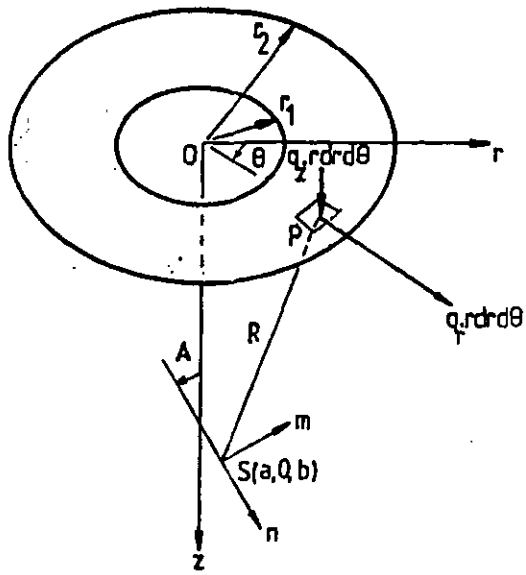
In Chapter 5 , several examples are given in which AXSYM is successfully used to capitalize on the economies and generality possible with axisymmetric analysis. In this respect it may be claimed that AXSYM is similar to the computer program by Mayr et al. (1980), which implements their semi-analytical boundary integral approach for axisymmetric elastic bodies with arbitrary boundary conditions. The work is quite independent however, although certain technical similarities occur.

2. Analysis

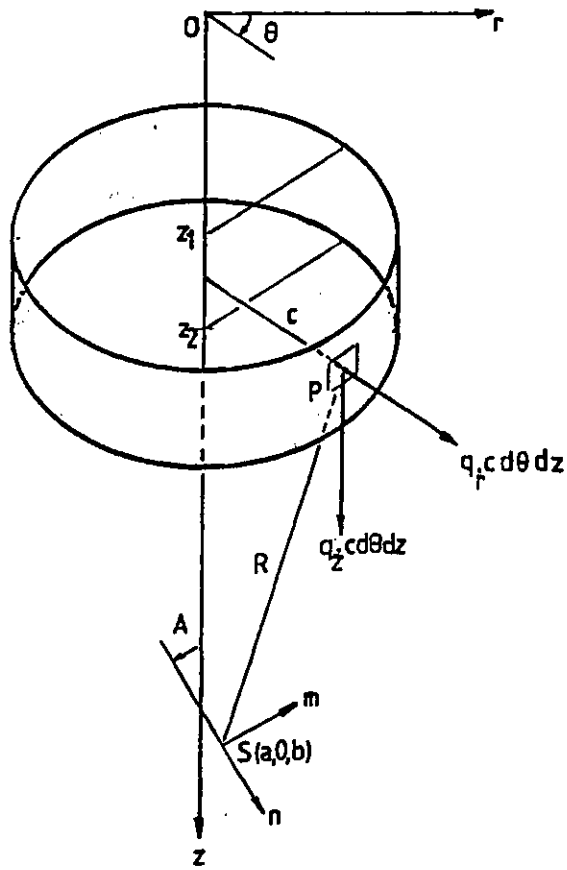
The Kelvin solution for stress and displacement at the point S, in Fig. 5.2.1, due to a concentrated load at the point P, is integrated over a radial and a vertical ring element for normal and tangential uniformly distributed loads. The resulting expressions are given below for each of the four cases in the form of double integrals, where the limits are 0 and 2π for θ, r_1 and r_2 for r, and z_1 and z_2 for z.

A fairly common procedure in the indirect method is to apply the fictitious loads to a surface which coincides with the real boundary. In this approach, however, an auxiliary boundary is used, the point S is positioned on the loaded surface of the body, and the fictitious load is applied at points P on the auxiliary surface so that the distance PS does not vanish (Fig. 5.2.1).

The method is not new and has been used here primarily to expedite the work and to avoid several technical problems which arise when these boundaries coincide. In particular, radial and axial elements could not have been used to model axisymmetric bodies with a curved surface in the axial section ; an inclined element would have had to precede their analysis. Althought not different in principle, the mathematical work involved in the creation of an inclined element is more complicated than for the radial and axial elements and it was not completed. It is also clear that for uniformly loaded linear elements the fictitious load discontinuities may be large. The amount of local disturbance within the model would therefore increase because they would be that much closer to it. Further consideration is given



(a)



(b)

FIG. 5.2.1: (a) RADIAL AND (b) AXIAL RING LOAD ELEMENTS

to these points later in the general discussion in section 5 of this chapter.

Radial ring element (Fig. 5.2.1(a))

Attention is now directed to the stresses and displacements induced by the normal and tangential loading of a radial ring element. Denoting the intensities of radial and axial loading by q_r and q_z respectively, the cylindrical components of stress and displacement are given by the following equations, where G designates shear modulus and ν Poisson's ratio.

$$\sigma_r = \frac{q_r}{8\pi(1-\nu)} \iint \left(3a^3\left(\frac{r\cos\theta}{R^5}\right) - 6a^2\left(\frac{r^2\cos^2\theta}{R^5}\right) - 3a^2\left(\frac{r^2}{R^5}\right) + 3a\left(\frac{r^3\cos^3\theta}{R^5}\right) + \right.$$

$$+ 6a\left(\frac{r^3\cos\theta}{R^5}\right) - 3\left(\frac{r^4\cos^2\theta}{R^5}\right) + (1-2\nu)a\left(\frac{r\cos\theta}{R^3}\right) +$$

$$\left. + (1-2\nu)\left(\frac{r^2}{R^3}\right) - 2(1-2\nu)\left(\frac{r^2\cos^2\theta}{R^3}\right)\right) \, dr d\theta$$

$$\sigma_\theta = \frac{q_r}{8\pi(1-\nu)} \iint \left(3a\left(\frac{r^3\cos\theta}{R^5}\right) - 3\left(\frac{r^4}{R^5}\right) - 3a\left(\frac{r^3\cos^3\theta}{R^5}\right) + 3\left(\frac{r^4\cos^2\theta}{R^5}\right) - \right.$$

$$\left. - (1-2\nu)a\left(\frac{r\cos\theta}{R^3}\right) + 2(1-2\nu)\left(\frac{r^2\cos^2\theta}{R^3}\right) - (1-2\nu)\left(\frac{r^2}{R^3}\right)\right) \, dr d\theta$$

...(5.2.1)

$$\sigma_z = \frac{q_r}{8\pi(1-\nu)} \iint \left(3ab^2\left(\frac{r\cos\theta}{R^5}\right) - 3b^2\left(\frac{r^2}{R^5}\right) - (1-2\nu)a\left(\frac{r\cos\theta}{R^3}\right) + (1-2\nu)\left(\frac{r^2}{R^3}\right)\right) \, dr d\theta$$

$$\tau_{zr} = \frac{q_r}{8\pi(1-\nu)} \iint \left(3a^2b\left(\frac{r\cos\theta}{R^5}\right) - 3ab\left(\frac{r^2\cos^2\theta}{R^5}\right) - 3ab\left(\frac{r^2}{R^5}\right) + 3b\left(\frac{r^3\cos\theta}{R^5}\right) + \right.$$

$$\left. + (1-2\nu)b\left(\frac{r\cos\theta}{R^3}\right)\right) \, dr d\theta$$

$$u_r = \frac{q_r}{16\pi(1-\nu)G} \iint \left(a^2\left(\frac{r\cos\theta}{R^3}\right) - a\left(\frac{r^2\cos^2\theta}{R^3}\right) - a\left(\frac{r^2}{R^3}\right) + \frac{r^3\cos\theta}{R^3} + (3-4\nu)\left(\frac{r\cos\theta}{R}\right)\right) dr d\theta$$

$$u_z = \frac{q_r}{16\pi(1-\nu)G} \iint \left(ab\left(\frac{r\cos\theta}{R^3}\right) - b\left(\frac{r^2}{R^3}\right)\right) \, dr d\theta$$

$$\tau_{r\theta} = \tau_{\theta z} = u_\theta = 0$$

$$\sigma_r = \frac{q_z}{8\pi(1-\nu)} \iint \left(3a^2 b\left(\frac{r}{R^5}\right) - 6ab\left(\frac{r^2\cos\theta}{R^5}\right) + 3b\left(\frac{r^3\cos^2\theta}{R^5}\right) - \right.$$

$$\left. -(1-2\nu)b\left(\frac{r}{R^3}\right)\right) \, dr d\theta$$

$$\sigma_\theta = \frac{q_z}{8\pi(1-\nu)} \iint \left(3b\left(\frac{r^3}{R^5}\right) - 3b\left(\frac{r^3\cos^2\theta}{R^5}\right) - \right.$$

$$\left. -(1-2\nu)\, b\left(\frac{r}{R^3}\right)\right) \, dr d\theta$$

$$\sigma_z = \frac{q_z}{8\pi(1-\nu)} \iint \left(3b^3\left(\frac{r}{R^5}\right) + (1-2\nu)b\left(\frac{r}{R^3}\right)\right) \, dr d\theta \qquad \ldots(5.2.2)$$

$$\tau_{zr} = \frac{q_z}{8\pi(1-\nu)} \iint \left(3ab^2\left(\frac{r}{R^5}\right) - 3b^2\left(\frac{r^2\cos\theta}{R^5}\right) + \right.$$

$$\left. +(1-2\nu)a\left(\frac{r}{R^3}\right) - (1-2\nu)\left(\frac{r^2\cos\theta}{R^3}\right)\right) \, dr d\theta$$

$$u_r = \frac{q_z}{16\pi(1-\nu)G} \iint \left(ab\left(\frac{r}{R^3}\right) - b\left(\frac{r^2\cos\theta}{R^3}\right)\right) \, dr d\theta$$

$$u_z = \frac{q_z}{16\pi(1-\nu)G} \iint \left(b^2\left(\frac{r}{R^3}\right) + (3-4\nu)\left(\frac{r}{R}\right)\right) \, dr d\theta$$

$$\tau_{r\theta} = \tau_{\theta z} = u_\theta = 0$$

The above expressions are written in an expanded form and showing that all the terms involving R and θ appearing in them are contained in Table 5.2.1

TABLE 5.2.1 TERMS INVOLVING R AND θ IN THE EXPRESSIONS FOR STRESS AND AND DISPLACEMENT DUE TO UNIFORMLY LOADED RING ELEMENTS

$\frac{1}{R}$	$\frac{\cos\theta}{R}$		
$\frac{1}{R^3}$	$\frac{\cos\theta}{R^3}$	$\frac{\cos^2\theta}{R^3}$	
$\frac{1}{R^5}$	$\frac{\cos\theta}{R^5}$	$\frac{\cos^2\theta}{R^5}$	$\frac{\cos^3\theta}{R^5}$

The integration is performed in the order θ, then r. As will be shown, the first integration leads to complete elliptic integrals of the first and second kinds. The second integration is carried out by Gaussian quadrature.

For the radial ring element,

$R = \sqrt{(a^2+b^2+r^2-2\ ar\ \cos\theta)}$.

By making the substitution

$\phi = \pi/2 - \theta/2$,

we obtain

$\cos\theta = -1+2\ \sin^2\phi$.

Hence we achieve the form

$$R = g\Delta \qquad \ldots(5.2.3)$$

where,

$g = \sqrt{((a+r)^2+b^2)}$

$\Delta = \sqrt{(1-k^2\sin^2\phi)}$

$k^2 = 4\ ar/g^2$

From the expressions for cos θ and Δ, it will be seen that,

$$\cos\theta = \frac{-1}{k^2}(2\Delta^2+(k^2-2)). \qquad \ldots(5.2.4)$$

Substitution of the expressions for R and cos θ from equations (5.2.3) and (5.2.4) gives the following results:

$$\frac{1}{R} = \frac{1}{g\Delta}\ ,\ \frac{1}{R^3} = \frac{1}{g^3\Delta^3}\ ,\ \frac{1}{R^5} = \frac{1}{g^5\Delta^5}$$

$$\frac{\cos\theta}{R} = \frac{-1}{gk^2}(2\Delta+(k^2-2)\Delta^{-1})$$

$$\frac{\cos\theta}{R^3} = \frac{-1}{g^3k^2}(2\Delta^{-1}+(k^2-2)\Delta^{-3})$$

$$\frac{\cos\theta}{R^5} = \frac{-1}{g^5k^2}(2\Delta^{-3}+(k^2-2)\Delta^{-5})$$

$$\frac{\cos^2\theta}{R^3} = \frac{1}{g^3k^4}(4\Delta+4(k^2-2)\Delta^{-1}+(k^2-2)^2\Delta^{-3})$$

$$\frac{\cos^2\theta}{R^5} = \frac{1}{g^5k^4}(4\Delta^{-1}+4(k^2-2)\Delta^{-3}+(k^2-2)^2\Delta^{-5})$$

$$\frac{\cos^3\theta}{R^5} = \frac{-1}{g^5k^6}(8\Delta+12(k^2-2)\Delta^{-1}+6(k^2-2)^2\Delta^{-3}+(k-2)^3\Delta^{-5})$$

These are the terms which have to be integrated in equation (5.2.1) and (5.2.2). We consider first the integration over θ from 0 to π. This is equivalent to minus twice the integral over ϕ from 0 to $\pi/2$.

Since $k^2 < 1$ we have, by definition,

$$\int_0^{\pi/2} \frac{1}{\Delta}\, d\phi = F_1$$

$$\int_0^{\pi/2} \Delta\, d\phi = E_1$$

where F_1 and E_1 are complete elliptic integrals of the first and second kind respectively. By differentiating the equation for F_1 w.r.t. k, as shown in Appendex A 5.2(a) we obtain,

$$\int_0^{\pi/2} \frac{1}{\Delta^3}\, d\phi = \frac{-1}{k^2-1} E_1$$

$$\int_0^{\pi/2} \frac{1}{\Delta^5}\, d\phi = \frac{1}{3(k^2-1)} F_1 - \frac{2(k^2-2)}{3(k^2-1)} E_1$$

These equations give the means of evaluating the integrals between 0 and $\pi/2$ of all the terms of Table 5.2.1.

When the point S approaches the z-axis, $k^2 \to 0$ and the limiting cases of the integrals are generated. They are obtained by dividing the corresponding limiting values obtained in Appendix A 5.2(b) by appropriate power of g. The resulting expressions are given in Table 5.2.2 below.

TABLE 5.2.2 LIMITING VALUES AS $k^2 \to 0$ OF THE INTEGRALS BETWEEN THE LIMITS OF 0 AND π FOR θ OF THE TERMS IN TABLE 5.2.1

$\frac{\pi}{2g}$	0		
$\frac{\pi}{2g}$	0	$\frac{\pi}{4g^2}$	
$\frac{\pi}{2g}$	0	$\frac{\pi}{4g^2}$	0

If f denotes the integrand of any of the expressions for stress or displacement components given by equation (5.2.1) and (5.2.2), it is seen that

$$\int_0^{2\pi} f(r,\cos\theta,\Delta(k,\phi))d\theta = 4\int_0^{\pi/2} F(r, \Delta(k,\phi))d\phi = \psi(F_1(r),E_1(r)).$$

Integration of ψ between the limits r_1 and r_2 for r by Gauss numerical methods gives the cylindrical components of stress and displacement at the point S due to a uniformly loaded ring element.

In general we shall need to evaluate the stress and displacement components referred to the m and n axes shown in Fig. 5.2.1(a), which lie in the r - z plane. They are determined by the following equations.

$$\sigma_m = \tfrac{1}{2}(\sigma_r + \sigma_z) + \tfrac{1}{2}(\sigma_r - \sigma_z)\cos 2A - \tau_{zr}\sin 2A$$

$$\sigma_n = \tfrac{1}{2}(\sigma_r + \sigma_z) - \tfrac{1}{2}(\sigma_r - \sigma_z)\cos 2A + \tau_{zr}\sin 2A$$

$$\tau_{nm} = \tau_{zr}\cos 2A + \tfrac{1}{2}(\sigma_r - \sigma_z)\sin 2A \qquad \ldots(5.2.5)$$

$$u_m = u_r \cos A - u_z \sin A$$

$$u_n = u_r \sin A + u_z \cos A$$

The θ component of normal stress is unaltered and, as before, the shear and displacement components vanish.

Axial ring element (Fig. 5.2.1(b))

Given that the intensities of radial and axial loading are q_r and q_z respectively, the expressions for the cylindrical components of stress for an axial ring element of radius c are as follows, where G designates shear modulus and ν Poisson's ratio.

$$\sigma_r = \frac{q_r}{8\pi(1-\nu)} \iint \left(-3c^3(b-z)\left(\frac{\cos^2\theta}{R^5}\right)+6ac^2(b-z)\left(\frac{\cos\theta}{R^5}\right)-3a^2c(b-z)\left(\frac{1}{R^5}\right) + \right.$$
$$\left. + (1-2\nu)c(b-z)\left(\frac{1}{R^3}\right)\right) dzd\theta$$

$$\sigma_\theta = \frac{q_r}{8\pi(1-\nu)} \iint \left(3c^3(b-z)\left(\frac{\cos^2\theta}{R^5}\right)-3c^3(b-z)\left(\frac{1}{R^5}\right) + \right.$$
$$\left. + (1-2\nu)c(b-z)\left(\frac{1}{R^3}\right)\right) dzd\theta$$

$$\sigma_z = \frac{q_r}{8\pi(1-\nu)} \iint \left(-3c(b-z)^3\left(\frac{1}{R^5}\right)-(1-2\nu)c(b-z)\left(\frac{1}{R^3}\right)\right) dzd\theta \qquad \ldots(5.2.6)$$

$$\tau_{zr} = \frac{q_r}{8\pi(1-\nu)} \iint \left(3c^2(b-z)^2\left(\frac{\cos\theta}{R^5}\right)-3ac(b-z)^2\left(\frac{1}{R^5}\right) + \right.$$
$$\left. +(1-2\nu)c^2\left(\frac{\cos\theta}{R^3}\right)-(1-2\nu)ac\left(\frac{1}{R^3}\right)\right) dzd\theta$$

$$u_r = \frac{q_r}{16\pi(1-\nu)G} \iint \left(c^2(b-z)\left(\frac{\cos\theta}{R^3}\right)-ac(b-z)\left(\frac{1}{R^3}\right)\right)dzd\theta$$

$$u_z = \frac{q_r}{16\pi(1-\nu)G} \iint \left(-c(b-z)^2\left(\frac{1}{R^3}\right)-(3-4\nu)c\left(\frac{1}{R}\right)\right) dzd\theta$$

$$\tau_{r\theta} = \tau_{\theta z} = u_\theta = 0$$

$$\sigma_r = \frac{q_z}{8\pi(1-\nu)} \iint \left(3ac^3\left(\frac{\cos^3\theta}{R^5}\right)+\left(-3c^4-6a^2c^2\right)\left(\frac{\cos^2\theta}{R^5}\right) + \right.$$

$$+(3a^3c+6ac^3)\left(\frac{\cos\theta}{R^5}\right)-3a^2c^2\left(\frac{1}{R^5}\right)-$$

$$\left.-2\ (1-2\nu)c^2\left(\frac{\cos^2\theta}{R^3}\right) + (1-2\nu)ac\left(\frac{\cos\theta}{R^3}\right) +(1-2\nu)c^2\left(\frac{1}{R^3}\right)\right)\ dzd\theta$$

$$\sigma_\theta = \frac{q_z}{8\pi(1-\nu)} \iint \left(-3ac^3\ \left(\frac{\cos^3\theta}{R^5}\right)+3c^4\ \left(\frac{\cos^2\theta}{R^5}\right)+3ac^3\left(\frac{\cos\theta}{R^5}\right)\ -\right.$$

$$\left.-3c^4\left(\frac{1}{R^5}\right)+2(1-2\nu)c^2\left(\frac{\cos^2\theta}{R^3}\right)-(1-2\nu)ac\left(\frac{\cos\theta}{R^3}\right)-(1-2\nu)\ c^2\left(\frac{1}{R^3}\right)\right)\ dzd\theta$$

...(5.2.7)

$$\sigma_z = \frac{q_z}{8\pi(1-\nu)} \iint \left(3(b-z)^2ac\left(\frac{\cos\theta}{R^5}\right)-3(b-z)^2c^2\ \left(\frac{1}{R^5}\right)\ -\right.$$

$$\left.-(1-2\nu)ac\left(\frac{\cos\theta}{R^3}\right)+(1-2\nu)c^2\left(\frac{1}{R^3}\right)\right)\ dzd\theta$$

$$\tau_{zr} = \frac{q_z}{8\pi(1-\nu)} \iint \left(-3ac^2(b-z)\left(\frac{\cos^2\theta}{R^5}\right)+3(a^2c+c^3)(b-z)\left(\frac{\cos\theta}{R^5}\right)\ -\right.$$

$$\left.-3ac^2(b-z)\left(\frac{1}{R^5}\right)+(1-2\nu)c(b-z)\left(\frac{\cos\theta}{R^3}\right)\right)\ dzd\theta$$

$$u_r = \frac{q_z}{16\pi(1-\nu)G} \iint \left(-ac^2\left(\frac{\cos^2\theta}{R^3}\right)+(a^2c+c^3)\left(\frac{\cos\theta}{R^3}\right)-ac^2\ \left(\frac{1}{R^3}\right)+(3-4\nu)c\ \left(\frac{\cos\theta}{R}\right)\right)\ dzd\theta$$

$$u_z = \frac{q_z}{16\pi(1-\nu)G} \iint \left(ac(b-z)\left(\frac{\cos\theta}{R^3}\right)-c^2(b-z)\left(\frac{1}{R^3}\right)\right)\ dzd\theta$$

$$\tau_{r\theta} = \tau_{\theta z} = u_\theta = 0$$

For the axial ring element

$$R = \sqrt{((a+c)^2 + (b-z)^2)}\ \sqrt{(1-k'^2\sin^2\phi)},$$

where

$$k'^2 = 4\ ac\ /((a+c)^2 + (b-z)^2) < 1$$

These equations are of the same form as those for the radial ring element, so that the analytical method used is unaltered and further details are omitted.

3. AXSYM procedure

The computer program AXSYM implements the previous analysis. The shape, mechanical properties and boundary condition of the body are specified, the last in terms of traction only. The body may be finite or infinite and may contain holes. Uniform field stresses are specified in the case of infinite bodies and mirror symmetry may be used in the problem description. The user chooses the position of the loaded ring elements relative to the points at which the tractions are prescribed. Good judgement exercised at this stage often greatly contributes to the efficiency of the analysis and the accuracy of the results.

The procedure followed in AXSYM divides naturally into four parts. In describing them it is convenient to refer to Fig.5.3.1. On the r, z plane shown, the traces of a radial and an axial ring element are denoted by 1' 2' and 1" 2" respectively. Other symbols used below are dashed in the same way to indicate their relationship with the particular type of element. The letter S denotes a typical point on the surface of the body. In the first part of the procedure, the coordinates of these points and the attitudes of the tangent planes passing through them are calculated, as well as the coordinates and attitudes of the elements. The specified surface traction components p_m and p_n at these points are also entered at this stage, as are the field stresses p_r and p_z if the body is infinite. For a finite body it is necessary to specify that the variables p_r and p_z are both zero.

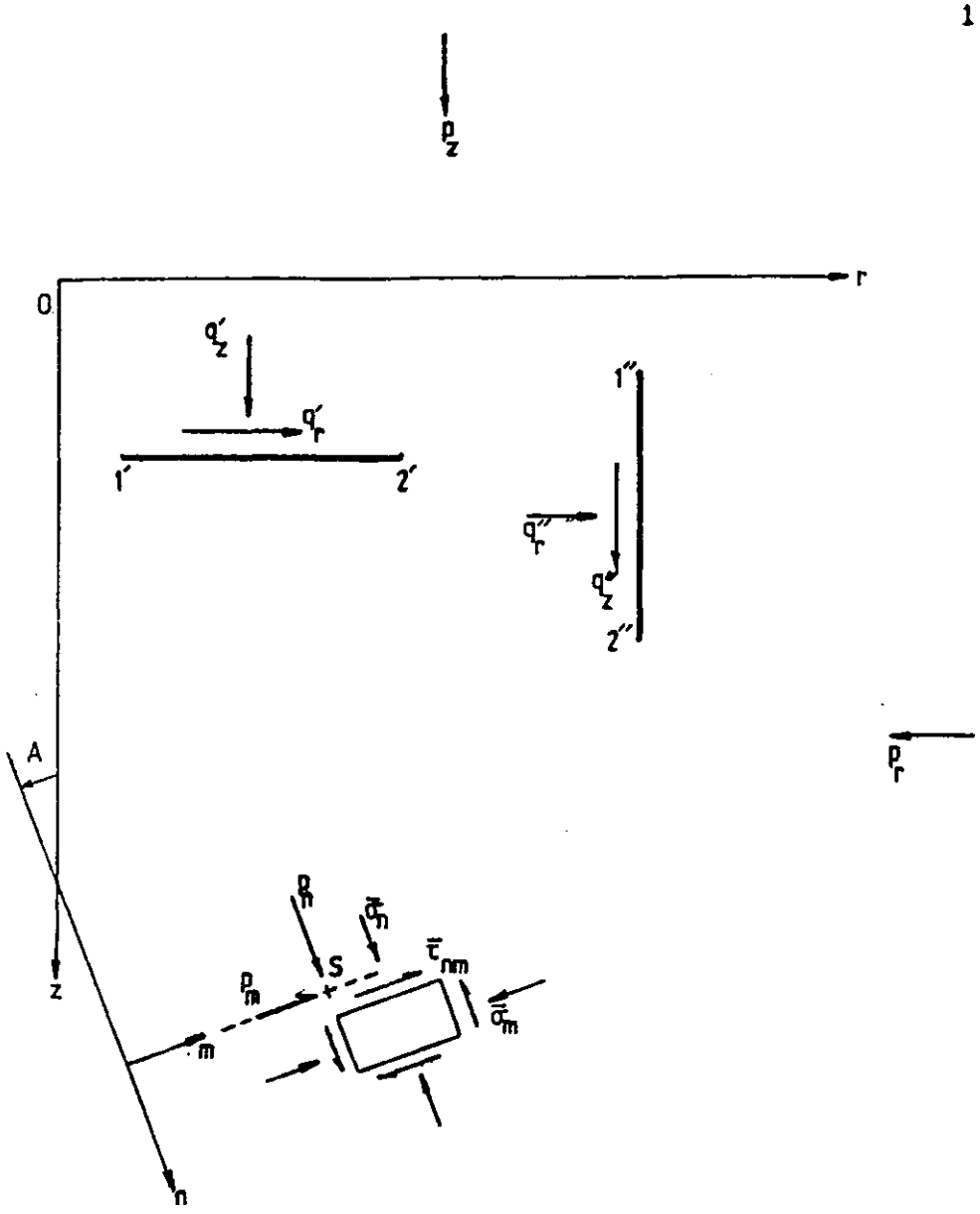


FIG. 5.3.1: GENERAL ARRANGEMENT OF A RADIAL AND AN AXIAL LOAD ELEMENT WITH A CORRESPONDING SURFACE POINT

The boundary element method cannot however deal directly with field stresses. To overcome this difficulty an alternative approach involving the repeated use of superposition is made by splitting the problem into parts which are solved separately and combining the results.

For simple illustration consider the calculation of the stress induced in a mass subject to field stresses p_r and p_z containing a cavity with a traction free surface. Initially stresses are considered at any point S in the infinite mass w.r.t. local axes m and n, shown in Fig. 5.3.1, due to the application of field stresses p_r and p_z. Denoting the tangential and normal traction component by $\bar{\bar{p}}_m$ and $\bar{\bar{p}}_n$ on a plane through the point S parallel to the m-axis, it is seen immediately from equation (5.2.5) that

$$\bar{\bar{p}}_m = \tfrac{1}{2} (p_r - p_z) \sin 2A$$

$$\bar{\bar{p}}_n = \tfrac{1}{2} (p_r + p_z) - \tfrac{1}{2} (p_r - p_z) \cos 2A.$$

The outline of the surface of the cavity in the intact mass is approximately represented by sections of such planes chosen to coincide with tangent planes at points S on the surface of the cavity. The boundary element method is used to arrange that traction components $-\bar{\bar{p}}_m$ and $-\bar{\bar{p}}_n$ are induced on these planes at points S in the intact mass. The stress at any point in the mass is then approximately determined by superposing the stress field obtained by the boundary element method and that due to the field stresses p_r and p_z when applied to an intact mass. This approach is easily extended to cover the problems of the stress induced in a mass subject to field stresses p_r and p_z containing a cavity loaded at various points S on its surface by traction components p_m and p_n (Fig. 5.3.1). Only one alteration to the approach already described is required by which the boundary element method is used to arrange that

modified tangential and normal component $\bar{p}_m$ and $\bar{p}_n$, instead of $-\bar{\bar{p}}_m$ and $-\bar{\bar{p}}_n$ respectively, are induced on corresponding planes, where

$$\bar{p}_m = p_m - \bar{\bar{p}}_m = p_m - \tfrac{1}{2}(p_r - p_z) \sin 2A$$

$$\bar{p}_n = p_n - \bar{\bar{p}}_n = p_n - \tfrac{1}{2}(p_r + p_z) + \tfrac{1}{2}(p_r - p_z) \cos 2A.$$

Most of the computing work is done in the second part of the AXSYM procedure. Here the 24 non-vanishing influence coefficients ${}_r\sigma'_r, {}_r\sigma'_\theta, \cdots {}_z u''_r, {}_z u''_z$ are calculated for each loaded element at every prescibed surface point. The expressions for the influence coefficients referred to the r, θ, z axes are those given for the corresponding stresses and displacements $\sigma_r, \sigma_\theta, \cdots u_r, u_z$ given in equations (5.2.1), (5.2.2), (5.2.6), and (5.2.7) with $q_r = 1, q_z = 1$. Two typical examples of this nomenclature are given as follows: ${}_r\sigma'_r = \sigma_r$, where σ_r is given in either equation (5.2.1) or (5.2.2) with $q_r = 1$, and ${}_z\sigma''_z = \sigma_z$ referring similarly to either equation (5.2.6) or (5.2.7) with $q_z = 1$. The influence coefficients denoted by ${}_r\sigma'_n, {}_r\tau'_{nm}, \cdots$ referred to m, n axes (Fig.5.3.1) are obtained from equations (5.2.5) with $q_r = 1, q_z = 1$.

Following the computation of the influence coefficients the values of the fictitious load intensities are obtained by solving the matrix equation (5.3.1).

$$\begin{bmatrix} \begin{bmatrix} r\tau'_{nm} & z\tau'_{nm} \\ r\sigma'_{n} & z\sigma'_{n} \end{bmatrix} & \cdot & \begin{bmatrix} r\tau''_{nm} & z\tau''_{mn} \\ r\sigma''_{n} & z\sigma''_{n} \end{bmatrix} & \cdots \\ \cdot & \cdot & \cdot & \cdots \\ \begin{bmatrix} & \\ \cdot & \end{bmatrix} & \cdot & \begin{bmatrix} & \\ \cdot & \end{bmatrix} & \cdots \\ \cdot & \cdot & \cdot & \cdots \\ \cdot & \cdot & \cdot & \cdots \\ \cdot & \cdot & \cdot & \cdots \end{bmatrix} \begin{bmatrix} q'_r \\ q'_z \\ \cdot \\ q''_r \\ q''_z \\ \cdot \\ \cdot \\ \cdot \\ \cdot \end{bmatrix} = \begin{bmatrix} \bar{p}_m \\ \bar{p}_n \\ \cdot \\ \\ \\ \cdot \\ \cdot \\ \cdot \\ \cdot \end{bmatrix} \qquad \ldots(5.3.1)$$

The l.h.s represents the superposition of the tractions due to the loaded elements at each of the points S and the r.h.s. is the vector of modified traction components.

The solution of the matrix equation (5.3.1) gives the fictitious load intensities required to create the traction and is indicated by $\bar{\sigma}_n = \bar{p}_n$ and $\bar{\tau}_{nm} = \bar{p}_m$ in Fig. 5.3.1. The other stress components and the displacements denoted by $\bar{\sigma}_m$, ... $\bar{u}_m$, may be obtained by using the values obtained for the fictitious load intensities in equation (5.3.2) given below. We may also recover $\bar{\sigma}_n$ and $\bar{\tau}_{nm}$ for verification. In these equations the summation is over all the elements and the displacements due to field stresses alone are ignored.

$$\bar{\sigma}_m = \Sigma\ ({}_r\sigma_m' q_r' + {}_z\sigma_m' q_z' + {}_r\sigma_m'' q_r'' + {}_z\sigma_m'' q_z'') +$$

$$+ \tfrac{1}{2}(p_r + p_z) + \tfrac{1}{2}(p_r - p_z) \cos 2A$$

$$\bar{\sigma}_\theta = \Sigma\ ({}_r\sigma_\theta' q_r' + {}_z\sigma_\theta' q_z' + {}_r\sigma_\theta'' q_r'' + {}_z\sigma_\theta'' q_z'') + p_r$$

$$\bar{\sigma}_n = \Sigma({}_r\sigma_n' q_r' + {}_z\sigma_n' q_z' + {}_r\sigma_n'' q_r'' + {}_z\sigma_n'' q_z'') +$$

$$+ \tfrac{1}{2}(p_r + p_z) - \tfrac{1}{2}(p_r - p_z) \cos 2A \qquad (5.3.2)$$

$$\bar{\tau}_{nm} = \Sigma({}_r\tau_{nm}' q_r' + {}_z\tau_{nm}' q_z' + {}_r\tau_{nm}'' q_r'' + {}_z\tau_{nm}'' q_z'') +$$

$$+ \tfrac{1}{2}(p_r - p_z) \sin 2A$$

$$\bar{u}_m = \Sigma({}_r u_m' q_r' + {}_z u_m' q_z' + {}_r u_m'' q_r'' + {}_z u_m'' q_z'')$$

$$\bar{u}_\theta = 0$$

$$\bar{u}_n = \Sigma({}_r u_n' q_r' + {}_z u_n' q_z' + {}_r u_n'' q_r'' + {}_z u_n'' q_z'')$$

The fourth and final part of the procedure is to use the fictitious loads to compute the non-vanishing stresses and displacements at the various points throughout the body. These quantities, denoted by $\bar{\sigma}_r$, ... $\bar{u}_z$ referred to the r, θ, z axes, are obtained by equations (5.3.3) where the summation is over all the elements. The fictitious load intensities q_r' , q_z', q_r'' , q_z'' , are those obtained by equation (5.3.1).

$$\bar{\sigma}_r = \Sigma\sigma_r = \Sigma\,({}_r\sigma_r' q_r' + {}_z\sigma_r' q_z' + {}_r\sigma_r'' q_r'' + {}_z\sigma_r'' q_z'') + p_r$$

$$\bar{\sigma}_\theta = \Sigma\sigma_\theta = \Sigma\,({}_r\sigma_\theta' q_r' + {}_z\sigma_\theta' q_z' + {}_r\sigma_\theta'' q_r'' + {}_z\sigma_\theta'' q_z'') + p_r$$

$$\bar{\sigma}_z = \Sigma\sigma_z = \Sigma\,({}_r\sigma_z' q_r' + {}_z\sigma_z' q_z' + {}_r\sigma_z'' q_r'' + {}_z\sigma_z'' q_z'') + p_z$$

$$\bar{\tau}_{zr} = \Sigma\tau_{zr} = \Sigma\,({}_r\tau_{zr}' q_r' + {}_z\tau_{zr}' q_z' + {}_r\tau_{zr}'' q_r'' + {}_z\tau_{zr}'' q_z'') \qquad \ldots(5.3.3)$$

$$\bar{u}_r = \Sigma u_r = \Sigma\,({}_r u_r' q_r' + {}_z u_r' q_z' + {}_r u_r'' q_r'' + {}_z u_r'' q_z'')$$

$$\bar{u}_z = \Sigma u_z = \Sigma\,({}_r u_z' q_r' + {}_z u_z' q_z' + {}_r u_z'' q_r'' + {}_z u_z'' q_z'')$$

4. Structure and operation of AXSYM

The program is made up of 23 subprograms comprising approximately 1500 Fortran statements. The function of each subprogram is briefly described in a Fortran comment statement immediately following its name. For convenience, these names and comments are also given in Table 5.4.1. The structure of the program is shown in Table 5.4.2, where the names of procedurally grouped subprograms are listed in columns and linked by lines denoting the various control paths. Generally the flow of control is from left to right and downwards. Appendix A5.4 contains the program listing.

TABLE 5.4.1 NAMES AND FUNCTIONS OF SUBPROGRAMS COMPRISING AXSYM

Name of subprogram	Function of Subprogram
AXSYM	Elastostatic analysis of axisymmetric body by the indirect Boundary Element Method using an auxiliary boundary
AXCRD	Reads input from cards and prints it out
AXGTY	Forms and prints out layout of structure
AXECO	Forms end coordinates and slopes of auxiliary boundary elements
AXCEN	Forms centre coordinates of elements in a segment and slopes of boundary elements
AXWCO	Prints out end coordinates and slopes of auxiliary boundary elements and coordinates of boundary points
AXWEN	Prints out centre coordinates of interior elements
AXBDT	Allocates equivalent boundary tractions equal to the applied boundary loads less the field stress on parallel planes
AXWDT	Prints out applied boundary loads and field stresses
AXEXE	Executes stress analysis and prints out results
AXELA	Calculates functions of elastic constants
AXCOE	Calculates stress and displacement coefficients
AXSDR	Calculates stresses and displacements induced by uniform loadings in the radial and axial directions along the surface of a disc.

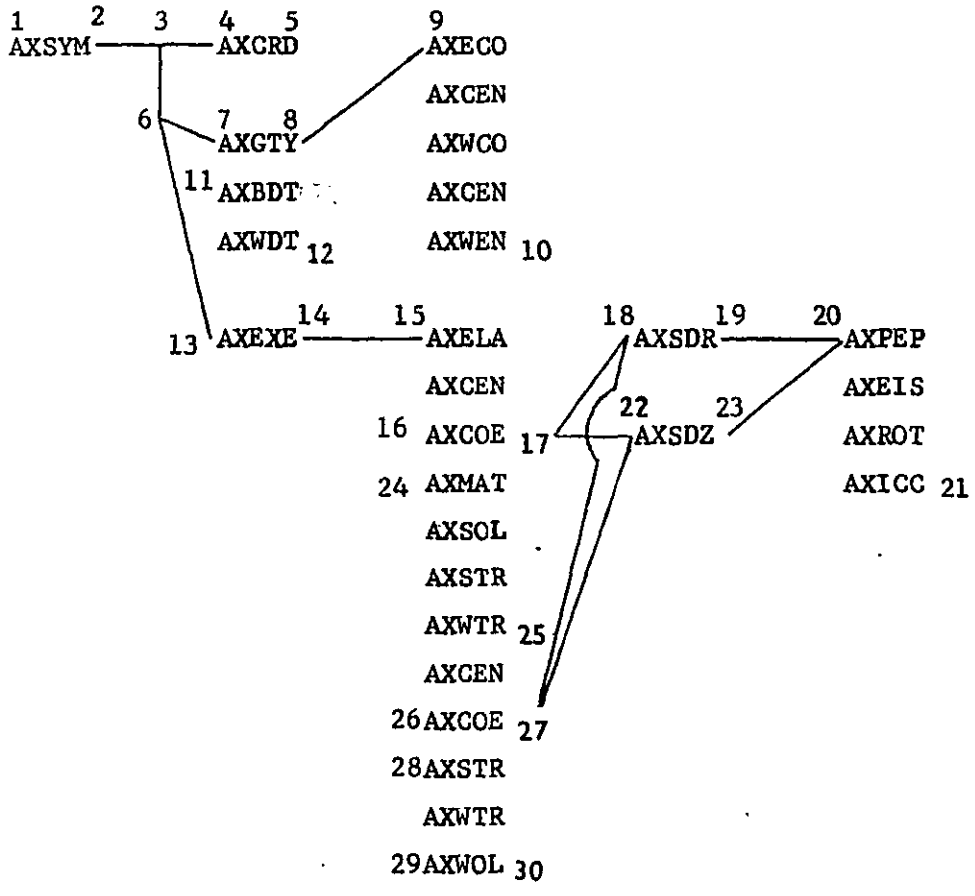
Table 5.4.1 (continued)

AXSDZ	Calculates stresses and displacements induced by uniform loadings in the radial and axial directions along the surface of a cylinder
AXPEP	Calculates point-element parameters
AXEIS	Calculates complete elliptic integrals using polynomial approximation 0.0.le. pam. lt. 1.0
AXICC	Calculates components of influence coefficients
AXROT	Transforms stresses and displacements from global to local axes
AXMAT	Forms matrix of influence coefficients and boundary traction vector
AXSOL	Solves for fictitious loads
AXSTR	Calculates stresses and displacements
AXWTR	Prints out stresses and displacements
AXWOL	Prints out fictitious loads

The numbers 1,2, 3 denote the three operating modes for the program. In mode 1, the input data is read from cards and printed out so that it can be checked and, if necessary, corrected. In mode 2 the coordinates of the auxiliary and body boundaries are calculated and specified boundary tractions are allocated to designated points. Again the information is printed out and may be checked before proceeding to mode 3. The main work of analysis is done in mode 3 where the stresses and displacements are calculated. In each mode all the work in the mode immediately prior to it is repeated before the new work is done.

The operational flow paths followed in each mode are shown by the guide number sequences in Table 5.4.2. The paths proceed downwards through each subprogram named in the columns unless noted otherwise. The guide numbers at the head and tail of a subprogram name refer respectively to entry and exit points. Possible iterations are denoted by round brackets and alternative paths by double banking. Any entry or exit number does not necessarily refer to the same point in a subprogram after an iteration. If no internal points have been specified in the problem description then the shorter flow path shown in mode 3 is required.

TABLE 5.4.2 STRUCTURE AND OPERATING MODES OF AXSYM



Operating mode	Guide number sequences indicating operational flow-paths
1	1 2 3 4 5
2	1 2 3 4 5 3 6 7 8 9 10 11 12
3	1 2 3 4 5 3 6 7 8 9 10 11 12 6 13 14 15 (17 18 19 22 23 20 21 16) 24 (27 18 19 22 23 20 21 26) 28 30
3 (without internal points)	1 2 3 4 5 3 6 7 8 9 10 11 12 6 13 14 15 (17 18 19 22 23 20 21 16) 25 29 30

The control variable MCRD is put equal to 1, 2, or 3 depending on the stage at which the operation of the program is to stop. The numerals and corresponding stages are: 1, read data only; 2, read data and calculate coordinates and slopes only; and 3, repeat the previous work and execute the stress analysis. The job title and load title must each not exceed 80 characters (i.e. 1 line). The symmetry code KRS is put equal to 0 or 1 depending on whether any mirror symmetry in the problem is ignored or included in the description.

The auxiliary boundary element cards define the elements by specifying segments divided into elements. The number of elements NEBS in a segment and the first and last coordinates of the segment RF_i ZF_i and RL_i and ZL_i are specified on a single card. The coordinate pairs may be interchanged. The total number of these cards is NCBS. The elements must be either radial or axial (i.e. horizontal or vertical) as shown in Fig. 5.4.1.

Boundary and interior element cards are used to specify points at the centre of each element. These elements are of two classes. The first defines the points corresponding to the auxiliary boundary elements at which tractions are specified. The second class generates true interior points. The first class must be specified by the same number of cards as the auxiliary boundary set and must define the same number of points as auxiliary boundary elements. The method of specification is the same as for the auxiliary boundary elements, but they may be defined at any attitude (Fig. 5.4.2).

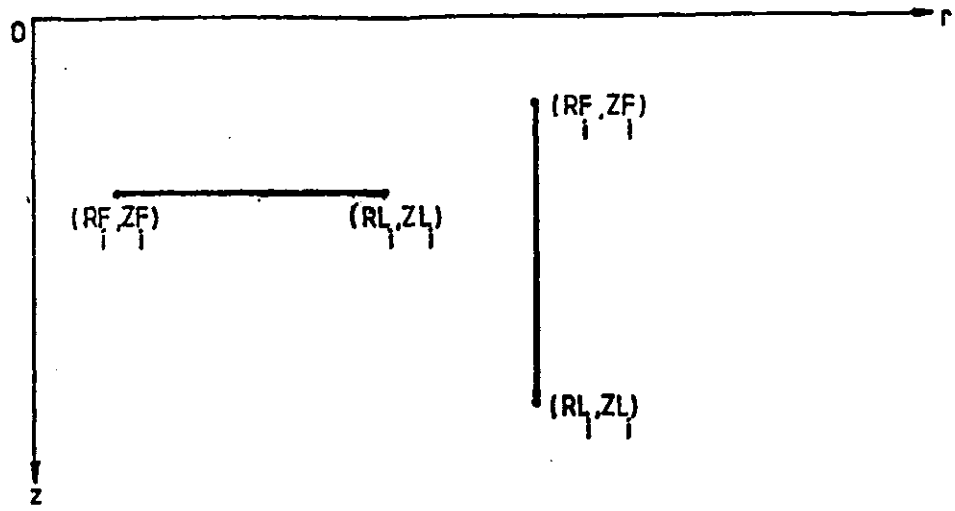


FIG. 5.4.1: SEGMENTS OF RADIAL AND AXIAL LOAD ELEMENTS IN THE r-z PLANE SHOWING NOTATION USED TO SPECIFY THE ELEMENT END POINTS

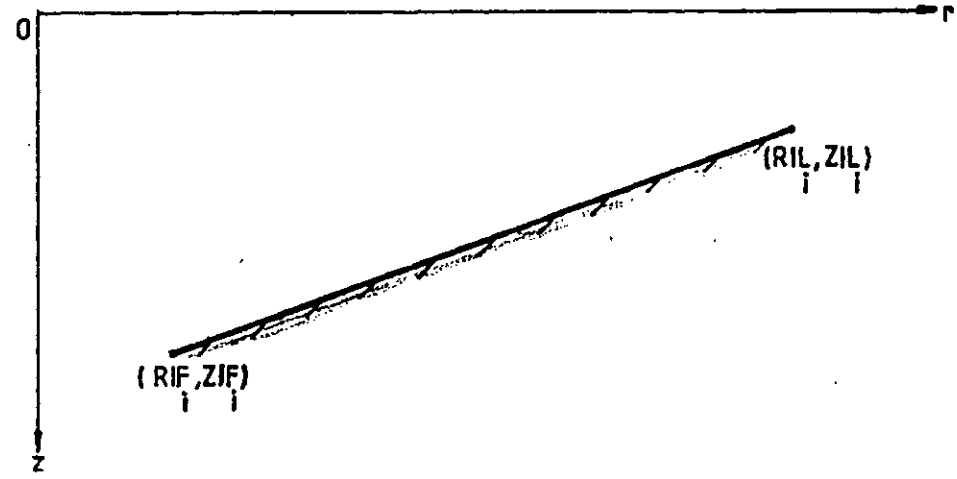


FIG. 5.4.2: SEGMENTS OF ELEMENTS IN THE r-z PLANE USED TO DEFINE POINTS SHOWING NOTATION USED TO SPECIFY THE ELEMENT END POINTS

Input data cards are presented in the order in which they are described in Table 5.4.3. The minimal set comprises 11 cards as shown in the first column. The notation is given in Table 5.4.4.

TABLE 5.4.3 NUMBER, FUNCTION AND SPECIFICATION OF INPUT CARDS FOR AXSYM

No. of cards	Function	Column number of input data card 1 5 10 20 30 40 50 80
1	Control	MCRD
1	Job title	
1	Symmetry	KRS
1	Mechanical properties	YG PN
1	Auxiliary boundary	NCBS
≥ 1		$NEBS_i$ RF_i ZF_i RL_i ZL_i
1	Boundary and interior elements	NCIS
≥ 1		$NEIS_i$ RIF_i ZIF_i RIL_i ZIL_i
1	Load title	
1	Boundary tractions	NCBL
≥ 0		LP_i LQ_i BPM_i BPN_i
1	Field stresses	FPR FPZ

TABLE 5.4.4 NOTATION SCHEME AND FIELD LENGTHS FOR INPUT VARIABLES USED IN AXSYM

MCRD	Operating mode
KRS	Symmetry code
YG	Young's modulus
PN	Poisson's ratio
NCBS	Number of cards defining auxiliary boundary segments
$NEBS_i$	Number of elements in an auxiliary boundary segment
RF_iZF_i	Coordinates of first point on straight line segment
RL_iZF_i	" " last " " " " " "
NCIS	Number of cards defining the boundary and interior points
$NEIS_i$	Number of elements in a boundary or interior points segment
RIF_iZIF_i	Coordinates of first point on straight line segment
RIL_iZIL_i	" " last " " " " " "
NCBL	Number of cards defining the boundary loads
LP_iLQ_i	Numbers of first and last elements to which the load is applied
BPM_iBPN_i	Components of load intensity in the tangential and normal directions(i.e. in the m-and n-direction respectively)
FPR FPZ	Principal field stresses

The subscript i indicates a variable array, where $i \leq 35$ in the version of the program presented. This can be altered, within limits, to suit the requirements of an particular problem. Almost all of the variables listed above are the same as those used within the program. The field length specification for MCRD and KRS is 4x, I1. The remaining field length specifications are either 3x, I2 or F10.0.

UNIVERSITY OF LONDON — General Coding Form

NAME:	USER.NUMBER:	DATE:
ADDRESS:	PROGRAM TITLE:	Page 1 of 1

1 5 10	15 20	25 30	35 40	45 50	55 60	65 70	75 80
3							
SPHERICAL CAVITY ϕF RADIUS 100·0 IN INFINITE MASS (4 ELEMENTS)							
1							
1·0	0·2						
4							
1	0·0	70·0	30·0	70·0			
1	30·0	70·0	30·0	30·0			
1	30·0	30·0	70·0	30·0			
1	70·0	30·0	70·0	0·0			
7							
1	6·129	100·310	25·871	97·110			
1	47·715	88·450	64·285	77·250			
1	77·250	64·285	88·450	47·715			
1	97·110	25·871	100·310	6·129			
10	0·0	95·0	0·0	195·0			
10	67·2	67·2	137·9	137·9			
10	95·0	0·0	195·0	0·0			
UNIT HYDROSTATIC FIELD STRESS							
0							
1·0	1·0						

PUNCHED BY: / DATE PUNCHED:	CODING CONVENTIONS (Please complete)	Zero	One	Two	Oh	I	Zed
		O	1	2	ϕ	I	Z

FIG. 5.4.3: EXAMPLE OF INPUT DATA FOR AXSYM (2)

INTERIOR POINTS

PT NO.	RC	ZC
35	70.736	70.736
36	77.807	77.807
37	84.877	84.877
38	91.948	91.948
39	99.019	99.019
40	106.091	106.091
41	113.162	113.162
42	120.233	120.233
43	127.304	127.304
44	134.375	134.375

STRESSES AND DISPLACEMENTS AT INTERIOR POINTS

PT.NO.	RR	TT	ZZ	ZR	DR	DZ
35	.774	1.492	.753	-.743	-41.477	-41.260
36	.823	1.371	.825	-.561	-34.372	-33.861
37	.861	1.287	.869	-.430	-28.895	-28.322
38	.890	1.225	.898	-.336	-24.619	-24.071
39	.912	1.180	.918	-.267	-21.226	-20.731
40	.929	1.147	.933	-.217	-18.491	-18.053
41	.941	1.121	.945	-.178	-16.255	-15.870
42	.951	1.101	.954	-.148	-14.403	-14.064
43	.959	1.085	.961	-.125	-12.851	-12.553
44	.965	1.072	.966	-.106	-11.539	-11.274

FIG. 5.4.4: EXAMPLE OF COMPUTER OUTPUT FOR AXSYM (2)

The main items of information printed out comprise the input data, the coordinates and slopes for the auxiliary boundary elements and for the boundary and interior points, the stresses at these points, and finally the fictitious loads.

An illustrative example of input data set out for punching on cards is given in Fig. 5.4.3. The four elements specified are shown in Fig.6.3.1 and are used to model a spherical cavity in an infinite mass with unit hydrostatic field stress. The model is one of a series for the spherical cavity discussed in Chapter 6 . Radial segments along the axes and diagonal, specifying points in the body, are included. The output reproduced in Fig.5.4.4 gives the calculated coordinates, stresses and displacements at points on such a diagonal for this four element model.

5. Discussion

Uniformly loaded radial and axial linear elements are perhaps amongst the simplest that could have been used to achieve the prescribed surface tractions. Local distrubances of the stress values caused by the inevitable local discontinuities at the end of contiguous elements would be reduced by allowing the load to vary linearly and equating the values at adjacent ends. For the general inclined linear element with linear variation of load, numerical integration would be used exclusively for both the general and the limiting values. A technique to obtain the latter is given by Watson (1972) involving the projection of the element onto the tangent plane and the calculation of the Cauchy principal values. With an element of this kind the auxiliary surface is obviously unnecessary. Its removal, however, would obviously intensify any problems due to linear representation of the surface and local variation of stress over an element.

In using AXSYM an awareness of the nature of stress and displacement distribution for solid bodies helps in making a suitable choice of load elements required to induce the prescribed surface tractions. Results for simple test loading may help to identify unsuitable choices quickly.

Development of the indirect method to a stage comparable with that reached at present using the direct method may well be possible. There is no doubt, however, that it is desirable, because it gives as much if not more scope for experiment and innovation based on an appreciation of the mechanics (as opposed to the mathematics) of the problem. Such features are welcome in elastostatic analysis.

The specification of the boundary conditions in AXSYM is limited to traction. It could, however, be readily extended to displacements, or to mixed conditions, at least for mirror symmetry problems. Scaling of the influence coefficients is obviously desirable in mixed conditions and should present no difficulty.

At the present state of development of the program, it is possible to obtain very good or alternatively poor results by positioning the same number of similar elements in what initially seem to be equally favourable arrangements. An important example of this effect is given in the next chapter where a spherical surface is modelled using different arrangements of elements.

6. Summary and conclusion

An elastostatic analysis for axisymmetric problems has been presented and its implementation by a computer program achieved. A considerable user contribution must be made for any given problem by positioning suitable numbers of load elements around the body. Where possible, the values obtained for simple test loading should be compared with the known solutions. AXSYM is essentially a research tool not suitable for ordinary general use in engineering. But even at this level of development,it is shown in the next chapter to be able to contribute substantially to the results previously available for axisymmetric problems.

CHAPTER 6 CHARACTERISTICS, VALIDATION, TESTING AND PRACTICAL APPLICATION OF AXSYM

1. Introduction

The contents of this chapter relate primarily to the results obtained using the computer program AXSYM. The characteristics of the load elements are considered first, followed by an account of the validation and additional special testing of the program. Two major analyses are then described, the result of which demonstrate the practical application of AXSYM.

The scope of the study of the characteristics is limited to a particular value of Poisson's ratio and to one radial and one axial element, each of certain length and distance from the z-axis. The results are useful, nevertheless, because they provide a guide to the stress patterns for a range of ratios of element length to axial distance.

All the bodies analysed have additional mirror symmetry in the plane normal to the axis of symmetry, except for the frustum of a cone. This case perhaps, provides the most severe test for the program and some of the results obtained for it are disappointingly inaccurate. On the other hand, the validation and other special testing produce good or very good agreement with several closed form solutions or known results. Simple checks are made, where possible,on the new results obtained.

In the first of the major analyses, the stresses and displacements are calculated around a series of complete circular toric tunnels in an infinite mass, subject to field stress. The second analysis is similar, and deals with two identical spherical cavities at different spacings. The surfaces of both bodies are assumed to be traction free.

2. Characteristics

The principal stresses in the r - z plane around a uniformly loaded radial and axial ring element are shown in Fig. 6.2.1 and Fig. 6.2.2, where the broad black lines represent traces of the elements. The groups of arrows adjacent to these lines represent the direction and intensity of the element loading. It has been assumed that Poisson's ratio $\nu = 0.25$. The crosses denote the position, direction, and magnitude of the induced principal stresses, with tension indicated by a dot. The scale of the crosses is such that the length of an arm represents magnitude relative to the length of the arrow shafts at the elements. In both cases there is rotational symmetry about the z-axis and stresses are not shown for negative values of z. The calculated values of the third principal stress are similar in magnitude to the other two. A listing of the program AXRAE used to obtain the above values is given in Appendix A6.2. Some subprograms called by AXRAE are included in Appendix A 5.4 . The specification of the input data is broadly similar to that for AXSYM and the output values are clearly labelled.

It can be seen from Fig. 6.2.1 and Fig. 6.2.2 that the radial loading induces comparable and slowly varying radial stresses adjacent to the regions encircled by either element. On the opposite side of the elements, the decay in stress magnitude is relatively rapid with increasing distance from the origin 0 because of the symmetry of loading. The figures also show the expected weaker interaction for axial stress due to axial loading. In general no axial stress is induced at the origin 0 by the loading on either element and no radial stress is induced there by axial loading.

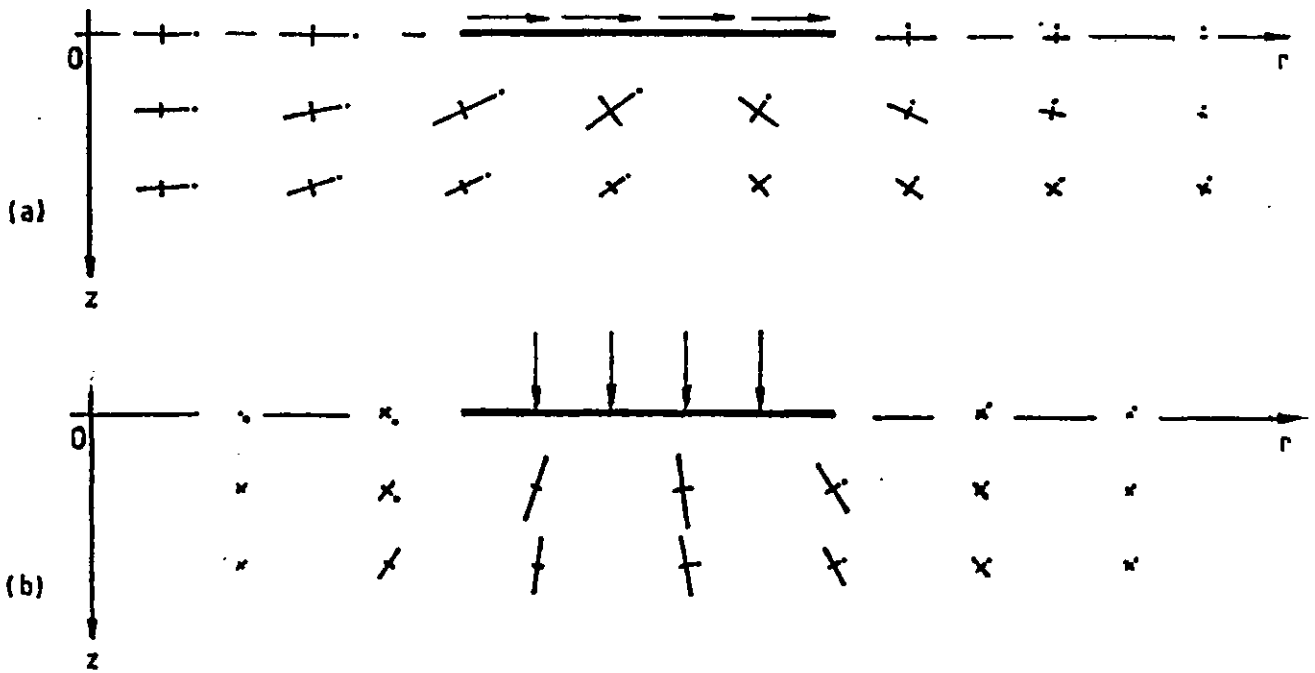


FIG. 6.2.1: DISTRIBUTIONS OF PRINCIPAL STRESSES INDUCED IN THE r-z PLANE AROUND A RADIAL RING LOAD ELEMENT DUE TO UNIT (a) RADIAL AND (b) AXIAL INTENSITIES OF LOADING

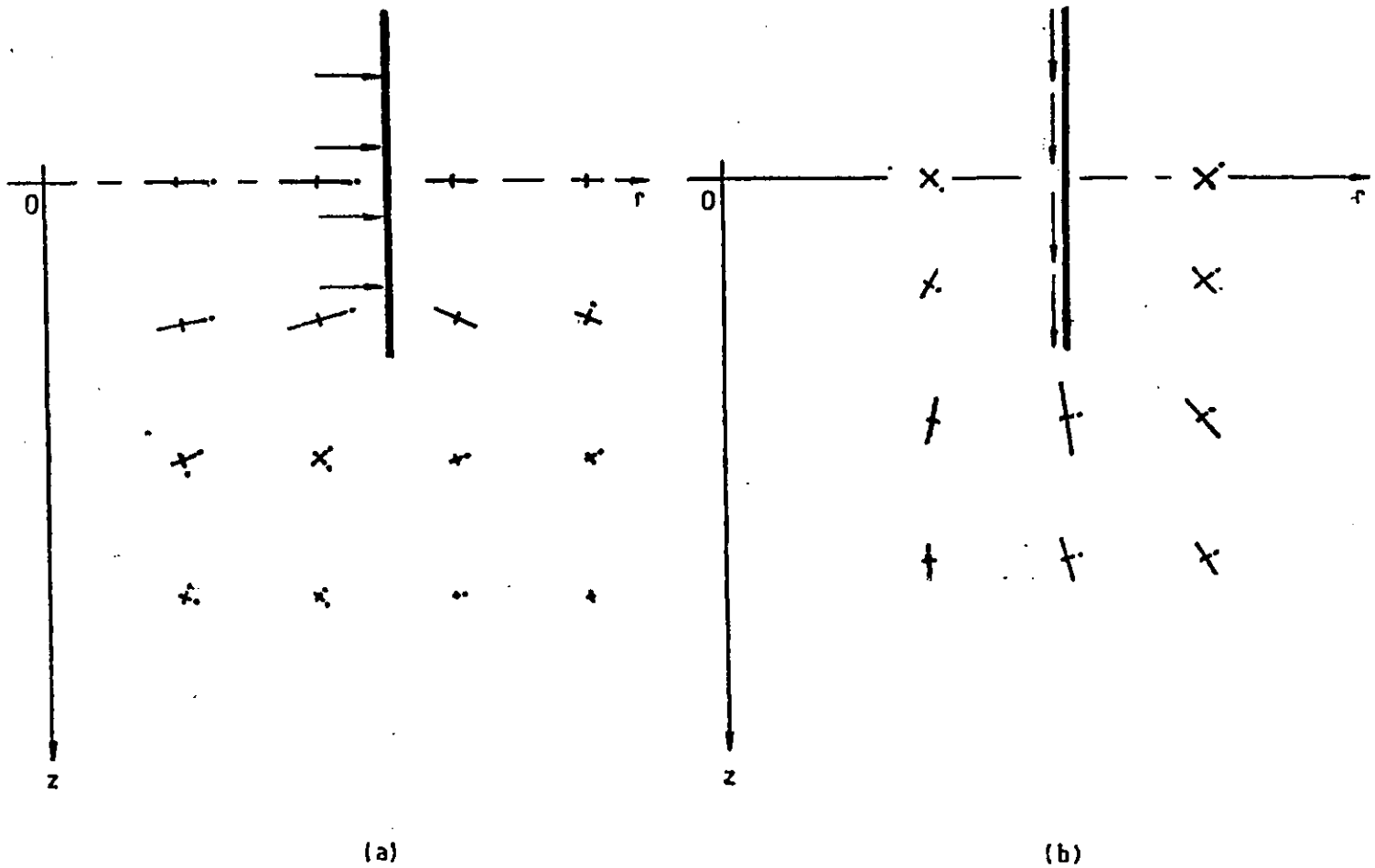


FIG. 6.2.2: DISTRIBUTIONS OF PRINCIPAL STRESSES INDUCED IN THE r-z PLANE AROUND AN AXIAL RING LOAD ELEMENT DUE TO UNIT (a) RADIAL AND (b) AXIAL INTENSITIES OF LOADING

The stress values show a steady variation as the elements are approached to within at least one fifth of their length. Stress values near limiting cases are sometimes very sensitive to the numerical integration method used, however, and some smoothing may have occurred. If closed form solutions were obtained for very simple cases such as, for example, along the r-axis in Fig. 6.2.1, it is thought that a better estimate could be made of the size of the regions of rapid change, especially near the ends of elements.

The above description of the stress distribution around the load elements provides some guidance in the selection of suitable numbers, positions, and types of elements for specific problems. It may also help in the interpretation of any unexpected results in the calculations.

3. Validation

The analytical solution due to Neuber (1946), given in Poulos and Davis (1974), for the stress around a spherical cavity in an infinite mass, subject to uniaxial compressive field stress p_z parallel to z-axis, was used in testing and validating AXSYM. The components of induced displacements u_r and u_z on the the surface of the spherical cavity, referred to cylindrical coordinates r, θ, z with the origin at the centre, are

$$u_r = \tfrac{1}{2}r\,(p_z/E)\,(3-5\nu)\,(1+\nu)\,/(7-5\nu)$$

$$u_z = \tfrac{1}{2}z\,(p_z/E)\,(15\nu-13)\,(1+\nu)\,/(7-5\nu)$$

where E and ν are Young's modulus and Poisson's ratio respectively (Bray (1982)).

Initially a stepped surface was used as a crude approximation to the spherical boundary. Mirror symmetric models were designed with 4, 8 or 12 load elements. Corresponding surface points were chosen on the coaxial radial and axial rings forming the boundary of the model. The load elements and corresponding surface points were generally positioned with an intervening distance of not less than one element length to reduce any unwanted variation In this, as in later models, the accuracy of the results generally increased with the number of elements used.

The layout of a four element model using mirror symmetry is shown in Fig.6.3.1. The traces of the four load elements and the corresponding points on the surface are indicated by dashed line segments and open circles respectively. The identification numbers for the elements and points are 4, 12, 19, 27. Gaps in the natural number sequence have been introduced for forward reference. The coordinates of the points are given in Table 6.3.1. Table 6.3.2(a) contains the results for the model together with the analytical results. Although the stress values differ considerably, the patterns are well represented and the displacements are comparable.

TABLE 6.3.1 IDENTIFICATION NUMBERS N AND COORDINATES r,z OF 30 POINTS ON THE SURFACE OF A SPHERE OF RADIUS 100

N	z r	r z	N
1	2.0	99.98	30
2	6.0	99.82	29
3	9.5	99.55	28
4	16.0	98.71	27
5	19.0	98.18	26
6	25.0	96.82	25
7	30.0	95.39	24
8	35.0	93.67	23
9	42.0	90.75	22
10	44.0	89.80	21
11	51.0	86.02	20
12	56.0	82.85	19
13	61.0	79.24	18
14	64.0	76.84	17
15	68.0	73.32	16

TABLE 6.3.2 COMPARATIVE VALUES OF STRESSES AND DISPLACEMENTS AROUND A SPHERICAL CAVITY IN AN INFINITE MASS SUBJECT TO A UNIT UNIAXIAL FIELD STRESS FOR THE FOUR LOAD ELEMENT MODEL OF THE SPHERICAL CAVITY AS SHOWN IN FIG.6.3.1 BY DASHED LINES, WHERE THE COORDINATES OF THE POINTS N ARE GIVEN IN TABLE 6.3.1

$E = 1.0$ $\nu = 0.2$

	Analytical results						AXSYM results					
	N	σ_r	σ_θ	σ_z	τ_{zr}	u_r	u_z	σ_r	σ_θ	σ_z	τ_{zr}	u_r	u_z
(a)	4	-0.425	-0.487	-0.011	0.069	3.20	-98.71	-0.549	-0.612	0.0	0.0	4.83	-70.94
	12	0.195	-0.343	0.089	-0.132	11.20	-82.85	0.0	-0.302	1.086	0.0	17.86	-35.74
	19	0.398	-0.186	0.672	-0.517	15.85	-61.00	1.027	-0.294	0.0	0.0	24.82	-39.93
	27	0.050	-0.013	1.886	-0.306	19.74	-16.00	0.0	0.005	2.179	0.0	22.80	-18.27
								AXSYM (1) results					
(b)	4	-0.425	-0.487	-0.011	0.069	3.20	-98.71	-0.355	-0.427	-0.011	0.069	2.47	-93.43
	12	0.195	-0.343	0.089	-0.132	11.20	-82.85	0.195	-0.268	0.223	-0.132	8.49	-75.74
	19	0.398	-0.186	0.672	-0.517	15.85	-61.00	0.221	-0.121	0.835	-0.564	10.99	-52.68
	27	0.050	-0.013	1.886	-0.306	19.74	-16.00	0.050	-0.004	1.819	-0.306	16.79	-14.98
								AXSYM (2) results					
	N	σ_m	σ_θ	σ_n	τ_{nm}	u_m	u_n	σ_m	σ_θ	σ_n	τ_{nm}	u_m	u_n
(c)	4	-0.436	-0.487	0.0	0.0	18.95	-96.93	-0.504	-0.682	0.0	0.0	21.70	-95.71
	12	0.284	-0.343	0.0	0.0	55.67	-62.37	0.434	-0.323	0.0	0.0	54.75	-59.99
	19	1.216	-0.157	0.0	0.0	55.67	-17.63	1.058	-0.171	0.0	0.0	55.40	-19.17
	27	1.936	-0.013	0.0	0.0	18.95	16.93	2.037	-0.005	0.0	0.0	20.83	17.82

Note: Underlined digit indicates prescribed traction component

By replacing the stepped surface by a spherical surface, a significant improvement was obtained in the accuracy of the results, as shown in Table 6.3.2(b). In this representation, the traction components parallel to the r- and z-axis for points on the unloaded surface do not vanish. Their values were obtained by use of the equations for stress transformation from spherical (polar) coordinates to rectangular coordinates. The Author found that the version of these equations given by Terzaghi and Richart (1952) is incorrect. In particular the sign of the shear stress component is reversed in the shear stress transformation equation and in all the related tables. This error also appears in the reproduction of their results in Poulos and Davis (1974).

The specification of boundary conditions in the way described above is rarely possible. Therefore the original program was altered to accept normal and tangential components of boundary traction. This version was called AXSYM (2) and the original program was renamed AXSYM (1). At the same time the number of points for Gaussian integration was increased from 5 to 10, and the number of terms in the polynomial approximation for complete elliptic integrals was increased from 3 to 5. Comparative runs were made for the four element model of the spherical cavity. The results for these and for the analytical solution are given in Table 6.3.2(c). The significant improvements noted earlier are maintained, but the quality of the results are otherwise unchanged. It is noted that the corresponding values for the fictitious load intensities acting on load elements denoted by the symbols q_r and q_z in Table 6.3.3, for the four element spherical model using AXSYM (1) and AXSYM (2) are quite different, although the results in both cases are relatively accurate.

TABLE 6.3.3 COMPARATIVE VALUES OF FICTITIOUS LOAD INTENSITIES q_r AND q_z ACTING IN THE r AND z DIRECTIONS RESPECTIVELY FOR THE FOUR ELEMENT MODEL OF THE SPHERICAL CAVITY IN AN INFINITE MASS SUBJECT TO UNIT UNIAXIAL FIELD STRESS SHOWN IN FIG. 6.3.1 BY DASHED LINES, WHERE THE COORDINATES OF THE POINTS N ARE GIVEN IN TABLE 6.3.1

	AXSYM (1) results		AXSYM (2) results	
N	q_r	q_z	q_r	q_z
4	-0.50	6.52	10.34	9.72
12	11.52	-3.22	6.41	-6.89
19	3.39	-10.78	5.55	-6.04
27	-5.59	0.13	-6.20	-5.38

It is of interest to investigate the performance of AXSYM (2) using its power as fully as can be conveniently arranged. Therefore 30 load elements and corresponding points with mirror symmetry were used to model a spherical cavity as shown by the full lines in Fig. 6.3.1. The coordinates of the points on the surface of the spherical cavity are given in Table 6.3.1. For unit hydrostatic field stress the results obtained are close to those for the analytical solution. The tangential surface stress in the r-z plane given in Table 6.3.4 are seen to be in good agreement generally with the closed form solution value of 1.5.

TABLE 6.3.4 VALUES OF TANGENTIAL SURFACE STRESSES σ_m AROUND A SPHERICAL CAVITY IN AN INFINITE MASS SUBJECT TO UNIT HYDROSTATIC FIELD STRESS FOR A 30 ELEMENT MODEL AS SHOWN IN FIG. 6.3.1 BY SOLID LINES, WHERE THE COORDINATES OF THE POINTS N ARE GIVEN IN TABLE 6.3.1

N	σ_m	N	σ_m	N	σ_m
1	1.432	11	1.517	21	1.585
2	1.756	12	1.437	22	1.616
3	1.450	13	1.488	23	1.430
4	1.449	14	1.465	24	1.465
5	1.538	15	1.213	25	1.529
6	1.488	16	1.589	26	1.494
7	1.524	17	1.592	27	1.526
8	1.687	18	1.543	28	1.543
9	1.394	19	1.518	29	1.397
10	1.443	20	1.516	30	1.536

Adequate representation of the spherical cavity by fewer than 30 elements is clearly desirable using AXSYM (2). Using mirror symmetry several different arrangements of 16 load elements were tried. Two arrangements are shown in Fig. 6.3.2 by dashed and solid lines and labelled A and B respectively. The corresponding surface points for each arrangement were the same. Hydrostatic field stress was used for testing because it was thought likely that the results for this

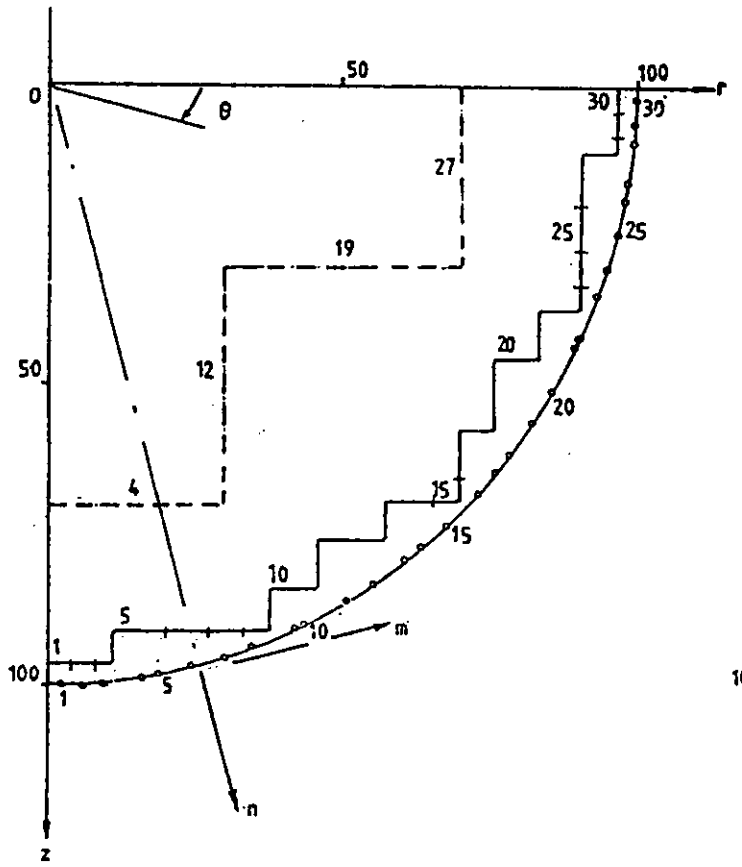


FIG. 6.3.1: LAYOUTS OF 4 AND 30 LOAD ELEMENTS USING MIRROR SYMMETRY FOR A MODEL OF A SPHERICAL CAVITY IN AN INFINITE MASS

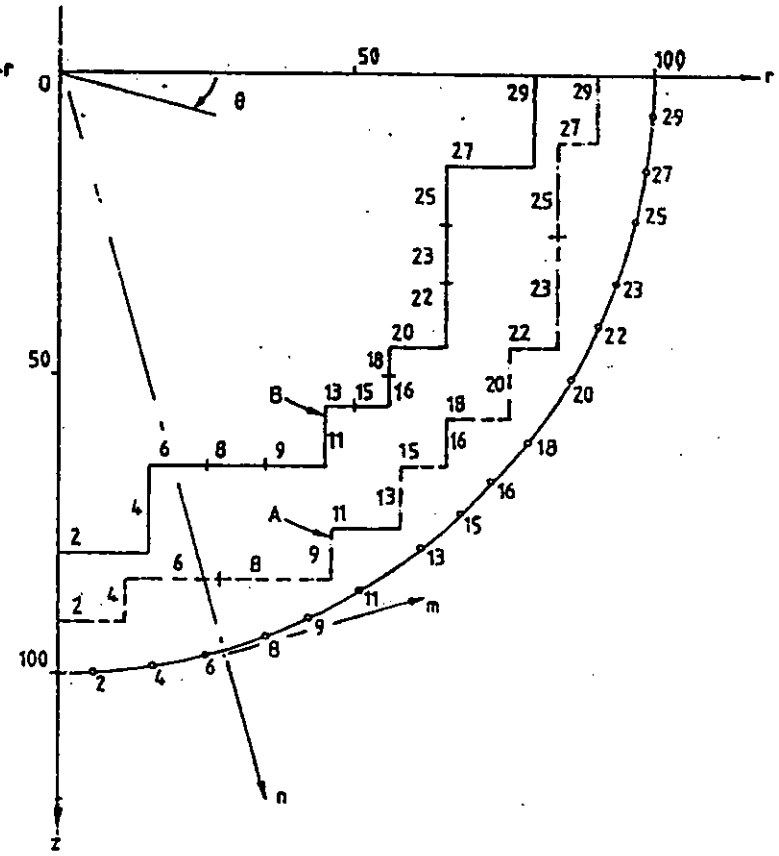


FIG. 6.3.2: LAYOUTS A AND B EACH OF 16 LOAD ELEMENTS USING MIRROR SYMMETRY FOR A MODEL OF A SPHERICAL CAVITY IN AN INFINITE MASS

loading would show up any deficiency quickly and clearly. The tangential surface stresses in the r - z plane for the two arrangements are given in Table 6.3.5. Arrangement A is obviously unsatisfactory, whereas the stress values for arrangement B are remarkably close to the correct value of 1.5. Comparative values for uniaxial field stress given in Table 6.3.6 are also remarkably close to the correct values.

TABLE 6.3.5 COMPARATIVE VALUES OF TANGENTIAL SURFACE STRESSES σ_m AROUND A SPHERICAL CAVITY IN AN INFINITE MASS SUBJECT TO UNIT HYDROSTATIC FIELD STRESS FOR TWO 16-ELEMENT MODELS SHOWN IN FIG. 6.3.2 LABELLED A AND B RESPECTIVELY WHERE THE COORDINATES OF THE POINTS N ARE GIVEN IN TABLE 6.3.1

	Analytical results	AXSYM (2) results A	B
N	σ_m	σ_m	σ_m
2	1.5	1.978	1.480
4	1.5	2.210	1.497
6	1.5	2.096	1.496
8	1.5	2.268	1.500
9	1.5	2.675	1.499
11	1.5	2.101	1.486
13	1.5	-10.631	1.520
15	1.5	11.946	1.499
16	1.5	12.881	1.490
18	1.5	-9.496	1.521
20	1.5	1.595	1.492
22	1.5	2.525	1.498
23	1.5	2.230	1.500
25	1.5	2.082	1.498
27	1.5	2.158	1.500
29	1.5	1.974	1.499

TABLE 6.3.6 COMPARATIVE VALUES OF THE TANGENTIAL SURFACE STRESSES σ_m AROUND A SPHERICAL CAVITY IN AN INFINITE MASS SUBJECT TO UNIT UNIAXIAL FIELD STRESS FOR TWO 16-ELEMENT MODELS, SHOWN IN FIG.6.3.2 LABELLED A AND B RESPECTIVELY, WHERE THE COORDINATES OF THE POINTS N ARE GIVEN IN TABLE 6.3.1

	Analytical results	AXSYM (2) results A	AXSYM (2) results B
N	σ_m	σ_m	σ_m
2	-0.491	-0.386	-0.491
4	-0.436	-0.276	-0.436
6	-0.344	-0.229	-0.344
8	-0.194	-0.050	-0.194
9	-0.059	0.162	-0.059
11	0.150	-0.138	0.145
13	0.430	-2.751	0.438
15	0.656	4.468	0.656
16	0.844	3.033	0.839
18	1.070	-1.950	1.078
20	1.350	1.771	1.347
22	1.559	1.941	1.558
23	1.694	1.960	1.694
25	1.844	2.050	1.843
27	1.936	2.158	1.936
29	1.991	2.147	1.990

The surface of the spherical cavity exhibits constant curvature and symmetry about the origin 0. On the other hand, the arrangement of the load elements of the model of the cavity is symmetric only about the z-axis and in the plane normal to it through the origin 0. The test posed by the spherical cavity is therefore a severe and searching one for the program. The results demonstrate beyond doubt that

problems of this kind can be successfully handled by AXSYM(2). The number of elements required for adequate modelling is not excessive, but considerable user input may be required in choosing a satisfactory arrangement. However once such an arrangement has been obtained it can be reused in different circumstances.

4. Testing of AXSYM

Arrangement B of the load elements shown in Fig. 6.3.2 forms the basis of the models used in dealing with the practical application of AXSYM. Before proceeding to that work, some other problems are considered for which either solutions are available for comparison, or simple checks may be made.

Spherical Shell (Fig. 6.4.1 and Fig. 6.3.2)

A sphere containing a concentric spherical cavity of half its radius was modelled using mirror symmetry by combining the element arrangement B in Fig.6.3.2 and that shown in Fig. 6.4.1. The results given in Table 6.4.1 are in excellent agreement with the closed form solution.

Cylinder with spherical cavity (Fig. 6.4.2 and Fig. 6.3.2)

A cylinder with height equal to diameter containing a concentric spherical cavity of half its diameter was modelled in a similar way to the spherical shell. The exterior element arrangement is shown in Fig. 6.4.2. Unit value of Young's modulus was assumed with Poisson's ratio $\nu = 0.25$. Two loadings were considered: (a) unit hydrostatic pressure externally and internally and (b) unit uniaxial pressure at the plane ends. For case (a) unit pressure was achieved to within 5% at most of the points sampled, but at a few surface points the departure reached a maximum of 26%. For case (b) no analytical solution is available. A check was made for equilibrium in the z-direction, however, and it was found that the load generated by the

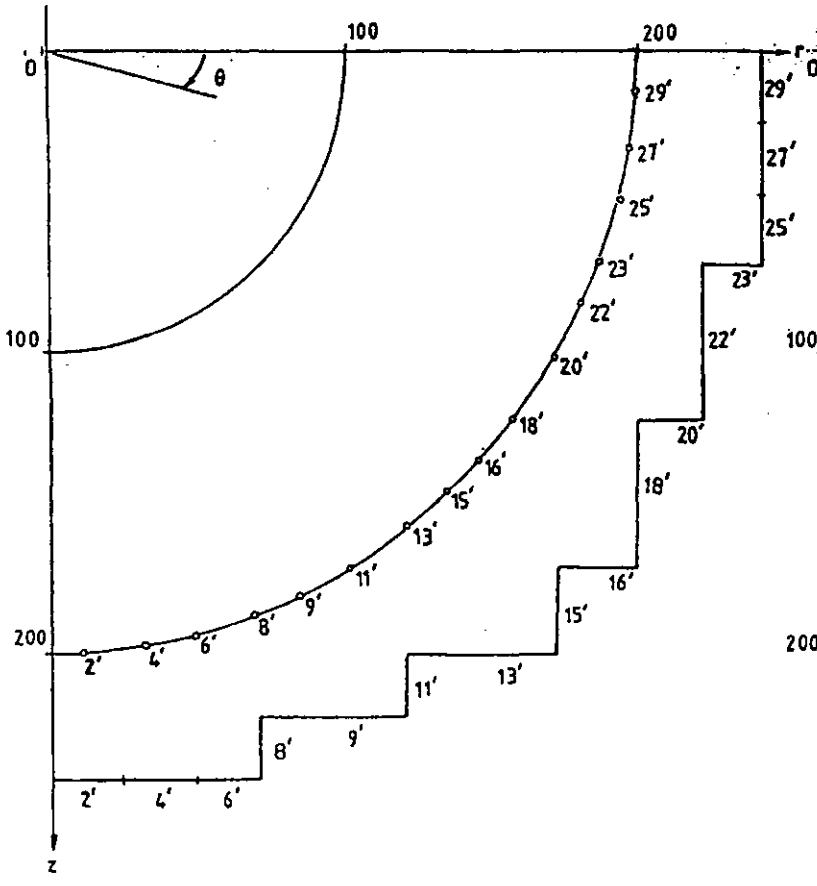


FIG. 6.4.1: LAYOUT OF 16 EXTERIOR LOAD ELEMENTS USING MIRROR SYMMETRY FOR A MODEL OF A SPHERE CONTAINING A SPHERICAL CAVITY OF HALF ITS RADIUS

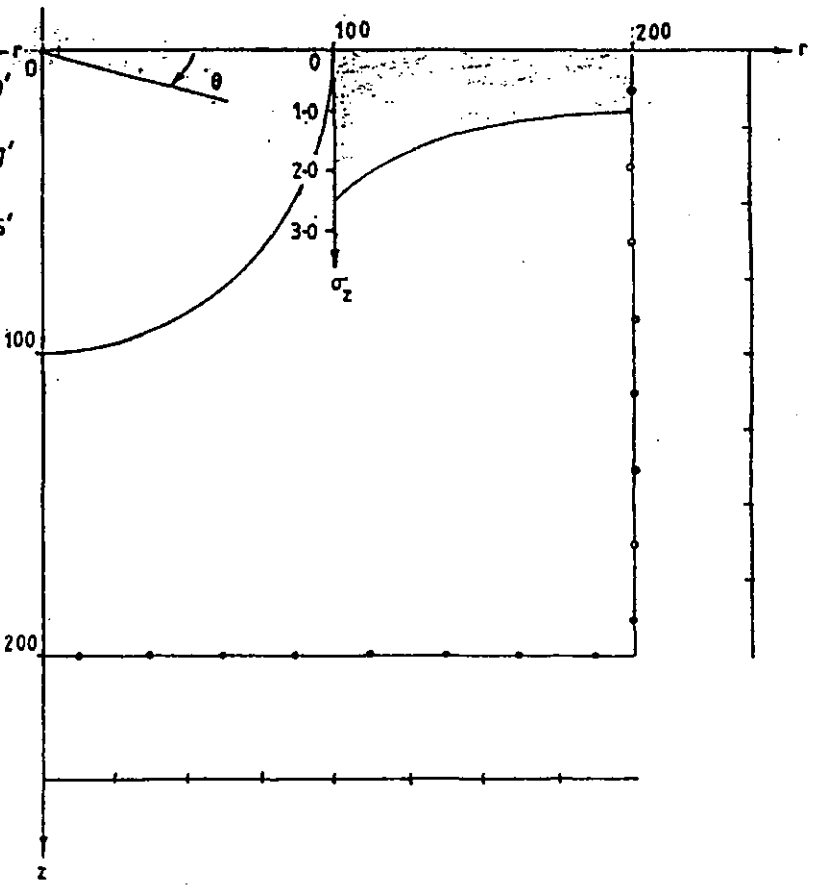


FIG. 6.4.2: LAYOUT OF 16 EXTERIOR LOAD ELEMENTS USING MIRROR SYMMETRY FOR A MODEL OF RIGHT CIRCULAR CYLINDER OF EQUAL HEIGHT AND DIAMETER CONTAINING A SPHERICAL CAVITY OF HALF ITS RADIUS

resulting distribution of normal stress σ_z along the r-axis, shown shaded in Fig. 6.4.2, is within 5% of the applied load.

TABLE 6.4.1. COMPARATIVE VALUES OF STRESSES AND DISPLACEMENTS ALONG THE r-AXIS OF A SPHERICAL SHELL, WITH INTERNAL RADIUS a AND EXTERNAL RADIUS 2a LOADED BY UNIT EXTERNAL PRESSURE AS SHOWN IN FIG.6.3.2 BY ARRANGEMENT B, AND IN FIG. 6.4.1, WHERE THE COORDINATES OF THE POINTS ON THE EXTERNAL SURFACE INDICATED BY DASHED NUMBERS ARE DOUBLE THOSE OF THE CORRESPONDING POINTS ON THE INTERIOR SURFACE

E = 1.0 $\quad\quad$ ν = 0.25 $\quad\quad$ a = 100.0

	Analytical results			AXSYM (2) results			
r/a	σ_r	$\sigma_\theta (=\sigma_z)$	u_r	σ_r	σ_θ	σ_z	u_r
2.0	1.000	1.214	-132.1	1.009	1.220	1.222	-132.4
1.9	0.976	1.226	-128.4	0.982	1.229	1.227	-128.5
1.8	0.947	1.241	-124.9	0.950	1.242	1.241	-127.1
1.7	0.910	1.259	-121.0	0.912	1.260	1.259	-122.0
1.6	0.864	1.282	-119.3	0.865	1.283	1.282	-119.4
1.5	0.804	1.312	-117.5	0.805	1.313	1.312	-117.6
1.4	0.726	1.351	-116.4	0.727	1.352	1.351	-116.5
1.3	0.623	1.403	-116.6	0.623	1.404	1.402	-116.6
1.2	0.481	1.474	-118.2	0.481	1.474	1.473	-118.3
1.1	0.284	1.572	-121.9	0.284	1.573	1.571	-122.0
1.0	0.000	1.714	-128.6	-0.001	1.714	1.712	-128.7

$$\tau_{zr} = u_z = 0$$

Frustum of a cone (Fig. 6.4.3)

Twenty load elements and surface points denoted by numbered line segments and numbered open circles respectively in Fig. 6.4.3, have been used to model a loaded frustum of a cone. The prescribed surface traction are in accordance with the solution for an axial load P at the apex of the cone shown in Fig. 6.4.4. The solution is given in Rekach (1979) using Lamé's coefficients and has been rewritten by the Author as equation (6.4.1) in terms of Young's modulus E and Poisson's ratio ν. The set of transformation equations for the h, v axes shown in Fig. 6.4.4 is given in equation (6.4.2) for convenience. Results obtained using AXSYM (2) are given in Table 6.4.2 for the stresses and displacements along the axis. It can be seen that the radial stresses are disappointingly inaccurate although the correct stress variation is generally achieved. On the other hand, the axial stresses are generally very close to the correct values as are the displacements when rigid body movement has been allowed for.

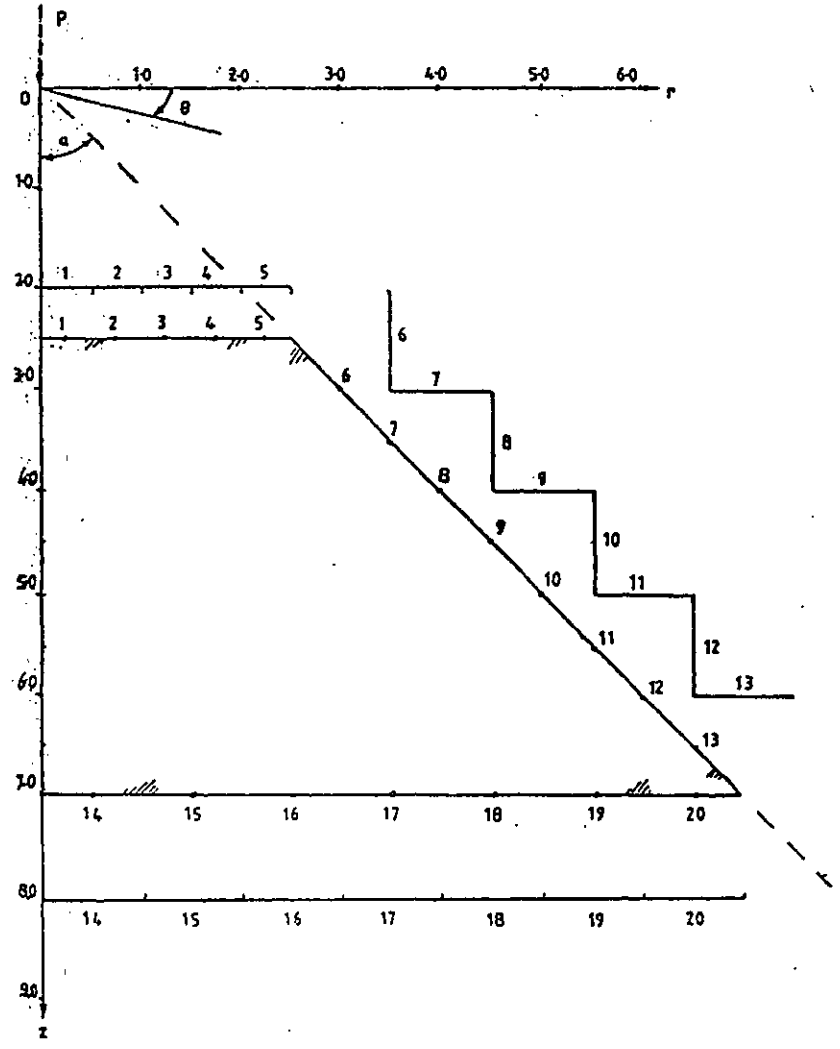


FIG. 6.4.3: LAYOUT OF 20 LOAD ELEMENTS FOR A MODEL OF A RIGHT CIRCULAR FRUSTUM OF A CONE

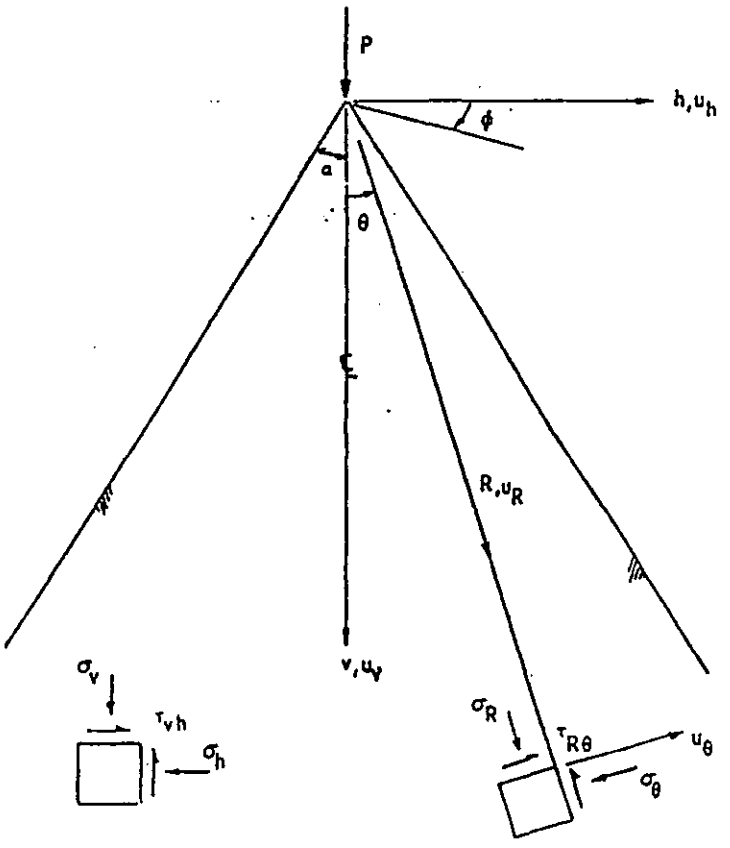


FIG. 6.4.4: INFINITE RIGHT CIRCULAR CONE OF SEMI-ANGLE α WITH A CONCENTRATED AXIAL LOAD P APPLIED AT THE APEX

$$\sigma_R = (C/R^2)((\nu-2)\cos\theta + \tfrac{1}{2}(1+\cos\alpha)(1-2\nu))$$

$$\sigma_\theta = \tfrac{1}{2}(C/R^2)(1-2\nu)(\cos\theta)(1-(1+\cos\alpha)/(1+\cos\theta))$$

$$\sigma_\phi = \tfrac{1}{2}(C/R^2)(1-2\nu)(\cos\theta-(1+\cos\alpha)/(1+\cos\theta))$$

...(6.4.1)

$$\tau_{R\theta} = \tfrac{1}{2}((C/R^2)(1-2\nu)(\sin\theta)(1-(1+\cos\alpha)/(1+\cos\theta))$$

$$u_R = -\tfrac{1}{2}(C/R)(1+\nu)(4(1-\nu)\cos\theta-(1+\cos\alpha)(1-2\nu))/E$$

$$u_\theta = -\tfrac{1}{2}(C/R)(1+\nu)(\sin\theta)(4\nu-3+(1+\cos\alpha)(1-2\nu)/(1+\cos\theta))/E$$

where

$$C = (-P/\pi)(1/(2\nu(1-\cos^3\alpha)+(1-2\nu)(1-\cos\alpha)(1+\cos^2\alpha))) .$$

$$\sigma_h = \tfrac{1}{2}(\sigma_R+\sigma_\theta) - \tfrac{1}{2}(\sigma_R-\sigma_\theta)\cos 2\theta + \tau_{R\theta}\sin 2\theta$$

$$\sigma_v = \tfrac{1}{2}(\sigma_R+\sigma_\theta) + \tfrac{1}{2}(\sigma_R-\sigma_\theta)\cos 2\theta - \tau_{R\theta}\sin 2\theta$$

$$\tau_{vh} = \tau_{R\theta}\cos 2\theta + \tfrac{1}{2}(\sigma_R-\sigma_\theta)\sin 2\theta$$

...(6.4.2)

$$u_h = u_R\sin\theta + u_\theta\cos\theta$$

$$u_v = u_R\cos\theta - u_\theta\sin\theta$$

TABLE 6.4.2 COMPARATIVE VALUES OF STRESSES AND DISPLACEMENTS ALONG THE AXIS OF THE FRUSTUM OF A CONE, AS SHOWN IN FIG. 6.4.3 LOADED ACCORDING TO THE SOLUTION FOR AN AXIAL LOAD P AT THE APEX OF AN INFINITE CONE WITH SEMI-ANGLE α GIVEN IN EQUATION (6.4.1)

$P = 10.0$ $E = 1.0$ $\nu = 0.25$ $\alpha = 45^{\circ}$

	Analytical results				AXSYM (2) results			
z	σ_r	σ_z	u_z	Δu_z	σ_r	σ_z	u_z	Δu_z
2.5	-0.034	1.241	3.146		-0.060	1.246	1.629	
				-0.524				-0.532
3.0	-0.024	0.862	2.622		-0.049	0.859	1.097	
				-0.375				-0.377
3.5	-0.018	0.633	2.247		-0.033	0.626	0.720	
				-0.281				-0.280
4.0	-0.013	0.485	1.966		-0.021	0.477	0.440	
				-0.218				-0.216
4.5	-0.011	0.383	1.748		-0.013	0.376	0.244	
				-0.175				-0.171
5.0	-0.009	0.310	1.573		-0.008	0.305	0.053	
				-0.143				-0.141
5.5	-0.007	0.256	1.430		-0.003	0.253	-0.088	
				-0.119				-0.116
6.0	-0.006	0.216	1.311		0.000	0.215	-0.204	
				-0.101				-0.100
6.5	-0.005	0.184	1.210		0.005	0.186	-0.304	
				-0.086				-0.085
7.0	-0.004	0.158	1.124		0.015	0.166	-0.389	

$\sigma_\theta = \sigma_r$ $\tau_{zr} = u_r = 0$

5. Practical application of AXSYM

Results in Appendix A 6.2 are for two major analyses made with AXSYM (2) and a combination of two sets of 16 load elements and corresponding points. For the first analysis the intrinsic arrangement of the elements of one of the sets is as shown in Fig. 6.3.2 by arrangement B, with the elements of the second set coincident with the position of the first when reflected in the z-axis. Additional symmetry is then used to complete the structure. A series of complete circular toric tunnels in an infinite mass with a void of radius a can be modelled by sliding the whole arrangement of 32 elements a distance c from the origin 0 along the r-axis as shown in Fig. 6.5.1. Results for c/a = 1⅛, 1¼, 1½, 2, 3 and 10, with Poisson's ratio ν = 0.0, 0.25, and 0.49 are given in Table A6.5.1 for uniform radial, axial and hydrostatic field stress of magnitude p. The symbols p_r and p_z denote radial and axial field stress respectively and E is Young's modulus. Although one of the loading cases is redundant all have been given for convenience. Stresses and displacements were calculated at points N = 1 to 22 inclusive around the origin and along normals to the surface of the void at 45° intervals from the axial direction to a depth of one radius.

The two identical spherical cavities of radius a and spaced at a distance 2d, as shown in Fig. 6.5.2, were modelled in the same way to that described above, but with the use of the r and z axes interchanged. Results for d/a = 1⅛, 1¼, 2 and 3 are given in Table A6.5.2 for the same Poisson's ratios and values of field stress.

AXSYM (2) carried out both major analyses without difficulty except for the two identical spherical cavities at d/a = 3 with $\nu = 0.49$. Here very large fictitious loads were generated giving uneven stress values and these results have not been included. The analysis was extended to d/a = 3½, however, where acceptable results were again obtained. A sample result from this calculation is given below for unit hydrostatic field stress with $\nu = 0.49$ at the point N = 14.

N	σ_r	σ_θ	σ_z	τ_{zr}	u_r	u_z
14	-0.001	1.502	1.495	0.004	-0.750	-0.009

All the results for d/a = 3½ are broadly comparable with those at d/a = 2½ given in Table A 6.5.2. Therefore it is considered that the instability is local to d/a = 3 and $\nu = 0.49$.

The small non-zero values for the normal stress at the unloaded surface of the voids which appear in the tables are functions of the approximate method used to analyse the problem. Usually they are relatively small and may be safely ignored. In general these errors are larger in the results of the calculations for the two identical spherical cavities than for the complete circular toric tunnels.

Complete circular toric tunnel (Fig. 6.5.1 and Table A6.5.1)

The following discussion of the results deals only with a few notable conclusions which can be drawn about the induced stresses and is not a comprehensive review. Consider first the principal stresses at the unloaded surface of the tunnel when c/a = 10 for points N = 8, 14 and 20. Values of these stresses are given in Table A6.5.1 and are reproduced below in Tables 6.5.1 and 2. At this relatively large distance from the z-axis the former table shows that the value of σ_r and σ_z are close to those given by plane strain analysis. The stress σ_θ normal to the plane is shown in the latter table to be near the limiting theoretical value for the three Poisson's ratios considered. The limiting theoretical value of σ_θ is obtained from the following equation:

$$0 = \bar{\sigma}_\theta - \nu(\bar{\sigma}_z + \bar{\sigma}_r)$$

where $\bar{\sigma}_\theta = \sigma_\theta - p_r$

$\bar{\sigma}_z = \sigma_z - p_z$

$\bar{\sigma}_r = \sigma_r - p_r$

and ν represent Poisson's ratio.

Results for c/a = 100, which are not included, show a much closer approximation to plane strain values. It is clear that at c/a = 10 these conditions are practically obtained.

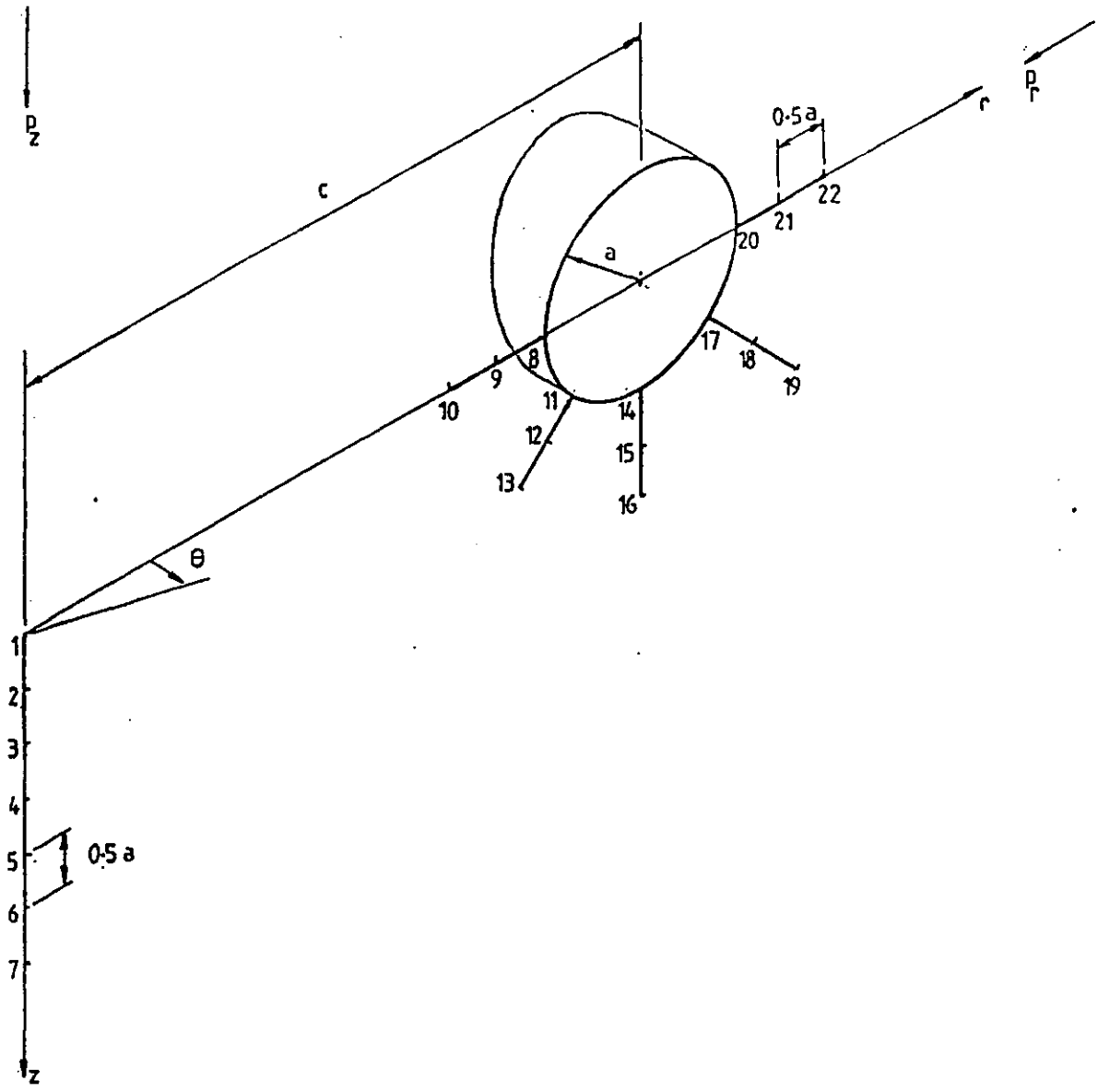


FIG. 6.5.1: COMPLETE CIRCULAR TORIC TUNNEL IN AN INFINITE MASS SUBJECT TO UNIFORM RADIAL AND AXIAL FIELD STRESS (Fig. A 6.5.1 bis)

TABLE 6.5.1 COMPARATIVE VALUES OF THE STRESS COMPONENTS σ_r AND σ_z AT THE SURFACE OF THE TUNNEL SHOWN IN FIG. 6.5.1 WHEN c/a = 10 AT POINTS N = 8, 14, AND 20 GIVEN IN TABLE A6.5.1 FOR POISSON'S RATIO ν = 0, 0.25 AND 0.49

$p_r = 1.0$, $p_z = 0.0$								
	Analytical results		AXSYM (2) results					
	(plane strain)		$\nu = 0.0$		$\nu = 0.25$		$\nu = 0.49$	
N	σ_r	σ_z	σ_r	σ_z	σ_r	σ_z	σ_r	σ_z
8	0.0	-1.0	(-0.003)	-1.003	0.0	-1.006	0.0	-1.013
14	3.0	0.0	2.903	(-0.003)	2.910	(-0.001)	2.911	-0.001
20	0.0	-1.0	(-0.003)	-0.920	0.0	-0.923	0.0	-0.929
$p_r = 0.0$ $p_z = 1.0$								
8	0.0	3.0	(-0.003)	3.082	(-0.001)	3.075	(-0.001)	3.047
14	-1.0	0.0	-0.951	(-0.003)	-0.958	0.0	-0.975	0.0
20	0.0	3.0	(-0.003)	2.889	(-0.001)	2.914	(-0.001)	2.947
$p_r = 1.0$ $p_z = 1.0$								
8	0.0	2.0	(-0.006)	2.078	(-0.001)	2.069	(-0.001)	2.034
14	2.0	0.0	1.952	(-0.006)	1.952	(-0.001)	1.935	(-0.001)
20	0.0	2.0	(-0.005)	1.968	(-0.001)	1.991	(-0.001)	2.018

Brackets indicate the exact value is zero

TABLE 6.5.2 COMPARATIVE VALUES OF THE STRESS COMPONENT σ_θ AT THE SURFACE OF THE TUNNEL SHOWN IN FIG. 6.5.1 WHEN c/a = 10 AT POINTS N = 8, 14, AND 20 GIVEN IN TABLE A6.5.1 FOR POISSON'S RATIO ν = 0, 0.25 AND 0.49

$p_r = 1.0$, $p_z = 0.0$						
Analytical results (plane strain)				AXSYM (2) results		
N	$\nu = 0.0$	$\nu = 0.25$	$\nu = 0.49$	$\nu = 0.0$	$\nu = 0.25$	$\nu = 0.49$
8	1.0	0.5	0.02	0.781	0.303	-0.131
14	1.0	1.5	1.98	1.008	1.489	1.953
20	1.0	0.5	0.02	1.170	0.686	0.199
$p_r = 0.0$, $p_z = 1.0$						
8	0.0	0.5	0.98	0.107	0.576	0.990
14	0.0	-0.5	-0.98	-0.008	-0.499	-0.975
20	0.0	0.5	0.98	-0.086	0.419	0.944
$p_r = 1.0$, $p_z = 1.0$						
8	1.0	1.0	1.0	0.887	0.879	0.860
14	1.0	1.0	1.0	1.000	0.991	0.978
20	1.0	1.0	1.0	1.084	1.105	1.143

As c/a decreases the changes in the principal stresses σ_θ and σ_z can be traced on the inner and outer face of the tunnel at points N = 8 and 20. For Poisson's ratio $\nu = 0.25$, and c/a = 10, 3 and $1\frac{1}{2}$, these values are given in Table A6.5.1 and are reproduced in Table 6.5.3 below. By considering the stress pairs at each of the points it is seen that as c/a reduces the principal stress differences on the inner face increase sharply but decrease on the outer face. The corresponding principal stress sums increase significantly on the inner face but only slightly on the outer face. Such information might well have an important bearing on the design of tunnels through certain materials.

TABLE 6.5.3 VALUES OF THE STRESS COMPONENTS σ_θ and σ_z AT THE SURFACE OF THE TUNNEL SHOWN IN FIG. 6.5.1, WHEN c/a = 10, 3, $1\frac{1}{2}$ AT POINTS N = 8 AND 20 GIVEN IN TABLE A 6.5.1 FOR POISSON'S RATIO $\nu = 0.25$

$p_r = p_z = 1$

	σ_θ		σ_z	
c/a	N = 8	N = 20	N = 8	N = 20
10	0.879	1.105	2.069	1.991
3	0.627	1.260	2.465	2.008
$1\frac{1}{2}$	0.406	1.349	3.725	1.984

At c/a = 10, the effect of the tunnel on the stresses near the origin is very small. In particular, the shading by the tunnel is negligble for a radial stress field. At the other extreme , with the tunnel closely coiled around the z-axis when c/a = $1\frac{1}{2}$, there are large variations in all the stresses and they vary noticeably with Poisson's ratio.

Two identical spherical cavities (Fig. 6.5.2 and Table A6.5.2)

Stress patterns induced in infinite masses by two identical spherical cavities are similar in several ways to those due to a complete circular toric tunnel. In other ways the patterns are quite different. But rather than pursue a general discussion of this kind it it thought that the attention should be restricted to the following two items. The first is Table 6.5.4 where a comparison is made with some results published by Sternberg and Sadowsky (1952). The second is a set of ratios indicating how the shape of the two spherical cavities changes as d/a is reduced in a hydrostatic stress field when Poisson's ratio $\nu = 0.49$.

The values given in Table 6.5.4. below show that AXSYM (2) has calculated the non-vanishing surface stresses to within 5% of Sternberg and Sadowsky's (1952) results.

TABLE 6.5.4 COMPARATIVE VALUES OF THE STRESS COMPONENTS σ_θ AND σ_z AT THE SURFACES OF THE TWO IDENTICAL SPHERICAL CAVITIES SHOWN IN FIG. 6.5.2 WHEN d/a = 2 AT POINTS N = 8, 14 & 20 GIVEN BY STERNBERG & SADOWSKY (1952) AND IN TABLE A6.5.2 WHEN POISSON'S RATIO $\nu = 0.25$

$p_r = p_z = 1$

	Sternberg & Sadowsky (1952)results			AXSYM (2) results		
N	σ_r	σ_θ	σ_z	σ_r	σ_θ	σ_z
8	1.57	1.57	0.000	1.624	1.624	(0.138)
14	0.00	1.50	1.47	(-0.004)	1.510	1.469
20	1.51	1.51	0.00	1.435	1.435	(-0.031)

Brackets indicate the exact value is zero.

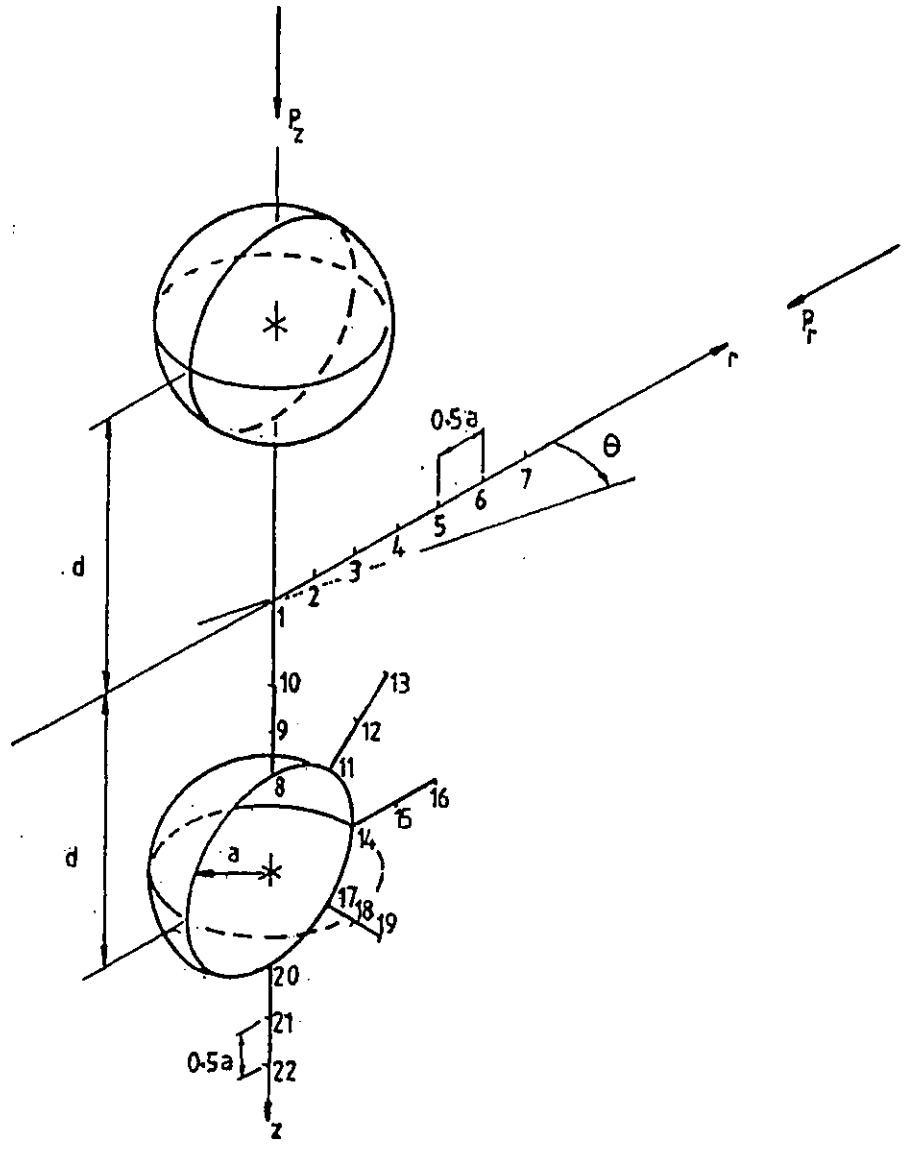


FIG. 6.5.2: TWO IDENTICAL SPHERICAL CAVITIES IN AN INFINITE MASS SUBJECT TO UNIFORM RADIAL AND AXIAL FIELD STRESS (Fig. A 6.5.2 bis)

Results given in Table A6.5.2. for a hydrostatic stress field where Poisson's ratio $\nu = 0.49$ show that the amount of compression parallel to the r-axis of two identical spherical cavities remains approximately the same as the ratio d/a is reduced from $2\frac{1}{2}$ to $1\frac{1}{2}$. On the other hand, the compression parallel to the z-axis is about $\frac{1}{3}$ less. Most of this reduction is due to the near faces of the two spherical cavities compressing less than the far faces. Hence as d/a is reduced the deformed shape of the two identical spherical cavities become like two identical imaginary dewdrops pendent from the origin 0 in opposite directions. Results for $d/a = 5$, which are not included, show that there is almost no interaction between the two identical spherical cavities.

6. Summary and conclusions

In calculating the large number of results given above AXSYM (2) has generally performed very well. Each computer run consumed about one unit on the CDC 7600 at ULCC. The total number of units used was approximately 500 and includes those used for the program testing and developing. Some of the methods used to reduce the amount of data preparation for the two major analyses were unusual and relatively inefficient in the use of machine time and storage.

Where possible the results obtained using AXSYM (2) have been checked against closed form solutions or published results and generally they are in good agreement. Where the results cannot be checked directly they have been shown to be consistent with equilibrium or to be self-consistent in various ways. Nevertheless, the calculated values should be treated with some caution, at least until and unless selected representative results are supported by one or more independent method. It is suggested that the computer program written by Watson (1979) or by Mayr et al. (1980) may be suitable for this work.

CHAPTER 7 CONCLUSION

1. Review

Engineering considerations principally determined the selection of the mathematical models which were developed and applied in the previous chapters. In particular, the choice of linear elastic continuum models is due to their general suitability for the problems considered as well as their relative simplicity and availability. Their key characteristic, however, is superposition.

In Chapter 2, the Author used linearity and superposition, often with dimensional analysis, to obtain solutions for models for the response of inhomogeneous ground to static surface loading. Speed of operation and efficiency were minor considerations in the evaluation by use of the computer of some of the resulting expressions.

In contrast, computing time considerations together with those of the scope and availability of some of the facilities in the existing computer programs used, and of the storage requirements for certain operations, were all of importance in the back analyses in Chapters 3 and 4. Some unusual analytical models had to be devised partly as a result of these factors. Despite the large size and complexity of the structures, their analysis based on these models were generally made with tolerable accuracy and the results obtained contributed to the understanding of their performance. All the results found by the Author were comparable with those of other researchers using different methods.

Because of certain mathematical difficulties, an auxiliary boundary was used in the Author's new computer program AXSYM as described in Chapters 5 and 6. Although this feature meant that a considerable user contribution was required in specifying some of the problems to be solved, it did not prevent the calculations of many results, given in Appendix A 6.5, which, it is thought, may be useful in the analysis of some underground structures.

2. Potential developments

The model for the response of inhomogeneous ground to surface loading presents problems of interpretation because the shear modulus vanishes at the surface. To overcome them it is suggested that the Author's solutions for surface loading could be used in the manner of the indirect formulation of the boundary integral method using an auxiliary boundary. In this way it may be possible to load a plane or other boundary in any prescribed way at some depth beneath the surface where the shear modulus does not vanish.

The models for the back analyses may be improved by the inclusion of more details of the original structure. The scope is limited, however, by the lack of certain facilities in the existing programs. Developments which would be welcome would allow the ready specification of both extensive single and multiple planes of weakness and of gradual variation of the elastic constants.

The necessity to choose suitable auxiliary boundaries with AXSYM (2) makes it hard to use. Difficulties encountered in evaluating certain mathematical limits which are closely linked to its inclusion may, perhaps, be removed without introducing other problems, by assuming that the intensity of element loading is proportional to the distance from the axis of symmetry.

3. Summary

This work deals with practical and theoretical aspects of investigating the structural behaviour of earthworks using mathematical models and back analyses. It is clear even from the limited variety of problems considered that there is a need in such investigations for imagination, approximation, and interpretation, just as there is for rigorous analysis. It is the concluding point of the thesis that such an approach has been shown to be essential in this field of engineering.

REFERENCES

ABRAMOWITZ M. and STEGUN I.A. (1970) Handbook of Mathematical Functions. Dover Publications.

ALEXANDER L.G. (1977) Discussion: Some results concerning displacements and stresses in a non-homogeneous elastic half-space. Géotechnique 27, No. 2, 253-254.

AWOJOBI A.O. and GIBSON R.E. (1973) Plane strain and axially symmetric problems of a linearly non-homogeneous elastic half-space. Q. Jnl Mech. Appl. Math.26, 285-302.

BRAY J.W. (1981) personal commumication.

BRAY J.W. (1982) personal communication.

BROWN P.T. and GIBSON R.E. (1979) Surface settlements of a finite elastic layer whose modulus increases linearly with depth. Int. J. Num. Analyt. Meth. Geomech. 3, No. 1, 37-47.

BURLAND J.B. (1969) Reply to discussion. Proc. Conf. on In Situ Investigations in Soils and Rocks. British Geotechnical Society, London.

BURLAND J.B. and LORD J.A. (1969) The load-deformation behaviour of Middle Chalk at Mundford, Norfolk; a comparison between full-scale performance and in situ and laboratory measurements. Proc. Conf. on In situ Investigations in Soils and Rocks, British Geotechnical Society, London.

BURLAND J.B., MOORE J.F.A. and SMITH P.D.K. (1972) A simple and precise borehole extensometer. Géotechnique 22, No. 1, 174-177.

BURLAND J.B. and MOORE J.F.A. (1973) The measurement of ground displacement around deep excavations. Proc. Symp. Field Instrumentation, British Geotechnical Society, London, 70-84.

BURLAND J.B., SILLS G.C. and GIBSON R.E. (1973) A field and theoretical study of the influence of non-homogeneity on settlement. Proc. 8th Int. Conf. Soil Mech., Moscow 1.3, 39-46.

BURLAND J.B. (1977) personal communication.

BURLAND J.B., LONGWORTH T.I. and MOORE J.F.A. (1977) A study of ground movement and progressive failure caused by a deep excavation in Oxford Clay. Géotechnique 27, No. 4, 557-591.

BURLAND J.B. (1978) Applications of the finite element method to prediction of ground movements. Developments in Soil Mechanics - 1 (ed. C.R. Scott) Applied Science Publishers, London.

CALLADINE C.R. and GREENWOOD J.A. (1978) Line and point loads on a non-homogeneous incompressible elastic half-space. Q. Jnl Mech. Appl. Math. 31, 507-529.

GAZIEV E.G. and ERLIKHMAN S.A. (1971) Stresses and strains in anisotropic rock foundation (model studies). Proc. of the International Symposium on Rock Mechanics, Nancy, II-1.

GIBSON R.E. (1967) Some results concerning displacements and stresses in a non-homogeneous elastic half-space. Géotechnique 17, No.1, 58-67 (see also corrigenda: 18, No. 2, 275-276; 19, No. 1, 160-161).

GIBSON R.E. (1974) Fourteenth Rankine Lecture: The analytical method in soil mechanics. Géotechnique 24, No. 2, 115-140.

LACHAT J.C. and WATSON J.O. (1975) A second generation boundary integral equation program for three dimensional elastic analysis. Boundary Integral Equation Method: Computational Applications in Applied Mechanics (eds. T.A. Cruse and F.J. Rizzo), ASME, New York, 85-100.

LEKHNITSKII S.G. (1962) Radial distribution of stresses in a wedge and in a half-plane with variable modulus of elasticity. Prinkl. Mat. Mekh, 26,1.

MAYR M., DREXLER W. and KUHN G. (1980) A semianalytical boundary integral approach for axisymmetric elastic bodies with arbitrary boundary conditions. Int. J. Solids Structures, Vol. 16, 863-871.

NEUBER J. (1946) Theory of notch stresses. Edwards Bros., Ann Arbor, Michigan.

PALMER A.C. and RICE J.R. (1973) The growth of slip surfaces in the progressive failure of overconsolidated clay. Proc. Roy. Soc. Series A, 332, 527-548.

POULOS J.G. and DAVIS E.H. (1974) Elastic solutions for soil and rock mechanics. John Wiley and Sons, New York.

REKACH V.G. (1979) Manual of the theory of elasticity. MIR Publishers, Moscow.

RIZZO F.J. (1967) An integral equation approach to boundary value problems of classical elastostatics. Quart. Appl. Math., Vol. 25, 83-95.

STERNBERG E. and SADOWSKY M.A. (1952) On the axisymmetric problem of the theory of elasticity for an infinite region containing two spherical cavities. Journal of Applied Mechanics, Vol. 19, 19-27.

TERZAGHI K. and RICHART F.E. (1952) Stresses in rock around cavities. Géotechnique, Vol. 3, 57-90.

TIMOSHENKO S. and GOODIER J.N. (1951) Theory of elasticity, McGraw-Hill, New York.

WATSON J.O. (1972) The analysis of thick shells with holes, by integral representation of displacement. Ph.D. Thesis, Univ. of Southampton, U.K.

WATSON J.O. (1979) Program for three dimensional elastic analysis: Specification for input data (unpublished).

WARD W.H., BURLAND J.B. and GALLOIS R.W. (1968) Geotechnical assessment of a site at Mundford, Norfolk, for a large proton accelerator. Géotechnique 18, No. 4, 399-431.

APPENDIX A.2

A 2.2(a) - Details of the methods used to perform the double integrals for specific uniformly loaded areas required in the expression for the surface settlement of a linear elastic, isotropic half-space, where the shear modulus is proportional to depth and Poisson's ratio is an arbitrary constant.

It is required to obtain the integral,

$$I = \iint_A \frac{dx\,dy}{x^2+y^2} \qquad \ldots(A\ 2.2.1)$$

for the areas A shown hatched in Fig. A 2.2.1. Note that the symbols a,b represent pure lengths between various points on the figures and are therefore always positive.

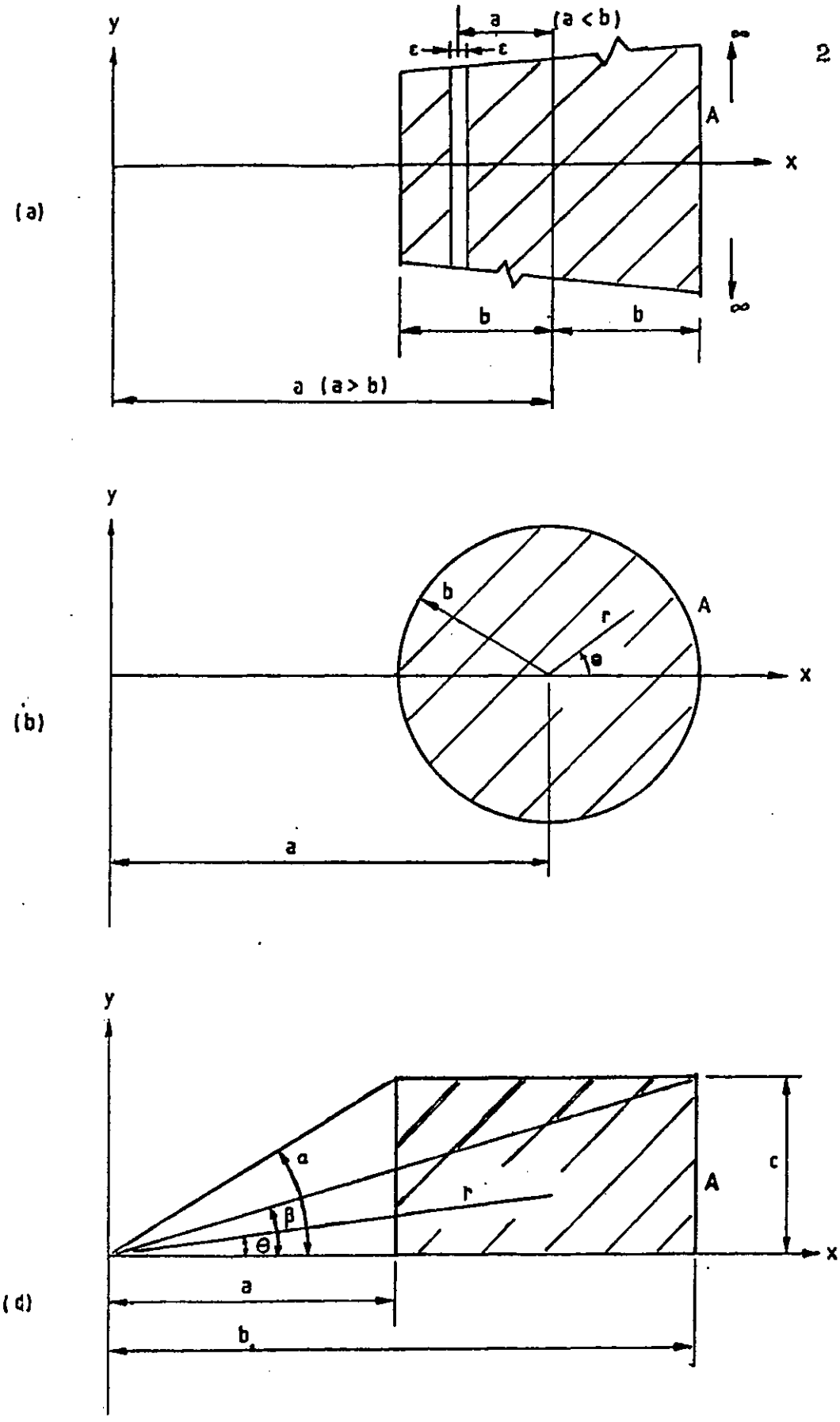


FIG. A 2.2.1: (a) INFINITE STRIP, (b) CIRCULAR AND (c) RECTANGULAR AREAS OF INTEGRATION FOR EQUATION A 2.2.1

For the infinite strip A shown in Fig. A.2.2.1(a)

$$I = \int_{x=a-b}^{a+b} \int_{y=-\infty}^{\infty} \frac{dx\, dy}{x^2+y^2}$$

$$I = 2 \int_{a-b}^{a+b} \left(\frac{1}{x} \tan^{-1} \frac{y}{x}\right)_{y=0}^{\infty} dx$$

$$I = \pm\pi \int_{a-b}^{a+b} \frac{dx}{x} \qquad \begin{matrix} , x > 0 \\ , x < 0 \end{matrix}$$

$$I = \begin{cases} \pi \log \left| \dfrac{a+b}{a-b} \right| & , \ a > b \\ \pi \left(\log \left| b^2 - a^2 \right| - \log(\varepsilon^2)\right) & , \ a < b \end{cases}$$

where the width 2ε of the thin strip shown in Fig. A 2.2.1(a), forming an area of exclusion, tends to zero.

For the circular area A shown in Fig. A 2.2.1(b), polar coordinates r, θ are used, where

$$x = a + r\cos\theta \quad , \quad y = r\sin\theta$$

We have, after substitution,

$$I = \int_{r=0}^{b} \int_{\theta=0}^{2\pi} \frac{r\, d\, r\, d\, \theta}{a^2 + r^2 + 2ar\cos\theta}$$

$$I = 4\int_{0}^{b} \left(\frac{1}{a^2 - r^2} \tan^{-1} \frac{a-r}{a+r} + \frac{1}{a^2 - r^2} \tan^{-1} \frac{a+r}{a-r} \right) r dr$$

$$I = \pm\pi \int_{0}^{b} \frac{2rdr}{a^2 - r^2} \quad , r < a \quad , r > a$$

The solutions are obtained in a similar way to the infinite strip described above. A thin concentric area of exclusion, which is omitted from Fig. A 2.2.1(b), is used for the interior case (a < b).

Integration is carried out separately for the two parts of the rectangle area A, shown hatched by single and double lines respectively, in Fig. A 2.2.1(c). Polar coordinates r, θ are used, such that

$$x = r\cos\theta \quad , \qquad y = r\sin\theta$$

Separation following substitution gives

$$I = \int_{\theta=0}^{\beta} \int_{r=\frac{a}{\cos\theta}}^{\frac{b}{\cos\theta}} \frac{dr d\theta}{r} + \int_{\theta=\beta}^{\alpha} \int_{r=\frac{a}{\cos\theta}}^{\frac{c}{\sin\theta}} \frac{dr d\theta}{r}$$

$$I = (\theta \log|\tan\theta|)_{\beta}^{\alpha} - \int_{\beta}^{\alpha} \log|\tan\theta| \, d\theta$$

$$I = \int_{\beta}^{\alpha} \frac{2\theta d\theta}{\sin 2\theta}$$

where $\alpha = \tan^{-1}\frac{c}{a}$ and $\beta = \tan^{-1}\frac{c}{b}$ as shown in Fig. A 2.2.1(c).

To obtain a form which does not contain an integral, we use the infinite series,

$$\log\left|\frac{\tan\theta}{\theta}\right| = a_2\theta^2 + a_4\theta^4 + \cdots + a_{2s}\theta^{2s} + \cdots \quad , \quad s = 1,2,\ldots$$

The values of a_2, a_4, etc., may be obtained by differentiation, series expansion, and equating coefficients. It follows that

$$\int_{\beta}^{\alpha} \log|\tan\theta| \, d\theta = (\theta \log|\theta| - \theta)_{\beta}^{\alpha} + \left(\sum_{s=1}^{\infty} \frac{a_{2s}}{2s+1}\theta^{2s+1}\right)_{\beta}^{\alpha}$$

For the interior case, thin strips forming areas of exclusion similar to the infinite strip analysis are used with superposition.

A 2.2 (b) - Listing of the computer program GSETT used in calculating surface settlements for a uniformly loaded rectangular area on the surface of an isotropic linear elastic half-space where the shear modulus is proportional to depth and Poisson's ratio is constant

```
      PROGRAM GSETT (INPUT,OUTPUT,TAPE1=INPUT,TAPE2=OUTPUT)
C     OBTAINS SCALED SURFACE SETTLEMENT
      DATA RTD /57.29578/
      DATA LUI,LUO /1,2/
      READ (LUI,100) NP
  100 FORMAT (3X,I2)
      WRITE (LUO,200)
  200 FORMAT (1H1)
      WRITE (LUO,201)
  201 FORMAT (/  43H     PT      OPF        ADF        THF      GTHF,
     1 52H          OPN        ADN        THN      GTHN      DGTH)
      DO 1 IA=1,NP
      READ (LUI,101) OPF,ADF,OPN,ADN
  101 FORMAT (4F10.0)
      TF=RTD*ATAN (OPF/ADF)
      TN=RTD*ATAN (OPN/ADN)
      CALL GLIST (TF,GTF)
      CALL GLIST (TN,GTN)
      DGT=GTF-GTN
      WRITE (LUO,202) IA,OPF,ADF,TF,GTF,OPN,ADN,TN,GTN,DGT
  202 FORMAT (1X,I5,3F10.3,1F10.6,2X,3F10.3,2F10.6)
    1 CONTINUE
      END


      SUBROUTINE GLIST (TH,GTH)
C     OBTAINS GTH CORRESPONDING TO TH
C     USING LINEAR INTERPOLATION
      DIMENSION GTP(45),GTN(45),GT(2)
      DATA GTP /0.915966,0.898511,0.881050,0.863574,0.846077,
     1          0.828551,0.810990,0.793386,0.775731,0.758019,
     2          0.740241,0.722390,0.704459,0.686439,0.668322,
     3          0.650101,0.631765,0.613308,0.594720,0.575991,
     4          0.557113,0.538076,0.518869,0.499483,0.479907,
     5          0.460129,0.440138,0.419922,0.399469,0.378765,
     6          0.357797,0.336551,0.315012,0.293164,0.270991,
     7          0.248477,0.225602,0.202348,0.178695,0.154621,
     8          0.130115,0.105123,0.079648,0.053656,0.027116/
      DATA GTN /0.0,0.027726,0.056096,0.085147,0.114918,
     1          0.145453,0.176797,0.209000,0.242116,0.276202,
     2          0.311321,0.347543,0.384940,0.423957,0.463601,
     3          0.505051,0.548057,0.592738,0.639228,0.687675,
     4          0.738247,0.791130,0.846536,0.904705,0.965909,
     5          1.030464,1.098732,1.171134,1.248165,1.330412,
     6          1.418572,1.513492,1.616204,1.727993,1.850478,
     7          1.985743,2.136535,2.306575,2.501083,2.727704,
     8          2.998295,3.332722,3.768234,4.388459,5.4602697
      IF (TH.LT.0.0) GOTO 999
      IF (TH.GT.89.0) GOTO 999
      ITH=TH
      REM=TH-ITH
      REC=1.0-REM
      JA=ITH+1
      DO 1 IA=1,2
      IF (JA.GE.46) GOTO 2
      GT(IA)=GTP(JA)
      GOTO 3
    2 JA=JA-45
      GT(IA)=-GTN(JA)
      JA=JA+45
    3 JA=JA+1
    1 CONTINUE
      GTH=REC*GT(1)+REM*GT(2)
      GOTO 4
C     TROUBLE
  999 STOP
    4 CONTINUE
      END
```

APPENDIX A 3

A 3.5 - Techniques for efficient numbering of nodes and elements and related preparation and specification of the network for use in Watson's computer program for three-dimensional elastic analysis, illustrated by reference to the stack model for the chalk at Mundford

The data input scheme for the program has been designed for convenience and economical use. A detailed description of the data specification, facilities and procedures has been documented by Watson (1979).

As a first step, algebraic surfaces are formed from the geometry of the body. The surfaces are then sectioned into finite and infinite elements as described in Chapter 3 in Figs. 3.5.2 to 5. For convenience, Figs. 3.5.1 to 5 are reproduced in this appendix as Figs. A 3.5.1 to 5 respectively. Each finite element is determined by four corner nodes and four midside nodes. All elements may be non-planar and have curved edges.

Node and element identification numbers must be unique. They can be generally selected to harmonize with progression along principal lines, surfaces or interfaces of a body. In order to assign these numbers conveniently, developments are made of the sectioned surfaces and interfaces of the solid. The isometric sketch and the sections and plans shown in Figs. A 3.5.1 to 15 inclusive will be used for illustration. The body represented is a layered horizontal half space with a plane-ended hollow circular shaft intersecting the surface. Clearly it is axisymmetric and can be completely specified by describing a quarter of it and invoking symmetry about both horizontal axes. Examples of sectioned surfaces with assigned node identification numbers are listed in Table A 3.5.1.

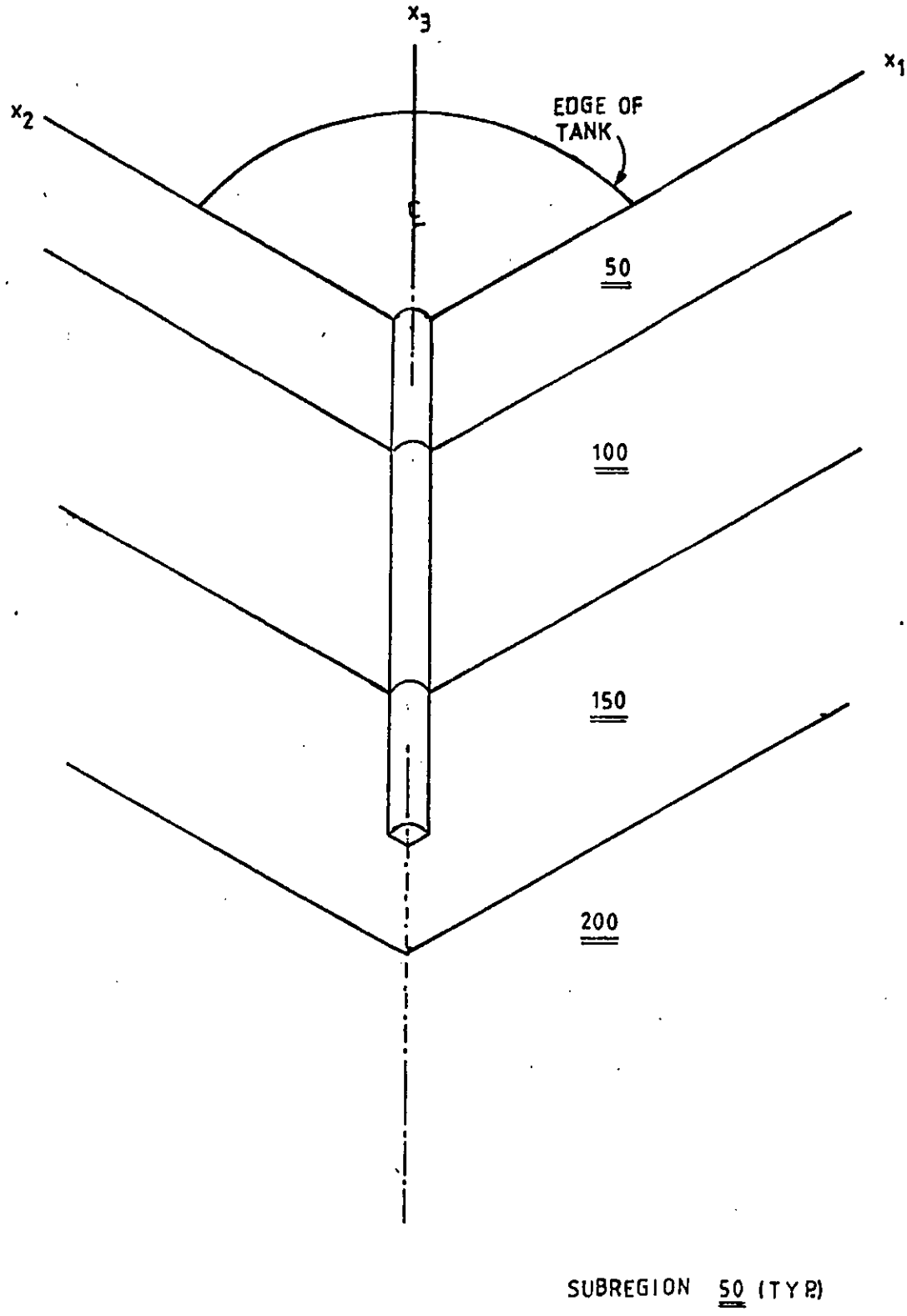


FIG. A 3.5.1: ISOMETRIC SKETCH OF THE MUNDFORD SITE STACK MODEL (FIG. 3.5.1 bis)

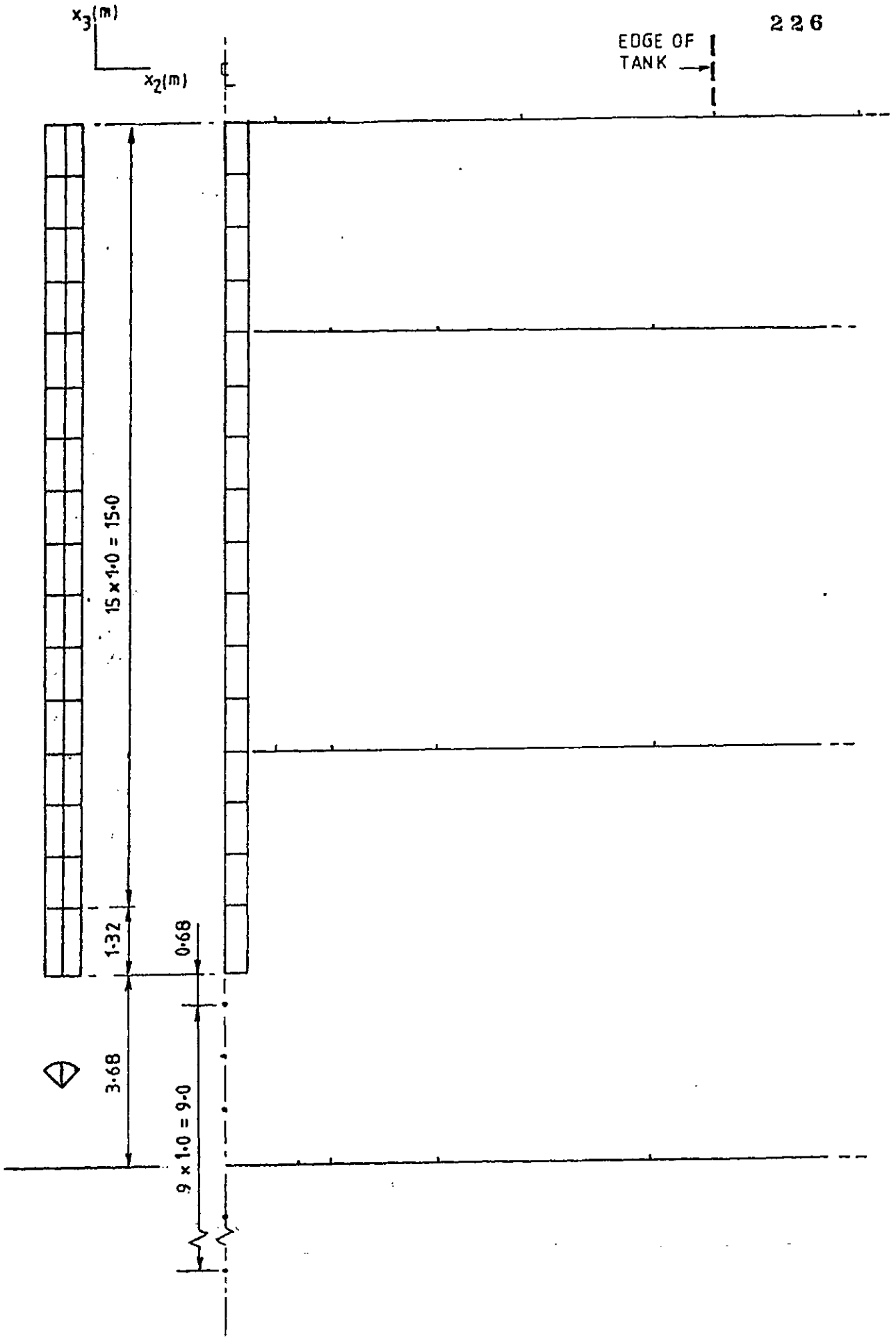


FIG. A 3.5.2: VERTICAL SECTION THROUGH THE MUNDFORD SITE STACK MODEL SHOWING BOUNDARY ELEMENT DIMENSIONS (FIG. 3.5.2 bis)

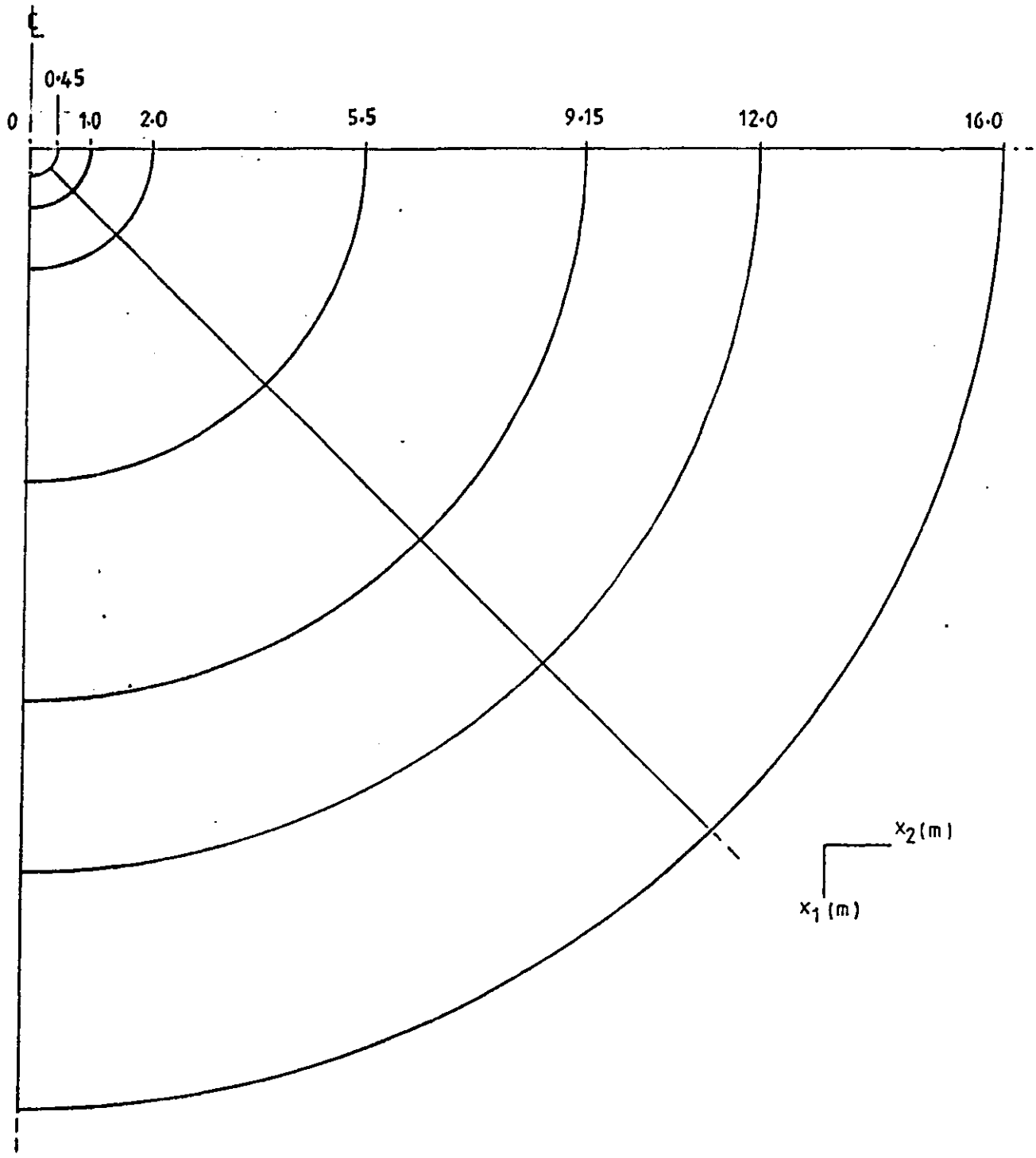


FIG. A 3.5.3: PLAN ON THE MUNDFORD SITE STACK MODEL ON TOP SURFACE OF SUBREGION 50 SHOWING BOUNDARY ELEMENT DIMENSIONS (FIG. 3.5.3 bis)

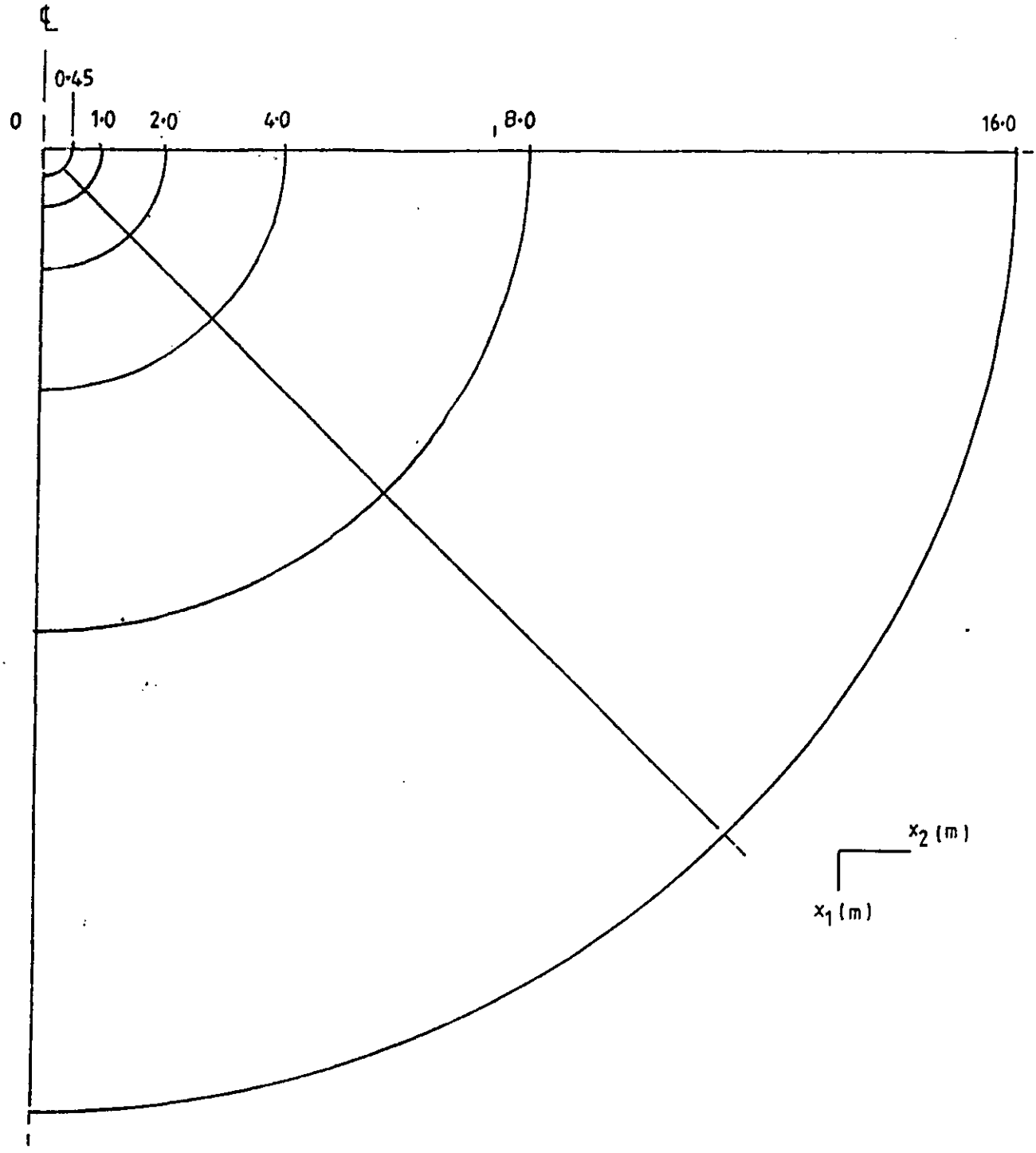


FIG. A 3.5.4: PLAN ON THE MUNDFORD SITE STACK MODEL ON THE TOP SURFACE OF SUBREGIONS 100 AND 150 SHOWING BOUNDARY ELEMENT DIMENSIONS (FIG. 3.5.4 bis)

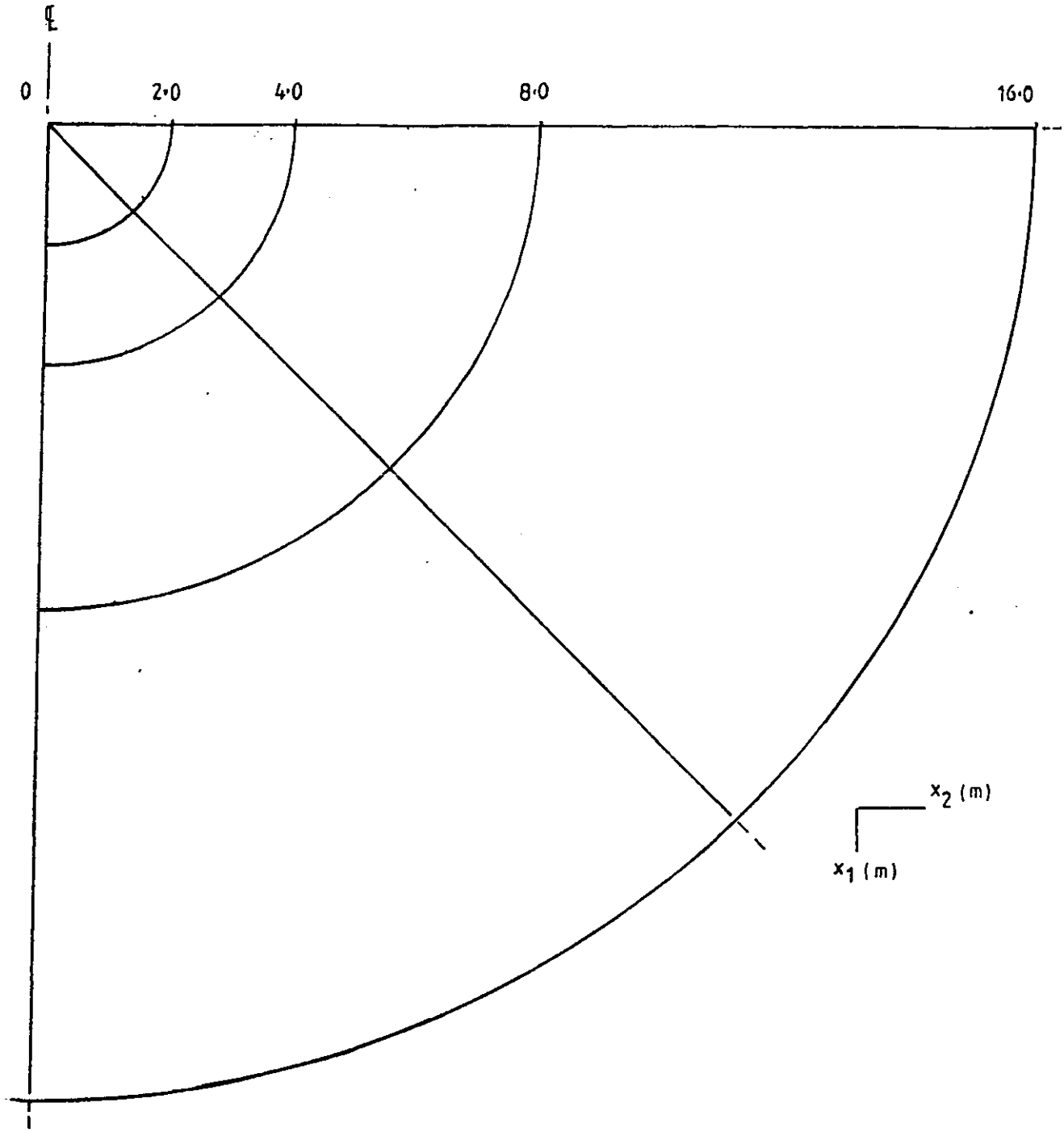


FIG. A 3.5.5: PLAN ON THE MUNDFORD SITE STACK MODEL ON THE TOP SURFACE OF SUBREGION 200 SHOWING BOUNDARY ELEMENT DIMENSIONS (FIG.3.5.5 bis)

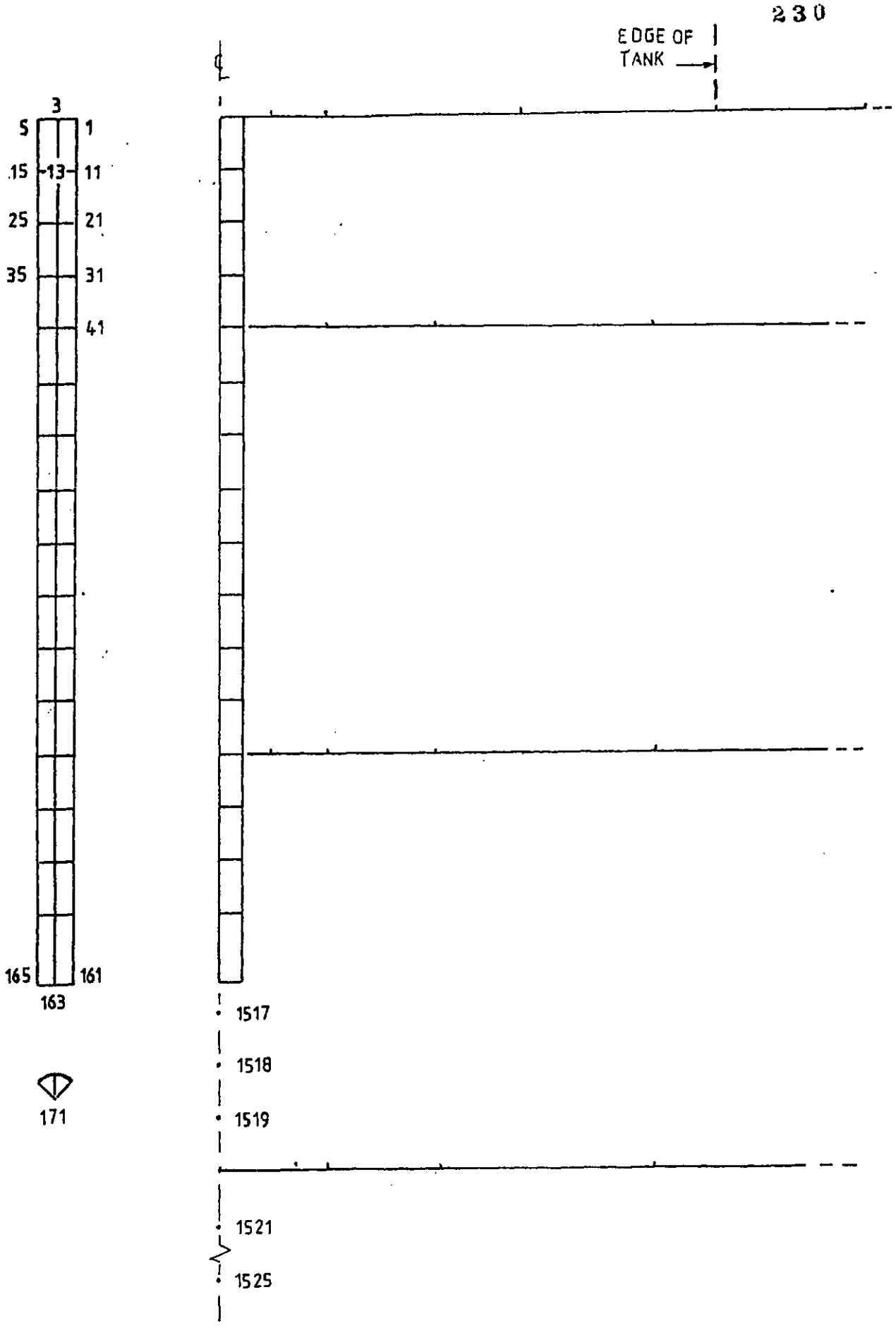


FIG. A 3.5.6: VERTICAL SECTION THROUGH THE MUNDFORD SITE STACK MODEL SHOWING ASSIGNED NODE IDENTIFICATION NUMBERS

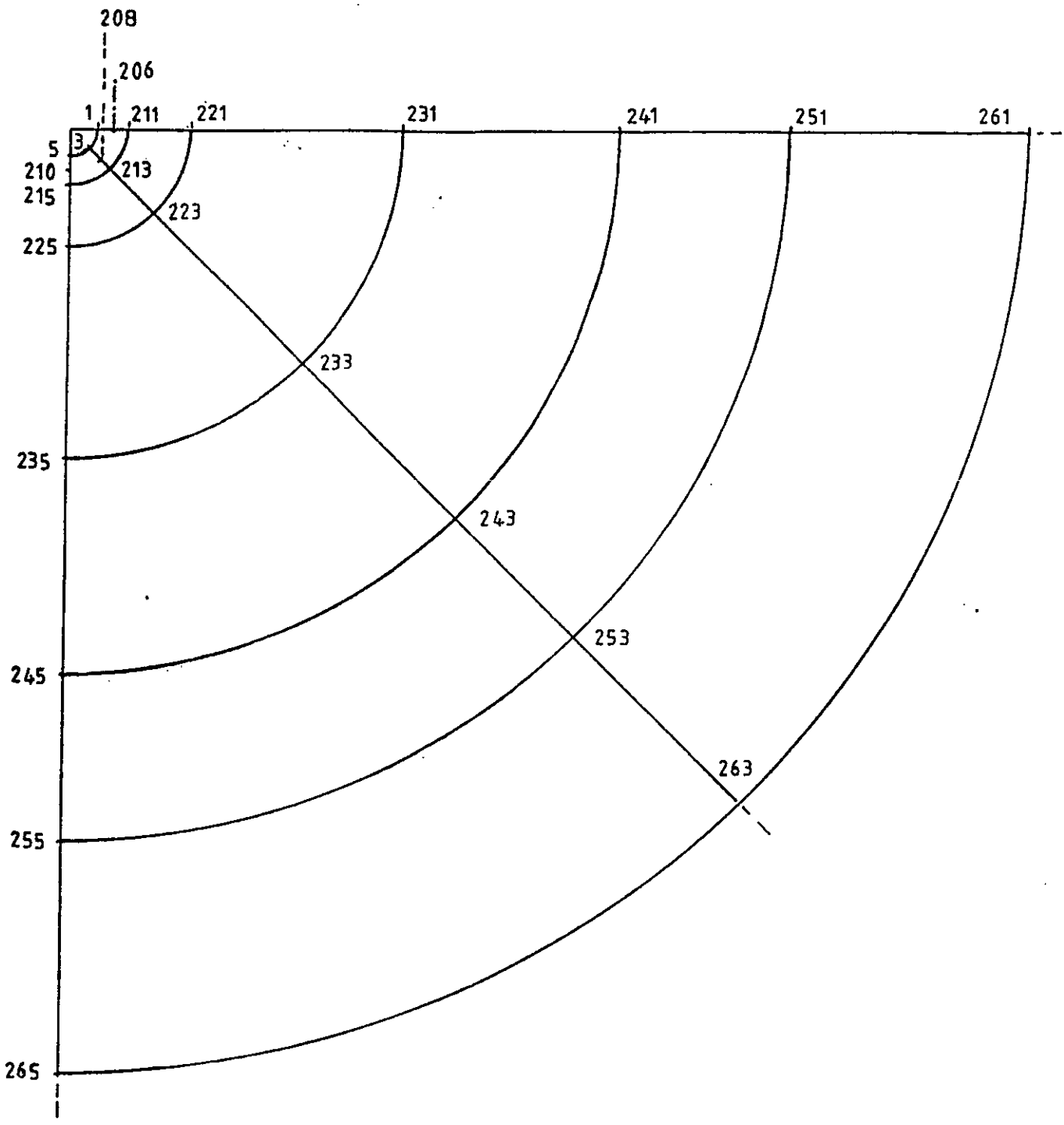


FIG. A 3.5.7: PLAN ON THE MUNDFORD SITE STACK MODEL ON THE TOP SURFACE OF SUBREGION 50 SHOWING ASSIGNED NODE IDENTIFICATION NUMBERS

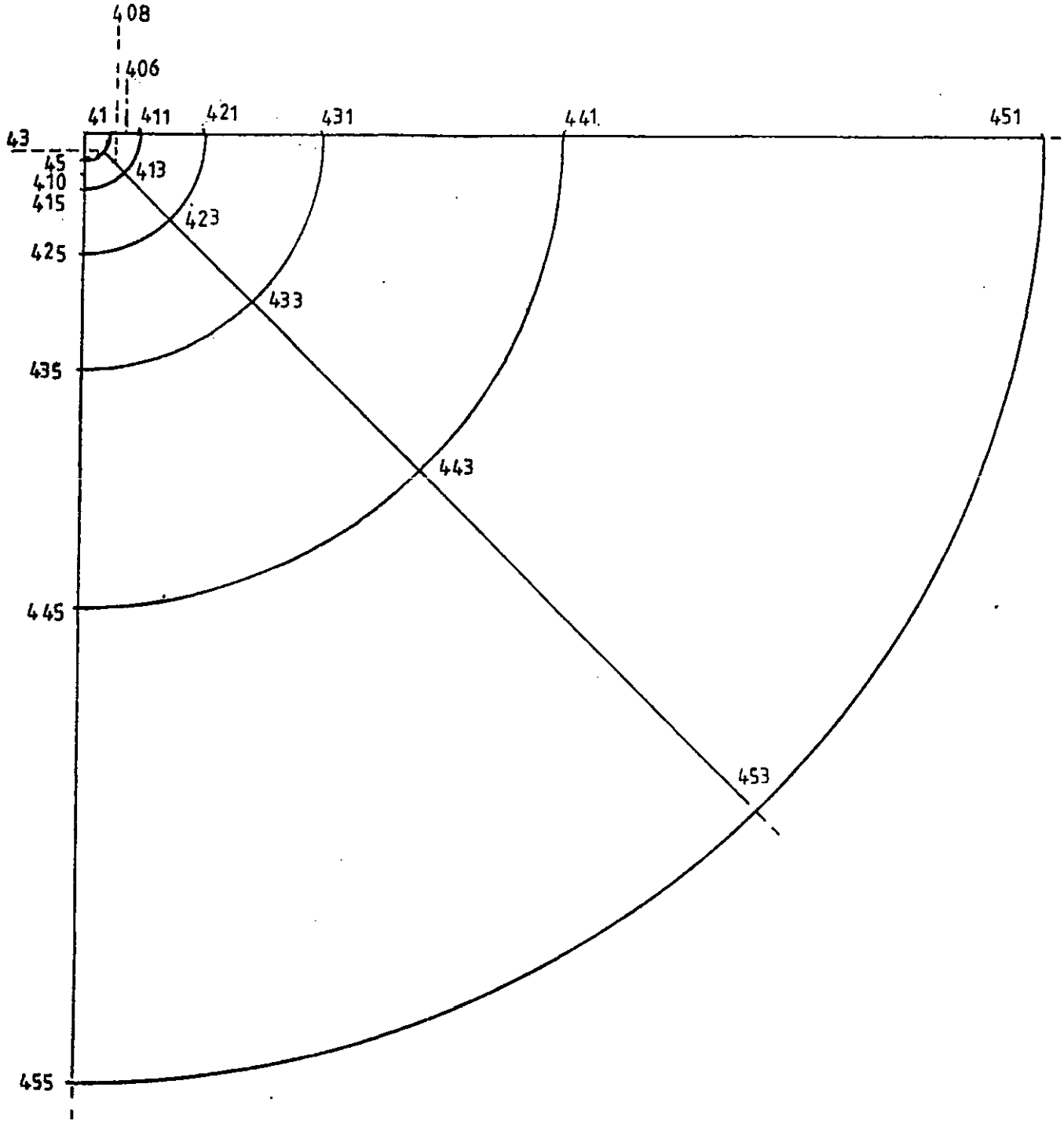


FIG. A 3.5.8: PLAN ON THE MUNDFORD SITE STACK MODEL ON THE TOP SURFACE OF SUBREGION 100 SHOWING ASSIGNED NODE IDENTIFICATION NUMBERS

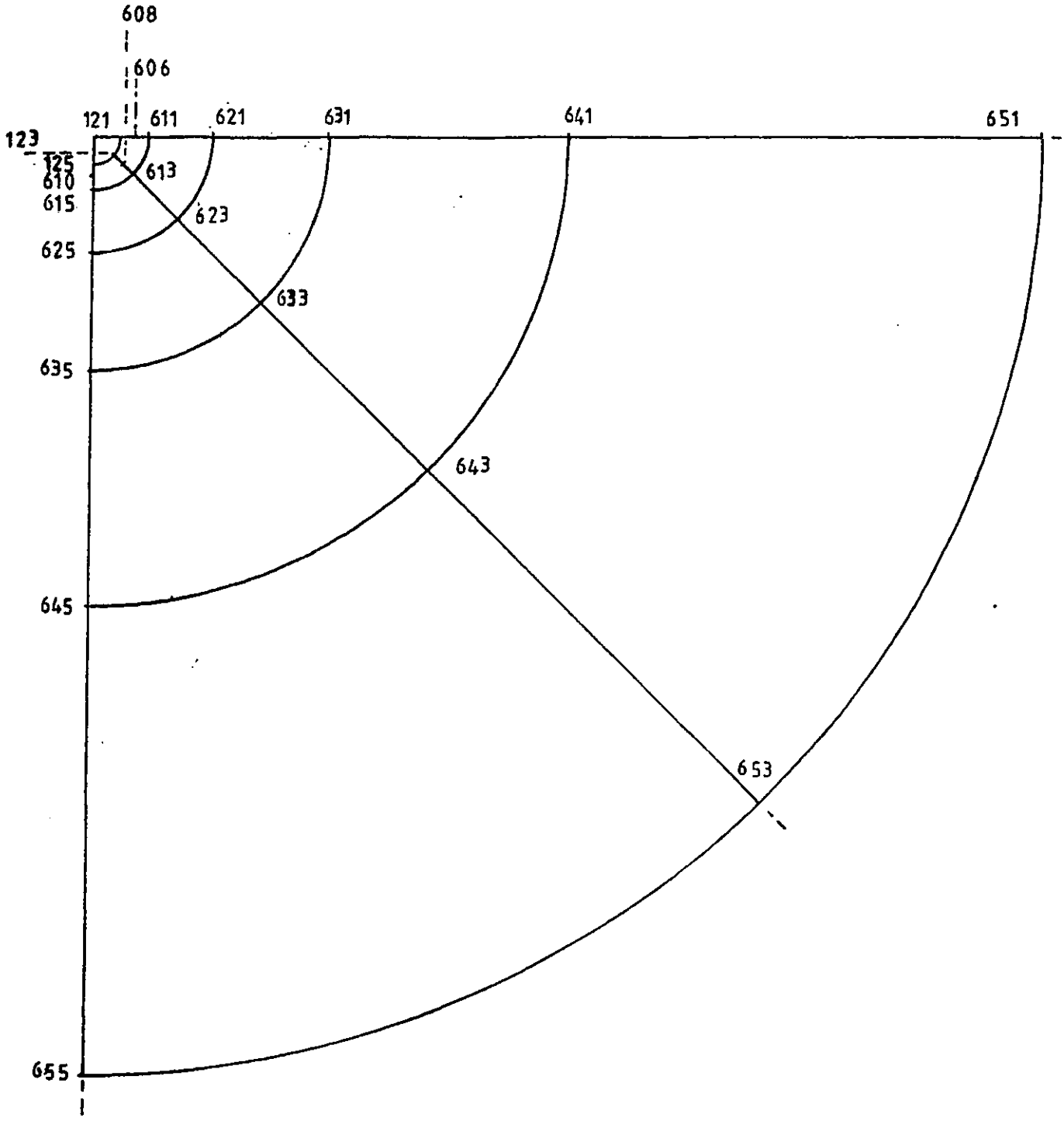


FIG. A 3.5.9: PLAN ON THE MUNDFORD SITE STACK MODEL ON THE TOP SURFACE OF SUBREGION 150 SHOWING ASSIGNED NODE IDENTIFICATION NUMBERS

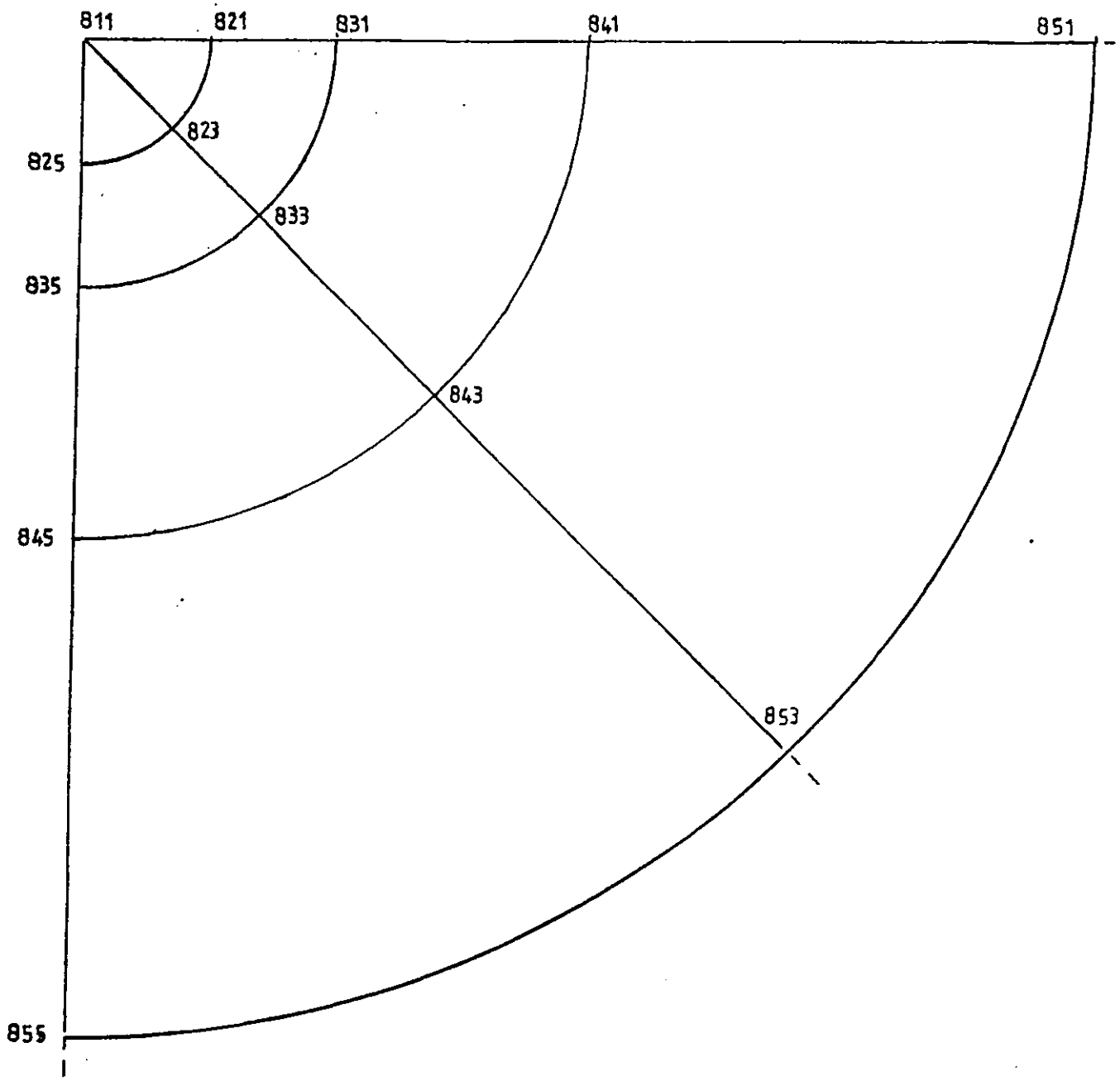


FIG. A.3.5.10: PLAN ON THE MUNDFORD SITE STACK MODEL ON THE TOP SURFACE OF SUBREGION 200 SHOWING ASSIGNED NODE IDENTIFICATION NUMBERS

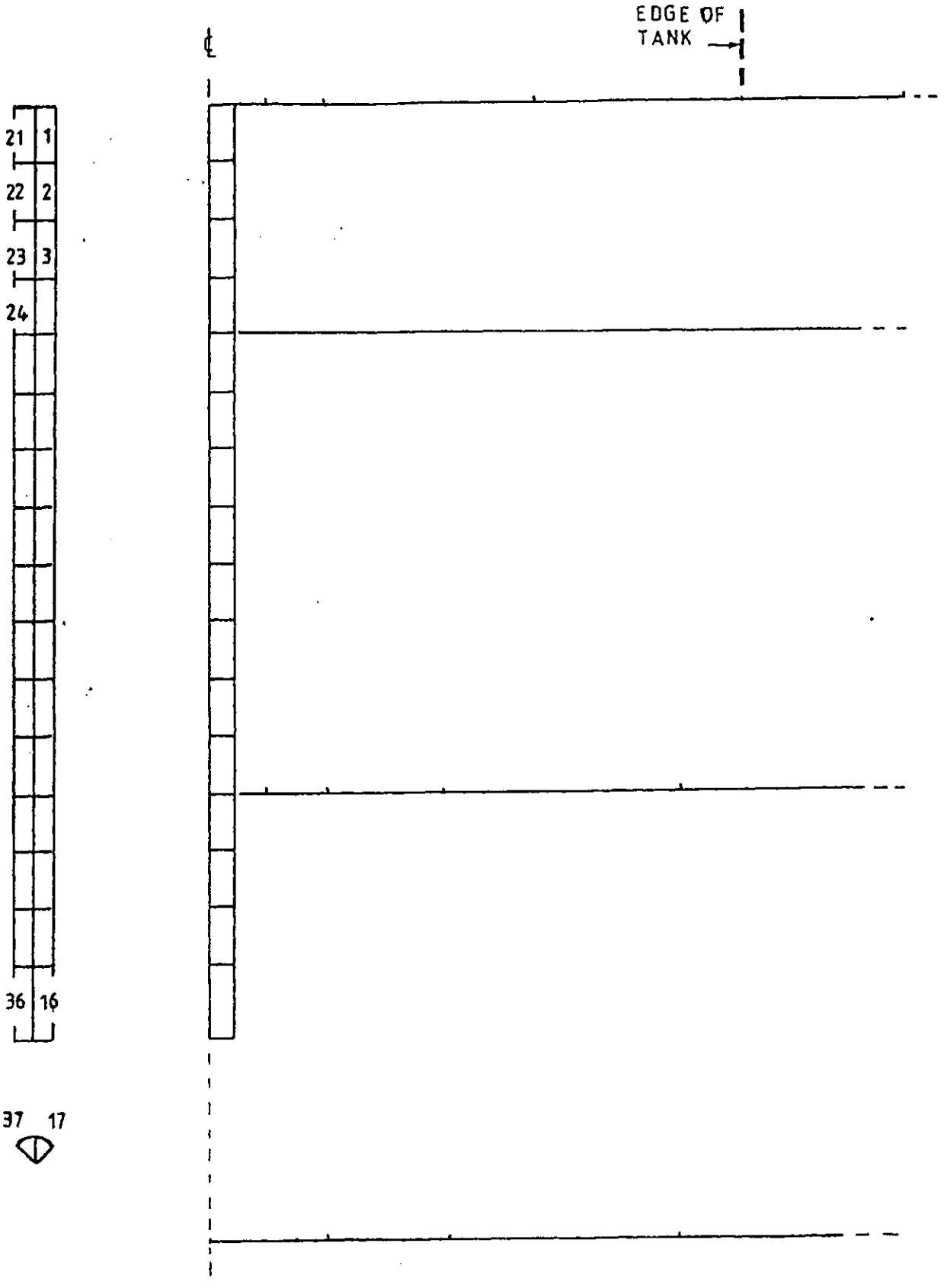


FIG. A 3.5.11: VERTICAL SECTION THROUGH THE MUNDFORD SITE STACK MODEL SHOWING ASSIGNED ELEMENT IDENTIFICATION NUMBERS

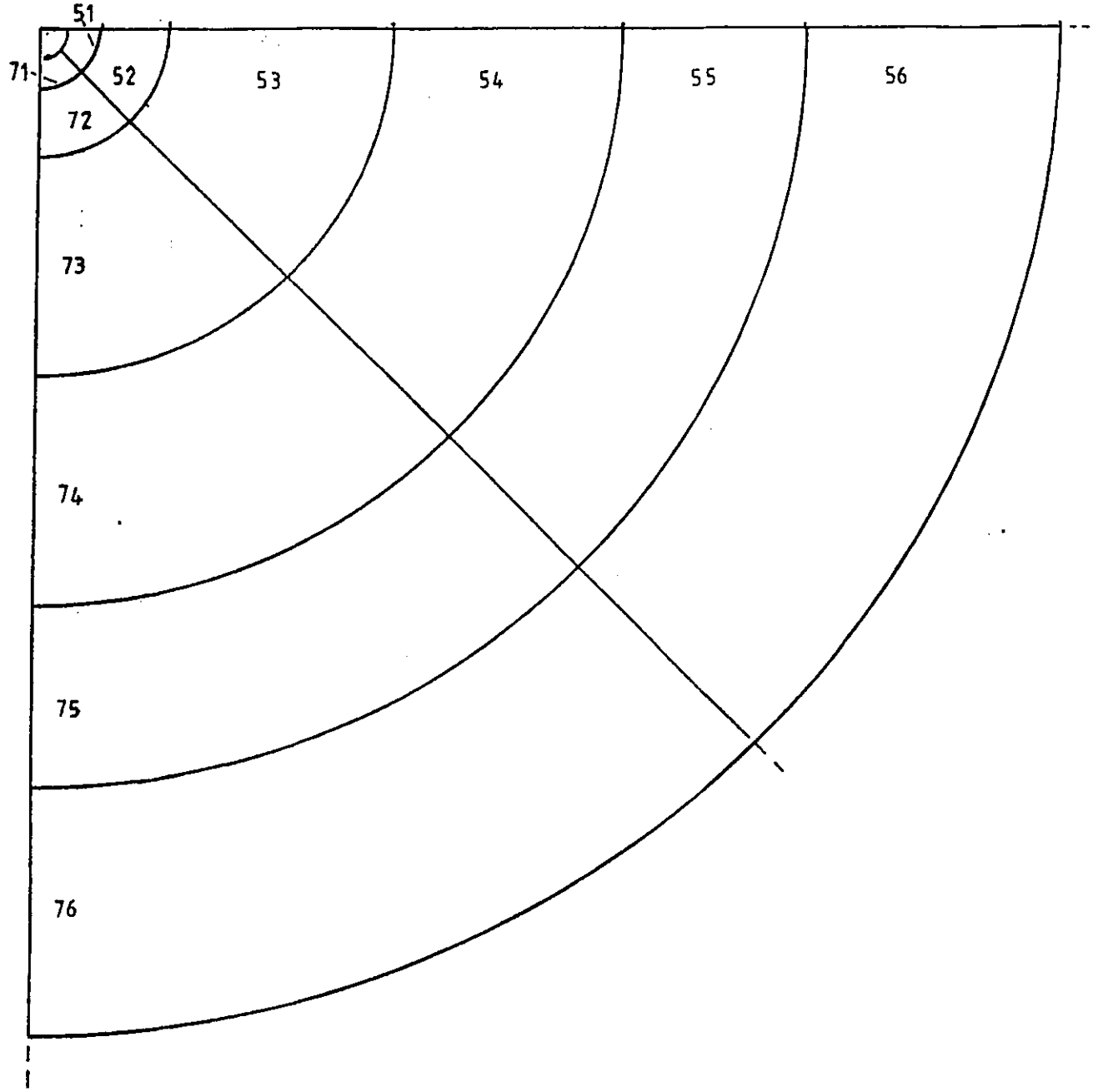


FIG. A 3.5.12: PLAN ON THE MUNDFORD SITE STACK MODEL ON THE TOP SURFACE OF SUBREGION 50 SHOWING ASSIGNED ELEMENT IDENTIFICATION NUMBERS

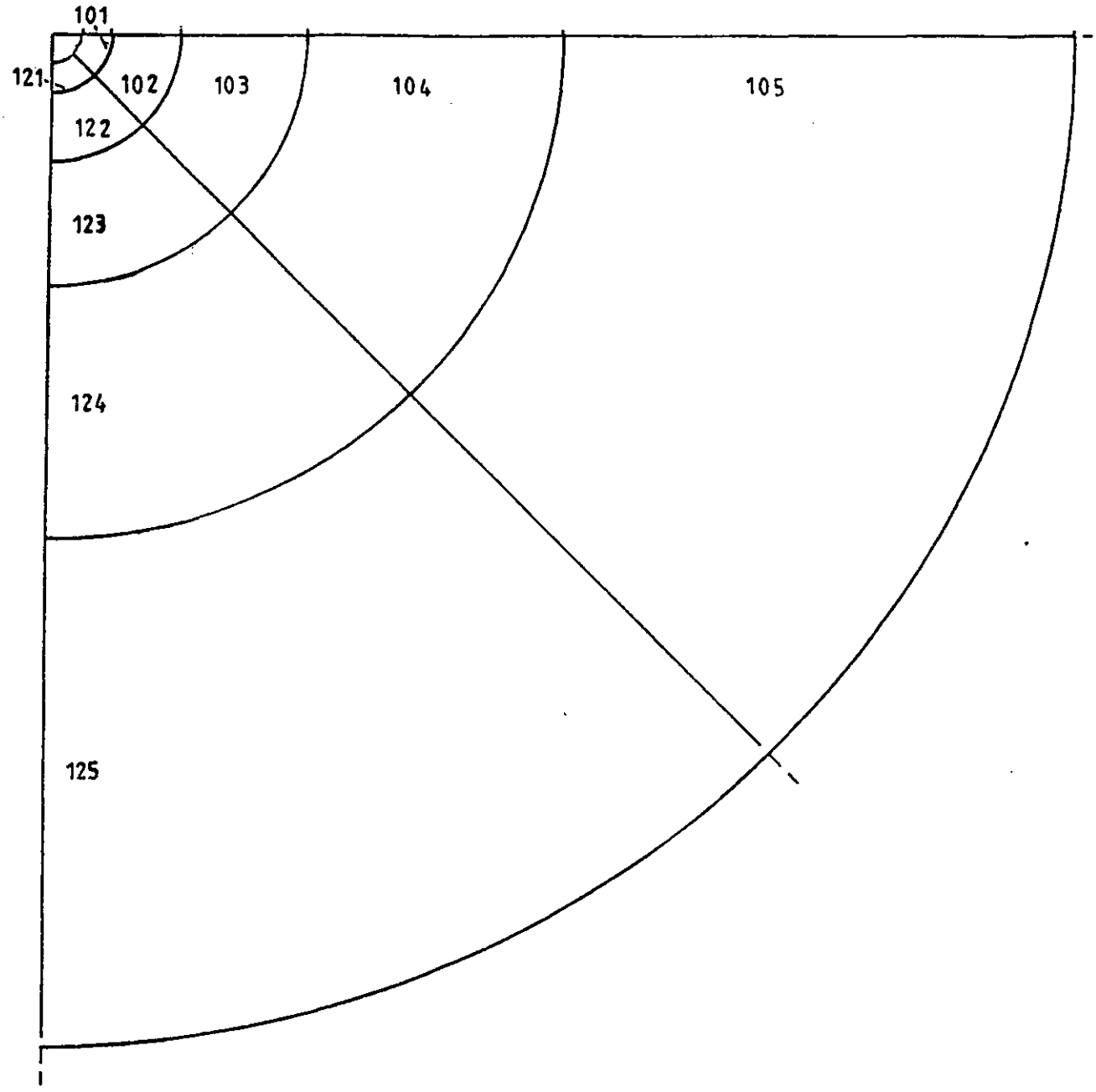


FIG. A 3.5.13: PLAN ON THE MUNDFORD SITE STACK MODEL ON THE TOP SURFACE OF SUBREGION 100 SHOWING ASSIGNED ELEMENT IDENTIFICATION NUMBERS

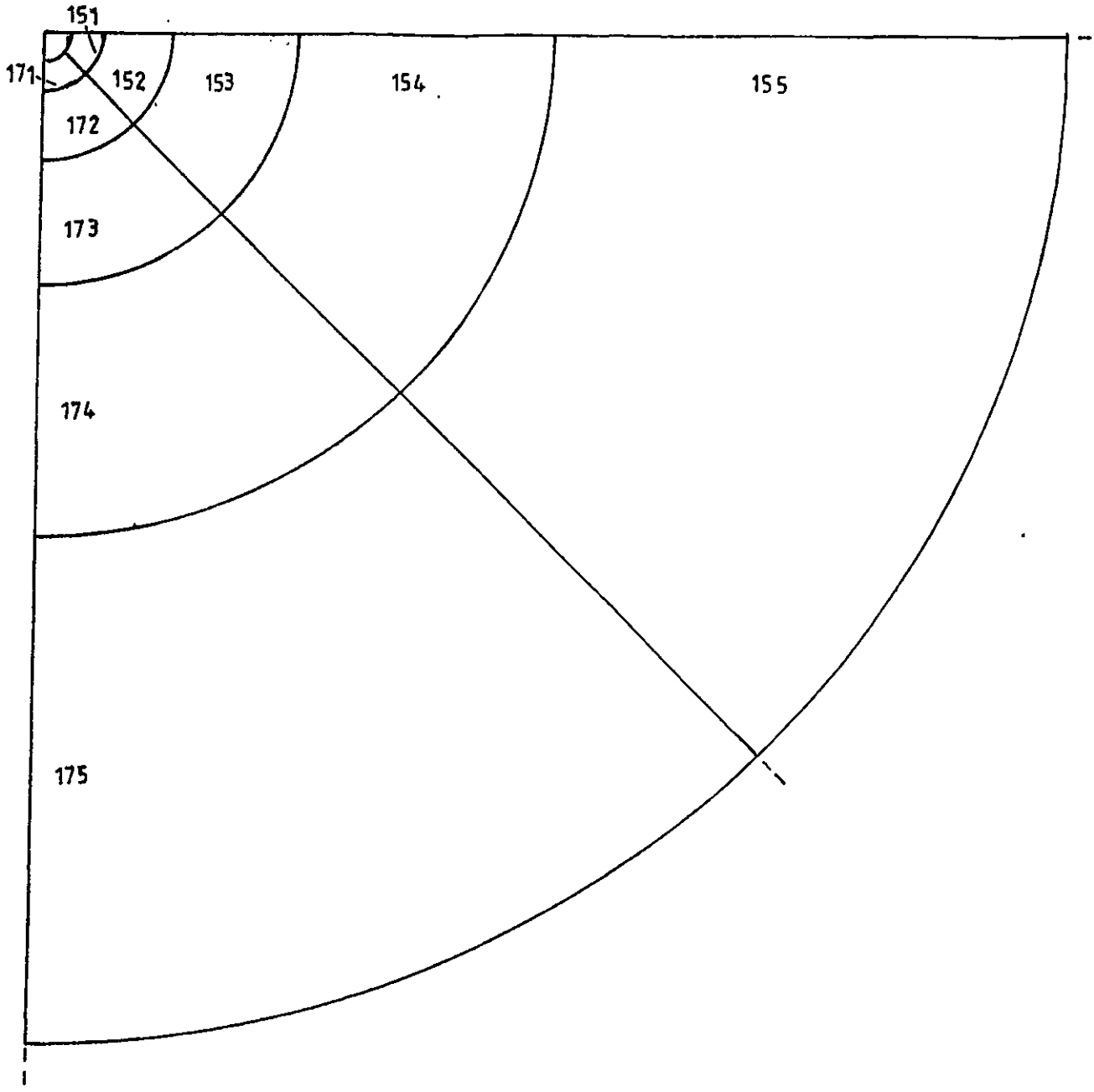


FIG. A 3.5.14: PLAN ON THE MUNDFORD SITE STACK MODEL ON THE TOP SURFACE OF SUBREGION 150 SHOWING ASSIGNED ELEMENT IDENTIFICATION NUMBERS

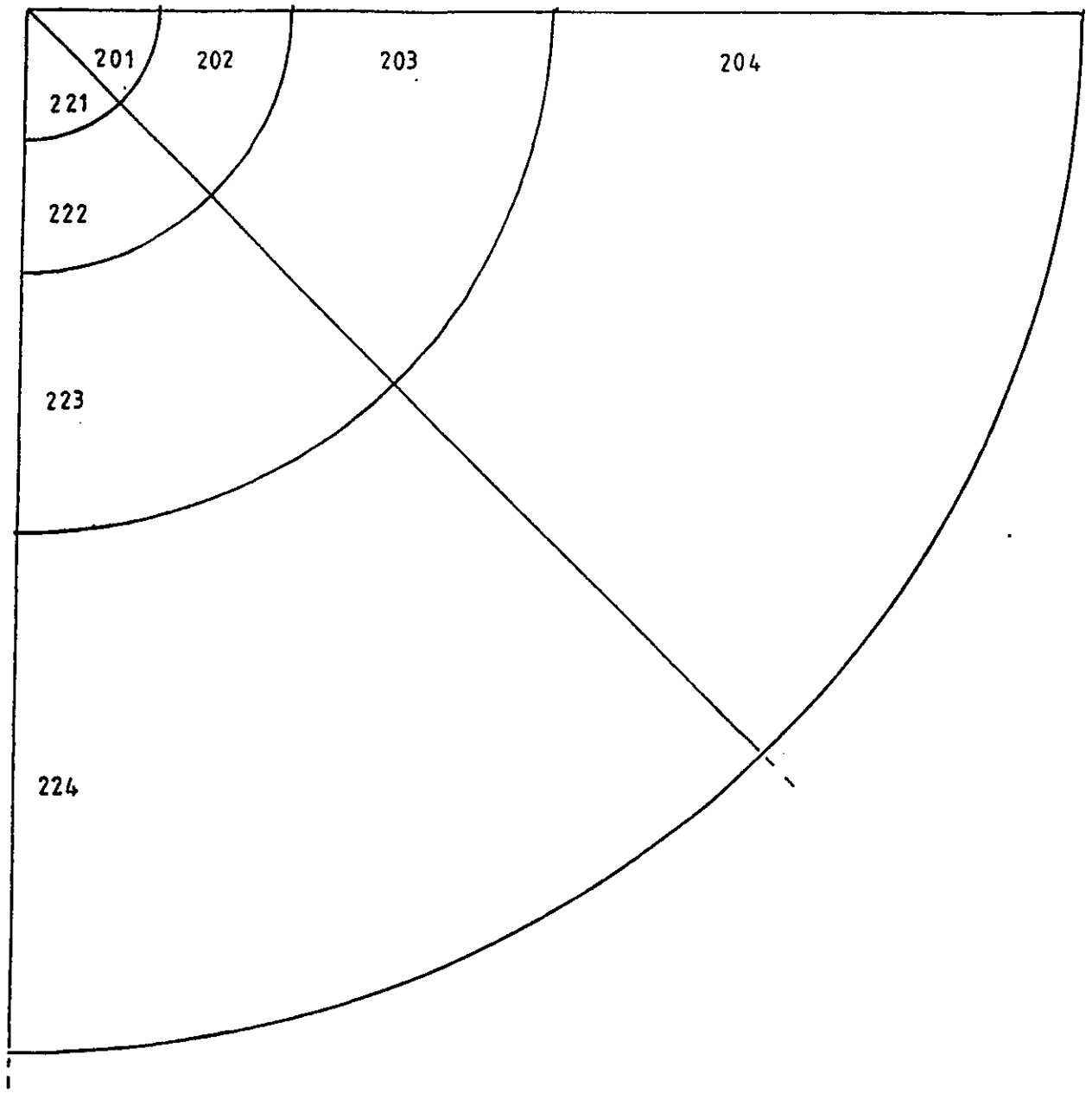


FIG. A 3.5.15: PLAN ON THE MUNDFORD SITE STACK MODEL ON THE TOP SURFACE OF SUBREGION 200 SHOWING ASSIGNED ELEMENT IDENTIFICATION NUMBERS

TABLE A 3.5.1 LIST OF SECTIONED SURFACES WITH ASSIGNED NODE IDENTIFICATION NUMBERS

Reference Figures	Node identification numbers
Fig. A.3.5.6	1, 3, 5; 11, 13, 15; etc. : 1, 11, 21, 31, 41, etc. : 1517, 1518, etc.
Fig. A.3.5.7	211, 213, 215; 221, 223, 225; etc. : 211, 221, 231, 241, etc. :
Fig. A.3.5.8	411, etc.

Finite element numbering is straightforward using only the unsigned integers in the range 1 to 400. Gaps are allowed. Examples of sectioned surfaces with assigned element identification numbers are given in Table A3.5.2.

TABLE A 3.5.2 LIST OF SECTIONED SURFACES WITH ASSIGNED ELEMENT IDENTIFICATION NUMBERS

Reference Figure	Element identification number
Fig. A.3.5.11	1, 2, 3, etc. ; 21, 22, 23, etc.

Infinite elements are treated quite differently from finite elements. In this case numbers are not employed but the directions of the two infinite sides and the two adjoining node numbers are stated. Either asymptotic variation of displacement or complete plane strain conditions are chosen. The maximum total number of finite and infinite elements which can be used for any subregion of a body is 150. All bodies must

have at least one subregion. The maximum aggregrate total of elements for any body is 400.

Node numbering is less simple than element numbering. Identification numbers must be unsigned integers from the range 1 to 2,400 but not more than 1,200 nodes may be used. A set of at least four nodes at the corners of each element is necessary to determine it. A triangular element is treated as a special case of the basic four-sided element. The identification numbers of automatically generated midside nodes are the average of the two adjacent corner node numbers and, unless required otherwise, they are positioned midway between them. Alternatively midside nodes are assigned identification numbers and/or positioned within reasonable limits as desired. Either none or all of the midside nodes of any four-sided element is identified by assigned numbers but for any triangular element all eights nodes are identified.

It is usual to arrange the node numbering of any group of associated elements - say on a plane or a cylinder - so that the difference between each of the corresponding node numbers for successive elements along either coordinate axis in the surface is a constant of a certain order of magnitude. The order of magnitude for each axis is usually different. These features are exhibited by the groups in TableA3.5.1. The data input scheme has been designed to use them to advantage in the economical specification of groups of elements which run along principal lines. Only the first and last element numbers and the constant differences need to be stated instead of the many separate details. If sets of element groups are required - say where there are many subregions defined by similarly shaped surfaces - then greater orders of magnitude may be used to distinguish

between the nodes of related element groups. Examples of input data for the specification of a group and an individual element are given on lines a and b respectively of Fig. A 3.5.16. At the intersection of subregions and on other occasions in which different groups of related elements meet, it is frequently not possible to use the grouping facility and each element is dealt with individually. Line c of Fig. A3.5.16 which refers to an element on the rim of the shaft exemplifies this difficulty.

The methods for the preparation and specification of input data for nodes and elements presented above are entirely general. The full number of input data for an initial run of the problem shown in Fig. A3.5.16 were reproduced by the preprocessor and are included for completeness.

The preprocessor checks the correctness of the input data very thoroughly at several levels including syntax and sufficiency. Generally redundancy is accepted but inconsistency and insufficiency are not. Where an error is detected the data perusal is not stopped but an appropriate error message is generated and a flag is set which prevents execution of the numerical work. The earlier an error is encountered, however, the less data checking is usually possible. Error messages which may be generated during preprocessing are listed in TableA3.5.3.

```
  INPUT DATA FOR PERUSAL BY SUBROUTINE PDECO      PAGE  1
***  COM     A7
***  T    FULL-SCALE TEST-TANK AT HUNDFORD
***  SYM     12
***  CYL      1  151   10        0.45       90.0        0.0       0.45      90.0     -15.0
***  CYL      2  152   10        0.45       67.5        0.0       0.45      67.5     -15.0

***  CYL      3  153   10        0.45       45.0        0.0       0.45      45.0     -15.0
***  CYL      4  154   10        0.45       22.5        0.0       0.45      22.5     -15.0
***  CYL      5  155   10        0.45        0.0        0.0       0.45       0.0     -15.0
***  CYL    161  165    1        0.45       90.0     -16.32       0.45       0.0    -16.32
***  CAR    171                   0.0        0.0     -16.32

***  CYL    211  215    1         1.0       90.0        0.0        1.0       0.0        0.0
***  CYL    221  225    1         2.0       90.0        0.0        2.0       0.0        0.0
***  CYL    231  235    1         5.5       90.0        0.0        5.5       0.0        0.0
***  CYL    241  245    1        9.15       90.0        0.0       9.15       0.0        0.0
***  CYL    251  255    1        12.0       90.0        0.0       12.0       0.0        0.0

***  CYL    261  265    1        16.0       90.0        0.0       16.0       0.0        0.0
***  CYL    411  415    1         1.0       90.0       -4.0        1.0       0.0       -4.0
***  CYL    421  425    1         2.0       90.0       -4.0        2.0       0.0       -4.0
***  CYL    431  435    1         4.0       90.0       -4.0        4.0       0.0       -4.0
***  CYL    441  445    1         8.0       90.0       -4.0        8.0       0.0       -4.0

***  CYL    451  455    1        16.0       90.0       -4.0       16.0       0.0       -4.0
***  CYL    611  615    1         1.0       90.0      -12.0        1.0       0.0      -12.0
***  CYL    621  625    1         2.0       90.0      -12.0        2.0       0.0      -12.0
***  CYL    631  635    1         4.0       90.0      -12.0        4.0       0.0      -12.0
***  CYL    641  645    1         8.0       90.0      -12.0        8.0       0.0      -12.0

***  CYL    651  655    1        16.0       90.0      -12.0       16.0       0.0      -12.0
***  CAR    811                   0.0        0.0      -20.0
***  CYL    821  825    1         2.0       90.0      -20.0        2.0       0.0      -20.0
***  CYL    831  835    1         4.0       90.0      -20.0        4.0       0.0      -20.0
***  CYL    841  845    1         8.0       90.0      -20.0        8.0       0.0      -20.0

***  CYL    851  855    1        16.0       90.0      -20.0       16.0       0.0      -20.0
***  CAR   1517 1519    1         0.0        0.0      -17.0        0.0       0.0      -19.0
***  CAR   1521 1530    1         0.0        0.0      -21.0        0.0       0.0      -30.0
***  CAR   1601 1603    1         0.0      12.12       -1.0        0.0     12.12       -3.0
***  CAR   1605 1611    1         0.0      12.12       -5.0        0.0     12.12      -11.0

***  CAR   1613 1619    1         0.0      12.12      -13.0        0.0     12.12      -19.0
***  CAR   1621 1630    1         0.0      12.12      -21.0        0.0     12.12      -30.0
line a →***  ELE      1   16   10    1    3   13   11
***  ELE     21   36   10    3    5   15   13
line b →***  ELE     17         161  163  171  171  166  162  167  171
```

```
  INPUT DATA FOR PERUSAL BY SUBROUTINE PDECO      PAGE  2

line c →***  ELE     37         163  165  171  171  167  164  168  171
***  ELE     51           1    3  213  211  206    2  208  212
***  ELE     52   56   10  211  213  223  221
***  ELE     71           3    5  215  213  208    4  210  214
***  ELE     72   76   10  213  215  225  223

***  ELE    101          41   43  413  411  406   42  408  412
***  ELE    102  105   10  411  413  423  421
***  ELE    121          43   45  415  413  408   44  410  414
***  ELE    122  125   10  413  415  425  423

***  ELE    151         121  123  613  611  606  122  608  612

***  ELE    152  155   10  611  613  623  621
***  ELE    171         123  125  615  613  608  124  610  614
***  ELE    172  175   10  613  615  625  623
***  ELE    201         811  811  823  821  816  811  817  822
***  ELE    202  204   10  821  823  833  831

***  ELE    221         811  811  825  823  817  811  818  824
***  ELE    222  224   10  823  825  835  833
***  IEL A          0.0       1.0       0.0  261  451  651  851
***  IEL A          1.0       1.0       0.0  263  453  653  853
***  IEL A          1.0       0.0       0.0  265  455  655  855

***  SUB     50    0.45E6      0.3                                              51
***  SUB    100    2.25E6     0.25                                             101
***  SUB    150    4.25E6     0.25                                         151 -201
***  SUB *  200    5.25E6     0.25                                             201
***  L    TEST-TANK FULL OF WATER WITH NO RADIAL FORCE ON INTERFACE

***  PEU          -180.0
***            51   52   53   54   71   72   73   74
***  END
```

FIG. A 3.5.16: EXAMPLE OF INPUT DATA REPRODUCED BY THE PREPROCESSOR IN WATSON'S PROGRAM FOR THREE-DIMENSIONAL ELASTOSTATIC ANALYSIS BY THE BOUNDARY INTEGRAL EQUATION METHOD

TABLE A 3.5.3 ERROR MESSAGES GENERATED BY PREPROCESSOR IN WATSON'S COMPUTER PROGRAM FOR THREE-DIMENSIONAL ELASTIC ANALYSIS

KEYWORD UNIDENTIFIED

BAD INTEGERS BAD REALS

END CARD MISSING

CARD **** ****

DUPLICATE CARD

CHECKPOINT SPECIFICATION ERROR

CARD MISSING OR MISPLACED

NO CARD T, LOAD OR INT

CARD T INCOMPATIBLE WITH CARD LOAD, INT

ILLEGAL SYMMETRY SPECIFICATION

ILLEGAL FUNCTIONAL VARIATION

PRECISION OF INTEGRATION OUTSIDE LIMITS

SUPERFLUOUS DATA

ERROR, ROTATION OF AXES - THE PROGRAM TAKES ZERO ROTATIONS

NODE NUMBER GREATER THAN

INTERPOLATION BETWEEN NODES AND

SIGN OF INCREMENT WRONG

THE DIFFERENCE BETWEEN THE NODE NUMBERS IS NOT DIVISIBLE BY THE INCREMENT

COORDINATES OF NODE OR NOT GIVEN

NODE NUMBER NEGATIVE

NO NODES

MORE THAN NODES

INTERPOLATION BETWEEN ELEMENTS AND

ELEMENT NUMBER GREATER THAN

ELEMENT NUMBER ZERO OR NEGATIVE

INCREMENT MISSING

NODE NUMBER ZERO OR NEGATIVE

ELEMENT GIVEN TWICE

THE NUMBER OF NODE OF ELEMENT CANNOT BE GENERATED

ERROR COLUMN 5

NULL VECTOR

MORE THAN LINES DEFINING INFINITE ELEMENTS

NO ELEMENTS

MORE THAN ELEMENTS

THE COORDINATES OF NODE OF ELEMENT ARE UNDEFINED

COORDINATE X OF NODE OF ELEMENT IS NEGATIVE

COORDINATES OF NODE UNDEFINED

INFINITE ELEMENT GEOMETRY AT NODE INCOMPATIBLE WITH SYMMETRY X

SUBREGION NUMBER OMITTED

SUBREGION DEFINED TWICE

MORE THAN SUBREGIONS

THE MODULUS OF ELASTICITY OF SUBREGION IS NOT POSITIVE

POISSONS RATIO OF SUBREGION NOT BETWEEN 0.0 AND 0.5

SURFACE OF SUBREGION UNDEFINED

ELEMENT NUMBER GREATER THAN SUBREGION

ELEMENT SUBREGION DOES NOT EXIST

NO SUBREGIONS

ZERO JACOBIAN ELEMENT

APPENDIX A 4

A 4.5 - Simplified two-dimensional elastic-plastic analysis of the horizontal displacement of a block of soil underlain by a horizontal plane crack at the bottom of a deep excavation in Oxford Clay at Saxon pit due to the relief of field stress

The layout of a simplified model of Saxon pit is shown by the typical vertical section normal to the face of excavation E'H in Fig. A 4.5.1. The floor of the pit is represented by the line AH. It is assumed that a horizontal plane crack GH underlies a block of soil which expands elastically, due to the relief of field stress, and slides along GH towards the point A, as the face E'H is excavated. It is also assumed that all the soil not within the zone directly above GH is rigid and that the normal stress on GH is uniformly distributed. Any effects due to groundwater are ignored.

The notation used in the analysis is as follows:

$\bar{u}_x = (1/h)\int_o^h u_x dz$ = average horizontal displacement over a vertical section, induced by excavation

$\bar{\varepsilon}_x = (1/h)\int_o^h \varepsilon_x dz$ = average horizontal strain over a vertical section, induced by excavation

$\bar{\sigma}_x = (1/h)\int_o^h \sigma_x dz$ = average horizontal normal stress over a vertical section, induced by excavation

E_h, ν = horizontal Young's modulus, Poisson's ratio

$E = E_h/(1-\nu^2)$ = plane strain value of Young's modulus

γ = unit weight of the soil

$p = \gamma h$ = normal stress on horizontal plane crack

In addition, the following set of primary data was used:

$E_h = 144$ MN/m^2 ; $\nu = 0.2$: $\gamma = 20$ kN/m^3 ; $h = 27$ m :

$\phi'_p = 27\frac{1}{2}^o$, $c'_p = 172$ kN/m^2 : $\phi'_r = 13^o$, $c'_r = 3\frac{1}{2}$ kN/m^2

Constant values derived from the primary data are as follows:

$E = 150$ MN/m^2

$p = 540$ kN/m^2

Peak shear strength $\tau_p = p \tan \phi'_p + c'_p = 453$ kN/m^2

Residual shear strength $\tau_r = p \tan \phi'_r + c'_r = 128$ kN/m^2

Assuming a shear strength rest value τ_o of 100 kN/m^2 the shear stress-shear displacement response curve may be approximated as shown in Fig. A 4.5.2. The three distinct phases shown by the graph corresponding to shear hardening, softening and residual strength and are designated (a), (b), and (c) respectively. Equations for each phase are as follows, where τ and u_x are measured in kN/m^2 and mm, respectively.

Phase (a) $\tau = 100 + 706\ u_x$ ...(A 4.5.1)

Phase (b) $\tau = 493.6 - 81.25\ u_x$ ...(A 4.5.2)

Phase (c) $\tau = 128$ ...(A 4.5.3)

In order to analyse the structure, consider the element of width dx shown in Fig. A 4.5.1 .

For horizontal equilibrium,

$$h d\bar{\sigma}_x + \tau dx = 0$$

It follows that,

$$\frac{d\bar{\sigma}_x}{dx} = -\frac{\tau}{h} \quad \text{...(A 4.5.4)}$$

$$\frac{d\bar{\varepsilon}_x}{dx} = -\frac{\tau}{hE} \quad \text{...(A 4.5.5)}$$

$$\frac{d^2 \bar{u}_x}{dx^2} = \frac{\tau}{hE} \quad \text{...(A 4.5.6)}$$

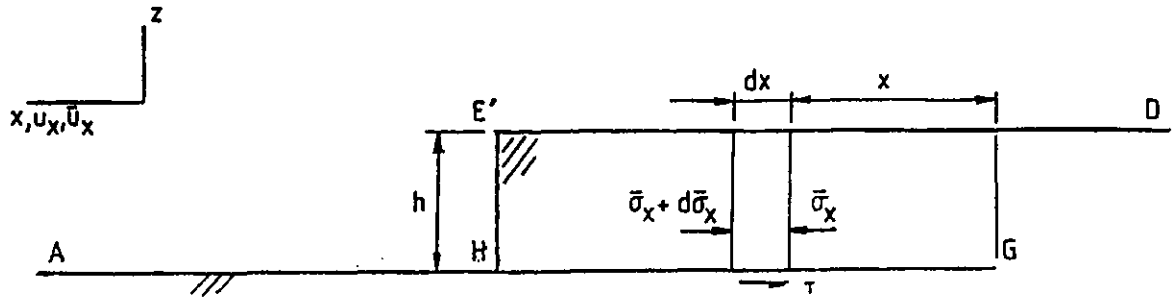


FIG. A 4.5.1: SIMPLIFIED SAXON PIT MODEL WITH INFINITELY REMOTE BOUNDARIES FOR TWO-DIMENSIONAL ANALYSIS

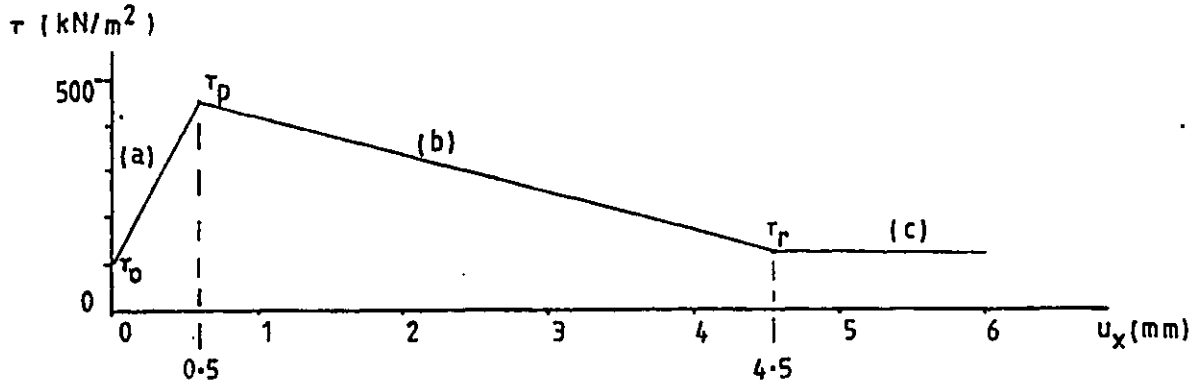


FIG. A 4.5.2: SIMPLIFIED SHEAR STRESS-DISPLACEMENT RESPONSE CURVE

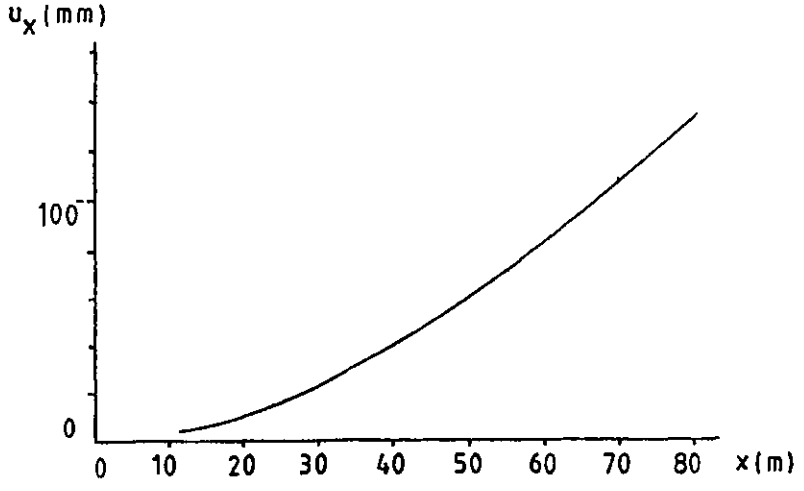


FIG. A 4.5.3: VARIATION OF HORIZONTAL DISPLACEMENT WITH DISTANCE FROM THE ROOT OF THE CRACK IN THE SIMPLIFIED SAXON PIT MODEL WITH INFINITELY REMOTE BOUNDARIES FOR TWO-DIMENSIONAL ANALYSIS

Three ordinary differential equations were obtained by substituting equation (A 4.5.6) in the equations for the shear strength-shear displacement response curve shown in Fig. A 4.5.2. By ignoring the difference between $\bar{u}_x$ and u_x and entering the numerical values of E and h in these equations, the solutions given below were obtained for the relevant boundary conditions, where u_x and x are measured in mm and m respectively.

Phase (a) $u_x = 0.14164\ (\exp\ (0.4175x)-1)$ ...(A 4.5.7)

Phase (b) $u_x = 6.0751 - 1.0856 \sin\ (0.14163x) - 5.7868 \cos\ (0.14163x)$ ...(A 4.5.8)

Phase (c) $u_x = 0.0158x^2 + 0.4721x - 2.1990$ ...(A 4.5.9)

A graph of equation (A 4.5.9) is plotted in Fig. A.4.5.3.

APPENDIX A 5

A5.2(a) Expressions for certain integrals related to and in terms of complete elliptic integrals of the first and second kind, denoted by F_1 and E_1 respectively

The equation,

$$\int_0^{\pi/2} \frac{d\phi}{\Delta} = F_1$$

is differentiated w.r.t. k, as shown below, to obtain the first relation required.

$$\int_0^{\pi/2} \frac{\partial}{\partial k}\left(\frac{1}{\Delta}\right) d\phi = \frac{dF_1}{dk}$$

$$\frac{1}{k}\int_0^{\pi/2} \left(\frac{1}{\Delta^3} - \frac{1}{\Delta}\right) d\phi = \frac{E_1}{k(1-k^2)} - \frac{F_1}{k}$$

$$\int_0^{\pi/2} \frac{d\phi}{\Delta^3} = \frac{E_1}{1-k^2}$$

Similarly, the second relation required is obtained as follows,

$$\int_0^{\pi/2} \frac{\partial}{\partial k}\left(\frac{1}{\Delta^3}\right) d\phi = \frac{d}{dk}\left(\frac{E_1}{1-k^2}\right)$$

$$\frac{3}{k}\int_0^{\pi/2} \left(\frac{1}{\Delta^5} - \frac{1}{\Delta^3}\right) d\phi = \frac{(1-k^2)(E_1 - F_1) + 2k^2 E_1}{k(1-k^2)^2}$$

$$\int_0^{\pi/2} \frac{d\phi}{\Delta^5} = \frac{F_1}{3(k^2-1)} - \frac{2(k^2-2)}{3(k^2-1)^2} E_1$$

A 5.2(b) Limiting values of certain integrals related to and in terms of complete elliptic integrals of the first and and second kind denoted by F_1 and E_1 respectively

Noting that for $k^2 < 1$ (Abramowitz and Stegun (1965))

$$F_1 = \frac{\pi}{2}\left(1+\frac{1}{4}k^2+\frac{9}{64}k^4+\frac{225}{2304}k^6+\ldots\right)$$

$$E_1 = \frac{\pi}{2}\left(1-\frac{1}{4}k^2-\frac{3}{64}k^4-\frac{45}{2304}k^6-\ldots\right),$$

we have, as $k^2 \to o$,

$$\text{Lim}\left(\int_o^{\pi/2}\Delta\, d\phi\right) = \text{Lim}\,(E_1) = \frac{\pi}{2}$$

$$\text{Lim}\left(\int_o^{\pi/2}\frac{1}{\Delta}\, d\phi\right) = \text{Lim}\,(F_1) = \frac{\pi}{2}$$

$$\text{Lim}\left(\int_o^{\pi/2}\frac{1}{\Delta^3}\, d\phi\right) = \text{Lim}\left(\frac{E_1}{1-k^2}\right) = \frac{\pi}{2}$$

$$\text{Lim}\left(\int_o^{\pi/2}\frac{1}{\Delta^5}\, d\phi\right) = \text{Lim}\left(\frac{F_1}{3(k^2-1)} - \frac{2(k^2-2)}{3(k^2-1)^2}E_1\right) = \frac{\pi}{2}$$

We also obtain the limiting values of the following two integrals as $k^2 \to 0$ by expressing them in terms of F_1 and E_1 and using partial fractions.

$$\text{Lim} \left(\int_0^{\pi/2} \frac{\cos^2\theta}{\Delta^3} \, d\phi \right)$$

$$= \text{Lim} \left(\int_0^{\pi/2} \frac{1}{k^4} (4\Delta + 4(k^2-2)\Delta^{-1} + (k^2-2)^2 \Delta^{-3}) d\phi \right)$$

$$= \text{Lim} \left(-\frac{8}{k^4} (F_1 - E_1) + \frac{4F_1}{k^2} \right) + \frac{\pi}{2}$$

$$= \frac{\pi}{4}$$

$$\text{Lim} \int_0^{\pi/2} \frac{\cos^2\theta}{\Delta^5} \, d\phi$$

$$= \text{Lim} \left(\int_0^{\pi/2} \frac{1}{k^4} (4\Delta^{-1} + (k^2-2)\Delta^{-3} + (k^2-2)^2\Delta^{-5}) \, d\phi \right)$$

$$= \text{Lim} \left(\frac{8}{3k^4} (E_1 - E_1) - \frac{4E_1}{3k^2} \right) - \frac{\pi}{6}$$

$$= \frac{\pi}{4}$$

In a similar way, it may be shown that, as $k^2 \to 0$

$$\text{Lim} \left(\int_0^{\pi/2} \frac{\cos\theta}{\Delta} \, d\phi \right) = \text{Lim} \left(\int_0^{\pi/2} \frac{\cos\theta}{\Delta^3} d\phi \right) = \text{Lim} \left(\int_0^{\pi/2} \frac{\cos\theta}{\Delta^5} d\phi \right)$$

$$= \text{Lim} \left(\int_0^{\pi/2} \frac{\cos^3\theta}{\Delta^5} \, d\phi \right) = 0$$

A 5.4 - Listing of the computer program AXSYM (2) for the elastostatic analysis of an axisymmetric homogeneous isotropic linear elastic body by the indirect formulation of the boundary element method using an auxiliary boundary and a list of the main variables in AXSYM (2)

```
      PROGRAM AXSYM (INPUT,OUTPUT,TAPE1=INPUT,TAPE2=OUTPUT)
C     ELASTOSTATIC ANALYSIS OF AXISYMMETRIC BODY
C     BY THE INDIRECT BOUNDARY ELEMENT METHOD
C     USING AN AUXILIARY BOUNDARY
      CALL AXCRD (JA)
      IF (JA.EQ.1) GOTO 1
      CALL AXGTY
      CALL AXPRT
      CALL AXWRT
      IF (JA.EQ.2) GOTO 1
      CALL AXEXE
    1 CONTINUE
      END


      SUBROUTINE AXCRD (MCRD)
C     READS INPUT FROM CARDS AND PRINTS IT OUT
      COMMON /MNPR/KRS,NCBS,NCIS,NCBL,NEBT,NEIT,
     1             YG,PN,FPR,FPZ
      COMMON /BDSG/NEBS(35),RF(35),ZF(35),RL(35),ZL(35),
     1             COSB(35),RP(35),ZP(35),RQ(35),ZQ(35)
      COMMON /INSG/NEIS(35),RIF(35),ZIF(35),RIL(35),ZIL(35),
     1             PIC(35),ZIC(35),SNA(35),CSA(35)
      COMMON /BOLD/LP(35),LQ(35),BPR(35),BPZ(35)
      COMMON /LINE/WORD(40)
      DATA LUI,LUO /1,2/
      READ (LUI,100) MCRD
  100 FORMAT (4X,I1)
      READ (LUI,101) ( WORD(IO),IO=1,20)
  101 FORMAT (20A4)
      READ (LUI,100) KRS
      READ (LUI,102) YG,PN
  102 FORMAT (2F10.0)
      READ (LUI,103) NCBS
  103 FORMAT (3X,I2)
      JA=1
    1 READ (LUI,104) NEBS(JA),RF(JA),ZF(JA),RL(JA),ZL(JA)
  104 FORMAT (3X,I2,5X,4F10.0)
      JA=JA+1
      IF (JA.LE.NCBS) GOTO 1
      READ (LUI,103) NCIS
      IF (NCIS.EQ.0) GOTO 2
      JA=1
    3 READ (LUI,104) NEIS(JA),RIF(JA),ZIF(JA),RIL(JA),ZIL(JA)
      JA=JA+1
      IF (JA.LE.NCIS) GOTO 3
    2 CONTINUE
      READ (LUI,101) ( WORD(IO),IO=21,40)
      READ (LUI,103) NCBL
      IF (NCBL.EQ.0) GOTO 4
      JA=1
    5 READ (LUI,105) LP(JA),LQ(JA),BPR(JA),BPZ(JA)
  105 FORMAT (2(3X,I2),2F10.0)
      JA=JA+1
      IF (JA.LE.NCBL) GOTO 5
    4 CONTINUE
      READ (LUI,106) FPR,FPZ
  106 FORMAT (2F10.0)
      WRITE (LUO,200)
  200 FORMAT (1H1)
      WRITE (LUO,201)
  201 FORMAT(/   11H INPUT DATA)
      WRITE (LUO,202) MCRD
  202 FORMAT (/   11H CARD       ,4X,I1,75X)
      WRITE (LUO,203) ( WORD(IO),IO=1,20)
  203 FORMAT (/   11H CARD       ,20A4)
      WRITE (LUO,202) KRS
      WRITE (LUO,204) YG,PN
  204 FORMAT (/   11H CARD       ,2F10.3,60X)
      WRITE (LUO,205) NCBS
  205 FORMAT (/   11H CARD       ,3X,I2,75X)
      JA=1
    6 WRITE (LUO,206) NEBS(JA),RF(JA),ZF(JA),RL(JA),ZL(JA)
  206 FORMAT (/   11H CARD       ,3X,I2,5X,4F10.3,30X)
      JA=JA+1
      IF (JA.LE.NCBS) GOTO 6
      WRITE (LUO,205) NCIS
      JA=1
    8 WRITE (LUO,206) NEIS(JA),RIF(JA),ZIF(JA),RIL(JA),ZIL(JA)
      JA=JA+1
      IF (JA.LE.NCIS) GOTO 8
      WRITE (LUO,203) ( WORD(IO),IO=21,40)
      WRITE (LUO,205) NCBL
      IF (NCBL.EQ.0) GOTO 9
      JA=1
   10 WRITE (LUO,207) LP(JA),LQ(JA),BPR(JA),BPZ(JA)
  207 FORMAT (/   11H CARD       ,2(3X,I2),2F10.4,50X)
      JA=JA+1
      IF (JA.LE.NCBL) GOTO 10
    9 CONTINUE
      WRITE (LUO,208) FPR,FPZ
  208 FORMAT (/   11H CARD       ,2F10.4,60X)
      RETURN
      END


      SUBROUTINE AXGTY
C     FORMS AND PRINTS OUT LAYOUT OF STRUCTURE
      COMMON /MNPR/KRS,NCBS,NCIS,NCBL,NEBT,NEIT,
     1             YG,PN,FPR,FPZ
      CALL AXFCO
      JA=1
      DO 1 IA=1,NCBS
      CALL AXCEN (IA,JA,JB)
      JA=JB+1
    1 CONTINUE
      CALL AXWCO
      IF (NCIS.EQ.NCBS) GOTO 2
      JA=NCBS+1
      JB=JB+1
      DO 3 IA=JA,NCIS
      CALL AXCEN (IA,JB,JC)
      CALL AXWEN (IA,JB,JC)
      JB=JC+1
    3 CONTINUE
      GOTO 4
    2 JA=1
      CALL AXWEN (JA,JA,JB)
      JC=JB
    4 NEIT=JC-NEBT
      RETURN
      END


      SUBROUTINE AXFCO
C     FORMS END COORDINATES AND SLOPES
C     OF AUXILIARY BOUNDARY ELEMENTS
      COMMON /MNPR/KRS,NCBS,NCIS,NCBL,NEBT,NEIT,
     1             YG,PN,FPR,FPZ
      COMMON /BDSG/NEBS(35),RF(35),ZF(35),RL(35),ZL(35),
     1             COSB(35),RP(35),ZP(35),RQ(35),ZQ(35)
      JA=1
      DO 1 IA=1,NCBS
      JB=NEBS(IA)
      RT=RF(IA)
      ZT=ZF(IA)
      DR=(RL(IA)-RT)/JB
      DZ=(ZL(IA)-ZT)/JB
      IF (ABS(DZ).LT.1.0E-3) GOTO 2
      COSBT=0.0
      GOTO 3
    2 COSBT=1.0
    3 CONTINUE
      DO 4 IB=1,JB
      COSB(JA)=COSBT
      RP(JA)=RT
      ZP(JA)=ZT
      RT=RT+DR
```

```
      ZT=ZT+DZ
      RQ(JA)=RT
      ZQ(JA)=ZT
      JA=JA+1
    4 CONTINUE
    1 CONTINUE
      NEBT=JA-1
      RETURN
      END


      SUBROUTINE AXCEN (IDSI,IDEP,IDEQ)
C     FORMS CENTRE COORDINATES OF ELEMENTS IN A SEGMENT
C     AND SLOPES OF BOUNDARY ELEMENTS
      COMMON /MNPR/KRS,NCBS,NCIS,NCBL,NEBT,NEIT,
     1            YG,PN,FPR,FPZ
      COMMON /INSG/NEIS(35),RIF(35),ZIF(35),RIL(35),ZIL(35),
     1            RIC(35),ZIC(35),SNA(35),CSA(35)
      JA=NEIS(IDSI)
      RT=RIF(IDSI)
      ZT=ZIF(IDSI)
      DR=(RIL(IDSI)-RT)/JA
      DZ=(ZIL(IDSI)-ZT)/JA
      RT=RT+DR/2.0
      ZT=ZT+DZ/2.0
      JB=IDEP
      IF (IDSI.LE.NCBS) GOTO 1
      JB=1
      GOTO 2
    1 DS=SQRT(DR*DR+DZ*DZ)
      SAU=-DZ/DS
      CAU=DR/DS
      DO 3 IA=1,JA
      SNA(JB)=SAU
      CSA(JB)=CAU
      JB=JB+1
    3 CONTINUE
      JB=IDEP
    2 CONTINUE
      DO 4 IA=1,JA
      RIC(JB)=RT
      ZIC(JB)=ZT
      RT=RT+DR
      ZT=ZT+DZ
      JB=JB+1
    4 CONTINUE
      IDEQ=IDEP+JA-1
      RETURN
      END


      SUBROUTINE AXWCO
C     PRINTS OUT END COORDINATES AND SLOPES OF AUXILIARY
C     BOUNDARY ELEMENTS AND COORDINATES OF BOUNDARY POINTS
      COMMON /MNPR/KRS,NCBS,NCIS,NCBL,NEBT,NEIT,
     1            YG,PN,FPR,FPZ
      COMMON /BDSG/NEBS(35),RF(35),ZF(35),RL(35),ZL(35),
     1            COSB(35),RP(35),ZP(35),RQ(35),ZQ(35)
      COMMON /INSG/NEIS(35),RIF(35),ZIF(35),RIL(35),ZIL(35),
     1            RIC(35),ZIC(35),SNA(35),CSA(35)
      DATA LUO /2/
      WRITE (LUO,200)
  200 FORMAT (1H1)
      WRITE (LUO,201)
  201 FORMAT (/  35H AXISYMMETRIC ELASTOSTATIC ANALYSIS,
     1 32H BY THE BOUNDARY INTEGRAL METHOD,
     2 28H USING AN AUXILIARY BOUNDARY//
     3 33H                          GEORGE A WATT,
     4 33H                IMPERIAL COLLEGE LONDON)
      WRITE (LUO,202)
  202 FORMAT (/  40H VERSION 1. UNIFORMLY DISTRIBUTED NORMAL,
     1 46H AND TANGENTIAL FICTITIOUS LOADS ON RADIAL AND//
     2 41H AXIAL RING ELEMENTS FORMING A VERTICALLY,
     3 32H AXISYMMETRIC AUXILIARY BOUNDARY)
      WRITE (LUO,203)
  203 FORMAT (/  36H SCHEME 2, A MAXIMUM OF 35 AUXILIARY,
     1 58H BOUNDARY ELEMENTS AND POINTS.10-POINT GAUSSIAN QUADRATURE//
     2 46H USING A STRAIGHT LINE VARIABLE,AND AN IN-CORE,
     3 43H SOLVER ALLOWING ZEROS ON THE MAIN DIAGONAL//
     4 39H WITH A 5-TERM POLYNOMIAL APPROXIMATION,
     5 32H FOR COMPLETE ELLIPTIC INTEGRALS////)
      IF (KRS.EQ.0) GOTO 1
      WRITE (LUO,204)
  204 FORMAT (/  36H MIRROR SYMMETRY WITH RESPECT TO THE,
     1 17H HORIZONTAL PLANE)
    1 CONTINUE
      WRITE (LUO,205)
  205 FORMAT (/  32H AUXILIARY BOUNDARY ELEMENTS AND,
     1 27H ASSOCIATED BOUNDARY POINTS)
      WRITE (LUO,206)
  206 FORMAT (/  35H  EL.NO.       R1          Z1          ,
     1 45H      R2          Z2          COS(B)      ,
     2 44H  PT NO.       RB          ZB       SIN(A)     COS(A))
      DO 2 IA=1,NEBT
      WRITE (LUO,207) IA,RP(IA),ZP(IA),
     1                RQ(IA),ZQ(IA),COSB(IA),
     2                IA,RIC(IA),ZIC(IA),SNA(IA),CSA(IA)
  207 FORMAT (1X,I5,3X,2F10.3,
     1      5X,2F10.3,5X,1F10.3,
     2     12X,I5,3X,4F10.3)
    2 CONTINUE
      RETURN
      END


      SUBROUTINE AXWEN (IDSI,IDEP,IDEQ)
C     PRINTS OUT CENTRE COORDINATES OF INTERIOR ELEMENTS
      COMMON /MNPR/KRS,NCBS,NCIS,NCBL,NEBT,NEIT,
     1            YG,PN,FPR,FPZ
      COMMON /INSG/NEIS(35),RIF(35),ZIF(35),RIL(35),ZIL(35),
     1            RIC(35),ZIC(35),SNA(35),CSA(35)
      DATA LUO /2/
  200 FORMAT (1H1)
      WRITE (LUO,200)
      WRITE (LUO,201)
  201 FORMAT (/  16H INTERIOR POINTS)
      IF (NCIS.EQ.NCBS) GOTO 1
      JA=IDEP
      IF (IDSI.LE.NCBS) GOTO 2
      JA=1
    2 CONTINUE
      WRITE (LUO,202)
  202 FORMAT (/  26H  PT NO.       RC          ZC)
      DO 3 IA=IDEP,IDEQ
      WRITE (LUO,203) IA,RIC(JA),ZIC(JA)
  203 FORMAT (1X,I5,3X,2F10.3)
      JA=JA+1
    3 CONTINUE
      GOTO 4
    1 WRITE (LUO,204)
  204 FORMAT (/   5H NONE)
    4 CONTINUE
      RETURN
      END


      SUBROUTINE AXBDT
C     ALLOCATES EQUIVALENT BOUNDARY TRACTIONS EQUAL TO APPLIED
C     BOUNDARY LOADS LESS THE FIELD STRESS ON PARALLEL PLANES.
      COMMON /MNPR/KRS,NCBS,NCIS,NCBL,NEBT,NEIT,
     1            YG,PN,FPR,FPZ
      COMMON /BDSG/NEBS(35),RF(35),ZF(35),RL(35),ZL(35),
     1            COSB(35),RP(35),ZP(35),RQ(35),ZQ(35)
      COMMON /INSG/NEIS(35),RIF(35),ZIF(35),RIL(35),ZIL(35),
     1            RIC(35),ZIC(35),SNA(35),CSA(35)
      COMMON /BDLD/LP(35),LQ(35),BPR(35),BPZ(35)
      COMMON /FTFB/FR(35),FZ(35),QR(35),QZ(35),
     1            FRR(35),FZZ(35),FZR(35)
      VA=0.5*(FPZ+FPR)
      VB=VA-FPR
      DO 1 IA=1,NEBT
      VC=SNA(IA)
```

```
      VO=CSA(IA)
      VE=VB*(VO*VO-VC*VC)
      FRR(IA)=VA-VE
      FZZ(IA)=VA+VE
      FZR(IA)=-2.0*VB*VC*VO
      PR(IA)=-FZR(IA)
      PZ(IA)=-FZZ(IA)
    1 CONTINUE
      IF (NC9L.EQ.0) GOTO 2
      DO 3 IA=1,NCBL
      JA=LP(IA)
      JB=LQ(IA)
      BR=BPR(IA)
      BZ=BPZ(IA)
      DO 4 I9=JA,JB
      PR(I9)=PR(I8)+BR
      PZ(I8)=PZ(I8)+BZ
    4 CONTINUE
    3 CONTINUE
    2 CONTINUE
      RETURN
      END


      SUBROUTINE AXWDI
C     PRINTS OUT APPLIED BOUNDARY LOADS AND FIELD STRESSES
      COMMON /MNPR/KPS,NCBS,NCIS,NCBL,NEBT,NEIT,
     1             YG,PN,FPR,FPZ
      COMMON /BDSG/NEBS(35),RF(35),ZF(35),RL(35),ZL(35),
     1             COSB(35),RP(35),ZP(35),RQ(35),ZQ(35)
      COMMON /BDLD/LP(35),LQ(35),BPR(35),BPZ(35)
      COMMON /INSG/NEIS(35),RIF(35),ZIF(35),RIL(35),ZIL(35),
     1             RIC(35),ZIC(35),SNA(35),CSA(35)
      DATA LUO /2/
      WRITE (LUO,200)
  200 FORMAT (1H1)
      WRITE (LUO,201)
  201 FORMAT (/  30H PRESCRIBED BOUNDARY TRACTIONS)
      IF (NCBL.EQ.0) GOTO 1
      WRITE (LUO,202)
  202 FORMAT (/  48H  PT NO.      BPR        BPN       SIN(A)     COS(A))
      JA=1
      JB=LQ(NCBL)+1
      DO 2 IA=1,NCBL
      JC=LP(IA)
      JD=LQ(IA)
      IF (JA.LT.JC) GOTO 3
    5 BR=BPR(IA)
      BZ=BPZ(IA)
      GOTO 4
    3 BR=0.0
      BZ=0.0
    4 WRITE (LUO,203) JA,BR,BZ,SNA(JA),CSA(JA)
  203 FORMAT (1X,I5,3X,4F10.3)
      JA=JA+1
      IF (JA.LT.JC) GOTO 4
      IF (JA.EQ.JC) GOTO 5
      IF (JA.LE.JD) GOTO 4
      IF (IA.LT.NCBL) GOTO 6
      IF (JA.GT.NEBT) GOTO 7
      IF (JA.EQ.JB) GOTO 3
      IF (JA.LE.NEBT) GOTO 4
    6 CONTINUE
    2 CONTINUE
    7 CONTINUE
      GOTO 8
    1 WRITE (LUO,204)
  204 FORMAT (/   5H NONE)
    8 WRITE (LUO,200)
      WRITE (LUO,205)
  205 FORMAT (/  15H FIELD STRESSES)
      WRITE (LUO,206)
  206 FORMAT (/  17H     FPR        FPZ)
      WRITE (LUO,207) FPR,FPZ
  207 FORMAT (1X,2F10.3)
      RETURN
      END


C     SUBROUTINE AXEXE
C     EXECUTES STRESS ANALYSIS AND PRINTS OUT RESULTS
      COMMON /MNPR/KPS,NCBS,NCIS,NCBL,NEBT,NEIT,
     1             YG,PN,FPR,FPZ
      CALL AXELA
      JA=1
      DO 1 IA=1,NCBS
      CALL AXCEN (IA,JA,JB)
      JA=JB+1
    1 CONTINUE
      JC=1
      CALL AXCOE (JC,JB)
      CALL AXMAT
      CALL AXSOL
      CALL AXSTR (JC,JB)
      CALL AXWTR (JC,JB)
      IF (NCIS.EQ.NCBS) GOTO 2
      JA=NCBS+1
      JB=JB+1
      DO 3 IA=JA,NCIS
      CALL AXCEN (IA,JC,JD)
      CALL AXCOE (JA,JD)
      CALL AXSTR (JA,JB)
      JD=JB+JD-1
      CALL AXWTR (JB,JD)
      JB=JD+1
    3 CONTINUE
    2 CONTINUE
      CALL AXWDL
      RETURN
      END


C     SUBROUTINE AXELA
C     CALCULATES FUNCTIONS OF ELASTIC CONSTANTS
C     ELASA=YG
C     ELASB=PN
C     ELASC=1-2PN
C     ELASD=3-4PN
C     ELASE=1/(8PI(1-PN))
C     ELASF=(1+PN)/(8PI(1-PN)YG)
      COMMON /MNPR/KPS,NCBS,NCIS,NCBL,NEBT,NEIT,
     1             YG,PN,FPR,FPZ
      COMMON /ELAS/ELASA,ELASB,ELASC,
     1             ELASD,ELASE,ELASF
      ELASA=YG
      ELASB=PN
      ELASC=1.0-2.0*ELASB
      ELASD=1.0+2.0*ELASC
      ELASE=0.039788673577/(1.0-ELASB)
      ELASF=ELASE*(1.0+ELASB)/ELASA
      RETURN
      END


      SUBROUTINE AXCOE (NCOE,NELC)
C     CALCULATES STRESS AND DISPLACEMENT COEFFICIENTS
      COMMON /MNPR/KPS,NCBS,NCIS,NCBL,NEBT,NEIT,
     1             YG,PN,FPR,FPZ
      COMMON /BDSG/NEBS(35),RF(35),ZF(35),RL(35),ZL(35),
     1             COSB(35),RP(35),ZP(35),RQ(35),ZQ(35)
      COMMON /INSG/NEIS(35),RIF(35),ZIF(35),RIL(35),ZIL(35),
     1             RIC(35),ZIC(35),SNA(35),CSA(35)
      COMMON /SDCU/RRRU,TTRU,ZZRU,
     1             ZRRU,DRRU,DZRU,
     2             RRZU,TTZU,ZZZU,
     3             ZRZU,DRZU,DZZU
      COMMON /SDCA/RRR(35,35),TTR(35,35),ZZR(35,35),
     1             ZRR(35,35),DRR(35,35),DZR(35,35),
     2             RRZ(35,35),TTZ(35,35),ZZZ(35,35),
     3             ZRZ(35,35),DRZ(35,35),DZZ(35,35)
```

```
      DO 1 IA=1,NELC
      RCU=RIC(IA)
      ZCU=ZIC(IA)
      SAU=SNA(IA)
      CAU=CSA(IA)
      DO 2 IB=1,NEBT
      RPU=RP(IB)
      ZPU=ZP(IB)
      RQU=RQ(IB)
      ZQU=ZQ(IB)
      IF (ABS(COSB(IB)).LT.1.0E-3) GOTO 3
      ZCV=ZCU-ZPU
      IF (RPU.GT.RQU) GOTO 4
      CALL AXSDS (RCU,ZCV,RPU,ZPU,RQU,ZQU)
      GOTO 5
    4 CALL AXSDR (RCU,ZCV,RQU,ZQU,RPU,ZPU)
      GOTO 5
    3 CONTINUE
      IF (ZPU.GT.ZQU) GOTO 6
      CALL AXSD7 (RCU,ZCU,RPU,ZPU,RQU,ZQU)
      GOTO 5
    6 CALL AXSDZ (RCU,ZCU,RQU,ZQU,RPU,ZPU)
    5 CONTINUE
      IF (NCOE.NE.1) GOTO 7
      CALL AXPOT (SAU,CAU)
    7 CONTINUE
      RRR(IA,IB)=RRRU
      TTR(IA,IB)=TTRU
      ZZR(IA,IB)=ZZRU
      ZRR(IA,IB)=ZRRU
      DRR(IA,IB)=DRRU
      DZR(IA,IB)=DZRU
      RRZ(IA,IB)=RRZU
      TTZ(IA,IB)=TTZU
      ZZZ(IA,IB)=ZZZU
      ZRZ(IA,IB)=ZRZU
      DRZ(IA,IB)=DRZU
      DZZ(IA,IB)=DZZU
    2 CONTINUE
    1 CONTINUE
      RETURN
      END


      SUBROUTINE AXSDR (PPI,PZI,ERF,EZF,ERL,EZL)
C     CALCULATES STRESSES AND DISPLACEMENTS
CC    INDUCED BY UNIFORM LOADINGS
C     IN THE RADIAL AND AXIAL DIRECTIONS
C     ALONG THE SURFACE OF A DISC
      DIMENSION GW(10),GP(10)
      COMMON /MNPR/KRS,NCBS,NCIS,NCBL,NEBT,NEIT,
     1             YG,PN,FPR,FPZ
      COMMON /SOCU/RRRU,TTRU,ZZRU,
     1             ZRRU,DRRU,DZRU,
     2             RRZU,TTZU,ZZZU,
     3             ZRZU,DRZU,DZZU
      COMMON /ICC/COC,COB,COA,
     1            CCC,CCB,CCA,
     2            CBB,CBA,CAA
      COMMON /ELAS/ELASA,ELASB,ELASC,
     1             ELASD,ELASE,ELASF
      COMMON /PEP/PAH,PAM,EF,ES
      DATA GW /0.2955242247,0.2955242247,
     1         0.2692667193,0.2692667193,
     2         0.2190863625,0.2190863625,
     3         0.1494513492,0.1494513492,
     4         0.0666713443,0.0666713443/

      DATA GP /0.1488743390,-0.1488743390,
     1         0.4333953941,-0.4333953941,
     2         0.6794095683,-0.6794095683,
     3         0.8650633667,-0.8650633667,
     4         0.9739065285,-0.9739065285/
      EZT=EZF
      EZF=0.0
      EZL=0.0

C     SYMMETRY
      ISYM=0
      RRRU=0.0
      TTRU=0.0
      ZZRU=0.0
      ZRRU=0.0
      DRRU=0.0
      DZRU=0.0
      RRZU=0.0
      TTZU=0.0
      ZZZU=0.0
      ZRZU=0.0
      DRZU=0.0
      DZZU=0.0
C     INTEGRATION BY GAUSSIAN QUADRATURE
    6 VA=0.5*(ERL+ERF)
      VB=0.5*(ERL-ERF)
      RRNA=0.0
      RRNB=0.0
      RRNC=0.0
      RRND=0.0
      TTNA=0.0
      TTNB=0.0
      TTNC=0.0
      ZZNA=0.0
      ZZNB=0.0
      ZRNA=0.0
      ZRNB=0.0
      ZRNC=0.0
      ZRND=0.0
      DRNA=0.0
      DRNB=0.0
      DZNA=0.0
      DZNB=0.0
      RRTA=0.0
      RRTB=0.0
      RRTC=0.0
      RRTD=0.0
      RRTE=0.0
      RRTF=0.0
      RRTG=0.0
      RRTH=0.0
      RRTI=0.0
      TTTA=0.0
      TTTB=0.0
      TTTC=0.0
      TTTD=0.0
      TTTE=0.0
      TTTF=0.0
      TTTG=0.0
      ZZTA=0.0
      ZZTB=0.0
      ZZTC=0.0
      ZZTD=0.0
      ZRTA=0.0
      ZRTB=0.0
      ZRTC=0.0
      ZPTD=0.0
      ZPTE=0.0
      DRTA=0.0
      DPTB=0.0
      DPTC=0.0
      DRTD=0.0
      DPTE=0.0
      DZTA=0.0
      DZTB=0.0
      DO 1 IA=1,10
      ERI=VA+VB*GP(IA)
      CALL AXPEP (PRI,PZI,ERI,EZF)
      IF (PAM.LT.0.01) GOTO 2
      CALL AXCIS
      CALL AXICC
      GOTO 3
    2 CONTINUE
      CDA=1.570796327
      CDB=1.570796327
```

```
      CDC=1.570796327
      CCA=0.0
      CCB=0.0
      CCC=0.0
      CBA=0.7853981635
      CBB=0.7853981635
      CAA=0.0
    3 CONTINUE
      CDA=CDA*PAH**5
      CDB=CDB*PAH**3
      CDC=CDC*PAH
      CCA=CCA*PAH**5
      CCB=CCB*PAH**3
      CCC=CCC*PAH
      CBA=CBA*PAH**5
      CBB=CBB*PAH**3
      CAA=CAA*PAH**5
      VC=4.0*VB*GW(IA)*EPI
      VD=VC*ERI
      VE=VC*ERI*ERI
      VF=VC*ERI*EPI*ERI
      VCCA=VC*CCA
      VCCB=VC*CCB
      VCCC=VC*CCC
      VCDA=VC*CDA
      VCDB=VC*CDB
      VCDC=VC*CDC
      VDBA=VD*CBA
      VDBB=VD*CBB
      VDCA=VD*CCA
      VDCB=VD*CCB
      VDDA=VD*CDA
      VDDB=VD*CDB
      VEAA=VE*CAA
      VEBA=VE*CBA
      VECA=VE*CCA
      VECB=VE*CCB
      VEDA=VE*CDA
      VFBA=VF*CBA
      VFDA=VF*CDA
      RRNA=RRNA+VCDA
      RRNB=RRNB+VDCA
      RRNC=RRNC+VEBA
      RRND=RRND+VCDB
      TTNA=TTNA+VEDA
      TTNB=TTNB+VEBA
      TTNC=TTNC+VCDB
      ZZNA=ZZNA+VCDA
      ZZNB=ZZNB+VCDB
      ZRNA=ZRNA+VCDA
      ZRNB=ZRNB+VCDB
      ZRNC=ZRNC+VDCA
      ZRND=ZRND+VDCB
      DRNA=DRNA+VCDB
      DRNB=DRNB+VDCB
      DZNA=DZNA+VCDB
      DZNB=DZNB+VCDC
      RRTA=RRTA+VCCA
      RRTB=RRTB+VDBA
      RRTC=RRTC+VDDA
      RRTD=RRTD+VEAA
      RRTE=RRTE+VECA
      RRTF=RRTF+VFBA
      RRTG=RRTG+VCCB
      RRTH=RRTH+VDDB
      RRTI=RRTI+VDBB
      TTTA=TTTA+VECA
      TTTB=TTTB+VFDA
      TTTC=TTTC+VEAA
      TTTD=TTTD+VFBA
      TTTE=TTTE+VCCB
      TTTF=TTTF+VDBB
      TTTG=TTTG+VDDB
      ZZTA=ZZTA+VCCA
      ZZTB=ZZTB+VDDA
      ZZTC=ZZTC+VCCB
      ZZTD=ZZTD+VDDB
      ZRTA=ZRTA+VCCA
      ZRTB=ZRTB+VDBA
      ZRTC=ZRTC+VDDA
      ZRTD=ZRTD+VECA
      ZRTE=ZRTE+VCCB
      ORTA=ORTA+VCCB
      ORTB=ORTB+VDBB
      DRTC=DRTC+VDDB
      DRTD=DRTD+VECB
      DRTE=DRTE+VCCC
      DZTA=DZTA+VCCB
      DZTB=DZTB+VDDB
    1 CONTINUE
C     ASSEMBLY OF COMPONENTS
      VA=PRI
      VB=PZI
      VC=VA*VA
      VD=VA*VB
      VE=VB*VB
      VF=VC*VA
      VG=VC*VB
      VH=VA*VE
      VI=VE*VB
      RRNA=3.0*VG*RRNA
      RRNB=-6.0*VD*RRNB
      RRNC=3.0*VB*RRNC
      RRND=-ELASC*VB*RRND
      RRNR=(RRNA+RRNB+RRNC+RRND)*ELASE
      TTNA=3.0*VB*TTNA
      TTNB=-3.0*VB*TTNB
      TTNC=-ELASC*VB*TTNC
      TTNR=(TTNA+TTNB+TTNC)*ELASE
      ZZNA=3.0*VI*ZZNA
      ZZNB=ELASC*VB*ZZNB
      ZZNR=(ZZNA+ZZNB)*ELASE
      ZRNA=3.0*VH*ZRNA
      ZRNB=ELASC*VA*ZRNB
      ZRNC=-3.0*VE*ZRNC
      ZRND=-ELASC*ZRND
      ZRNR=(ZRNA+ZRNB+ZRNC+ZRND)*ELASE
      DRNA=VD*DRNA
      DRNB=-VB*DRNB
      DRNR=(DRNA+DRNB)*ELASE
      DZNA=VE*DZNA
      DZNB=ELASD*DZNB
      DZNR=(DZNA+DZNB)*ELASE
      RRTA=3.0*VF*RRTA
      RRTB=-6.0*VC*RRTB
      RRTC=-3.0*VC*RRTC
      RRTD=3.0*VA*RRTD
      RRTE=6.0*VA*RRTE
      RRTF=-3.0*RRTF
      RRTG=ELASC*VA*RRTG
      RRTH=ELASC*RRTH
      RRTI=-2.0*ELASC*RRTI
      RRTR=RRTA+RRTB+RRTC+RRTD+RRTE+RRTF
      RRTR=(RRTR+RRTG+RRTH+RRTI)*ELASE
      TTTA=3.0*VA*TTTA
      TTTB=-3.0*TTTB
      TTTC=-3.0*VA*TTTC
      TTTD=3.0*TTTD
      TTTE=-ELASC*VA*TTTE
      TTTF=2.0*ELASC*TTTF
      TTTG=-ELASC*TTTG
      TTTR=TTTA+TTTB+TTTC+TTTD+TTTE
      TTTR=(TTTR+TTTF+TTTG)*ELASE
      ZZTA=3.0*VH*ZZTA
      ZZTB=-3.0*VE*ZZTB
      ZZTC=-ELASC*VA*ZZTC
      ZZTD=ELASC*ZZTD
      ZZTR=(ZZTA+ZZTB+ZZTC+ZZTD)*ELASE
      ZRTA=3.0*VG*ZRTA
```

```
      ZRTB=-3.0*VD*ZRTB
      ZRTC=-1.0*VD*ZRTC
      ZRTD=3.0*VB*ZRTD
      ZRTE=ELASC*VB*ZRTE
      ZRTR=ZRTA+ZRTB+ZRTC+ZRTD
      ZRTR=(ZRTR+ZRTE)*ELASF
      DRTA=VC*DRTA
      DRTB=-VA*DRTB
      DRTC=-VA*DRTC
      DRTE=ELASD*DRTE
      DRTR=DRTA+DRTB+DRTC+DRTD
      DRTR=(DRTR+DRTE)*ELASF
      DZTA=VD*DZTA
      DZTB=-VB*DZTB
      DZTR=(DZTA+DZTB)*ELASF
      RRZU=RRNR-RRZU
      TTZU=TTNR-TTZU
      ZZZU=ZZNR-ZZZU
      ZRZU=ZRNR-ZRZU
      DRZU=DRNR-DRZU
      DZZU=DZNR-DZZU
      RRRU=RRTR+RRRU
      TTRU=TTTR+TTRU
      ZZRU=ZZTR+ZZRU
      ZRRU=ZRTR+ZRRU
      DRRU=DRTR+DRRU
      DZRU=DZTR+DZRU
      IF (KRS.EQ.0) GOTO 4
      ISYM=ISYM+1
      IF (ISYM.EQ.2) GOTO 5
      PZI=PZI+2.0*EZT
      IF (ISYM.EQ.1) GOTO 6
    5 CONTINUE
      RRZU=-RRZU
      TTZU=-TTZU
      ZZZU=-ZZZU
      ZRZU=-ZRZU
      DRZU=-DRZU
      DZZU=-DZZU
    4 CONTINUE
      RETURN
      END


      SUBROUTINE AXSDZ (PRI,PZI,ERF,EZF,ERL,EZL)
C     CALCULATES STRESSES AND DISPLACEMENTS
CC    INDUCED BY UNIFORM LOADINGS
C     IN THE RADIAL AND AXIAL DIRECTIONS
      ALONG THE SURFACE OF A CYLINDER
      DIMENSION GW(10),GP(10)
      COMMON /MNPR/KRS,NCBS,NCIS,NCBL,NEBT,NEIT,
     1             YG,PN,FPR,FPZ
      COMMON /SDCU/RRRU,TTRU,ZZRU,
     1             ZRRU,DRRU,DZRU,
     2             RRZU,TTZU,ZZZU,
     3             ZRZU,DRZU,DZZU
      COMMON /ICC/CDC,CDB,CDA,
     1            CCC,CCB,CCA,
     2            CBB,CBA,CAA
      COMMON /ELAS/ELASA,ELASB,ELASC,
     1             ELASD,ELASE,ELASF
      COMMON /PEP/PAH,PAM,EF,ES
      DATA GW /0.2955242247,0.2955242247,
     1         0.2692667193,0.2692667193,
     2         0.2190863625,0.2190863625,
     3         0.1494513492,0.1494513492,
     4         0.0666713443,0.0666713443/
      DATA GP /0.1488743390,-0.1488743390,
     1         0.4333953941,-0.4333953941,
     2         0.6794095683,-0.6794095683,
     3         0.8650633667,-0.8650633667,
     4         0.9739065285,-0.9739065285/
C     SYMMETRY
      ISYM=0
      RRRU=0.0
      TTRU=0.0
      ZZRU=0.0
      ZRRU=0.0
      DRRU=0.0
      DZRU=0.0
      RRZU=0.0
      TTZU=0.0
      ZZZU=0.0
      ZRZU=0.0
      DRZU=0.0
      DZZU=0.0
C     INTEGRATION BY GAUSSIAN QUADRATURE
    6 VA=0.5*(EZL+EZF)
      VB=0.5*(EZL-EZF)
      RRNA=0.0
      RRNB=0.0
      RRNC=0.0
      RRND=0.0
      RRNE=0.0
      RRNF=0.0
      RRNG=0.0
      TTNA=0.0
      TTNB=0.0
      TTNC=0.0
      TTND=0.0
      TTNE=0.0
      TTNF=0.0
      TTNG=0.0
      ZZNA=0.0
      ZZNB=0.0
      ZZNC=0.0
      ZZND=0.0
      ZRNA=0.0
      ZRNB=0.0
      ZRNC=0.0
      ZRND=0.0
      DRNA=0.0
      DRNB=0.0
      DRNC=0.0
      DRND=0.0
      DZNA=0.0
      DZNB=0.0
      RRTA=0.0
      RRTB=0.0
      RRTC=0.0
      RRTD=0.0
      TTTA=0.0
      TTTB=0.0
      TTTC=0.0
      ZZTA=0.0
      ZZTB=0.0
      ZRTA=0.0
      ZRTB=0.0
      ZRTC=0.0
      ZRTD=0.0
      DRTA=0.0
      DRTB=0.0
      DZTA=0.0
      DZTB=0.0
      DO 1 IA=1,10
      EZI=VA+VB*GP(IA)
      CALL AXPEP (PRI,PZI,EPF,EZI)
      IF (PAM.LT.0.01) GOTO 2
      CALL AXFIS
      CALL AXICC
      GOTO 3
    2 CONTINUE
      COA=1.570796327
      COB=1.570796327
      COC=1.570796327
      CCA=0.0
      CCB=0.0
      CCC=0.0
      CBA=0.7853981635
      CBB=0.7853981635
      CAA=0.0
    3 CONTINUE
```

```
      CDA=CDA*PAH**5
      CDB=CDB*PAH**3
      CDC=CDC*PAH
      CCA=CCA*PAH**5
      CCB=CCB*PAH**3
      CCC=CCC*PAH
      CBA=CBA*PAH**5
      CBB=CBB*PAH**3
      CAA=CAA*PAH**5
      VC=4.0*VB*GW(IA)
      VD=VC*(PZI-EZI)
      VE=VC*(PZI-EZI)**2
      VF=VC*(PZI-EZI)**3
      VCAA=VC*CAA
      VCBA=VC*CBA
      VCBB=VC*CBB
      VCCA=VC*CCA
      VCCB=VC*CCB
      VCCC=VC*CCC
      VCDA=VC*CDA
      VCDB=VC*CDB
      VCDC=VC*CDC
      VDBA=VD*CBA
      VDCA=VD*CCA
      VDCB=VD*CCB
      VDDA=VD*CDA
      VDDB=VD*CDB
      VECA=VE*CCA
      VEDA=VE*CDA
      VEDB=VE*CDB
      VFDA=VF*CDA
      RRNA=RRNA+VCAA
      RRNB=RRNB+VCBA
      RRNC=RRNC+VCCA
      RRND=RRND+VCDA
      RRNE=RRNE+VCBB
      RRNF=RRNF+VCCB
      RRNG=RRNG+VCDB
      TTNA=TTNA+VCAA
      TTNB=TTNB+VCBA
      TTNC=TTNC+VCCA
      TTND=TTND+VCDA
      TTNE=TTNE+VCBB
      TTNF=TTNF+VCCB
      TTNG=TTNG+VCDB
      ZZNA=ZZNA+VECA
      ZZNB=ZZNB+VEDA
      ZZNC=ZZNC+VCCB
      ZZND=ZZND+VCDB
      ZRNA=ZRNA+VDBA
      ZRNB=ZRNB+VDCA
      ZRNC=ZRNC+VDDA
      ZRND=ZRND+VDCB
      DRNA=DRNA+VCBB
      DRNB=DRNB+VCCB
      DRNC=DRNC+VCDB
      DRND=DRND+VCCC
      DZNA=DZNA+VDCB
      DZNB=DZNB+VDDB
      RRTA=RRTA+VDBA
      RRTB=RRTB+VDCA
      RRTC=RRTC+VDDA
      RRTD=RRTD+VDDB
      TTTA=TTTA+VDBA
      TTTB=TTTB+VDDA
      TTTC=TTTC+VDDB
      ZZTA=ZZTA+VFDA
      ZZTB=ZZTB+VDDB
      ZRTA=ZRTA+VECA
      ZRTB=ZRTB+VEDA
      ZRTC=ZRTC+VCCB
      ZRTD=ZRTD+VCDB
      DRTA=DRTA+VDCB
      DRTB=DRTB+VDDB
      DZTA=DZTA+VEDB
      DZTB=DZTB+VCDC
    1 CONTINUE
C     ASSEMBLY OF COMPONENTS
      VA=PRI
      VB=ERF
      VC=VA*VA
      VD=VA*VB
      VE=VB*VB
      VF=VC*VA
      VG=VC*VB
      VH=VA*VE
      VI=VE*VB
      VJ=VF*VB
      VK=VC*VE
      VL=VA*VI
      VM=VE*VE
      RRNA=3.0*VL*RRNA
      RRNB=-3.0*(VM+2.0*VK)*RRNB
      RRNC=3.0*(VJ+2.0*VL)*RRNC
      RRND=-3.0*VK*RRND
      RRNE=-2.0*ELASC*VE*RRNE
      RRNF=ELASC*VD*RRNF
      RRNG=ELASC*VE*RRNG
      RRNZ=RRNA+RRNB+RRNC+RRND+RRNE
      RRNZ=(RRNZ+RRNF+RRNG)*ELASE
      TTNA=-3.0*VL*TTNA
      TTNB=3.0*VM*TTNB
      TTNC=3.0*VL*TTNC
      TTND=-3.0*VM*TTND
      TTNE=2.0*ELASC*VE*TTNE
      TTNF=-ELASC*VD*TTNF
      TTNG=-ELASC*VE*TTNG
      TTNZ=TTNA+TTNB+TTNC+TTND+TTNE
      TTNZ=(TTNZ+TTNF+TTNG)*ELASE
      ZZNA=3.0*VD*ZZNA
      ZZNB=-3.0*VE*ZZNB
      ZZNC=-ELASC*VD*ZZNC
      ZZND=ELASC*VE*ZZND
      ZZNZ=(ZZNA+ZZNB+ZZNC+ZZND)*ELASE
      ZRNA=-3.0*VM*ZRNA
      ZRNB=3.0*(VG+VI)*ZRNB
      ZRNC=-3.0*VM*ZRNC
      ZRND=ELASC*VB*ZRND
      ZRNZ=(ZRNA+ZRNB+ZRNC+ZRND)*ELASE
      DRNA=-VM*DRNA
      DRNB=(VG+VI)*DRNB
      DRNC=-VM*DRNC
      DRND=ELASD*VB*DRND
      DRNZ=(DRNA+DRNB+DRNC+DRND)*ELASF
      DZNA=VD*DZNA
      DZNB=-VE*DZNB
      DZNZ=(DZNA+DZNB)*ELASF
      RRTA=3.0*VI*RRTA
      RRTB=-6.0*VM*RRTB
      RRTC=3.0*VG*RRTC
      RRTD=-ELASC*VB*RRTD
      RRTZ=(RRTA+RRTB+RRTC+RRTD)*ELASE
      TTTA=-3.0*VI*TTTA
      TTTB=3.0*VI*TTTB
      TTTC=-ELASC*VB*TTTC
      TTTZ=(TTTA+TTTB+TTTC)*ELASE
      ZZTA=3.0*VB*ZZTA
      ZZTB=ELASC*VB*ZZTB
      ZZTZ=(ZZTA+ZZTB)*ELASE
      ZRTA=-3.0*VE*ZRTA
      ZRTB=3.0*VD*ZRTB
      ZRTC=-ELASC*VE*ZRTC
      ZRTD=ELASC*VD*ZRTD
      ZRTZ=(ZRTA+ZRTB+ZRTC+ZRTD)*ELASE
      DRTA=-VE*DRTA
      DRTB=VD*DRTB
      DRTZ=(DRTA+DRTB)*ELASF
      DZTA=VB*DZTA
      DZTB=ELASD*VB*DZTB
      DZTZ=(DZTA+DZTB)*ELASF
      RRZU=RRTZ-RRZU
      TTZU=TTTZ-TTZU
      ZZZU=ZZTZ-ZZZU
```

```
      ZRZU=ZRTZ-ZRZU
      DRZU=DRTZ-DRZU
      DZZU=DZTZ-DZZU
      RRRU=RRNZ+RRRU
      TTRU=TTNZ+TTRU
      ZZRU=ZZNZ+ZZRU
      ZRRU=ZRNZ+ZRRU
      DRRU=DRNZ+DRRU
      DZRU=DZNZ+DZRU
      IF (KRS.EQ.0) GOTO 4
      ISYM=ISYM+1
      IF (ISYM.EQ.2) GOTO 5
      EZU=-EZF
      EZF=-EZL
      EZL=EZU
      IF (ISYM.EQ.1) GOTO 6
    5 CONTINUE
      RRZU=-RRZU
      TTZU=-TTZU
      ZZZU=-ZZZU
      ZRZU=-ZRZU
      DRZU=-DRZU
      DZZU=-DZZU
    4 CONTINUE
      RETURN
      END


      SUBROUTINE AXPEP (VA,VB,VC,VD)
C     CALCULATES POINT-ELEMENT PARAMETERS
      COMMON /PEP/PAM,PAM,EF,ES
      VE=VA+VC
      VF=VE*VE
      VG=VB-VD
      VH=VG*VG
      VI=VF+VH
      PAM=1.0/SQRT(VI)
      VJ=4.0*VA*VC
      PAM=VJ/VI
      RETURN
      END

      SUBROUTINE AXEIS
C     CALCULATES COMPLETE ELLIPTIC INTEGRALS
CC    USING POLYNOMIAL APPROXIMATIONS
CC    0.0.LE.PAM.LT.1.0
      COMMON /PEP/PAM,PAM,EF,ES
      DATA AZEF,BZEF /1.38629436112,0.5/,
     1     AONF,BONF /0.09666344259,0.12498593597/,
     2     ATHF,BTHF /0.03590092383,0.06880248576/,
     3     ATHF,BTHF /0.03742563713,0.03328355346/,
     4     AFOF,BFOF /0.01451196212,0.00441787012/,
     5     AONS,BONS /0.44325141463,0.24998368310/,
     6     ATHS,BTHS /0.06260601220,0.09200180037/,
     7     ATHS,BTHS /0.04757383546,0.04069697526/,
     8     AFOS,BFOS /0.01736506451,0.00526449639/
      DATA PAMU /0.99999999999/
      VA=AMIN1 (PAMU,PAM)
      VB=1.0-VA
      VC=VB*VB
      VD=VC*VB
      VE=VD*VB
      VF=VE*AFOF
      VG=VD*ATHF
      VH=VC*ATHF
      VI=VB*AONF
      VI=VI+VH+VG+VF+AZEF
      VH=VE*AFOS
      VG=VD*ATHS
      VF=VC*ATHS
      VJ=VB*AONS
      VJ=VJ+VF+VG+VH+1.0
      VF=VE*BFOF
      VG=VD*BTHF
      VH=VC*BTHF
      VK=VB*BONF
      VK=VK+VH+VG+VF+BZEF
      VH=VE*BFOS
      VG=VD*BTHS
      VF=VC*BTHS
      VL=VB*BONS
      VL=VL+VF+VG+VH
      VM=ALOG(VB)
      EF=VI-VK*VM
      ES=VJ-VL*VM
      RETURN
      END


      SUBROUTINE AXICC
C     CALCULATES COMPONENTS OF INFLUENCE COEFFICIENTS
      COMMON /ICC/CDC,CDB,CDA,
     1            CCC,CCB,CCA,
     2            CBB,CBA,CAA
      COMMON /PEP/PAM,PAM,EF,ES
      CDC=EF
      VA=PAM-1.0
      VB=1.0/VA
      VC=VA-1.0
      CDB=-VB*ES
      VD=CDC-2.0*VC*VB*ES
      CDA=VD*VB/3.0
      VE=-1.0/PAM
      CCC=VE*(2.0*ES+VC*CDC)
      CCB=VE*(2.0*CDC+VC*CDB)
      CCA=VE*(2.0*CDB+VC*CDA)
      VF=VE*VE
      VG=4.0*CDC+VC*CDB
      CBB=VF*(4.0*ES+VC*VG)
      VH=4.0*CDB+VC*CDA
      CBA=VF*(4.0*CDC+VC*VH)
      VI=VE*VF
      VJ=6.0*CDB+VC*CDA
      VK=12.0*CDC+VC*VJ
      CAA=VI*(8.0*ES+VC*VK)
      RETURN
      END


      SUBROUTINE AXROT (SN,CS)
C     TRANSFORMS STRESSES AND DISPLACEMENTS
CC    FROM GLOBAL TO LOCAL AXES
      COMMON /SOCU/RRRU,TTRU,ZZRU,
     1             ZRRU,DRRU,DZRU,
     2             RRZU,TTZU,ZZZU,
     3             ZRZU,DRZU,DZZU
      SNT=2.0*SN*CS
      CST=CS*CS-SN*SN
      VA=0.5*(ZZRU+RRRU)
      VB=VA-RRRU
      VC=VB*CST+ZRRU*SNT
      RRRU=VA-VC
      ZZRU=VA+VC
      ZRRU=ZRRU*CST-VB*SNT
      VA=DRRU
      DRRU=VA*CS-DZRU*SN
      DZRU=VA*SN+DZRU*CS
      VA=0.5*(ZZZU+RRZU)
      VB=VA-RRZU
      VC=VB*CST+ZRZU*SNT
      RRZU=VA-VC
      ZZZU=VA+VC
      ZRZU=ZRZU*CST-VB*SNT
      VA=DRZU
      DRZU=VA*CS-DZZU*SN
      DZZU=VA*SN+DZZU*CS
      RETURN
      END
```

```
      SUBROUTINE AXMAT
C     FORMS MATRIX OF INFLUENCE COEFFICIENTS
C     AND BOUNDARY TRACTIONS VECTOR
      COMMON /MNPR/KRS,NCBS,NCIS,NCBL,NEBT,NEIT,
     1             YG,PN,FPR,FPZ
      COMMON /SDCA/RRR(35,35),TTR(35,35),ZZR(35,35),
     1             ZRR(35,35),DRR(35,35),DZR(35,35),
     2             RRZ(35,35),TTZ(35,35),ZZZ(35,35),
     3             ZRZ(35,35),DRZ(35,35),DZZ(35,35)
      COMMON /FTFB/PR(35),PZ(35),QR(35),QZ(35),
     1             FRR(35),FZZ(35),FZR(35)
      COMMON /SOLV/AO(70,71)
      JA=1
      JB=2
      JC=2*NEBT+1
      DO 1 IA=1,NEBT
      JD=1
      JE=2
      DO 2 IB=1,NEBT
      AO(JA,JD)=ZRR(IA,IB)
      AO(JA,JE)=ZRZ(IA,IB)
      AO(JB,JD)=ZZR(IA,IB)
      AO(JB,JE)=ZZZ(IA,IB)
      JD=JD+2
      JE=JD+1
    2 CONTINUE
      AO(JA,JC)=PR(IA)
      AO(JB,JC)=PZ(IA)
      JA=JA+2
      JB=JA+1
    1 CONTINUE
      RETURN
      END


      SUBROUTINE AXSOL
C     SOLVES FOR FICTITIOUS LOADS
      COMMON /MNPR/KRS,NCBS,NCIS,NCBL,NEBT,NEIT,
     1             YG,PN,FPR,FPZ
      COMMON /FTFB/PR(35),PZ(35),QR(35),QZ(35),
     1             FRR(35),FZZ(35),FZR(35)
      COMMON /SOLV/AO(70,71)
      DATA EPS /1.0E-5/
      DATA LUO /2/
      JA=2*NEBT
      JB=JA+1
      DO 1 IA=1,JA
      DO 2 IB=IA,JA
      JC=IB
      AT=ABS(AO(IB,IA))
      IF (AT.GT.EPS) GOTO 3
    2 CONTINUE
      GOTO 4
    3 CONTINUE
      DO 5 IB=1,JB
      AT=AO(IA,IB)
      AO(IA,IB)=AO(JC,IB)
      AO(JC,IB)=AT
    5 CONTINUE
      AT=1.0/AO(IA,IA)
      DO 6 IB=1,JB
      AO(IA,IB)=AT*AO(IA,IB)
    6 CONTINUE
      DO 7 I9=1,JA
      IF (I9.EQ.IA) GOTO 8
      AT=-AO(I8,IA)
      DO 9 IC=1,JB
      AO(I8,IC)=AO(I8,IC)+AT*AO(IA,IC)
    9 CONTINUE
    8 CONTINUE
    7 CONTINUE
    1 CONTINUE
      JA=1
      JC=2
      DO 10 IA=1,NEBT
      QR(IA)=AO(JA,JB)
      QZ(IA)=AO(JC,JB)
      JA=JA+2
      JC=JA+1
   10 CONTINUE
      GOTO 11
    4 WRITE (LUO,200)
  200 FORMAT (1H1)
      WRITE (LUO,201)
  201 FORMAT (/  19H NO UNIQUE SOLUTION)
      STOP
   11 CONTINUE
      RETURN
      END


      SUBROUTINE AXSTR (MSTR,NELS)
C     CALCULATES STRESSES AND DISPLACEMENTS
      COMMON /MNPR/KRS,NCBS,NCIS,NCBL,NEBT,NEIT,
     1             YG,PN,FPR,FPZ
      COMMON /FTFB/PR(35),PZ(35),QR(35),QZ(35),
     1             FRR(35),FZZ(35),FZR(35)
      COMMON /SDCA/RRR(35,35),TTR(35,35),ZZR(35,35),
     1             ZRR(35,35),DRR(35,35),DZR(35,35),
     2             RRZ(35,35),TTZ(35,35),ZZZ(35,35),
     3             ZRZ(35,35),DRZ(35,35),DZZ(35,35)
      COMMON /STDA/RR(35),TT(35),ZZ(35),
     1             ZR(35),DR(35),DZ(35)
      DO 1 IA=1,NELS
      IF (MSTR.NE.1) GOTO 2
      RRU=FRR(IA)
      ZZU=FZZ(IA)
      ZRU=FZR(IA)
      GOTO 3
    2 RRU=FPR
      ZZU=FPZ
      ZRU=0.0
    3 TTU=FPR
      DRU=0.0
      DZU=0.0
      DO 4 IB=1,NEBT
      QRU=QR(IB)
      QZU=QZ(IB)
      RRU=RRU+QRU*RRR(IA,IB)+QZU*RRZ(IA,IB)
      TTU=TTU+QRU*TTR(IA,IB)+QZU*TTZ(IA,IB)
      ZZU=ZZU+QRU*ZZR(IA,IB)+QZU*ZZZ(IA,IB)
      ZRU=ZRU+QRU*ZRR(IA,IB)+QZU*ZRZ(IA,IB)
      DRU=DRU+QRU*DRR(IA,IB)+QZU*DRZ(IA,IB)
      DZU=DZU+QRU*DZR(IA,IB)+QZU*DZZ(IA,IB)
    4 CONTINUE
      RR(IA)=RRU
      TT(IA)=TTU
      ZZ(IA)=ZZU
      ZR(IA)=ZRU
      DR(IA)=DRU
      DZ(IA)=DZU
    1 CONTINUE
      RETURN
      END
```

```
      SUBROUTINE AXWTR (IDEP,IDEQ)
C     PRINTS OUT STRESSES AND DISPLACEMENTS
      COMMON /LINE/WORD(40)
      COMMON /BDSG/NEBS(35),RF(35),ZF(35),RL(35),ZL(35),
     1             COSB(35),RP(35),ZP(35),RQ(35),ZQ(35)
      COMMON /STDA/RR(35),TT(35),ZZ(35),
     1             ZR(35),DR(35),DZ(35)
      DATA LUO /2/
      WRITE (LUO,200)
  200 FORMAT (1H1)
      IF (IDEP.GT.1) GOTO 1
      WRITE (LUO,206) (WORD(IO),IO=1,40)
  206 FORMAT (/1X,20A4//1X,20A4)
      WRITE (LUO,201)
  201 FORMAT (/  46H STRESSES AND DISPLACEMENTS AT BOUNDARY POINTS)
      WRITE (LUO,202)
  202 FORMAT (/  30H  PT.NO.       NN          TT     ,
     1 36H     NN          MN          DN          DN)
      GOTO 2
    1 CONTINUE
      WRITE (LUO,203)
  203 FORMAT (/  46H STRESSES AND DISPLACEMENTS AT INTERIOR POINTS)
      WRITE (LUO,204)
  204 FORMAT (/  30H  PT.NO.       RR          TT     ,
     1 36H     ZZ          ZR          DR          DZ)
    2 CONTINUE
      JA=1
      DO 3 IA=IDEP,IDEQ
      WRITE (LUO,205) IA,RR(JA),TT(JA),ZZ(JA),
     1                   ZR(JA),DR(JA),DZ(JA)
  205 FORMAT (1X,I5,3X,6F10.3)
      JA=JA+1
    3 CONTINUE
      RETURN
      END


      SUBROUTINE AXWDL
C     PRINTS OUT FICTITIOUS LOADS
      COMMON /MNPR/KRS,NCBS,NCIS,NCBL,NEBT,NEIT,
     1             YG,PN,FPR,FPZ
      COMMON /BDSG/NEBS(35),RF(35),ZF(35),RL(35),ZL(35),
     1             COSB(35),RP(35),ZP(35),RQ(35),ZQ(35)
      COMMON /FTFB/PR(35),PZ(35),QR(35),QZ(35),
     1             FRR(35),FZZ(35),FZR(35)
      DATA LUO /2/
      WRITE (LUO,200)
  200 FORMAT (1H1)
      WRITE (LUO,201)
  201 FORMAT (/  17H FICTITIOUS LOADS)
      WRITE (LUO,202)
  202 FORMAT (/  36H  EL.NO.       QR.         QZ       COS(B))
      DO 1 IA=1,NEBT
      WRITE (LUO,203) IA,QR(IA),QZ(IA),COSB(IA)
  203 FORMAT (1X,I5,3X,3F10.3)
    1 CONTINUE
      RETURN
      END
```

LIST OF MAIN VARIABLES IN AXSYM (2)

(The subscripts i, j indicate arrays)

MCRD	Operating mode; 1 for read data only, 2 for 1 and calculate geometry, 3 for 2 and execute
KRS	Symmetry code; 0 for not used, 1 for used
NCBS	Number of cards defining auxiliary boundary segements
NCIS	Number of cards defining the boundary and interior points
NCBS	Number of cards defining boundary loads
NEBT	Number of boundary points
NEIT	Number of interior points
YG	Young's modulus
PN	Poisson's ratio
FPR	$p_r(=p_\theta)$ field stress component
FPZ	p_z field stress component
$NEBS_i$	Number of elements in an auxiliary boundary segment
RF_i, ZF_i	Coordinates of first point on straight line segment
RL_i, ZL_i	Coordinates of last point on straight line segment
$COSB_i$	cos (angle between load element and r-axis)
RP_i, ZP_i	Coordinates of end 1 of body boundary element
RQ_i, ZQ_i	Coordinates of end 2 of body boundary element
$NEIS_i$	Number of elements in a boundary or interior point segment
RIF_i, ZIF_i	Coordinates of first point on straight line segment
RIL_i, ZIL_i	Coordinates of last point on straight line segment
RIC_i, ZIC_i	Coordinates of centre point of element
SNA_i	sin A
CSA_i	cos A
LP_i	Number of first element to which the load is applied
LQ_i	Number of last element to which the load is applied
BPR_i	p_m
BPZ_i	p_n
PR_i	$\bar{p}_m$
PZ_i	$\bar{p}_n$
QR_i	q_r
QZ_i	q_z
FRR_i	m-component of field stress
FZZ_i	n-component of field stress
FZR_i	nm-component of field stress
ELASA	E
ELASB	ν
ELASC	$1 - 2\nu$
ELASD	$3 - 4\nu$
ELASE	$1/(8\pi(1 - \nu))$
ELASF	$(1 + \nu)/(8\pi(1 - \nu)E)$

LIST OF MAIN VARIABLES IN AXSYM (2) (contd.)

(The subscripts i, j indicate arrays)

RRR_{ij}	$r\sigma'_r$ or $r\sigma''_r$, $r\sigma'_m$ or $r\sigma''_m$
TTR_{ij}	$r\sigma'_\theta$ or $r\sigma''_\theta$, $r\sigma'_\theta$ or $r\sigma''_\theta$
ZZR_{ij}	$r\sigma'_z$ or $r\sigma''_z$, $r\sigma'_n$ or $r\sigma''_n$
ZRR_{ij}	$r\tau'_{zr}$ or $r\tau''_{zr}$, $r\tau'_{nm}$ or $r\tau''_{nm}$
DRR_{ij}	ru'_r or ru''_r , ru'_m or ru''_m
DZR_{ij}	ru'_z or ru''_z , ru'_n or ru''_n
RRZ_{ij}	$z\sigma'_r$ or $z\sigma''_r$, $z\sigma'_m$ or $z\sigma''_m$
TTZ_{ij}	$z\sigma'_\theta$ or $z\sigma''_\theta$, $z\sigma'_\theta$ or $z\sigma''_\theta$
ZZZ_{ij}	$z\sigma'_z$ or $z\sigma''_z$, $z\sigma'_n$ or $z\sigma''_n$
ZRZ_{ij}	$z\tau'_{zr}$ or $z\tau''_{zr}$, $z\tau'_{nm}$ or $z\tau''_{nm}$
DRZ_{ij}	zu'_r or zu''_r , zu'_m or zu''_m
DZZ_{ij}	zu'_z or zu''_z , zu'_n or zu''_n
RRRU	
TTRU	
ZZRU	
ZRRU	
DRRU	
DZRU	ditto
RRZU	
TTZU	
ZZZU	
ZRZU	
DRZU	
DZZU	

RR_i	$\bar{\sigma}_r$
TT_i	$\bar{\sigma}_\theta$
ZZ_i	$\bar{\sigma}_z$
ZR_i	$\bar{\tau}_{zr}$
DR_i	$\bar{u}_r$
DZ_i	$\bar{u}_z$
GW_i	Weight factor for Gaussian integration
GP_i	Abscissa for Gaussian integration
PAH	$1/\sqrt{((a+b)^2+b^2)}$ or $1/\sqrt{((a+c)^2+(b-z)^2)}$
PAM	k^2 or k'^2 in $\sqrt{(1-k^2\sin^2\phi)}$ or $\sqrt{(1-k'^2\sin^2\phi)}$
EF	F_1 complete elliptic integral of the first kind
ES	E_1 complete elliptic integral of the second kind

CDC	$1/Z$
CDB	$1/Z^3$
CDA	$1/Z^5$
CCC	$\cos\theta/Z$
CCB	$\int_0^{\pi/2} (\cos\theta/Z^3)\,d\phi$ where $Z = \Delta$ or $Z = \Delta/PAH = R$
CCA	$\cos\theta/Z^5$
CBB	$\cos^2\theta/Z^3$
CBA	$\cos^2\theta/Z^5$
CAA	$\cos^3\theta/Z^5$

APPENDIX A 6

A 6.2 - Listing of the computer program AXRAE used in calculating principal stresses due to normal or tangential loads of unit intensity applied to a radial or an axial element within a homogeneous isotropic linear elastic space where subprograms AXSDR and AXSDZ are listed in Appendix A 5.4

```
      PROGRAM AXRAE (INPUT,OUTPUT,TAPE1=INPUT,TAPE2=OUTPUT)
C     CALCULATES PRINCIPAL STRESSES DUE TO
C     RADIAL AND AXIAL ELEMENTS WITH
C     UNIT LOAD INTENSITIES
      COMMON /LINE/WORD(20)
      COMMON /MNPR/KRS,NCRS,NCIS,NC9L,NEBT,NEIT,
     1             YG,PN,FRR,FRZ
      COMMON /JNSG/NEIS(35),RIF(35),ZIF(35),RIL(35),ZIL(35)
      COMMON /SDCU/RRRU,TTRU,ZZRU,
     1             ZRRU,DRRU,DZRU,
     2             RRZU,TTZU,ZZZU,
     3             ZRZU,DRZU,DZZU
      DATA LUI,LUO /1,2/
      DATA KRS /0/
      READ (LUI,100) (WORD(IO),IO=1,20)
  100 FORMAT (20A4)
      READ (LUI,101) IRZ
  101 FORMAT (4X,I1)
      READ (LUI,102) YG,PN
  102 FORMAT (2F10.0)
      READ (LUI,103) RF,ZF,RL,ZL
  103 FORMAT (10X,4F10.0)
      READ (LUI,104) NCIS
  104 FORMAT (3X,I2)
      JA=1
    1 READ (LUI,105) NEIS(JA),RIF(JA),ZIF(JA),RIL(JA),ZIL(JA)
  105 FORMAT (3X,I2,5X,4F10.0)
      JA=JA+1
      IF (JA.LE.NCIS) GOTO 1
      WRITE (LUO,200)
  200 FORMAT (1H1)
      WRITE (LUO,201)
  201 FORMAT (/  11H INPUT DATA)
      WRITE (LUO,202) (WORD(IO),IO=1,20)
  202 FORMAT (/  11H CARD       ,20A4)
      WRITE (LUO,203) IRZ
  203 FORMAT (/  11H CARD       ,4X,I1,75X)
      WRITE (LUO,204) YG,PN
  204 FORMAT (/  11H CARD       ,2F10.3,60X)
      WRITE (LUO,205) RF,ZF,RL,ZL
  205 FORMAT (/  11H CARD       ,10X,4F10.3,30X)
      WRITE (LUO,206) NCIS
  206 FORMAT (/  11H CARD       ,3X,I2,75X)
      JA=1
    2 WRITE (LUO,207) NEIS(JA),RIF(JA),ZIF(JA),RIL(JA),ZIL(JA)
  207 FORMAT (/  11H CARD       ,3X,I2,5X,4F10.3,30X)
      JA=JA+1
      IF (JA.LE.NCIS) GOTO 2
      CALL AXELA
      DO 3 IA=1,NCIS
      WRITE (LUO,206)
  208 FORMAT (1H1)
      WRITE (LUO,209) (WORD(IO),IO=1,20)
  209 FORMAT (/1X,20A4)
      WRITE (LUO,210)
  210 FORMAT (/  43H PRINCIPAL STRESSES AROUND A SINGLE ELEMENT)
      WRITE (LUO,211)
  211 FORMAT (// 41H    IRZ NCIS NEIS        R         Z     ,
     1 40H R,ALPHA/RR SIG1/ZZ   SIG2/ZR   SIGTHE  ,
     2 40H Z,ALPHA/RR SIG1/ZZ   SIG2/ZR   SIGTHE  )
      JA=NEIS(IA)
      VA=RIF(IA)
      VB=ZIF(IA)
      VC=RIL(IA)
      VD=ZIL(IA)
      VE=(VC-VA)/JA
      VF=(VD-VB)/JA
      VA=VA+0.5*VE
      VB=VB+0.5*VF
      VG=RF
      VH=ZF
      VI=RL
      VJ=ZL
      VK=VB-VH
      DO 4 IB=1,JA
      IF (IRZ.EQ.2) GOTO 5
      CALL AXSOR (VA,VK,VG,VH,VI,VJ)
      GOTO 6
    5 CALL AXSOZ (VA,VB,VG,VH,VI,VJ)
    6 CALL AXPRS (VL,VM,VN,RRRU,ZZRU,ZRRU)
      CALL AXPRS (VO,VP,VQ,RRZU,ZZZU,ZRZU)
      WRITE (LUO,212) IRZ,IA,IB,VA,VE,
     1                VL,VP,VN,TTRU,
     2                VO,VP,VQ,TTZU
  212 FORMAT (1X,3I5,5X,2F10.3,F10.0,3F10.3,F10.0,3F10.3)
      WRITE (LUO,213) RRRU,ZZRU,ZRRU,TTRU,
     2                RRZU,ZZZU,ZRZU,TTZU
  213 FORMAT (41X,8F10.3)
      WRITE (LUO,214)
  214 FORMAT (/)
      VA=VA+VE
      VB=VB+VF
      VK=VK+VF
    4 CONTINUE
    3 CONTINUE
      END


C     SUBROUTINE AXPRS (ALP,SON,STW,RR,ZZ,ZR)
C     CALCULATES PRINCIPAL STRESSES
      DATA RTD /57.29578/
      DATA DEL /1.0E-10/
      VA=RR*RR+ZZ*ZZ+ZR*ZR
      VA=SQRT (VA)
      EPS=VA*DEL
      IF (ABS(RR).GT.EPS) GOTO 1
      IF (ABS(ZZ).GT.EPS) GOTO 1
      IF (ABS(ZR).GT.EPS) GOTO 2
      SON=0.0
      STW=0.0
      ALP=0.0
      GOTO 3
    2 CONTINUE
      IF (ZR.LT.-EPS) GOTO 4
      SON=ZR
      STW=-ZR
      ALP=45.0
      GOTO 3
    4 SON=-ZR
      STW=ZR
      ALP=-45.0
      GOTO 3
    1 CONTINUE
      IF (ABS(ZR).GT.EPS) GOTO 5
      IF (RR.GT.ZZ) GOTO 6
      SON=ZZ
      STW=RR
      ALP=0.0
      GOTO 3
    6 SON=RR
      STW=ZZ
      ALP=90.0
      GOTO 3
    5 VA=0.5*(ZZ-RR)
      VB=VA+RR
      VA=VA*VA
      VC=ZR*ZR
      VA=SQRT (VA+VC)
      SON=VB+VA
      STW=VB-VA
      VC=(SON-ZZ)/ZR
      ALP=RTD*ATAN (VC)
    3 CONTINUE
      RETURN
      END
```

A 6.5 - Results obtained using the computer program AXSYM (2) for the total stresses and induced displacements associated with a complete circular toric tunnel (Fig. A 6.5.1) and two identical spherical cavities (Fig. A 6.5.2) in a homogeneous isotropic linear elastic mass with uniform field stress

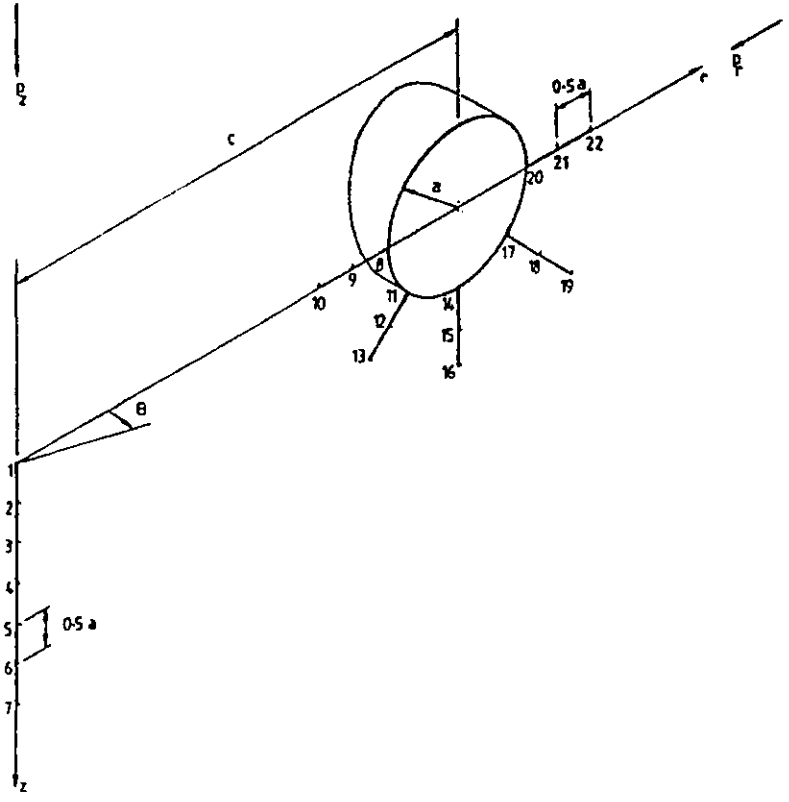


FIG. A 6.5.1: COMPLETE CIRCULAR TORIC TUNNEL IN AN INFINITE MASS SUBJECT TO UNIFORM RADIAL AND AXIAL FIELD STRESS

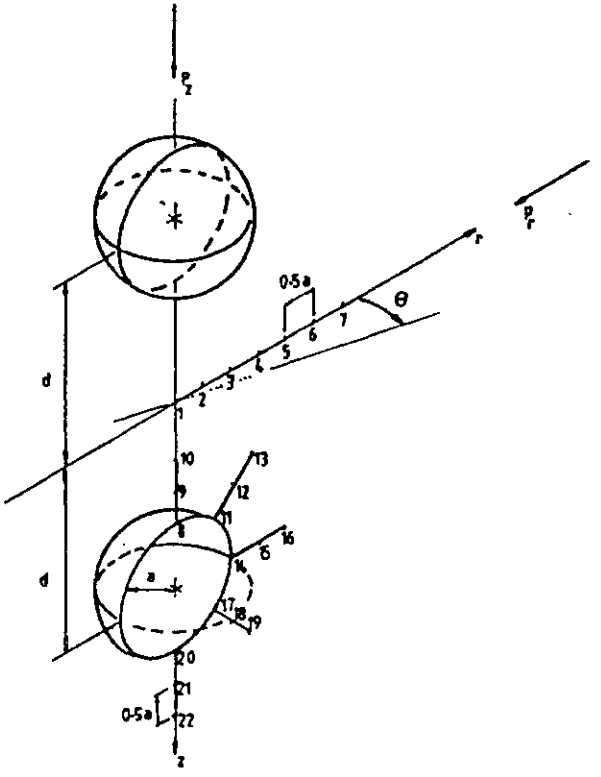


FIG. A 6.5.2: TWO IDENTICAL SPHERICAL CAVITIES IN AN INFINITE MASS SUBJECT TO UNIFORM RADIAL AND AXIAL FIELD STRESS

TABLE A 6.5.1 TOTAL STRESSES AND INDUCED DISPLACEMENTS ASSOCIATED WITH A COMPLETE CIRCULAR TORIC TUNNEL IN A HOMOGENEOUS ISOTROPIC LINEAR ELASTIC INFINITE MASS WITH UNIFORM FIELD STRESS (Fig. A 6.5.1)

$E/p = 1$ $p_r/p = 1$ $p_z/p = 0$ $c/a = 1\ 1/8$ $\nu = 0$

N.	σ_r/p	σ_θ/p	σ_z/p	τ_{zr}/p	Eu_r/ap	Eu_z/ap
1	-0.018	-0.018	-0.375	0	0	0
2	-0.003	-0.003	-0.047	0	0	0.119
3	0.811	0.811	-0.277	0	0	0.181
4	1.153	1.153	-0.204	0	0	0.320
5	1.118	1.118	-0.005	0	0	0.369
6	1.061	1.061	0.079	0	0	0.346
7	1.028	1.028	0.096	0	0	0.300
8	(-0.004)	-0.011	-0.426	0	0.126	0
9						
10						
11	0.045	0.216	0.047	0.073	0.328	0.262
12	0.904	0.891	-0.296	0.008	0.007	0.200
13						
14	2.003	1.201	(-0.002)	0	-0.226	0.563
15	1.139	1.154	0.208	0.074	-0.173	0.475
16	1.048	1.088	0.153	-0.024	-0.099	0.385
17	0.318	1.497	0.321	-0.335	-0.910	0.408
18	0.906	1.212	-0.059	-0.119	-0.463	0.181
19	0.978	1.114	-0.063	-0.062	-0.290	0.109
20	(-0.002)	1.554	-0.574	0	-1.177	0
21	0.372	1.291	-0.043	0	-0.763	0
22	0.638	1.167	0.008	0	-0.523	0

Brackets indicate the exact value is zero.

$\tau_{r\theta} = \tau_{\theta z} = u_\theta = 0$

$E/p = 1$ $p_r/p = 0$ $p_z/p = 1$ $c/a = 1\ 1/8$ $\nu = 0$

N.	σ_r/p	σ_θ/p	σ_z/p	τ_{zr}/p	Eu_r/ap	Eu_z/ap
1	0.322	0.322	6.989	0	0	0
2	0.073	0.073	2.176	0	0	-1.873
3	-0.195	-0.195	0.679	0	0	-1.968
4	-0.100	-0.100	0.359	0	0	-1.711
5	0.016	0.016	0.356	0	0	-1.380
6	0.055	0.055	0.475	0	0	-1.086
7	0.059	0.059	0.600	0	0	-0.856
8	(-0.013)	0.218	7.839	0	-0.027	0
9						
10						
11	0.118	0.037	0.129	0.197	-0.016	-2.263
12	-0.186	-0.211	0.608	0.030	0.014	-1.949
13						
14	-0.360	-0.253	(-0.005)	0	0.284	-1.933
15	0.023	-0.040	0.211	-0.337	0.045	-1.471
16	0.035	0.031	0.444	-0.189	-0.035	-1.139
17	0.598	-0.269	0.597	-0.638	0.493	-1.107
18	0.011	-0.093	1.082	-0.240	0.203	-0.595
19	-0.052	-0.041	1.085	-0.123	0.103	-0.394
20	(-0.004)	-0.265	2.475	0	0.562	0
21	0.275	-0.171	1.382	0	0.450	0
22	0.198	-0.106	1.158	0	0.331	0

Brackets indicate the exact value is zero.

$\tau_{r\theta} = \tau_{\theta z} = u_\theta = 0$

$E/p = 1$ $p_r/p = 1$ $p_z/p = 1$ $c/a = 1\ 1/8$ $\nu = 0$

N.	σ_r/p	σ_θ/p	σ_z/p	τ_{zr}/p	Eu_r/ap	Eu_z/ap
1	0.304	0.304	6.614	0	0	0
2	0.070	0.070	2.129	0	0	-1.753
3	0.616	0.616	0.402	0	0	-1.787
4	1.054	1.054	0.154	0	0	-1.390
5	1.134	1.134	0.350	0	0	-1.012
6	1.116	1.116	0.554	0	0	-0.740
7	1.088	1.088	0.696	0	0	-0.555
8	(-0.017)	0.207	7.413	0	0.099	0
9						
10						
11	0.163	0.253	0.176	0.270	0.312	-2.001
12	0.718	0.680	0.312	0.038	0.021	-1.748
13						
14	1.643	0.948	(-0.007)	0	0.058	-1.371
15	1.162	1.114	0.419	-0.263	-0.129	-0.996
16	1.083	1.119	0.597	-0.213	-0.134	-0.754
17	0.916	1.228	0.918	-0.973	-0.418	-0.699
18	0.917	1.119	1.024	-0.359	-0.260	-0.415
19	0.926	1.073	1.022	-0.185	-0.187	-0.286
20	(-0.006)	1.289	1.901	0	-0.615	0
21	0.647	1.119	1.339	0	-0.313	0
22	0.836	1.061	1.166	0	-0.192	0

Brackets indicate the exact value is zero.

$\tau_{r\theta} = \tau_{\theta z} = u_\theta = 0$

TABLE A 6.5.1 TOTAL STRESSES AND INDUCED DISPLACEMENTS ASSOCIATED WITH A COMPLETE CIRCULAR TORIC TUNNEL IN A HOMOGENEOUS ISOTROPIC LINEAR ELASTIC INFINITE MASS WITH UNIFORM FIELD STRESS (Fig. A 6.5.1)

E/p = 1 p_r/p = 1 p_z/p = 0 c/a = 1 1/8 ν = 0.25

N	σ_r/p	σ_θ/p	σ_z/p	τ_{zr}/p	Eu_r/ap	Eu_z/ap
1	-0.053	-0.053	-1.213	0	0	0
2	-0.020	-0.020	-0.312	0	0	0.142
3	0.795	0.795	-0.300	0	0	0.092
4	1.201	1.201	-0.206	0	0	0.251
5	1.169	1.169	0.003	0	0	0.347
6	1.099	1.099	0.094	0	0	0.352
7	1.055	1.055	0.110	0	0	0.317
8	(-0.001)	-0.046	-1.348	0	0.057	0
9						
10						
11	-0.004	0.143	-0.011	-0.003	0.252	0.221
12	0.895	0.888	-0.313	0.005	0	0.108
13						
14	2.145	1.510	0	0	-0.252	0.417
15	1.211	1.269	0.227	-0.090	-0.179	0.432
16	1.096	1.145	0.171	-0.029	-0.088	0.374
17	0.388	1.480	0.393	-0.392	-0.980	0.321
18	0.964	1.190	-0.066	-0.137	-0.472	0.108
19	1.015	1.099	-0.072	-0.071	-0.287	0.055
20	0	1.184	-0.662	0	-1.274	0
21	0.349	1.152	-0.048	0	-0.857	0
22	0.623	1.098	0.010	0	-0.593	0

Brackets indicate the exact value is zero.

$\tau_{r\theta} = \tau_{\theta z} = u_\theta = 0$

E/p = 1 p_r/p = 0 p_z/p = 1 c/a = 1 1/8 ν = 0.25

N	σ_r/p	σ_θ/p	σ_z/p	τ_{zr}/p	Eu_r/ap	Eu_z/ap
1	0.315	0.315	7.182	0	0	0
2	0.119	0.119	2.162	0	0	-1.863
3	-0.290	-0.290	0.673	0	0	-1.972
4	-0.244	-0.244	0.370	0	0	-1.794
5	-0.092	-0.092	0.345	0	0	-1.504
6	-0.014	-0.014	0.453	0	0	-1.213
7	0.014	0.014	0.578	0	0	-0.971
8	(-0.003)	0.275	7.976	0	0.184	0
9						
10						
11	0.218	-0.033	0.249	0.241	-0.042	-2.244
12	-0.319	-0.298	0.610	0.027	0.008	-1.962
13						
14	-0.732	-0.573	(-0.001)	0	0.157	-1.973
15	-0.126	-0.182	0.171	-0.173	-0.064	-1.576
16	-0.054	-0.048	0.412	-0.184	-0.126	-1.250
17	0.562	-0.174	0.551	-0.564	0.370	-1.158
18	-0.078	-0.034	1.093	-0.216	0.083	-0.590
19	-0.109	-0.006	1.098	-0.111	0.009	-0.382
20	(-0.001)	0.192	2.605	0	0.445	0
21	0.308	0.012	1.391	0	0.428	0
22	0.218	-0.011	1.156	0	0.327	0

Brackets indicate the exact value is zero.

$\tau_{r\theta} = \tau_{\theta z} = u_\theta = 0$

E/p = 1 p_r/p = 1 p_z/p = 1 c/a = 1 1/8 ν = 0.25

N	σ_r/p	σ_θ/p	σ_z/p	τ_{zr}/p	Eu_r/ap	Eu_z/ap
1	0.262	0.262	5.969	0	0	0
2	0.099	0.099	1.851	0	0	-1.722
3	0.505	0.505	0.373	0	0	-1.881
4	0.957	0.957	0.163	0	0	-1.542
5	1.077	1.077	0.349	0	0	-1.157
6	1.084	1.084	0.547	0	0	-0.862
7	1.069	1.069	0.688	0	0	-0.653
8	(-0.003)	0.230	6.628	0	0.241	0
9						
10						
11	0.213	0.110	0.238	0.238	0.210	-2.023
12	0.576	0.590	0.297	0.033	0.008	-1.854
13						
14	1.412	0.937	(-0.001)	0	-0.095	-1.556
15	1.084	1.087	0.399	-0.263	-0.243	-1.145
16	1.042	1.097	0.583	-0.213	-0.214	-0.875
17	0.950	1.307	0.944	-0.956	-0.610	-0.837
18	0.886	1.156	1.027	-0.352	-0.389	-0.482
19	0.906	1.093	1.026	-0.181	-0.278	-0.327
20	(-0.001)	1.376	1.943	0	-0.830	0
21	0.657	1.164	1.344	0	-0.429	0
22	0.841	1.087	1.166	0	-0.267	0

Brackets indicate the exact value is zero.

$\tau_{r\theta} = \tau_{\theta z} = u_\theta = 0$

TABLE A 6.5.1 TOTAL STRESSES AND INDUCED DISPLACEMENTS ASSOCIATED WITH A COMPLETE CIRCULAR TORIC TUNNEL IN A HOMOGENEOUS ISOTROPIC LINEAR ELASTIC INFINITE MASS WITH UNIFORM FIELD STRESS (Fig. A 6.5.1)

$E/p = 1$ $p_r/p = 1$ $p_z/p = 0$ $c/a = 1\frac{1}{8}$ $\nu = 0.49$

N	σ_r/p	σ_θ/p	σ_z/p	τ_{zr}/p	Eu_r/ap	Eu_z/ap
1	-0.067	-0.067	-1.730	0	0	0
2	-0.027	-0.027	-0.467	0	0	0.058
3	0.800	0.800	-0.306	0	0	-0.128
4	1.268	1.268	-0.205	0	0	0.068
5	1.236	1.236	0.017	0	0	0.242
6	1.147	1.147	0.113	0	0	0.298
7	1.088	1.088	0.130	0	0	0.291
8	(0.001)	-0.064	-1.908	0	-0.045	0
9						
10						
11	-0.073	0.088	-0.031	-0.053	0.155	0.046
12	0.875	0.939	-0.316	0.004	-0.010	-0.116
13						
14	2.331	1.873	(-0.001)	0	-0.249	0.076
15	1.305	1.408	0.254	-0.108	-0.151	0.273
16	1.159	1.215	0.195	-0.033	-0.047	0.287
17	0.451	1.469	0.472	-0.465	-0.928	0.092
18	1.040	1.164	-0.076	-0.158	-0.397	-0.051
19	1.064	1.079	-0.083	-0.082	-0.226	-0.058
20	0	0.699	-0.781	0	-1.214	0
21	0.317	0.917	-0.055	0	-0.873	0
22	0.604	1.009	0.012	0	-0.614	0

Brackets indicate the exact value is zero.

$\tau_{r\theta} = \tau_{\theta z} = u_\theta = 0$

$E/p = 1$ $p_r/p = 0$ $p_z/p = 1$ $c/a = 1\frac{1}{8}$ $\nu = 0.49$

N	σ_r/p	σ_θ/p	σ_z/p	τ_{zr}/p	Eu_r/ap	Eu_z/ap
1	0.277	0.277	6.608	0	0	0
2	0.120	0.120	1.950	0	0	-1.610
3	-0.393	-0.393	0.628	0	0	-1.702
4	-0.412	-0.412	0.370	0	0	-1.663
5	-0.221	-0.221	0.325	0	0	-1.482
6	-0.100	-0.100	0.422	0	0	-1.241
7	-0.042	-0.042	0.546	0	0	-1.016
8	(-0.001)	0.279	7.286	0	0.350	0
9						
10						
11	0.259	-0.071	0.208	0.204	-0.079	-1.922
12	-0.443	-0.416	0.579	0.020	0	-1.705
13						
14	-1.173	-1.009	0	0	-0.063	-1.698
15	-0.308	-0.369	0.120	-0.153	-0.240	-1.496
16	-0.164	-0.151	0.370	-0.180	-0.268	-1.237
17	0.476	-0.073	0.454	-0.467	0.070	-1.015
18	-0.190	0.032	1.109	-0.184	-0.158	-0.459
19	-0.183	0.034	1.116	-0.094	-0.170	-0.283
20	(-0.001)	0.811	2.772	0	0.120	0
21	0.351	0.255	1.404	0	0.301	0
22	0.244	0.114	1.154	0	0.255	0

Brackets indicate the exact value is zero.

$\tau_{r\theta} = \tau_{\theta z} = u_\theta = 0$

$E/p = 1$ $p_r/p = 1$ $p_z/p = 1$ $c/a = 1\frac{1}{8}$ $\nu = 0.49$

N	σ_r/p	σ_θ/p	σ_z/p	τ_{zr}/p	Eu_r/ap	Eu_z/ap
1	0.209	0.209	4.877	0	0	0
2	0.093	0.093	1.484	0	0	-1.553
3	0.407	0.407	0.322	0	0	-1.830
4	0.856	0.856	0.165	0	0	-1.595
5	1.014	1.014	0.341	0	0	-1.240
6	1.048	1.048	0.535	0	0	-0.943
7	1.046	1.046	0.676	0	0	-0.724
8	0	0.214	5.378	0	0.305	0
9						
10						
11	0.186	0.017	0.177	0.187	0.076	-1.875
12	0.432	0.523	0.263	0.025	-0.010	-1.821
13						
14	1.158	0.865	0	0	-0.312	-1.622
15	0.996	1.039	0.373	-0.261	-0.391	-1.223
16	0.995	1.065	0.565	-0.214	-0.315	-0.950
17	0.926	1.396	0.927	-0.932	-0.851	-0.009
18	0.849	1.197	1.034	-0.341	-0.555	-0.006
19	0.881	1.113	1.033	-0.176	-0.396	-0.004
20	(-0.001)	1.510	1.990	0	-1.094	0
21	0.668	1.226	1.349	0	-0.572	0
22	0.849	1.122	1.166	0	-0.359	0

Brackets indicate the exact value is zero.

$\tau_{r\theta} = \tau_{\theta z} = u_\theta = 0$

TABLE A 6.5.1 TOTAL STRESSES AND INDUCED DISPLACEMENTS ASSOCIATED WITH A COMPLETE CIRCULAR TORIC TUNNEL IN A HOMOGENEOUS ISOTROPIC LINEAR ELASTIC INFINITE MASS WITH UNIFORM FIELD STRESS (Fig. A 6.5.1)

$E/p = 1$ $p_r/p = 1$ $p_z/p = 0$ $c/a = 1\frac{1}{2}$ $\nu = 0$

N.	σ_r/p	σ_θ/p	σ_z/p	τ_{zr}/p	Eu_r/ap	Eu_z/ap
1	-0.023	-0.023	-0.190	0	0	0
2	0.052	0.052	-0.031	0	0	0.059
3	0.796	0.796	-0.287	0	0	0.130
4	1.134	1.134	-0.242	0	0	0.279
5	1.123	1.123	-0.049	0	0	0.349
6	1.069	1.069	0.053	0	0	0.344
7	1.035	1.035	0.083	0	0	0.308
8	(-0.003)	-0.014	-0.237	0	0.254	0
9						
10						
11	0.102	0.277	0.099	0.120	0.392	0.268
12	0.889	0.877	-0.297	0.023	0.023	0.164
13						
14	2.046	1.186	(-0.001)	0	-0.232	0.574
15	1.146	1.148	0.215	-0.073	-0.185	0.483
16	1.046	1.090	0.154	-0.030	-0.112	0.391
17	0.324	1.481	0.329	-0.338	-0.941	0.416
18	0.907	1.211	-0.061	-0.123	-0.487	0.185
19	0.977	1.116	-0.066	-0.065	-0.309	0.112
20	(-0.001)	1.539	-0.585	0	-1.213	0
21	0.361	1.289	-0.044	0	-0.796	0
22	0.624	1.169	0.008	0	-0.550	0

Brackets indicate the exact value is zero.

$\tau_{r\theta} = \tau_{\theta z} = u_\theta = 0$

$E/p = 1$ $p_r/p = 0$ $p_z/p = 1$ $c/a = 1\frac{1}{2}$ $\nu = 0.0$

N.	σ_r/p	σ_θ/p	σ_z/p	τ_{zr}/p	Eu_r/ap	Eu_z/ap
1	0.424	0.424	4.515	0	0	0
2	0.158	0.158	2.510	0	0	-1.348
3	-0.189	-0.189	1.125	0	0	-1.694
4	-0.134	-0.134	0.608	0	0	-1.607
5	-0.016	-0.016	0.474	0	0	-1.366
6	0.037	0.037	0.522	0	0	-1.111
7	0.051	0.051	0.614	0	0	-0.894
8	(-0.005)	0.298	5.623	0	-0.074	0
9						
10						
11	0.329	0.105	0.317	0.361	0.057	-2.070
12	-0.182	-0.195	0.960	0.126	0.037	-1.725
13						
14	-0.399	-0.223	(-0.003)	0	0.279	-1.934
15	0.035	-0.047	0.222	-0.164	0.059	-1.474
16	0.041	0.019	0.461	-0.169	-0.024	-1.150
17	0.613	-0.261	0.617	-0.637	0.511	-1.126
18	0.009	-0.094	1.087	-0.241	0.216	-0.610
19	-0.052	-0.043	1.089	-0.125	0.114	-0.406
20	(-0.003)	-0.261	2.505	0	0.587	0
21	0.283	-0.172	1.392	0	0.472	0
22	0.205	-0.108	1.163	0	0.349	0

Brackets indicate the exact value is zero.

$\tau_{r\theta} = \tau_{\theta z} = u_\theta = 0$

$E/p = 1$ $p_r/p = 1$ $p_z/p = 1$ $c/a = 1\frac{1}{2}$ $\nu = 0.0$

N.	σ_r/p	σ_θ/p	σ_z/p	τ_{zr}/p	Eu_r/ap	Eu_z/ap
1	0.402	0.402	4.325	0	0	0
2	0.210	0.210	2.479	0	0	-1.289
3	0.607	0.607	0.839	0	0	-1.564
4	1.001	1.001	0.366	0	0	-1.328
5	1.106	1.106	0.426	0	0	-1.017
6	1.107	1.107	0.574	0	0	-0.767
7	1.085	1.085	0.697	0	0	-0.586
8	(-0.008)	0.284	5.386	0	0.179	0
9						
10						
11	0.431	0.382	0.416	0.481	0.335	-1.803
12	0.706	0.682	0.664	0.149	0.060	-1.561
13						
14	1.647	0.962	(-0.004)	-0.001	0.047	-1.361
15	1.181	1.101	0.437	-0.237	-0.126	-0.991
16	1.087	1.109	0.616	-0.199	-0.136	-0.759
17	0.937	1.220	0.946	-0.975	-0.430	-0.710
18	0.916	1.117	1.026	-0.365	-0.271	-0.425
19	0.925	1.073	1.024	-0.189	-0.195	-0.295
20	(-0.004)	1.278	1.921	0	-0.626	0
21	0.644	1.118	1.348	0	-0.323	0
22	0.832	1.062	1.171	0	-0.201	0

Brackets indicate the exact value is zero.

$\tau_{r\theta} = \tau_{\theta z} = u_\theta = 0$

TABLE A 6.5.1 TOTAL STRESSES AND INDUCED DISPLACEMENTS ASSOCIATED WITH A COMPLETE CIRCULAR TORIC TUNNEL IN A HOMOGENEOUS ISOTROPIC LINEAR ELASTIC INFINITE MASS WITH UNIFORM FIELD STRESS (Fig. A 6.5.1)

$E/p = 1$ $p_r/p = 1$ $p_z/p = 0$ $c/a = 1\frac{1}{2}$ $\nu = 0.25$

N.	σ_r/p	σ_θ/p	σ_z/p	τ_{zr}/p	Eu_r/ap	Eu_z/ap
1	-0.066	-0.066	-0.721	0	0	0
2	0.016	0.016	-0.323	0	0	0.014
3	0.773	0.773	-0.352	0	0	0.004
4	1.171	1.171	-0.265	0	0	0.180
5	1.170	1.170	-0.054	0	0	0.303
6	1.107	1.107	0.058	0	0	0.332
7	1.062	1.062	0.092	0	0	0.313
8	(-0.001)	-0.056	-0.878	0	0.147	0
9						
10						
11	0.009	0.200	0.005	0.011	0.301	0.182
12	0.872	0.868	-0.349	0.011	0.002	0.036
13						
14	2.176	1.501	0	0	-0.259	0.411
15	1.210	1.266	0.230	-0.094	-0.196	0.425
16	1.091	1.149	0.168	-0.039	-0.105	0.367
17	0.393	1.462	0.396	-0.396	-1.007	0.321
18	0.965	1.188	-0.068	-0.141	-0.495	0.106
19	1.014	1.100	-0.074	-0.074	-0.306	0.053
20	0	1.164	-0.669	0	-1.307	0
21	0.339	1.146	-0.047	0	-0.889	0
22	0.614	1.097	0.011	0	-0.620	0

Brackets indicate the exact value is zero.

$\tau_{r\theta} = \tau_{\theta z} = u_\theta = 0$

$E/p = 1$ $p_r/p = 0$ $p_z/p = 1$ $c/a = 1\frac{1}{2}$ $\nu = 0.25$

N.	σ_r/p	σ_θ/p	σ_z/p	τ_{zr}/p	Eu_r/ap	Eu_z/ap
1	0.415	0.415	4.714	0	0	0
2	0.199	0.199	2.541	0	0	-1.327
3	-0.244	-0.244	1.118	0	0	-1.168
4	-0.252	-0.252	0.618	0	0	-1.667
5	-0.116	-0.116	0.469	0	0	-1.472
6	-0.032	-0.032	0.505	0	0	-1.229
7	0.004	0.004	0.594	0	0	-1.006
8	(-0.001)	0.368	5.749	0	0.205	0
9						
10						
11	0.431	0.020	0.421	0.434	-0.031	-2.047
12	-0.256	-0.273	0.962	0.120	0.038	-1.721
13						
14	-0.737	-0.561	(-0.001)	0	0.159	-1.966
15	-0.103	-0.192	0.186	-0.145	-0.046	-1.570
16	-0.044	-0.061	0.433	-0.163	-0.115	-1.253
17	0.558	-0.164	0.565	-0.564	0.381	-1.117
18	-0.078	-0.034	1.098	-0.217	0.091	-0.601
19	-0.109	-0.007	1.103	-0.111	0.015	-0.391
20	(-0.001)	0.203	2.631	0	0.450	0
21	0.314	0.017	1.401	0	0.444	0
22	0.224	-0.009	1.161	0	0.341	0

Brackets indicate the exact value is zero.

$\tau_{r\theta} = \tau_{\theta z} = u_\theta = 0$

$E/p = 1$ $p_r/p = 1$ $p_z/p = 1$ $c/a = 1\frac{1}{2}$ $\nu = 0.25$

N.	σ_r/p	σ_θ/p	σ_z/p	τ_{zr}/p	Eu_r/ap	Eu_z/ap
1	0.349	0.349	3.993	0	0	0
2	0.214	0.214	2.218	0	0	-1.313
3	0.529	0.529	0.765	0	0	-1.677
4	0.919	0.919	0.354	0	0	-1.487
5	1.054	1.054	0.416	0	0	-1.170
6	1.075	1.075	0.563	0	0	-0.897
7	1.066	1.066	0.686	0	0	-0.693
8	(-0.002)	0.312	4.870	0	0.351	0
9						
10						
11	0.440	0.220	0.426	0.445	0.270	-1.865
12	0.616	0.594	0.613	0.130	0.040	-1.685
13						
14	1.439	0.940	(-0.001)	0	-0.101	-1.555
15	1.107	1.074	0.416	-0.239	-0.242	-1.146
16	1.047	1.088	0.600	-0.202	-0.220	-0.885
17	0.952	1.298	0.962	-0.960	-0.626	-0.851
18	0.886	1.154	1.031	-0.358	-0.404	-0.494
19	0.905	1.093	1.029	-0.186	-0.291	-0.338
20	(-0.001)	1.367	1.962	0	-0.848	0
21	0.653	1.163	1.353	0	-0.445	0
22	0.838	1.088	1.172	0	-0.279	0

Brackets indicate the exact value is zero.

$\tau_{r\theta} = \tau_{\theta z} = u_\theta = 0$

TABLE A 6.5.1 TOTAL STRESSES AND INDUCED DISPLACEMENTS ASSOCIATED WITH A COMPLETE CIRCULAR TORIC TUNNEL IN A HOMOGENEOUS ISOTROPIC LINEAR ELASTIC INFINITE MASS WITH UNIFORM FIELD STRESS (Fig. A 6.5.1)

E/p = 1 $p_r/p = 1$ $p_z/p = 0$ c/a = 1½ ν = 0.49

N.	σ_r/p	σ_θ/p	σ_z/p	τ_{zr}/p	Eu_r/ap	Eu_z/ap
1	-0.091	-0.091	-1.077	0	0	0
2	-0.006	-0.006	-0.512	0	0	-0.105
3	0.768	0.768	-0.388	0	0	-0.229
4	1.224	1.224	-0.276	0	0	-0.024
5	1.230	1.230	-0.051	0	0	0.175
6	1.154	1.154	0.070	0	0	0.259
7	1.096	1.096	0.107	0	0	0.273
8	(0.001)	-0.087	-1.294	0	-0.009	0
9						
10						
11	-0.087	0.136	-0.044	-0.066	0.168	-0.018
12	0.873	0.875	-0.378	0.003	-0.023	-0.204
13						
14	2.341	1.868	(-0.001)	0	-0.264	0.556
15	1.294	1.407	0.252	-0.115	-0.175	0.251
16	1.149	1.220	0.187	-0.046	-0.069	0.266
17	0.452	1.451	0.477	-0.468	-0.951	0.084
18	1.038	1.163	-0.076	-0.162	-0.419	-0.059
19	1.061	1.080	-0.084	-0.086	-0.244	-0.065
20	0	0.679	-0.782	0	-1.241	0
21	0.310	0.963	-0.053	0	-0.900	0
22	0.596	1.006	0.014	0	-0.639	0

Brackets indicate the exact value is zero.

$\tau_{r\theta} = \tau_{\theta z} = u_\theta = 0$

E/p = 1 $p_r/p = 0$ $p_z/p = 1$ c/a = 1½ ν = 0.49

N.	σ_r/p	σ_θ/p	σ_z/p	τ_{zr}/p	Eu_r/ap	Eu_z/ap
1	0.378	0.378	4.449	0	0	0
2	0.196	0.196	2.353	0	0	-1.138
3	-0.323	-0.323	1.037	0	0	-1.448
4	-0.395	-0.395	0.597	0	0	-1.538
5	-0.236	-0.236	0.444	0	0	-1.443
6	-0.116	-0.116	0.473	0	0	-1.251
7	-0.053	-0.053	0.563	0	0	-1.048
8	(-0.001)	0.386	5.351	0	0.436	0
9						
10						
11	0.464	-0.036	0.403	0.438	-0.016	-1.761
12	-0.357	-0.370	0.904	0.102	0.028	-1.493
13						
14	-1.140	-1.005	0	0	-0.054	-1.691
15	-0.275	-0.379	0.138	-0.128	-0.223	-1.486
16	-0.151	-0.162	0.392	-0.161	-0.262	-1.234
17	0.484	-0.066	0.453	-0.471	0.070	-1.024
18	-0.187	0.033	1.115	-0.186	-0.158	-0.466
19	-0.182	0.034	1.120	-0.095	-0.172	-0.289
20	(-0.001)	0.826	2.794	0	0.119	0
21	0.355	0.265	1.413	0	0.305	0
22	0.249	0.120	1.159	0	0.261	0

Brackets indicate the exact value is zero.

$\tau_{r\theta} = \tau_{\theta z} = u_\theta = 0$

E/p = 1 $p_r/p = 1$ $p_z/p = 1$ c/a = 1½ ν = 0.49

N.	σ_r/p	σ_θ/p	σ_z/p	τ_{zr}/p	Eu_r/ap	Eu_z/ap
1	0.287	0.287	3.371	0	0	0
2	0.190	0.190	1.841	0	0	-1.243
3	0.445	0.445	0.650	0	0	-1.677
4	0.829	0.829	0.321	0	0	-1.562
5	0.994	0.994	0.393	0	0	-1.268
6	1.038	1.038	0.543	0	0	-0.992
7	1.043	1.043	0.669	0	0	-0.776
8	(-0.001)	0.299	4.057	0	0.427	0
9						
10						
11	0.377	0.100	0.359	0.372	0.152	-1.780
12	0.516	0.505	0.526	0.106	0.005	-1.697
13						
14	1.201	0.863	0	0	-0.318	-1.635
15	1.019	1.029	0.389	-0.243	-0.398	-1.234
16	0.999	1.058	0.579	-0.207	-0.331	-0.969
17	0.936	1.385	0.930	-0.939	-0.881	-0.941
18	0.850	1.195	1.039	-0.348	-0.577	-0.525
19	0.880	1.115	1.036	-0.180	-0.415	-0.354
20	(-0.001)	1.505	2.013	0	-1.122	0
21	0.664	1.228	1.360	0	-0.595	0
22	0.845	1.125	1.173	0	-0.378	0

Brackets indicate the exact value is zero.

$\tau_{r\theta} = \tau_{\theta z} = u_\theta = 0$

TABLE A 6.5.1 TOTAL STRESSES AND INDUCED DISPLACEMENTS ASSOICATED WITH A COMPLETE CIRCULAR TORIC TUNNEL IN A HOMOGENEOUS ISOTROPIC LINEAR ELASTIC INFINITE MASS WITH UNIFORM FIELD STRESS (Fig. A 6.5.1)

$E/p = 1$ $p_r/p = 1$ $p_z/p = 0$ $c/a = 1\frac{1}{2}$ $\nu = 0$

N	σ_r/p	σ_θ/p	σ_z/p	τ_{zr}/p	Eu_r/ap	Eu_z/ap
1	-0.048	-0.048	0.027	0	0	0
2	0.165	0.165	0.003	0	0	0.157
3	0.771	0.771	-0.268	0	0	0.052
4	1.092	1.092	-0.279	0	0	0.201
5	1.122	1.122	-0.120	0	0	0.302
6	1.082	1.082	-0.002	0	0	0.329
7	1.047	1.047	0.052	0	0	0.314
8	(-0.003)	-0.033	-0.183	0	0.516	0
9	-0.048	-0.048	0.027	0	0	0
10						
11	0.193	0.371	0.191	0.213	0.499	0.303
12	0.894	0.853	0.262	0.056	0.064	0.135
13	1.069	1.063	0.297	0.008	0.005	0.178
14	2.123	1.162	(0.002)	0	0.242	0.600
15	1.164	1.135	0.229	-0.067	0.203	0.504
16	1.045	1.090	0.161	-0.036	0.135	0.406
17	0.329	1.451	0.333	-0.345	-0.994	0.432
18	0.911	1.207	-0.066	-0.131	-0.529	0.194
19	0.978	1.118	-0.071	-0.070	-0.343	0.118
20	(-0.002)	1.512	-0.607	0	-1.281	0
21	0.341	1.286	-0.047	0	-0.857	0
22	0.608	1.172	0.009	0	-0.601	0

Brackets indicate the exact value is zero.

$\tau_{r\theta} = \tau_{\theta z} = u_\theta = 0$

$E/p = 1$ $p_r/p = 0$ $p_z/p = 1$ $c/a = 1\frac{1}{2}$ $\nu = 0$

N	σ_r/p	σ_θ/p	σ_z/p	τ_{zr}/p	Eu_r/ap	Eu_z/ap
1	0.519	0.519	2.774	0	0	0
2	0.243	0.243	2.252	0	0	-0.789
3	-0.133	-0.133	1.533	0	0	-1.229
4	-0.165	-0.165	0.994	0	0	-1.351
5	-0.070	-0.070	0.718	0	0	-1.268
6	-0.002	-0.002	0.064	0	0	-1.103
7	0.028	0.028	0.669	0	0	-0.930
8	(-0.004)	0.384	4.232	0	0	0
9	0.519	0.519	2.774	0	0	0
10						
11	0.460	0.156	0.448	0.487	-0.124	-1.829
12	-0.124	-0.144	1.216	0.256	0.063	-1.404
13	-0.171	-0.180	1.062	0.039	0.015	-1.351
14	-0.469	-0.178	(-0.003)	0	0.267	-1.925
15	0.053	-0.055	0.235	-0.124	0.083	-1.466
16	0.056	-0.001	0.486	-0.133	0.001	-1.152
17	0.607	-0.245	0.611	-0.631	0.540	-1.152
18	0.004	-0.093	1.094	-0.242	0.238	-0.630
19	-0.053	-0.045	1.096	-0.125	0.132	-0.423
20	(-0.002)	-0.251	2.548	0	0.628	0
21	0.294	-0.170	1.406	0	0.509	0
22	0.216	-0.109	1.170	0	0.381	0

Brackets indicate the exact value is zero.

$\tau_{r\theta} = \tau_{\theta z} = u_\theta = 0$

$E/p = 1$ $p_r/p = 1$ $p_z/p = 1$ $c/a = 1\frac{1}{2}$ $\nu = 0$

N	σ_r/p	σ_θ/p	σ_z/p	τ_{zr}/p	Eu_r/ap	Eu_z/ap
1	0.471	0.471	2.801	0	0	0
2	0.408	0.408	2.255	0	0	-0.805
3	0.638	0.638	1.265	0	0	-1.178
4	0.926	0.926	0.715	0	0	-1.150
5	1.052	1.052	0.598	0	0	-0.967
6	1.080	1.080	0.645	0	0	-0.774
7	1.075	1.075	0.721	0	0	-0.616
8	(-0.007)	0.351	4.048	0	0.324	0
9	0.471	0.471	2.801	0	0	0
10						
11	0.653	0.527	0.639	0.700	0.375	-1.525
12	0.770	0.709	0.954	0.312	0.128	-1.269
13	0.897	0.883	0.765	0.031	0.010	-1.173
14	1.654	0.983	(0.005)	0	0.025	-1.326
15	1.216	1.080	0.463	-0.191	-0.120	-0.963
16	1.101	1.089	0.647	-0.169	-0.134	-0.746
17	0.936	1.206	0.944	-0.976	-0.455	-0.720
18	0.915	1.114	1.028	-0.373	-0.291	-0.436
19	0.925	1.073	1.025	-0.195	-0.211	-0.305
20	(-0.004)	1.261	1.941	0	-0.653	0
21	0.635	1.116	1.359	0	-0.348	0
22	0.824	1.063	1.179	0	-0.220	0

Brackets indicate the exact value is zero.

$\tau_{r\theta} = \tau_{\theta z} = u_\theta = 0$

TABLE A 6.5.1 TOTAL STRESSES AND INDUCED DISPLACEMENTS ASSOCIATED WITH A COMPLETE CIRCULAR TORIC TUNNEL IN A HOMOGENEOUS ISOTROPIC LINEAR ELASTIC INFINITE MASS WITH UNIFORM FIELD STRESS (Fig. A 6.5.1)

E/p = 1 p_r/p = 1 p_z/p = 0 c/a = 1½ ν = 0.25

N	σ_r/p	σ_θ/p	σ_z/p	τ_{zr}/p	Eu_r/ap	Eu_z/ap
1	-0.091	-0.091	-0.305	0	0	0
2	0.111	0.111	-0.232	0	0	-0.124
3	0.738	0.738	-0.365	0	0	-0.125
4	1.111	1.111	-0.329	0	0	0.050
5	1.160	1.160	-0.146	0	0	0.207
6	1.118	1.118	-0.013	0	0	0.279
7	1.075	1.075	0.049	0	0	0.290
8	(-0.001)	-0.089	-0.592	0	0.345	0
9	-0.091	-0.091	-0.305	0	0	0
10						
11	0.075	0.299	0.070	0.077	0.386	0.153
12	0.860	0.841	-0.342	0.028	0.017	-0.044
13	1.080	1.077	-0.352	-0.011	-0.012	0.019
14	2.236	1.489	0	0	-0.271	0.405
15	1.216	1.216	0.238	-0.095	-0.222	0.417
16	1.083	1.153	0.168	-0.051	-0.136	0.357
17	0.401	1.429	0.405	-0.404	-1.055	0.322
18	0.967	1.183	-0.070	-0.149	-0.535	0.104
19	1.014	1.101	-0.077	-0.080	-0.340	0.050
20	0	1.127	-0.681	0	-1.367	0
21	0.322	1.134	-0.047	0	-0.947	0
22	0.598	1.094	0.013	0	-0.670	0

Brackets indicate the exact value is zero.

$\tau_{r\theta} = \tau_{\theta z} = u_\theta = 0$

E/p = 1 p_r/p = 0 p_z/p = 1 c/a = 1½ ν = 0.25

N	σ_r/p	σ_θ/p	σ_z/p	τ_{zr}/p	Eu_r/ap	Eu_z/ap
1	0.523	0.523	2.955	0	0	0
2	0.278	0.278	2.320	0	0	-0.748
3	-0.149	-0.149	1.534	0	0	-1.187
4	-0.241	-0.241	1.001	0	0	-1.367
5	-0.150	-0.150	0.719	0	0	-1.336
6	-0.066	-0.066	0.639	0	0	-1.196
7	-0.019	-0.019	0.657	0	0	-1.027
8	(-0.001)	0.495	4.317	0	0.167	0
9	0.523	0.523	2.955	0	0	0
10						
11	0.586	0.069	0.576	0.588	-0.023	-1.790
12	-0.155	-0.202	1.232	0.255	0.097	-1.372
13	-0.243	-0.249	1.069	0.039	0.018	-1.357
14	-0.742	-0.543	0	0	0.162	-1.937
15	-0.064	-0.207	0.207	-0.101	-0.011	-1.543
16	-0.020	-0.082	0.464	-0.123	-0.086	-1.237
17	0.554	-0.152	0.561	-0.559	0.398	-1.188
18	-0.079	-0.035	1.104	-0.218	0.106	-0.614
19	-0.108	-0.009	1.108	-0.112	0.027	-0.403
20	0	0.223	2.665	0	0.484	0
21	0.322	0.027	1.413	0	0.470	0
22	0.232	-0.004	1.167	0	0.364	0

Brackets indicate the exact value is zero.

$\tau_{r\theta} = \tau_{\theta z} = u_\theta = 0$

E/p = 1 p_r/p = 1 p_z/p = 1 c/a = 1½ ν = 0.25

N	σ_r/p	σ_θ/p	σ_z/p	τ_{zr}/p	Eu_r/ap	Eu_z/ap
1	0.432	0.432	2.650	0	0	0
2	0.388	0.388	2.088	0	0	-0.872
3	0.589	0.589	1.169	0	0	-1.313
4	0.870	0.870	0.672	0	0	-1.317
5	1.010	1.010	0.573	0	0	-1.129
6	1.052	1.052	0.626	0	0	-0.917
7	1.057	1.057	0.706	0	0	-0.736
8	0	0.406	3.725	0	0.513	0
9	0.432	0.432	2.650	0	0	0
10						
11	0.661	0.368	0.646	0.665	0.363	-1.639
12	0.706	0.639	0.889	0.283	0.114	-1.416
13	0.837	0.828	0.718	0.028	0.005	-1.338
14	1.493	0.946	(-0.001)	0	-0.109	-1.533
15	1.152	1.054	0.445	-0.196	-0.232	-1.126
16	1.064	1.072	0.632	-0.175	-0.222	-0.880
17	0.955	1.278	0.966	-0.963	-0.657	-0.866
18	0.888	1.148	1.034	-0.367	-0.430	-0.510
19	0.906	1.091	1.031	-0.192	-0.313	-0.353
20	0	1.349	1.984	0	-0.884	0
21	0.644	1.161	1.366	0	-0.477	0
22	0.830	1.090	1.181	0	-0.306	0

Brackets indicate the exact value is zero.

$\tau_{r\theta} = \tau_{\theta z} = u_\theta = 0$

TABLE A 6.5.1 TOTAL STRESSES AND INDUCED DISPLACEMENTS ASSOCIATED WITH A COMPLETE CIRCULAR TORIC TUNNEL IN A HOMOGENEOUS ISOTROPIC LINEAR ELASTIC INFINITE MASS WITH UNIFORM FIELD STRESS (Fig. A 6.5.1)

E/p = 1 $p_r/p = 1$ $p_z/p = 0$ c/a = 1½ ν = 0.49

N.	σ_r/p	σ_θ/p	σ_z/p	τ_{zr}/p	Eu_r/ap	Eu_z/ap
1	-0.121	-0.121	-0.549	0	0	0
2	0.074	0.074	-0.403	0	0	-0.279
3	0.720	0.720	-0.430	0	0	-0.380
4	1.140	1.140	-0.360	0	0	-0.188
5	1.206	1.206	-0.160	0	0	0.036
6	1.160	1.160	-0.015	0	0	0.167
7	1.108	1.108	0.054	0	0	0.220
8	0	-0.134	-0.888	0	0.105	0
9	-0.121	-0.121	-0.549	0	0	0
10						
11	-0.043	0.230	-0.010	-0.028	0.201	-0.092
12	0.842	0.839	-0.396	0.008	-0.049	-0.313
13	1.087	1.115	-0.386	-0.013	-0.022	-0.228
14	2.367	1.862	(-0.001)	0	-0.288	0.023
15	1.282	1.406	0.253	0.122	-0.216	0.217
16	1.132	1.226	0.180	-0.064	-0.111	0.229
17	0.460	1.421	0.480	-0.474	-0.993	0.069
18	1.036	1.159	-0.076	-0.169	-0.458	-0.074
19	1.058	1.082	-0.086	-0.092	-0.277	-0.780
20	0	0.643	-0.781	0	-1.289	0
21	0.297	0.948	-0.049	0	-0.950	0
22	0.583	0.999	0.017	0	-0.683	0

Brackets indicate the exact value is zero.

$\tau_{r\theta} = \tau_{\theta z} = u_\theta = 0$

E/p = 1 $p_r/p = 0$ $p_z/p = 1$ c/a = 1½ ν = 0.49

N.	σ_r/p	σ_θ/p	σ_z/p	τ_{zr}/p	Eu_r/ap	Eu_z/ap
1	0.492	0.492	2.880	0	0	0
2	0.268	0.268	2.218	0	0	-0.610
3	-0.198	-0.198	1.450	0	0	-0.999
4	-0.340	-0.340	0.959	0	0	-1.239
5	-0.249	-0.249	0.687	0	0	-1.290
6	-0.143	-0.143	0.607	0	0	-1.202
7	-0.075	-0.075	0.626	0	0	-1.059
8	(-0.001)	0.532	4.100	0	0.493	0
9	0.492	0.492	2.880	0	0	0
10						
11	0.625	0.004	0.578	0.607	0.076	-1.540
12	-0.221	-0.284	1.176	0.234	0.115	-1.173
13	-0.350	-0.332	1.023	0.036	0.015	-1.215
14	-1.076	-0.997	(0.001)	0	-0.030	-1.662
15	-0.214	-0.394	0.165	-0.085	-0.180	-1.449
16	-0.117	-0.181	0.428	-0.121	-0.234	-1.207
17	0.485	-0.060	0.458	-0.474	0.071	-1.032
18	-0.181	0.031	1.120	-0.189	-0.155	-0.474
19	-0.178	0.033	1.126	-0.096	-0.170	-0.295
20	(-0.001)	0.845	2.821	0	0.118	0
21	0.359	0.280	1.425	0	0.312	0
22	0.255	0.129	1.166	0	0.270	0

Brackets indicate the exact value is zero.

$\tau_{r\theta} = \tau_{\theta z} = u_\theta = 0$

E/p = 1 $p_r/p = 1$ $p_z/p = 1$ c/a = 1½ ν = 0.49

N.	σ_r/p	σ_θ/p	σ_z/p	τ_{zr}/p	Eu_r/ap	Eu_z/ap
1	0.371	0.371	2.330	0	0	0
2	0.341	0.341	1.815	0	0	-0.888
3	0.522	0.522	1.019	0	0	-1.378
4	0.800	0.800	0.599	0	0	-1.427
5	0.957	0.957	0.528	0	0	-1.254
6	1.017	1.017	0.592	0	0	-1.035
7	1.034	1.034	0.680	0	0	-0.840
8	(-0.001)	0.399	3.213	0	0.598	0
9	0.371	0.371	2.330	0	0	0
10						
11	0.582	0.234	0.568	0.580	0.277	-1.632
12	0.621	0.556	0.780	0.242	0.066	-1.486
13	0.738	0.782	0.637	0.023	-0.008	-1.443
14	1.291	0.864	0	0	-0.318	-1.639
15	1.068	1.012	0.418	-0.206	-0.396	-1.233
16	1.015	1.045	0.608	-0.186	-0.345	-0.978
17	0.945	1.361	0.939	-0.948	-0.922	-0.964
18	0.855	1.190	1.044	-0.358	-0.613	-0.547
19	0.881	1.115	1.040	-0.188	-0.447	-0.373
20	(-0.001)	1.488	2.040	0	-1.172	0
21	0.656	1.228	1.376	0	-0.638	0
22	0.838	1.128	1.183	0	-0.413	0

Brackets indicate the exact value is zero.

$\tau_{r\theta} = \tau_{\theta z} = u_\theta = 0$

TABLE A 6.5.1 TOTAL STRESSES AND INDUCED DISPLACEMENTS ASSOCIATED WITH A COMPLETE CIRCULAR TORIC TUNNEL IN A HOMOGENEOUS ISOTROPIC LINEAR ELASTIC INFINITE MASS WITH UNIFORM FIELD STRESS (Fig. A 6.5.1)

$E/p = 1$ $p_r/p = 1$ $p_z/p = 0$ $c/a = 2$ $\nu = 0$

N.	σ_r/p	σ_θ/p	σ_z/p	τ_{zr}/p	Eu_r/ap	Eu_z/ap
1	0.096	0.096	0.237	0	0	0
2	0.311	0.311	0.080	0	0	-0.091
3	0.730	0.730	-0.189	0	0	-0.061
4	1.006	1.006	-0.278	0	0	-0.066
5	1.093	1.093	-0.201	0	0	0.189
6	1.090	1.090	-0.095	0	0	0.263
7	1.065	1.065	-0.019	0	0	0.290
8	(-0.003)	0.033	-0.419	0	0.967	0
9	0.034	0.075	0.157	0	0.462	0
10	0.096	0.096	0.237	0	0	0
11	0.336	0.482	0.336	0.360	0.670	0.399
12	0.940	0.829	-0.192	0.113	0.161	0.147
13	1.023	0.991	-0.257	-0.006	0.005	0.109
14	2.262	1.126	(-0.002)	0	-0.252	0.658
15	1.207	1.110	0.257	-0.048	-0.220	0.552
16	1.049	1.083	0.183	-0.035	-0.165	0.442
17	0.336	1.400	0.340	-0.356	-1.083	0.464
18	0.924	1.196	-0.077	-0.142	-0.599	0.213
19	0.984	1.117	-0.081	-0.077	-0.401	0.131
20	(0.002)	1.466	-0.652	0	-1.396	0
21	0.310	1.275	-0.053	0	-0.961	0
22	0.578	1.172	0.009	0	-0.690	0

Brackets indicate the exact value is zero.

$\tau_{r\theta} = \tau_{\theta z} = u_\theta = 0$

$E/p = 1$ $p_r/p = .0$ $p_z/p = 1$ $c/a = 2$ $\nu = 0$

N.	σ_r/p	σ_θ/p	σ_z/p	τ_{zr}/p	Eu_r/ap	Eu_z/ap
1	0.483	0.483	1.681	0	0	0
2	0.295	0.295	1.683	0	0	-0.342
3	-0.007	-0.007	1.579	0	0	-0.665
4	-0.132	-0.132	1.322	0	0	-0.894
5	-0.114	-0.114	1.060	0	0	-0.986
6	-0.061	-0.061	0.894	0	0	-0.970
7	-0.019	-0.019	0.820	0	0	-0.896
8	(-0.003)	0.414	3.552	0	-0.414	0
9	0.474	0.482	1.924	0	-0.241	0
10	0.483	0.483	1.681	0	0	0
11	0.487	0.175	0.477	0.513	-0.226	-1.632
12	-0.075	-0.056	1.249	0.306	0.053	-1.115
13	-0.124	-0.125	1.258	0.176	0.074	-0.983
14	-0.569	-0.124	(-0.003)	0	0.247	-1.916
15	0.062	0.056	0.237	0.082	0.112	-1.455
16	0.079	-0.021	0.504	-0.086	0.041	-1.146
17	0.592	-0.216	0.595	-0.617	0.584	-1.189
18	-0.007	-0.089	1.103	-0.241	0.273	-0.658
19	-0.057	-0.047	1.105	-0.126	0.162	-0.447
20	(-0.003)	-0.231	2.610	0	0.693	0
21	0.310	-0.162	1.425	0	0.568	0
22	0.231	-0.108	1.180	0	0.432	0

Brackets indicate the exact value is zero.

$\tau_{r\theta} = \tau_{\theta z} = u_\theta = 0$

$E/p = 1$ $p_r/p = 1$ $p_z/p = 1$ $c/a = 2$ $\nu = 0$

N.	σ_r/p	σ_θ/p	σ_z/p	τ_{zr}/p	Eu_r/ap	Eu_z/ap
1	0.578	0.578	1.918	0	0	0
2	0.606	0.606	1.763	0	0	-0.433
3	0.723	0.723	1.390	0	0	-0.726
4	0.874	0.874	1.044	0	0	-0.828
5	0.979	0.979	0.858	0	0	-0.797
6	1.029	1.029	0.799	0	0	-0.708
7	1.045	1.045	0.801	0	0	-0.606
8	(-0.006)	0.447	3.133	0	0.553	0
9	0.508	0.557	2.081	0	0.222	0
10	0.578	0.578	1.918	0	0	0
11	0.823	0.657	0.813	0.873	0.444	-1.233
12	0.866	0.773	1.057	0.419	0.213	-0.968
13	0.899	0.866	1.002	0.170	0.079	-0.874
14	1.692	1.002	(-0.005)	0	-0.004	-1.258
15	1.268	1.054	0.494	-0.130	-0.108	-0.903
16	1.128	1.062	0.686	-0.121	-0.124	-0.704
17	0.929	1.185	0.935	-0.973	-0.500	-0.725
18	0.917	1.106	1.026	-0.383	-0.326	-0.445
19	0.927	1.070	1.025	-0.204	-0.239	-0.316
20	(-0.005)	1.235	1.959	0	-0.704	0
21	0.620	1.112	1.372	0	-0.393	0
22	0.810	1.064	1.189	0	-0.258	0

Brackets indicate the exact value is zero.

$\tau_{r\theta} = \tau_{\theta z} = u_\theta = 0$

TABLE A 6.5.1 TOTAL STRESSES AND INDUCED DISPLACEMENTS ASSOCIATED WITH A COMPLETE CIRCULAR TORIC TUNNEL IN A HOMOGENEOUS ISOTROPIC LINEAR ELASTIC INFINITE MASS WITH UNIFORM FIELD STRESS (Fig. A 6.5.1)

E/p = 1 $p_r/p = 1$ $p_z/p = 0$ c/a = 2 v = 0.25

N.	σ_r/p	σ_θ/p	σ_z/p	τ_{zr}/p	Eu_r/ap	Eu_z/ap
1	0.044	0.044	0.040	0	0	0
2	0.257	0.257	0.273	0	0	-0.221
3	0.691	0.691	-0.278	0	0	-0.263
4	1.001	1.001	-0.334	0	0	-0.136
5	1.111	1.111	-0.242	0	0	0.029
6	1.116	1.116	-0.123	0	0	0.149
7	1.090	1.090	-0.037	0	0	0.213
8	(-0.001)	-0.122	-0.620	0	0.716	0
9	-0.005	0.003	-0.051	0	0.366	0
10	0.044	0.044	0.040	0	0	0
11	0.212	0.444	0.210	0.214	0.532	0.177
12	0.926	0.869	-0.292	0.050	0.034	-0.091
13	1.014	0.994	-0.317	-0.018	-0.041	-0.097
14	2.347	1.477	0	0	-0.282	0.415
15	1.243	1.251	0.261	-0.083	-0.250	0.425
16	1.078	1.155	0.182	-0.057	-0.179	0.357
17	0.413	1.375	0.415	-0.416	-1.132	0.329
18	0.977	1.171	-0.076	-0.161	-0.600	0.102
19	1.018	1.099	-0.083	-0.088	-0.395	0.047
20	0	1.062	-0.708	0	-1.467	0
21	0.295	1.110	-0.047	0	-1.044	0
22	0.571	1.086	0.016	0	-0.755	0

Brackets indicate the exact value is zero.

$\tau_{r\theta} = \tau_{\theta z} = u_\theta = 0$

E/p = 1 $p_r/p = 0$ $p_z/p = 1$ c/a = 2 v = 0.25

N.	σ_r/p	σ_θ/p	σ_z/p	τ_{zr}/p	Eu_r/ap	Eu_z/ap
1	0.506	0.506	1.803	0	0	0
2	0.321	0.321	1.759	0	0	-0.284
3	0	0	1.601	0	0	-0.591
4	-0.160	-0.160	1.330	0	0	-0.851
5	-0.160	-0.160	1.065	0	0	-0.989
6	-0.108	-0.108	0.895	0	0	-1.008
7	-0.060	-0.060	0.817	0	0	-0.953
8	(-0.001)	0.623	3.580	0	0.022	0
9	0.486	0.536	2.047	0	-0.076	0
10	0.506	0.506	1.803	0	0	0
11	0.623	0.091	0.613	0.624	-0.042	-1.563
12	-0.067	-0.109	1.279	0.320	0.152	-1.048
13	-0.151	-0.167	1.272	0.179	0.115	-0.938
14	-0.756	-0.523	0	0	0.167	-1.893
15	-0.021	-0.221	0.220	-0.051	0.041	-1.498
16	0.020	-0.107	0.492	-0.071	-0.031	-1.200
17	0.544	-0.133	0.551	-0.549	0.424	-1.206
18	-0.081	-0.035	1.109	-0.219	0.130	-0.629
19	-0.107	-0.012	1.115	-0.113	0.049	-0.417
20	(-0.001)	0.254	2.711	0	0.521	0
21	0.333	0.044	1.428	0	0.510	0
22	0.244	0.004	1.175	0	0.402	0

Brackets indicate the exact value is zero.

$\tau_{r\theta} = \tau_{\theta z} = u_\theta = 0$

E/p = 1 $p_r/p = 1$ $p_z/p = 1$ c/a = 2 v = 0.25

N.	σ_r/p	σ_θ/p	σ_z/p	τ_{zr}/p	Eu_r/ap	Eu_z/ap
1	0.550	0.550	1.843	0	0	0
2	0.578	0.578	1.686	0	0	-0.505
3	0.691	0.691	1.324	0	0	-0.855
4	0.841	0.841	0.995	0	0	-0.987
5	0.951	0.951	0.823	0	0	-0.959
6	1.008	1.008	0.772	0	0	-0.859
7	1.030	1.030	0.781	0	0	-0.740
8	(-0.001)	0.501	2.959	0	0.738	0
9	0.481	0.539	1.996	0	0.290	0
10	0.550	0.550	1.843	0	0	0
11	0.834	0.535	0.823	0.839	0.490	-1.386
12	0.824	0.717	1.006	0.398	0.226	-1.126
13	0.863	0.828	0.955	0.160	0.074	-1.036
14	1.591	0.955	(0.001)	0	-0.114	-1.478
15	1.221	1.030	0.481	-0.137	-0.209	-1.073
16	1.099	1.048	0.674	-0.129	-0.209	-0.844
17	0.957	1.242	0.966	-0.965	-0.707	-0.877
18	0.896	1.136	1.033	-0.380	-0.470	-0.527
19	0.911	1.087	1.031	-0.202	-0.346	-0.370
20	(-0.001)	1.316	2.002	0	-0.946	0
21	0.628	1.155	1.381	0	-0.534	0
22	0.815	1.090	1.192	0	-0.353	0

Brackets indicate the exact value is zero.

$\tau_{r\theta} = \tau_{\theta z} = u_\theta = 0$

TABLE A 6.5.1 TOTAL STRESSES AND INDUCED DISPLACEMENTS ASSOCIATED WITH A COMPLETE CIRCULAR TORIC TUNNEL IN A HOMOGENEOUS ISOTROPIC LINEAR ELASTIC INFINITE MASS WITH UNIFORM FIELD STRESS (Fig. A 6.5.1)

$E/p = 1$ $p_r/p = 1$ $p_z/p = 0$ $c/a = 2$ $\nu = 0.49$

N.	σ_r/p	σ_θ/p	σ_z/p	τ_{zr}/p	Eu_r/ap	Eu_z/ap
1	0.005	0.005	-0.117	0	0	0
2	0.215	0.215	-0.196	0	0	-0.380
3	0.633	0.633	-0.348	0	0	-0.520
4	1.003	1.003	-0.377	0	0	-0.404
5	1.133	1.133	-0.270	0	0	-0.199
6	1.144	1.144	-0.141	0	0	-0.026
7	1.117	1.117	-0.047	0	0	0.084
8	0	-0.234	-0.786	0	0.359	0
9	-0.036	-0.052	-0.216	0	0.219	0
10	0.005	0.005	-0.117	0	0	0
11	0.081	0.384	0.112	0.097	0.285	-0.131
12	0.851	0.823	-0.334	0.048	-0.057	-0.380
13	1.010	1.002	-0.363	-0.029	-0.102	-0.376
14	2.434	1.861	(-0.001)	0	-0.316	-0.013
15	1.285	1.404	0.267	-0.115	-0.267	0.183
16	1.112	1.233	0.185	-0.077	-0.174	0.188
17	0.467	1.369	0.489	-0.481	-1.058	0.048
18	1.037	1.150	-0.077	-0.180	-0.519	-0.096
19	1.057	1.081	-0.088	-0.100	-0.331	-0.098
20	0	0.581	-0.786	0	-1.368	0
21	0.277	0.919	-0.045	0	-1.033	0
22	0.562	0.986	0.023	0	-0.759	0

Brackets indicate the exact value is zero.

$\tau_{r\theta} = \tau_{\theta z} = u_\theta = 0$

$E/p = 1$ $p_r/p = 0$ $p_z/p = 1$ $c/a = 2$ $\nu = 0.49$

N.	σ_r/p	σ_θ/p	σ_z/p	τ_{zr}/p	Eu_r/ap	Eu_z/ap
1	0.491	0.491	1.807	0	0	0
2	0.309	0.309	1.738	0	0	-0.182
3	-0.026	-0.026	1.557	0	0	-0.442
4	-0.211	-0.211	1.289	0	0	-0.723
5	-0.222	-0.222	1.033	0	0	-0.911
6	-0.166	-0.166	0.687	0	0	-0.978
7	-0.108	-0.108	0.792	0	0	-0.956
8	(-0.001)	0.735	3.452	0	0.467	0
9	0.467	0.545	2.041	0	0.097	0
10	0.491	0.491	1.807	0	0	0
11	0.678	0.029	0.637	0.662	0.162	-1.329
12	-0.095	-0.179	1.252	0.311	0.241	-0.861
13	-0.202	-0.230	1.237	0.173	0.145	-0.797
14	-0.993	-0.983	0	0	0.014	-1.610
15	-0.133	-0.410	0.191	-0.136	-0.104	-1.385
16	-0.057	-0.206	0.466	-0.067	-0.168	-1.147
17	0.487	-0.055	0.460	-0.476	0.079	-1.037
18	-0.169	0.025	1.123	-0.194	-0.144	-0.480
19	-0.168	0.029	1.130	-0.098	-0.160	-0.301
20	(-0.001)	0.865	2.848	0	0.119	0
21	0.363	0.301	1.439	0	0.323	0
22	0.261	0.142	1.174	0	0.285	0

Brackets indicate the exact value is zero.

$\tau_{r\theta} = \tau_{\theta z} = u_\theta = 0$

$E/p = 1$ $p_r/p = 1$ $p_z/p = 1$ $c/a = 2$ $\nu = 0.49$

N	σ_r/p	σ_θ/p	σ_z/p	τ_{zr}/p	Eu_r/ap	Eu_z/ap
1	0.496	0.496	1.690	0	0	0
2	0.525	0.525	1.542	0	0	-0.563
3	0.637	0.637	1.209	0	0	-0.962
4	0.792	0.792	0.913	0	0	-1.127
5	0.912	0.912	0.762	0	0	-1.110
6	0.979	0.979	0.726	0	0	-1.004
7	1.010	1.010	0.745	0	0	-0.872
8	(-0.001)	0.501	2.666	0	0.825	0
9	0.431	0.493	1.824	0	0.316	0
10	0.496	0.496	1.690	0	0	0
11	0.759	0.413	0.749	0.759	0.448	-1.460
12	0.756	0.644	0.918	0.359	0.185	-1.241
13	0.808	0.773	0.875	0.143	0.042	-1.173
14	1.441	0.877	0	0	-0.302	-1.623
15	1.152	0.994	0.458	-0.151	-0.371	-1.202
16	1.055	1.027	0.651	0.144	-0.342	-0.959
17	0.954	1.314	0.949	-0.957	-0.979	-0.988
18	0.868	1.175	1.046	-0.374	-0.663	-0.576
19	0.889	1.110	1.042	-0.198	-0.491	-0.399
20	(-0.001)	1.446	2.062	0	-1.249	0
21	0.640	1.220	1.395	0	-0.710	0
22	0.823	1.128	1.197	0	-0.473	0

Brackets indicate the exact value is zero.

$\tau_{r\theta} = \tau_{\theta z} = u_\theta = 0$

TABLE A 6.5.1 TOTAL STRESSES AND INDUCED DISPLACEMENTS ASSOCIATED WITH A COMPLETE CIRCULAR TORIC TUNNEL IN A HOMOGENEOUS ISOTROPIC LINEAR ELASTIC INFINITE MASS WITH UNIFORM FIELD STRESS (Fig. A 6.5.1)

E/p = 1 $p_r/p = 1$ $p_z/p = 0$ c/a = 3 $\nu = 0$

N.	σ_r/p	σ_θ/p	σ_z/p	τ_{zr}/p	Eu_r/ap	Eu_z/ap
1	0.463	0.463	0.219	0	0	0
2	0.540	0.540	0.144	0	0	-0.096
3	0.715	0.715	-0.014	0	0	-0.130
4	0.886	0.886	-0.139	0	0	-0.088
5	0.996	0.996	-0.181	0	0	-0.005
6	1.046	1.046	-0.161	0	0	0.083
7	1.058	1.058	-0.115	0	0	0.152
8	(-0.003)	0.270	-0.738	0	1.460	0
9	0.117	0.356	0.100	0	0.966	0
10	0.325	0.419	0.204	0	0.581	0
11	0.470	0.598	0.472	0.497	0.922	0.538
12	1.043	0.820	0.138	0.189	0.349	0.211
13	1.054	0.922	-0.184	0.063	0.123	0.110
14	2.486	1.077	(-0.002)	0	-0.232	0.760
15	1.292	1.076	0.300	-0.015	-0.210	0.639
16	1.078	1.059	0.221	-0.017	-0.178	0.508
17	0.352	1.324	0.356	-0.375	-1.200	0.522
18	0.959	1.169	-0.094	-0.157	-0.686	0.245
19	1.007	1.108	-0.097	-0.086	-0.475	0.155
20	(-0.002)	1.390	-0.729	0	-1.560	0
21	0.270	1.247	-0.063	0	-1.111	0
22	0.540	1.164	0.009	0	-0.820	0

Brackets indicate the exact value is zero.

$\tau_{r\theta} = \tau_{\theta z} = u_\theta = 0$

E/p = 1 $p_r/p = 0$ $p_z/p = 1$ c/a = 3 $\nu = 0$

N.	σ_r/p	σ_θ/p	σ_z/p	τ_{zr}/p	Eu_r/ap	Eu_z/ap
1	0.295	0.295	1.194	0	0	0
2	0.236	0.236	1.230	0	0	-0.103
3	0.107	0.107	1.287	0	0	-0.233
4	-0.007	-0.007	1.291	0	0	-0.381
5	-0.063	-0.063	1.228	0	0	-0.513
6	-0.073	-0.073	1.136	0	0	-0.604
7	-0.060	-0.060	1.049	0	0	-0.650
8	(-0.003)	0.335	3.281	0	-0.671	0
9	0.414	0.341	1.655	0	-0.510	0
10	0.358	0.316	1.322	0	-0.316	0
11	0.455	0.164	0.447	0.480	-0.375	-1.528
12	-0.098	0.019	1.196	0.271	-0.036	-0.950
13	-0.104	-0.034	1.225	0.182	0.054	-0.743
14	-0.707	-0.707	(-0.003)	0	0.210	-1.926
15	0.039	-0.041	0.222	-0.056	0.124	-1.459
16	0.090	-0.026	0.499	-0.052	0.077	-1.145
17	0.571	-0.172	0.572	-0.595	0.639	-1.241
18	-0.030	-0.078	1.114	-0.238	0.316	-0.695
19	-0.070	-0.045	1.117	-0.127	0.200	-0.478
20	(-0.003)	-0.196	2.696	0	0.782	0
21	0.330	-0.145	1.449	0	0.651	0
22	0.250	-0.101	1.191	0	0.505	0

Brackets indicate the exact value is zero.

$\tau_{r\theta} = \tau_{\theta z} = u_\theta = 0$

E/p = 1 $p_r/p = 1$ $p_z/p = 1$ c/a = 3 $\nu = 0$

N.	σ_r/p	σ_θ/p	σ_z/p	τ_{zr}/p	Eu_r/ap	Eu_z/ap
1	0.758	0.758	1.413	0	0	0
2	0.776	0.776	1.373	0	0	-0.200
3	0.821	0.821	1.273	0	0	-0.363
4	0.879	0.879	1.151	0	0	-0.469
5	0.933	0.933	1.047	0	0	-0.517
6	0.973	0.973	0.975	0	0	-0.521
7	0.999	0.999	0.935	0	0	-0.498
8	(-0.006)	0.605	2.544	0	0.790	0
9	0.531	0.697	1.755	0	0.455	0
10	0.638	0.735	1.525	0	0.265	0
11	0.925	0.761	0.919	0.977	0.547	-0.990
12	0.945	0.839	1.058	0.460	0.312	-0.739
13	0.950	0.888	1.041	0.245	0.178	-0.633
14	1.779	1.007	(-0.005)	0	-0.021	-1.166
15	1.331	1.029	0.522	-0.071	-0.086	-0.820
16	1.168	1.034	0.720	-0.069	-0.101	-0.637
17	0.923	1.151	0.928	-0.970	-0.561	-0.720
18	0.929	1.091	1.020	-0.396	-0.371	-0.449
19	0.937	1.062	1.020	-0.213	-0.275	-0.323
20	(-0.005)	1.195	1.967	0	-0.778	0
21	0.600	1.102	1.386	0	-0.460	0
22	0.790	1.063	1.200	0	-0.315	0

Brackets indicate the exact value is zero.

$\tau_{r\theta} = \tau_{\theta z} = u_\theta = 0$

TABLE A 6.5.1 TOTAL STRESSES AND INDUCED DISPLACEMENTS ASSOCIATED WITH A COMPLETE CIRCULAR TORIC TUNNEL IN A HOMOGENEOUS ISOTROPIC LINEAR ELASTIC INFINITE MASS WITH UNIFORM FIELD STRESS (Fig. A 6.5.1)

$E/p = 1$ $p_r/p = 1$ $p_z/p = 0$ $c/a = 3$ $\nu = 0.25$

N.	σ_r/p	σ_θ/p	σ_z/p	τ_{zr}/p	Eu_r/ap	Eu_z/ap
1	0.417	0.417	0.129	0	0	0
2	0.497	0.497	0.063	0	0	-0.192
3	0.681	0.681	-0.077	0	0	-0.293
4	0.867	0.867	-0.185	0	0	-0.280
5	0.991	0.991	-0.217	0	0	-0.193
6	1.051	1.051	-0.189	0	0	-0.084
7	1.069	1.069	-0.137	0	0	0.014
8	0	-0.040	-0.814	0	1.174	0
9	0.094	0.221	-0.017	0	0.823	0
10	0.286	0.344	0.102	0	0.504	0
11	0.370	0.604	0.370	0.373	0.759	0.265
12	0.986	0.834	-0.198	0.155	0.220	0.034
13	1.028	0.932	-0.230	0.044	0.028	-0.108
14	2.535	1.473	0	0	-0.267	0.463
15	1.310	1.236	0.299	-0.051	-0.251	0.474
16	1.094	1.147	0.217	-0.043	-0.208	0.389
17	0.428	1.296	0.429	-0.431	-1.229	0.351
18	1.004	1.146	-0.089	-0.175	-0.679	0.108
19	1.035	1.090	-0.096	-0.097	-0.415	0.048
20	0	0.960	-0.763	0	-1.604	0
21	0.262	1.065	-0.052	0	-1.181	0
22	0.538	1.065	0.019	0	-0.879	0

Brackets indicate the exact value is zero.

$\tau_{r\theta} = \tau_{\theta z} = u_\theta = 0$

$E/p = 1$ $p_r/p = 0$ $p_z/p = 1$ $c/a = 3$ $\nu = 0.25$

N.	σ_r/p	σ_θ/p	σ_z/p	τ_{zr}/p	Eu_r/ap	Eu_z/ap
1	0.319	0.319	1.251	0	0	0
2	0.257	0.257	1.279	0	0	-0.056
3	0.119	0.119	1.319	0	0	-0.159
4	-0.006	-0.006	1.308	0	0	-0.305
5	-0.074	-0.074	1.238	0	0	-0.455
6	-0.092	-0.092	1.141	0	0	-0.572
7	-0.081	-0.081	1.052	0	0	-0.641
8	(-0.001)	0.667	3.279	0	-0.195	0
9	0.420	0.464	1.725	0	-0.266	0
10	0.377	0.372	1.386	0	-0.182	0
11	0.572	0.087	0.565	0.574	-0.120	-1.434
12	-0.067	-0.031	1.224	0.293	0.137	-0.859
13	-0.099	-0.099	1.243	0.194	0.167	-0.668
14	-0.806	-0.507	0	0	0.165	-1.863
15	-0.007	-0.226	0.215	-0.027	0.086	-1.466
16	0.054	-0.124	0.495	-0.034	0.033	-1.166
17	0.532	-0.106	0.537	-0.537	0.459	-1.230
18	-0.089	-0.033	1.116	-0.220	0.162	-0.648
19	-0.109	-0.015	1.122	-0.115	0.079	-0.434
20	(-0.001)	0.300	2.771	0	0.572	0
21	0.345	0.072	1.448	0	0.566	0
22	0.257	0.019	1.185	0	0.456	0

Brackets indicate the exact value is zero.

$\tau_{r\theta} = \tau_{\theta z} = u_\theta = 0$

$E/p = 1$ $p_r/p = 1$ $p_z/p = 1$ $c/a = 3$ $\nu = 0.25$

N.	σ_r/p	σ_θ/p	σ_z/p	τ_{zr}/p	Eu_r/ap	Eu_z/ap
1	0.736	0.736	1.380	0	0	0
2	0.754	0.754	1.341	0	0	-0.248
3	0.800	0.800	1.242	0	0	-0.452
4	0.860	0.860	1.123	0	0	-0.585
5	0.917	0.917	1.021	0	0	-0.648
6	0.960	0.960	0.952	0	0	-0.655
7	0.988	0.988	0.915	0	0	-0.627
8	(-0.001)	0.627	2.465	0	0.978	0
9	0.515	0.684	1.708	0	0.557	0
10	0.663	0.716	1.488	0	0.322	0
11	0.942	0.691	0.935	0.947	0.639	-1.169
12	0.919	0.802	1.026	0.449	0.356	-0.893
13	0.929	0.862	1.012	0.239	0.195	-0.776
14	1.729	0.966	(-0.001)	0	-0.102	-1.400
15	1.304	1.010	0.514	-0.078	-0.166	-0.993
16	1.149	1.023	0.712	-0.077	-0.175	-0.777
17	0.966	1.189	0.967	-0.968	-0.770	-0.878
18	0.915	1.113	1.027	-0.396	-0.518	-0.541
19	0.926	1.075	1.026	-0.213	-0.386	-0.386
20	(-0.001)	1.260	2.008	0	-1.032	0
21	0.607	1.137	1.395	0	-0.615	0
22	0.795	1.085	1.204	0	-0.423	0

Brackets indicate the exact value is zero.

$\tau_{r\theta} = \tau_{\theta z} = u_\theta = 0$

TABLE A 6.5.1 TOTAL STRESSES AND INDUCED DISPLACEMENTS ASSOCIATED WITH A COMPLETE CIRCULAR TORIC TUNNEL IN A HOMOGENEOUS ISOTROPIC LINEAR ELASTIC INFINITE MASS WITH UNIFORM FIELD STRESS (Fig. A 6.5.1)

E/p = 1 $p_r/p = 1$ $p_z/p = 0$ c/a = 3 v = 0.49

N	σ_r/p	σ_θ/p	σ_z/p	τ_{zr}/p	Eu_r/ap	Eu_z/ap
1	0.379	0.379	0.051	0	0	0
2	0.462	0.462	-0.007	0	0	-0.306
3	0.654	0.654	-0.131	0	0	-0.491
4	0.851	0.851	-0.224	0	0	-0.519
5	0.988	0.988	-0.246	0	0	-0.435
6	1.058	1.058	-0.211	0	0	-0.305
7	1.081	1.081	-0.155	0	0	-0.178
8	0	0.284	0.886	0	0.721	0
9	0.076	0.108	-0.117	0	0.573	0
10	0.254	0.280	0.015	0	0.362	0
11	0.249	0.572	0.282	0.267	0.454	-0.107
12	0.936	0.839	-0.248	0.124	0.016	-0.360
13	1.006	0.940	-0.269	0.027	-0.110	-0.397
14	2.577	1.879	(-0.001)	0	-0.319	-0.026
15	1.330	1.406	0.299	-0.081	-0.294	0.183
16	1.112	1.236	0.213	-0.067	-0.230	0.178
17	0.473	1.292	0.499	-0.489	-1.134	0.032
18	1.051	1.129	-0.085	-0.193	-0.590	-0.120
19	1.066	1.075	-0.096	-0.108	-0.396	-0.122
20	0	0.480	-0.811	0	-1.469	0
21	0.251	0.866	-0.043	0	-1.146	0
22	0.534	0.959	0.028	0	-0.867	0

Brackets indicate the exact value is zero.

$\tau_{r\theta} = \tau_{\theta z} = u_\theta = 0$

E/p = 1 $p_r/p = 0$ $p_z/p = 1$ c/a = 3 v = 0.49

N	σ_r/p	σ_θ/p	σ_z/p	τ_{zr}/p	Eu_r/ap	Eu_z/ap
1	0.315	0.315	1.266	0	0	0
2	0.252	0.252	1.287	0	0	0.007
3	0.109	0.109	1.315	0	0	-0.055
4	-0.024	-0.024	1.295	0	0	-0.191
5	-0.099	-0.099	1.221	0	0	-0.355
6	-0.120	-0.120	1.123	0	0	-0.497
7	-0.110	-0.110	1.035	0	0	-0.593
8	(-0.001)	0.899	3.198	0	0.356	0
9	0.407	0.540	1.733	0	0.029	0
10	0.370	0.395	1.400	0	-0.018	0
11	0.635	0.031	0.596	0.620	0.188	-1.192
12	-0.063	-0.090	1.218	0.299	0.321	-0.667
13	-0.115	-0.118	1.230	0.198	0.276	-0.519
14	-0.941	-0.972	0	0	0.062	-1.559
15	-0.073	-0.422	0.200	-0.008	-0.017	-1.324
16	-0.005	-0.227	0.482	-0.025	-0.072	-1.081
17	0.492	-0.048	0.461	-0.479	0.094	-1.039
18	-0.155	0.016	1.126	-0.200	-0.123	-0.486
19	-0.157	0.021	1.134	-0.102	-0.141	-0.306
20	(-0.001)	0.887	2.875	0	0.125	0
21	0.365	0.326	1.455	0	0.340	0
22	0.268	0.159	1.183	0	0.308	0

Brackets indicate the exact value is zero.

$\tau_{r\theta} = \tau_{\theta z} = u_\theta = 0$

E/p = 1 $p_r/p = 1$ $p_z/p = 1$ c/a = 3 v = 0.49

N	σ_r/p	σ_θ/p	σ_z/p	τ_{zr}/p	Eu_r/ap	Eu_z/ap
1	0.695	0.695	1.318	0	0	0
2	0.713	0.713	1.280	0	0	-0.299
3	0.763	0.763	1.185	0	0	-0.546
4	0.827	0.827	1.071	0	0	-0.711
5	0.889	0.889	0.975	0	0	-0.790
6	0.938	0.938	0.912	0	0	-0.802
7	0.971	0.971	0.880	0	0	-0.771
8	(-0.001)	0.614	2.312	0	1.076	0
9	0.483	0.647	1.616	0	0.601	0
10	0.624	0.675	1.415	0	0.344	0
11	0.885	0.604	0.878	0.887	0.643	-1.299
12	0.873	0.749	0.969	0.423	0.337	-1.027
13	0.891	0.823	0.960	0.225	0.166	-0.915
14	1.636	0.907	(-0.001)	0	-0.257	-1.585
15	1.257	0.984	0.499	-0.092	-0.310	-1.141
16	1.117	1.009	0.696	-0.092	-0.302	-0.904
17	0.965	1.244	0.961	-0.969	-1.040	-1.007
18	0.896	1.145	1.041	-0.393	-0.713	-0.606
19	0.909	1.096	1.038	-0.211	-0.537	-0.428
20	(-0.001)	1.367	2.064	0	-1.344	0
21	0.616	1.193	1.411	0	-0.806	0
22	0.802	1.118	1.212	0	-0.559	0

Brackets indicate the exact value is zero.

$\tau_{r\theta} = \tau_{\theta z} = u_\theta = 0$

TABLE A 6.5.1 TOTAL STRESSES AND INDUCED DISPLACEMENTS ASSOCIATED WITH A COMPLETE CIRCULAR TORIC TUNNEL IN A HOMOGENEOUS ISOTROPIC LINEAR ELASTIC INFINITE MASS WITH UNIFORM FIELD STRESS (Fig. A 6.5.1)

$E/p = 1$ $p_r/p = 1$ $p_z/p = 0$ $c/a = 10$ $\nu = 0$

N	σ_r/p	σ_θ/p	σ_z/p	τ_{zr}/p	Eu_r/ap	Eu_z/ap
1	0.939	0.939	0.030	0	0	0
2	0.940	0.940	0.029	0	0	-0.015
3	0.943	0.943	0.026	0	0	-0.029
4	0.947	0.947	0.022	0	0	-0.041
5	0.952	0.952	0.016	0	0	-0.050
6	0.958	0.958	0.009	0	0	-0.056
7	0.965	0.965	0.003	0	0	-0.059
8	(-0.003)	0.781	-1.003	0	1.972	0
9	0.168	0.825	-0.037	0	1.484	0
10	0.449	0.857	0.070	0	1.144	0
11	0.513	0.856	0.516	0.541	1.336	0.697
12	1.164	0.919	-0.140	0.236	0.724	0.322
13	1.162	0.944	-0.157	0.133	0.479	0.198
14	2.903	1.008	(-0.003)	0	-0.083	0.953
15	1.476	1.008	0.360	0.012	-0.076	0.810
16	1.187	1.008	0.274	0.009	-0.076	0.650
17	0.421	1.128	0.424	-0.447	-1.370	0.656
18	1.053	1.072	-0.134	-0.196	-0.795	0.318
19	1.102	1.050	-0.138	-0.108	-0.566	0.207
20	(-0.003)	1.170	-0.920	0	-1.870	0
21	0.260	1.122	-0.081	0	-1.400	0
22	0.484	1.090	0.016	0	-1.080	0

Brackets indicate the exact value is zero.

$\tau_{r\theta} = \tau_{\theta z} = u_\theta = 0$

$E/p = 1$ $p_r/p = 0$ $p_z/p = 1$ $c/a = 10$ $\nu = 0$

N	σ_r/p	σ_θ/p	σ_z/p	τ_{zr}/p	Eu_r/ap	Eu_z/ap
1	0.034	0.034	1.009	0	0	0
2	0.033	0.033	1.010	0	0	-0.005
3	0.031	0.031	1.011	0	0	-0.010
4	0.028	0.028	1.014	0	0	-0.016
5	0.025	0.025	1.017	0	0	-0.024
6	0.020	0.020	1.020	0	0	-0.033
7	0.016	0.016	1.023	0	0	-0.044
8	(-0.003)	0.107	3.082	0	-0.959	0
9	0.378	0.095	1.540	0	-0.808	0
10	0.290	0.080	1.228	0	-0.639	0
11	0.450	0.068	0.446	0.474	-0.633	-1.451
12	-0.156	0.029	1.156	0.222	-0.263	-0.843
13	-0.158	0.016	1.168	0.128	-0.141	-0.604
14	-0.951	-0.008	(-0.003)	0	0.084	-1.984
15	-0.050	-0.006	0.191	-0.024	0.060	-1.504
16	0.048	-0.005	0.473	-0.021	0.051	-0.175
17	0.514	-0.067	0.512	0.538	0.712	-1.355
18	-0.106	-0.032	1.138	-0.228	0.359	-0.771
19	-0.124	-0.021	1.143	-0.127	0.240	-0.541
20	(-0.003)	-0.086	2.889	0	0.948	0
21	0.360	-0.070	1.495	0	0.804	0
22	0.276	-0.054	1.210	0	0.644	0

Brackets indicate the exact value is zero.

$\tau_{r\theta} = \tau_{\theta z} = u_\theta = 0$

$E/p = 1$ $p_r/p = 1$ $p_z/p = 1$ $c/a = 10$ $\nu = 0$

N	σ_r/p	σ_θ/p	σ_z/p	τ_{zr}/p	Eu_r/ap	Eu_z/ap
1	0.973	0.973	1.039	0	0	0
2	0.974	0.974	1.038	0	0	-0.019
3	0.974	0.974	1.037	0	0	-0.038
4	0.975	0.975	1.035	0	0	-0.057
5	0.977	0.977	1.033	0	0	-0.074
6	0.979	0.979	1.029	0	0	-0.089
7	0.981	0.981	1.026	0	0	-0.103
8	(-0.006)	0.887	2.078	0	1.013	0
9	0.547	0.920	1.503	0	0.677	0
10	0.739	0.937	1.298	0	0.505	0
11	0.963	0.924	0.961	1.015	0.702	-0.754
12	1.008	0.948	1.016	0.458	0.461	-0.521
13	1.004	0.961	1.011	0.262	0.337	-0.406
14	1.952	1.000	(-0.006)	0	0.001	-1.030
15	1.425	1.002	0.550	-0.012	-0.016	-0.694
16	1.236	1.002	0.747	-0.012	-0.025	-0.525
17	0.935	1.061	0.936	-0.985	-0.658	-0.699
18	0.976	1.039	1.004	-0.424	-0.436	-0.453
19	0.978	1.029	1.005	-0.235	-0.326	-0.334
20	(-0.005)	1.084	1.968	0	-0.925	0
21	0.566	1.052	1.415	0	-0.595	0
22	0.760	1.036	1.226	0	-0.433	0

Brackets indicate the exact value is zero.

$\tau_{r\theta} = \tau_{\theta z} = u_\theta = 0$

TABLE A 6.5.1 TOTAL STRESSES AND INDUCED DISPLACEMENTS ASSOCIATED WITH A COMPLETE CIRCULAR TORIC TUNNEL IN A HOMOGENEOUS ISOTROPIC LINEAR ELASTIC INFINITE MASS WITH UNIFORM FIELD STRESS (Fig. A 6.5.1)

$E/p = 1$ $p_r/p = 1$ $p_z/p = 0$ $c/a = 10$ $\nu = 0.25$

N	σ_r/p	σ_θ/p	σ_z/p	τ_{zr}/p	Eu_r/ap	Eu_z/ap
1	0.932	0.932	0.022	0	0	0
2	0.933	0.933	0.021	0	0	-0.028
3	0.936	0.936	0.018	0	0	-0.054
4	0.940	0.940	0.014	0	0	-0.078
5	0.946	0.946	0.008	0	0	-0.098
6	0.953	0.953	0.002	0	0	-0.113
7	0.960	0.960	0.004	0	0	-0.124
8	0	0.303	-1.006	0	1.755	0
9	0.166	0.614	-0.061	0	1.378	0
10	0.441	0.739	0.050	0	1.073	0
11	0.497	0.871	0.497	0.501	1.188	0.414
12	1.139	0.930	-0.157	0.224	0.584	0.093
13	1.146	0.953	-0.169	0.125	0.358	0.011
14	2.910	1.489	(-0.001)	0	-0.118	0.591
15	1.599	1.252	0.363	-0.004	-0.118	0.627
16	1.188	1.127	0.272	-0.004	-0.114	0.510
17	0.471	1.112	0.472	-0.475	-1.345	0.420
18	1.101	1.061	-0.128	-0.206	-0.756	0.131
19	1.114	1.042	-0.134	-0.114	-0.534	0.061
20	0	0.686	-0.923	0	-1.833	0
21	0.205	0.908	-0.070	0	-1.424	0
22	0.486	0.970	0.024	0	-1.110	0

Brackets indicate the exact value is zero.

$\tau_{r\theta} = \tau_{\theta z} = u_\theta = 0$

$E/p = 1$ $p_r/p = 0$ $p_z/p = 1$ $c/a = 10$ $\nu = 0.25$

N	σ_r/p	σ_θ/p	σ_z/p	τ_{zr}/p	Eu_r/ap	Eu_z/ap
1	0.038	0.038	1.014	0	0	0
2	0.037	0.037	1.015	0	0	0.002
3	0.035	0.035	1.016	0	0	0.004
4	0.032	0.032	1.019	0	0	0.003
5	0.027	0.027	1.021	0	0	0.001
6	0.023	0.023	1.024	0	0	-0.005
7	0.017	0.017	1.027	0	0	-0.012
8	(-0.001)	0.576	3.075	0	-0.517	0
9	0.378	0.298	1.554	0	-0.555	0
10	0.293	0.191	1.241	0	-0.461	0
11	0.502	0.036	0.499	0.505	-0.335	-1.352
12	-0.138	0.009	1.163	0.233	-0.029	-0.745
13	-0.147	0.001	1.172	0.136	0.043	-0.522
14	-0.958	-0.499	0	0	0.089	-1.867
15	-0.055	-0.223	0.191	-0.011	0.068	-1.473
16	0.044	-0.126	0.474	-0.011	0.056	-1.164
17	0.508	-0.041	0.509	-0.512	0.490	-1.291
18	-0.128	-0.015	1.135	-0.221	0.182	-0.694
19	-0.138	-0.008	1.142	-0.121	0.103	-0.474
20	(-0.001)	0.419	2.914	0	0.648	0
21	0.364	0.156	1.491	0	0.659	0
22	0.276	0.075	1.205	0	0.550	0

Brackets indicate the exact value is zero.

$\tau_{r\theta} = \tau_{\theta z} = u_\theta = 0$

$E/p = 1$ $p_r/p = 1$ $p_z/p = 1$ $c/a = 10$ $\nu = 0.25$

N	σ_r/p	σ_θ/p	σ_z/p	τ_{zr}/p	Eu_r/ap	Eu_z/ap
1	0.970	0.970	1.036	0	0	0
2	0.970	0.970	1.036	0	0	-0.031
3	0.971	0.971	1.035	0	0	-0.056
4	0.972	0.972	1.033	0	0	-0.075
5	0.974	0.974	1.030	0	0	-0.097
6	0.975	0.975	1.027	0	0	-0.118
7	0.978	0.978	1.023	0	0	-0.136
8	(-0.001)	0.879	2.069	0	1.238	0
9	0.544	0.912	1.493	0	0.823	0
10	0.734	0.930	1.291	0	0.612	0
11	0.999	0.907	0.997	1.005	0.853	-0.938
12	1.000	0.940	1.006	0.457	0.555	-0.652
13	0.999	0.954	1.004	0.261	0.401	-0.511
14	1.952	0.991	(-0.001)	0	-0.029	-1.277
15	1.421	0.998	0.550	-0.015	-0.049	-0.863
16	1.232	1.000	0.746	-0.015	-0.057	-0.654
17	0.979	1.070	0.981	-0.981	-0.856	-0.872
18	0.973	1.043	1.007	-0.427	-0.573	-0.563
19	0.976	1.034	1.008	-0.236	-0.431	-0.413
20	(-0.001)	1.105	1.991	0	-1.185	0
21	0.569	1.064	1.421	0	-0.766	0
22	0.762	1.045	1.229	0	-0.560	0

Brackets indicate the exact value is zero.

$\tau_{r\theta} = \tau_{\theta z} = u_\theta = 0$

TABLE A 6.5.1 TOTAL STRESSES AND INDUCED DISPLACEMENTS ASSOCIATED WITH A COMPLETE CIRCULAR TORIC TUNNEL IN A HOMOGENEOUS ISOTROPIC LINEAR ELASTIC INFINITE MASS WITH UNIFORM FIELD STRESS (Fig. A 6.5.1)

$E/p = 1$ $p_r/p = 1$ $p_z/p = 0$ $c/a = 10$ $\nu = 0.49$

N	σ_r/p	σ_θ/p	σ_z/p	τ_{zr}/p	Eu_r/ap	Eu_z/ap
1	0.925	0.925	0.015	0	0	0
2	0.926	0.926	0.014	0	0	-0.044
3	0.929	0.929	0.011	0	0	-0.085
4	0.934	0.934	0.007	0	0	-0.123
5	0.941	0.941	0.002	0	0	-0.156
6	0.948	0.948	-0.004	0	0	-0.183
7	0.956	0.956	-0.010	0	0	-0.203
8	0	-0.131	-1.013	0	1.300	0
9	0.163	0.419	-0.083	0	1.105	0
10	0.435	-0.629	0.031	0	0.875	0
11	0.442	0.868	0.478	0.463	0.862	-0.012
12	1.115	0.936	-0.170	0.212	0.328	-0.234
13	1.131	0.959	-0.179	0.117	0.152	-0.252
14	2.911	1.953	(-0.001)	0	-0.173	0.012
15	1.476	1.425	0.357	-0.020	-0.171	0.265
16	1.189	1.241	0.270	-0.017	-0.160	0.259
17	0.482	1.109	0.516	-0.502	-1.179	0.026
18	1.119	1.055	-0.121	-0.215	-0.625	-0.156
19	1.125	1.036	-0.130	-0.120	-0.437	-0.158
20	0	0.199	-0.929	0	-1.588	0
21	0.205	-0.696	-0.059	0	-1.317	0
22	0.488	0.852	0.032	0	-1.048	0

Brackets indicate the exact value is zero.

$\tau_{r\theta} = \tau_{\theta z} = u_\theta = 0$

$E/p = 1$ $p_r/p = 0$ $p_z/p = 1$ $c/a = 10$ $\nu = 0.49$

N	σ_r/p	σ_θ/p	σ_z/p	τ_{zr}/p	Eu_r/ap	Eu_z/ap
1	0.038	0.038	1.017	0	0	0
2	0.037	0.037	1.017	0	0	0.010
3	0.035	0.035	1.018	0	0	0.019
4	0.031	0.031	1.021	0	0	0.025
5	0.027	0.027	1.023	0	0	0.029
6	0.022	0.022	1.026	0	0	0.028
7	0.016	0.016	1.028	0	0	0.024
8	(-0.001)	0.990	3.047	0	0.110	0
9	0.373	0.476	1.557	0	-0.176	0
10	0.291	0.286	1.245	0	-0.189	0
11	0.541	0.013	0.504	0.526	0.088	-1.095
12	-0.124	-0.012	1.162	0.239	0.276	-0.544
13	-0.139	-0.017	1.171	0.141	0.275	-0.363
14	-0.975	-0.975	0	0	0.071	-1.521
15	-0.063	-0.433	0.190	-0.001	0.049	-1.287
16	-0.037	-0.243	0.473	-0.004	0.033	-1.037
17	0.504	-0.022	0.469	-0.490	0.093	-1.057
18	-0.148	0.005	1.137	-0.213	-0.115	-0.505
19	-0.153	0.007	1.146	-0.115	-0.127	-0.324
20	(-0.001)	0.944	2.947	0	0.110	0
21	0.369	0.390	1.491	0	0.356	0
22	0.278	0.207	1.203	0	0.340	0

Brackets indicate the exact value is zero.

$\tau_{r\theta} = \tau_{\theta z} = u_\theta = 0$

$E/p = 1$ $p_r/p = 1$ $p_z/p = 1$ $c/a = 10$ $\nu = 0.49$

N	σ_r/p	σ_θ/p	σ_z/p	τ_{zr}/p	Eu_r/ap	Eu_z/ap
1	0.963	0.963	1.031	0	0	0
2	0.963	0.963	1.031	0	0	-0.034
3	0.964	0.964	1.029	0	0	-0.073
4	0.966	0.966	1.027	0	0	-0.098
5	0.967	0.967	1.025	0	0	-0.127
6	0.970	0.970	1.021	0	0	-0.154
7	0.972	0.972	1.018	0	0	-0.179
8	(-0.001)	0.880	2.034	0	1.409	0
9	0.536	0.896	1.473	0	0.929	0
10	0.725	0.915	1.276	0	0.686	0
11	0.983	0.881	0.982	0.989	0.950	-1.108
12	0.990	0.924	0.992	0.452	0.604	-0.778
13	0.992	0.942	0.991	0.259	0.427	-0.615
14	1.935	0.978	(-0.001)	0	-0.102	-1.509
15	1.412	0.992	0.547	-0.020	-0.122	-1.023
16	1.225	0.997	0.742	-0.021	-0.127	-0.778
17	0.986	1.088	0.985	-0.992	-1.086	-1.037
18	0.970	1.060	1.016	-0.428	-0.740	-0.661
19	0.972	1.043	1.015	-0.236	-0.564	-0.482
20	(-0.001)	1.143	2.018	0	-1.478	0
21	0.574	1.086	1.431	0	-0.962	0
22	0.766	1.059	1.235	0	-0.708	0

Brackets indicate the exact value is zero.

$\tau_{r\theta} = \tau_{\theta z} = u_\theta = 0$

TABLE A 6.5.2 TOTAL STRESSES AND INDUCED DISPLACEMENTS ASSOCIATED WITH TWO IDENTICAL SPHERICAL CAVITIES IN A HOMOGENEOUS ISOTROPIC LINEAR ELASTIC INFINITE MASS WITH UNIFORM FIELD STRESS (Fig. A 6.5.2)

$E/p = 1$ $p_r/p = 1$ $p_z/p = 0$ $d/a = 1\frac{1}{8}$ $\nu = 0$

N	σ_r/p	σ_θ/p	σ_z/p	τ_{zr}/p	Eu_r/ap	Eu_z/ap
1	1.795	1.795	0.218	0	0	0
2	1.206	1.542	0.279	0	-0.271	0
3	0.974	1.297	0.007	0	-0.297	0
4	0.919	1.179	-0.074	0	-0.268	0
5	0.906	1.111	0.046	0	-0.223	0
6	0.919	1.071	-0.021	0	-0.178	0
7	0.936	1.047	-0.009	0	-0.142	0
8	1.999	1.999	0	0	0	-0.019
9						
10						
11	0.426	1.762	0.428	0.419	-0.539	-0.104
12	0.959	1.280	-0.017	0.028	-0.297	0.001
13	0.872	1.210	-0.065	-0.073	-0.297	-0.021
14	(0.001)	1.728	-0.359	0	-0.728	0.673
15	0.579	1.260	-0.005	-0.015	-0.390	0.465
16	0.806	1.123	0.004	0	-0.245	0.259
17	0.335	1.721	0.342	-0.330	-0.510	0.341
18	0.969	1.163	-0.006	-0.052	-0.173	0.151
19	1.013	1.062	-0.015	-0.013	-0.088	0.089
20	1.722	1.722	(0.012)	0	0	0.463
21	1.075	1.075	0.289	0	0	0.327
22	1.011	1.011	0.168	0	0	0.215

Brackets indicate the exact value is zero.

$\tau_{r\theta} = \tau_{\theta z} = u_\theta = 0$

$E/p = 1$ $p_r/p = 0$ $p_z/p = 1$ $d/a = 1\frac{1}{8}$ $\nu = 0$

N	σ_r/p	σ_θ/p	σ_z/p	τ_{zr}/p	Eu_r/ap	Eu_z/ap
1	0.088	0.088	0.011	0	0	0
2	0.077	0.084	0.073	0	-0.042	0
3	-0.086	0.039	0.579	0	-0.039	0
4	-0.079	-0.006	1.042	0	0.009	0
5	-0.028	-0.017	1.061	0	0.034	0
6	-0.001	-0.016	1.042	0	0.041	0
7	0.007	-0.013	1.026	0	0.039	0
8	0.102	0.102	0	0	0	0.013
9						
10						
11	0.177	-0.036	0.173	0.168	0.026	0.295
12	-0.094	0.031	0.824	0.015	-0.032	0.014
13	-0.068	-0.011	1.039	0.013	0.015	0.083
14	(0.001)	-0.168	1.795	0	0.017	-0.096
15	0.115	-0.074	1.117	-0.043	0.011	-0.087
16	0.056	-0.035	1.041	-0.028	0.069	-0.060
17	0.430	-0.195	0.437	-0.427	0.014	-0.699
18	-0.033	-0.033	0.925	-0.172	0.029	-0.319
19	-0.037	0.008	0.977	-0.084	-0.012	-0.190
20	-0.197	-0.197	(0.010)	0	0	-0.960
21	0.081	0.081	0.420	0	0	-0.551
22	0.056	0.056	0.709	0	0	-0.343

Brackets indicate the exact value is zero.

$\tau_{r\theta} = \tau_{\theta z} = u_\theta = 0$

$E/p = 1$ $p_r/p = 1$ $p_z/p = 1$ $d/a = 1\frac{1}{8}$ $\nu = 0$

N	σ_r/p	σ_θ/p	σ_z/p	τ_{zr}/p	Eu_r/ap	Eu_z/ap
1	1.884	1.884	0.229	0	0	0
2	1.283	1.625	0.352	0	-0.313	0
3	0.888	1.335	0.765	0	-0.335	0
4	0.839	1.173	0.968	0	-0.259	0
5	0.879	1.094	1.015	0	-0.188	0
6	0.917	1.055	1.021	0	-0.137	0
7	0.944	1.034	1.017	0	-0.103	0
8	2.101	2.101	0	0	0	0.105
9						
10						
11	0.603	1.725	0.601	0.589	-0.513	0.192
12	0.865	1.311	0.807	0.043	-0.330	0.013
13	0.804	1.199	0.974	-0.060	-0.282	-0.012
14	(0.001)	1.559	1.436	0	-0.559	-0.029
15	0.694	1.186	1.112	-0.034	-0.279	-0.041
16	0.861	1.088	1.045	-0.029	-0.176	-0.034
17	0.764	1.526	0.779	-0.757	-0.372	-0.358
18	0.936	1.161	0.919	-0.224	-0.170	-0.169
19	0.976	1.070	0.961	-0.096	-0.100	-0.101
20	1.524	1.524	(0.022)	0	0	-0.498
21	1.156	1.156	0.709	0	0	-0.224
22	1.067	1.067	0.877	0	0	-0.129

Brackets indicate the exact value is zero.

$\tau_{r\theta} = \tau_{\theta z} = u_\theta = 0$

TABLE A 6.5.2 TOTAL STRESSES AND INDUCED DISPLACEMENTS ASSOCIATED WITH TWO IDENTICAL SPHERICAL CAVITIES IN A HOMOGENEOUS ISOTROPIC LINEAR ELASTIC INFINITE MASS WITH UNIFORM FIELD STRESS (Fig. A 6.5.2)

E/p = 1 $p_r/p = 1$ $p_z/p = 0$ d/a = 1 1/8 $\nu = 0.25$

N	σ_r/p	σ_θ/p	σ_z/p	τ_{zr}/p	Eu_r/ap	Eu_z/ap
1	2.268	2.268	0.276	0	0	0
2	1.457	1.778	0.339	0	-0.289	0
3	1.082	1.333	0.008	0	-0.311	0
4	0.961	1.165	-0.090	0	-0.296	0
5	0.918	1.094	-0.056	0	-0.257	0
6	0.920	1.058	-0.026	0	-0.211	0
7	0.934	1.038	-0.011	0	-0.171	0
8	2.553	2.553	0	0	0	0.061
9						
10						
11	0.502	1.884	0.510	0.511	-0.623	-0.056
12	1.056	1.305	-0.021	0.034	-0.314	0.007
13	0.913	1.192	-0.080	-0.089	-0.331	-0.035
14	(-0.001)	1.476	-0.440	0	-0.836	0.070
15	0.556	1.196	-0.007	0.012	-0.462	0.044
16	0.795	1.096	0.004	-0.001	-0.292	0.019
17	0.402	1.776	0.398	-0.403	-0.584	0.309
18	1.030	1.171	-0.006	-0.062	-0.175	0.129
19	1.045	1.065	-0.019	-0.015	-0.082	0.076
20	2.096	2.096	(-0.003)	0	0	0.414
21	1.158	1.158	0.352	0	0	0.364
22	1.043	1.043	0.206	0	0	0.248

Brackets indicate the exact value is zero.

$\tau_{r\theta} = \tau_{\theta z} = u_\theta = 0$

E/p = 1 $p_r/p = 0$ $p_z/p = 1$ d/a = 1 1/8 $\nu = 0.25$

N	σ_r/p	σ_θ/p	σ_z/p	τ_{zr}/p	Eu_r/ap	Eu_z/ap
1	-0.188	-0.188	-0.024	0	0	0
2	-0.096	-0.118	0.019	0	-0.075	0
3	-0.175	-0.011	0.754	0	-0.094	0
4	-0.118	-0.001	1.056	0	-0.024	0
5	-0.040	-0.040	1.070	0	0.024	0
6	-0.004	-0.005	1.046	0	0.040	0
7	0.009	-0.005	1.028	0	0.042	0
8	-0.211	-0.211	0	0	0	0.115
9						
10						
11	0.079	-0.215	0.081	0.085	0.003	0.297
12	-0.176	-0.007	0.825	0.010	-0.085	0.084
13	-0.106	-0.003	0.052	0.027	-0.016	0.021
14	(-0.001)	0.078	1.869	0	0.139	-0.116
15	0.136	-0.013	1.118	-0.047	0.115	-0.100
16	0.065	-0.010	1.041	-0.029	0.073	-0.065
17	0.356	-0.240	0.354	-0.359	0.119	-0.764
18	-0.090	-0.007	0.927	-0.161	-0.036	-0.343
19	-0.067	0.007	0.980	-0.081	-0.041	-0.204
20	-0.565	-0.565	(-0.002)	0	0	-1.047
21	0.003	0.003	0.359	0	0	-0.647
22	0.027	0.027	0.674	0	0	-0.410

Brackets indicate the exact value is zero.

$\tau_{r\theta} = \tau_{\theta z} = u_\theta = 0$

E/p = 1 $p_r/p = 1$ $p_z/p = 1$ d/a = 1 1/8 $\nu = 0.25$

N	σ_r/p	σ_θ/p	σ_z/p	τ_{zr}/p	Eu_r/ap	Eu_z/ap
1	2.080	2.080	0.252	0	0	0
2	1.361	1.660	0.358	0	-0.365	0
3	0.907	1.322	0.763	0	-0.404	0
4	0.843	1.165	0.965	0	-0.318	0
5	0.879	1.090	1.014	0	-0.233	0
6	0.916	1.053	1.020	0	-0.172	0
7	0.943	1.033	1.017	0	-0.129	0
8	2.342	2.342	0	0	0	0.176
9						
10						
11	0.581	1.669	0.592	0.596	-0.619	0.241
12	0.881	1.297	0.804	0.044	-0.399	0.016
13	0.807	1.190	0.971	-0.062	-0.347	-0.014
14	(-0.001)	1.554	1.429	0	-0.697	-0.046
15	0.692	1.183	1.111	-0.035	-0.348	-0.056
16	0.860	1.086	1.045	-0.030	-0.219	-0.046
17	0.758	1.536	0.752	-0.762	-0.466	-0.455
18	0.940	1.164	0.920	-0.223	-0.211	-0.214
19	0.978	1.072	0.961	-0.096	-0.123	-0.128
20	1.531	1.531	(-0.005)	0	0	-0.632
21	1.161	1.161	0.711	0	0	-0.283
22	1.069	1.069	0.879	0	0	-0.162

Brackets indicate the exact value is zero.

$\tau_{r\theta} = \tau_{\theta z} = u_\theta = 0$

TABLE A 6.5.2 TOTAL STRESSES AND INDUCED DISPLACEMENTS ASSOCIATED WITH TWO IDENTICAL SPHERICAL CAVITIES IN A HOMOGENEOUS ISOTROPIC LINEAR ELASTIC INFINITE MASS WITH UNIFORM FIELD STRESS (Fig. A 6.5.2)

E/p = 1 p_r/p= 1 p_z/p = 0 d/a = 1 1/8 ν = 0.49

N	σ_r/p	σ_θ/p	σ_z/p	τ_{zr}/p	Eu_r/ap	Eu_z/ap
1	3.089	3.089	0.383	0	0	0
2	1.906	2.143	0.485	0	-0.231	0
3	1.254	1.375	-0.027	0	-0.264	0
4	1.012	1.140	-0.125	0	-0.293	0
5	0.928	1.067	0.073	0	-0.277	0
6	0.917	0.038	-0.033	0	-0.238	0
7	0.928	1.024	-0.014	0	-0.198	0
8	3.497	3.497	(0.059)	0	0	0.238
9						
10						
11	1.009	2.279	0.725	0.668	-0.650	0.069
12	1.205	1.329	-0.060	0.048	-0.274	0.021
13	0.959	1.159	-0.112	-0.115	-0.331	-0.060
14	(-0.001)	1.100	-0.563	0.016	-0.866	0.067
15	0.523	1.100	-0.012	0.012	-0.509	0.027
16	0.780	1.057	0.003	-0.004	-0.327	-0.002
17	0.201	1.647	0.361	-0.502	-0.609	0.171
18	1.121	1.199	0.009	-0.063	-0.144	0.063
19	1.091	1.078	-0.017	-0.011	-0.059	0.036
20	2.634	2.634	(0.121)	0	0	0.222
21	1.274	1.274	0.427	0	0	0.350
22	1.089	1.089	0.254	0	0	0.260

Brackets indicate the exact value is zero.

$\tau_{r\theta} = \tau_{\theta z} = u_\theta = 0$

E/p = 1 p_r/p = 0 p_z/p = 1 d/a = 1 1/8 ν = 0.49

N	σ_r/p	σ_θ/p	σ_z/p	τ_{zr}/p	Eu_r/ap	Eu_z/ap
1	-0.651	-0.651	0.083	0	0	0
2	-0.368	-0.417	-0.055	0	-0.140	0
3	-0.311	-0.080	0.745	0	-0.197	0
4	-0.176	0.009	1.076	0	-0.868	0
5	-0.058	0.015	1.083	0	-0.006	0
6	-0.007	0.011	1.052	0	0.028	0
7	0.011	0.008	1.031	0	0.038	0
8	-0.750	-0.750	(0.005)	0	0	0.048
9						
10						
11	-0.016	-0.437	-0.031	-0.037	-0.053	0.229
12	-0.299	-0.059	0.823	0.003	-0.185	0.000
13	-0.163	0.012	1.070	0.049	-0.082	0.044
14	0	0.440	1.980	0.001	0.040	-0.128
15	0.167	0.077	1.119	-0.052	0.095	-0.102
16	0.079	0.026	1.039	-0.030	0.063	-0.059
17	0.240	-0.316	0.249	-0.257	0.047	-0.716
18	-0.174	-0.012	0.931	-0.144	0.113	-0.310
19	-0.112	0.006	0.986	-0.076	0.097	-0.183
20	-1.108	-1.108	(0.011)	0	0	-0.974
21	-0.115	-0.115	0.269	0	0	-0.698
22	-0.017	-0.017	0.621	0	0	-0.456

Brackets indicate the exact value is zero.

$\tau_{r\theta} = \tau_{\theta z} = u_\theta = 0$

E/p = 1 p_r/p = 1 p_z/p = 1 d/a = 1 1/8 ν = 0.49

N	σ_r/p	σ_θ/p	σ_z/p	τ_{zr}/p	Eu_r/p	Eu_z/p
1	2.438	2.438	0.300	0	0	0
2	1.538	1.725	0.430	0	-0.370	0
3	0.943	1.295	0.719	0	-0.460	0
4	0.836	1.149	0.951	0	-0.380	0
5	0.870	1.083	1.010	0	-0.283	0
6	0.910	1.050	1.019	0	-0.210	0
7	0.939	1.032	1.017	0	-0.160	0
8	2.747	2.747	(0.064)	0	0	0.286
9						
10						
11	0.993	1.842	0.695	0.631	-0.704	0.298
12	0.905	1.270	0.763	0.051	-0.459	0.021
13	0.796	1.171	0.958	-0.067	-0.413	-0.016
14	(-0.001)	1.540	1.418	0.017	-0.826	-0.061
15	0.691	1.177	1.107	-0.040	-0.414	-0.075
16	0.859	1.083	1.042	-0.034	-0.263	-0.061
17	0.441	1.331	0.611	-0.759	-0.562	-0.545
18	0.947	1.187	0.939	-0.206	-0.258	-0.246
19	0.979	1.085	0.968	-0.087	-0.156	-0.147
20	1.525	1.525	(0.131)	0	0	-0.752
21	1.159	1.159	0.695	0	0	-0.348
22	1.072	1.072	0.876	0	0	-0.196

Brackets indicate the exact value is zero.

$\tau_{r\theta} = \tau_{\theta z} = u_\theta = 0$

TABLE A 6.5.2 TOTAL STRESSES AND INDUCED DISPLACEMENTS ASSOCIATED WITH TWO IDENTICAL SPHERICAL CAVITIES IN A HOMOGENEOUS ISOTROPIC LINEAR ELASTIC INFINITE MASS WITH UNIFORM FIELD STRESS (Fig. A 6.5.2)

$E/p = 1$ $p_r/p = 1$ $p_z/p = 0$ $d/a = 1\frac{1}{2}$ $\nu = 0$

N	σ_r/p	σ_θ/p	σ_z/p	τ_{zr}/p	Eu_r/ap	Eu_z/ap
1	1.438	1.438	0.352	0	0	0
2	1.192	1.336	0.304	0	-0.168	0
3	1.038	1.218	0.240	0	-0.218	0
4	0.968	1.145	-0.065	0	-0.218	0
5	0.938	1.096	-0.047	0	-0.192	0
6	0.937	1.064	-0.024	0	-0.160	0
7	0.946	1.044	-0.011	0	-0.131	0
8	1.749	1.749	(0.002)	0	0	-0.061
9						
10						
11	0.429	1.719	0.429	0.418	-0.508	-0.129
12	0.996	1.224	0.001	0.064	-0.238	0
13	0.963	1.161	-0.061	-0.040	-0.227	-0.010
14	(0.001)	1.719	-0.365	0	-0.719	0.061
15	0.577	1.254	-0.003	0.012	-0.381	0.046
16	0.807	1.118	0.007	0.004	-0.236	0.028
17	0.336	1.718	0.343	-0.328	-0.508	0.337
18	0.968	1.162	-0.007	-0.052	-0.172	0.148
19	1.012	1.061	-0.016	-0.013	-0.086	0.088
20	1.720	1.720	(0.005)	0	0	0.458
21	1.073	1.073	0.288	0	0	0.324
22	1.011	1.011	0.167	0	0	0.212

Brackets indicate the exact value is zero.

$\tau_{r\theta} = \tau_{\theta z} = u_\theta = 0$

$E/p = 1$ $p_r/p = 0$ $p_z/p = 1$ $d/a = 1\frac{1}{2}$ $\nu = 0$

N	σ_r/p	σ_θ/p	σ_z/p	τ_{zr}/p	Eu_r/ap	Eu_z/ap
1	0.096	0.096	-0.007	0	0	0
2	0.074	0.094	0.163	0	-0.047	0
3	-0.073	0.045	0.758	0	-0.046	0
4	-0.078	0.001	1.020	0	-0.002	0
5	-0.033	-0.013	1.052	0	0.026	0
6	-0.007	-0.014	1.040	0	0.035	0
7	0.004	-0.120	1.026	0	0.036	0
8	0.092	0.092	(0.001)	0	0	0.250
9						
10						
11	0.232	-0.066	0.230	0.223	0.047	0.346
12	-0.079	0.031	0.825	0.042	-0.033	0.035
13	-0.080	0.003	1.005	0.001	-0.005	0
14	(0.001)	-0.174	1.809	0	0.174	-0.091
15	0.120	-0.076	1.120	-0.038	0.114	-0.084
16	0.060	-0.035	1.046	-0.027	0.071	-0.060
17	0.431	-0.197	0.437	-0.427	0.139	-0.699
18	-0.034	-0.003	0.926	-0.172	0.003	-0.319
19	-0.037	0.008	0.977	-0.083	-0.011	-0.190
20	-0.199	-0.199	(0.003)	0	0	-0.961
21	0.081	0.081	0.426	0	0	-0.551
22	0.056	0.056	0.709	0	0	-0.344

Brackets indicate the exact value is zero.

$\tau_{r\theta} = \tau_{\theta z} = u_\theta = 0$

$E/p = 1$ $p_r/p = 1$ $p_z/p = 1$ $d/a = 1\frac{1}{2}$ $\nu = 0$

N	σ_r/p	σ_θ/p	σ_z/p	τ_{zr}/p	Eu_r/ap	Eu_z/ap
1	1.535	1.535	0.345	0	0	0
2	1.265	1.429	0.467	0	-0.215	0
3	0.965	1.262	0.782	0	-0.262	0
4	0.890	1.146	0.955	0	-0.219	0
5	0.904	1.083	1.005	0	-0.166	0
6	0.930	1.050	1.015	0	-0.125	0
7	0.950	1.032	1.015	0	-0.095	0
8	1.841	1.841	(0.003)	0	0	0.189
9						
10						
11	0.661	1.653	0.658	0.641	-0.462	0.217
12	0.918	1.255	0.826	0.106	-0.271	0.035
13	0.833	1.164	0.944	-0.038	-0.232	-0.010
14	(0.002)	1.546	1.444	0	-0.546	-0.031
15	0.698	1.178	1.118	-0.026	-0.266	-0.038
16	0.866	1.083	1.047	-0.023	-0.165	-0.032
17	0.767	1.521	0.780	0.755	-0.369	-0.362
18	0.934	1.158	0.919	-0.224	-0.168	-0.171
19	0.975	1.069	0.961	-0.096	-0.098	0.102
20	1.521	1.521	(0.008)	0	0	-0.503
21	1.155	1.155	0.708	0	0	-0.227
22	1.066	1.066	0.876	0	0	-0.131

Brackets indicate the exact value is zero.

$\tau_{r\theta} = \tau_{\theta z} = u_\theta = 0$

TABLE A 6.5.2 TOTAL STRESSES AND INDUCED DISPLACEMENTS ASSOCIATED WITH TWO IDENTICAL SPHERICAL CAVITIES IN A HOMOGENEOUS ISOTROPIC LINEAR ELASTIC INFINITE MASS WITH UNIFORM FIELD STRESS (Fig. A 6.5.2)

E/p = 1 $p_r/p = 1$ $p_z/z = 0$ d/a = 1½ $\nu = 0.25$

N	σ_r/p	σ_θ/p	σ_z/p	τ_{zr}/p	Eu_r/ap	Eu_z/ap
1	1.720	1.720	0.427	0	0	0
2	1.385	1.510	0.368	0	-0.161	0
3	1.142	1.255	0.031	0	-0.212	0
4	1.015	1.138	-0.079	0	-0.231	0
5	0.955	1.083	-0.057	0	-0.216	0
6	0.942	1.053	-0.030	0	-0.186	0
7	0.947	1.035	-0.014	0	-0.155	0
8	2.133	2.133	0	0	0	0.032
9						
10						
11	0.501	1.824	0.508	0.509	-0.581	-0.077
12	1.089	1.248	0.002	0.077	-0.239	0.016
13	1.016	1.155	-0.074	-0.048	-0.240	-0.020
14	(-0.001)	1.461	-0.448	0	-0.823	0.064
15	0.554	1.188	-0.003	0.015	-0.450	0.046
16	0.796	1.091	0.009	0.005	-0.280	0.024
17	0.398	1.769	0.395	-0.400	-0.580	0.306
18	1.027	1.168	-0.008	-0.062	-0.173	0.126
19	1.044	1.063	-0.019	-0.015	-0.081	0.074
20	2.092	2.092	0	0	0	0.411
21	1.156	1.156	0.350	0	0	0.361
22	1.041	1.041	0.204	0	0	0.245

Brackets indicate the exact value is zero.

$\tau_{r\theta} = \tau_{\theta z} = u_\theta = 0$

E/p = 1 $p_r/p = 0$ $p_z/p = 1$ d/a = 1½ $\nu = 0.25$

N	σ_r/p	σ_θ/p	σ_z/p	τ_{zr}/p	Eu_r/ap	Eu_z/ap
1	-0.112	-0.112	-0.063	0	0	0
2	-0.080	-0.056	0.105	0	-0.094	0
3	-0.163	0.003	0.751	0	-0.106	0
4	-0.121	0.004	1.032	0	-0.052	0
5	-0.050	-0.002	1.062	0	0.003	0
6	-0.012	-0.004	1.045	0	0.031	0
7	0.003	-0.004	1.028	0	0.036	0
8	-0.170	-0.170	(-0.001)	0	0	0.243
9						
10						
11	0.134	-0.210	0.138	0.139	0.020	0.352
12	-0.159	0.001	0.823	0.031	-0.090	0.028
13	-0.128	0.004	1.016	0.009	-0.045	0.007
14	0	0.078	1.885	0	0.143	-0.110
15	0.142	-0.013	1.120	-0.041	0.118	-0.097
16	0.070	-0.010	1.038	-0.028	0.074	-0.661
17	0.357	-0.241	0.355	-0.358	0.120	-0.763
18	-0.090	-0.007	0.928	-0.161	-0.035	-0.342
19	-0.067	0.007	0.981	-0.080	-0.041	-0.204
20	-0.565	-0.565	0	0	0	-1.046
21	0.002	0.002	0.359	0	0	-0.647
22	0.027	0.027	0.674	0	0	-0.410

Brackets indicate the exact value is zero.

$\tau_{r\theta} = \tau_{\theta z} = u_\theta = 0$

E/p = 1 $p_r/p = 1$ $p_z/p = 1$ d/a = 1½ $\nu = 0.25$

N	σ_r/p	σ_θ/p	σ_z/p	τ_{zr}/p	Eu_r/ap	Eu_z/ap
1	1.608	1.608	0.364	0	0	0
2	1.304	1.454	0.473	0	-0.255	0
3	0.979	1.258	0.782	0	-0.318	0
4	0.895	1.142	0.953	0	-0.269	0
5	0.905	1.081	1.004	0	-0.206	0
6	0.930	1.049	1.015	0	-0.156	0
7	0.950	1.031	1.014	0	-0.119	0
8	1.964	1.964	(-0.001)	0	0	0.275
9						
10						
11	0.634	1.614	0.645	0.649	-0.561	0.274
12	0.929	1.249	0.825	0.108	-0.329	0.044
13	0.888	1.159	0.942	-0.039	-0.284	-0.012
14	(-0.001)	1.539	1.437	0	-0.680	-0.046
15	0.696	1.175	1.117	-0.027	-0.332	-0.052
16	0.866	1.081	1.047	-0.023	-0.206	-0.042
17	0.755	1.528	0.750	-0.758	-0.461	-0.458
18	0.938	1.161	0.920	-0.223	-0.209	-0.216
19	0.977	1.070	0.962	-0.096	-0.121	-0.129
20	1.527	1.527	0	0	0	-0.635
21	1.158	1.158	0.709	0	0	-0.286
22	1.068	1.068	0.878	0	0	-0.165

Brackets indicate the exact value is zero.

$\tau_{r\theta} = \tau_{\theta z} = u_\theta = 0$

TABLE A 6.5.2 TOTAL STRESSES AND INDUCED DISPLACEMENTS ASSOCIATED WITH TWO IDENTICAL SPHERICAL CAVITIES IN A HOMOGENEOUS ISOTROPIC LINEAR ELASTIC INFINITE MASS WITH UNIFORM FIELD STRESS (Fig. A 6.5.2)

E/p = 1 $p_r/p = 1$ $p_z/p = 0$ d/a = 1½ ν = 0.49

N	σ_r/p	σ_θ/p	σ_z/p	τ_{zr}/p	Eu_r/ap	Eu_z/ap
1	2.142	2.142	0.543	0	0	0
2	1.681	1.762	0.468	0	-0.099	0
3	1.298	1.309	0.036	0	-0.145	0
4	1.084	1.126	-0.101	0	-0.201	0
5	0.980	1.062	-0.073	0	-0.214	0
6	0.949	1.035	-0.038	0	-0.197	0
7	0.947	1.022	-0.018	0	-0.170	0
8	2.705	2.705	(0.012)	0	0	0.229
9						
10						
11	0.662	2.003	0.664	0.646	-0.596	0.058
12	1.226	1.282	0	0.098	-0.182	0.049
13	1.093	1.145	-0.095	-0.061	-0.207	-0.036
14	0	1.077	-0.568	0.002	-0.846	0.582
15	0.520	1.089	-0.004	0.018	-0.490	0.341
16	0.781	1.051	0.011	0.006	-0.306	0.084
17	0.450	1.819	0.501	-0.505	-0.597	0.159
18	1.115	1.180	-0.008	-0.077	-0.135	0.047
19	1.090	1.067	-0.024	-0.019	-0.049	0.026
20	2.631	2.631	(0.025)	0	0	0.207
21	1.276	1.276	0.439	0	0	0.349
22	1.087	1.087	0.256	0	0	0.256

Brackets indicate the exact value is zero.

$\tau_{r\theta} = \tau_{\theta z} = u_\theta = 0$

E/p = 1 $p_r/p = 0$ $p_z/p = 1$ d/a = 1½ ν = 0.49

N	σ_r/p	σ_θ/p	σ_z/p	τ_{zr}/p	Eu_r/ap	Eu_z/ap
1	-0.431	-0.431	-0.148	0	0	0
2	-0.310	-0.280	0.020	0	-0.176	0
3	-0.296	-0.059	0.739	0	-0.214	0
4	-0.185	0.008	1.050	0	-0.111	0
5	-0.075	0.014	1.076	0	-0.028	0
6	-0.019	0.011	1.052	0	0.013	0
7	0.003	0.007	1.032	0	0.028	0
8	-0.584	-0.584	(0.003)	0	0	0.156
9						
10						
11	0.025	-0.399	0.025	0.016	-0.047	0.279
12	-0.279	-0.043	0.818	0.014	-0.194	0.006
13	-0.199	0.005	1.032	0.020	-0.123	0.021
14	0	0.447	1.998	0.001	0.042	-0.123
15	0.175	0.080	1.121	-0.047	0.098	-0.102
16	0.084	0.027	1.036	-0.030	0.063	-0.063
17	0.244	-0.311	0.258	-0.258	0.047	-0.716
18	-0.174	-0.012	0.932	-0.144	-0.113	-0.309
19	-0.111	0.006	0.987	-0.076	-0.096	-0.184
20	-1.109	-1.109	(0.008)	0	0	-0.974
21	-0.114	-0.114	0.269	0	0	-0.698
22	-0.017	-0.017	0.622	0	0	-0.456

Brackets indicate the exact value is zero.

$\tau_{r\theta} = \tau_{\theta z} = u_\theta = 0$

E/p = 1 $p_r/p = 1$ $p_z/p = 1$ d/a = 1½ ν = 0.49

N	σ_r/p	σ_θ/p	σ_z/p	τ_{zr}/p	Eu_r/ap	Eu_z/ap
1	1.711	1.711	0.396	0	0	0
2	1.371	1.482	0.488	0	-0.276	0
3	1.002	1.250	0.774	0	-0.360	0
4	0.900	1.134	0.949	0	-0.312	0
5	0.906	1.076	1.003	0	-0.242	0
6	0.929	1.046	1.014	0	-0.184	0
7	0.949	1.029	1.014	0	-0.141	0
8	2.121	2.121	(0.014)	0	0	0.385
9						
10						
11	0.687	1.604	0.688	0.662	-0.643	0.337
12	0.946	1.239	0.818	0.113	-0.376	0.055
13	0.895	1.151	0.937	-0.041	-0.330	-0.015
14	0	1.525	1.431	0.002	-0.804	-0.065
15	0.695	1.169	1.117	-0.028	-0.392	-0.068
16	0.865	1.078	1.046	-0.024	-0.243	-0.055
17	0.694	1.508	0.758	-0.763	-0.549	-0.557
18	0.941	1.167	0.924	-0.221	-0.248	-0.262
19	0.979	1.073	0.963	-0.094	-0.145	-0.157
20	1.522	1.522	(0.033)	0	0	-0.767
21	1.161	1.161	0.708	0	0	-0.348
22	1.070	1.070	0.878	0	0	-0.201

Brackets indicate the exact value is zero.

$\tau_{r\theta} = \tau_{\theta z} = u_\theta = 0$

TABLE A 6.5.2 TOTAL STRESSES AND INDUCED DISPLACEMENTS ASSOCIATED WITH TWO IDENTICAL SPHERICAL CAVITIES IN A HOMOGENEOUS ISOTROPIC LINEAR ELASTIC INFINITE MASS WITH UNIFORM FIELD STRESS (Fig. A 6.5.2)

$E/p = 1$ $p_r/p = 1$ $p_z/p = 0$ $d/a = 1\frac{1}{2}$ $\nu = 0$

N	σ_r/p	σ_θ/p	σ_z/p	τ_{zr}/p	Eu_r/ap	Eu_z/ap
1	1.158	1.158	0.441	0	0	0
2	1.121	1.143	0.300	0	0.716	0
3	1.075	1.121	0.055	0	-0.121	0
4	1.020	1.096	-0.042	0	-0.144	0
5	0.981	1.072	-0.044	0	-0.144	0
6	0.966	1.052	-0.028	0	-0.129	0
7	0.964	1.037	-0.015	0	-0.111	0
8	1.662	1.662	(-0.002)	0	0	-0.169
9	1.158	1.158	0.441	0	0	0
10						
11	0.389	1.696	0.391	0.391	-0.492	-0.169
12	0.995	1.178	0.018	0.082	-0.188	-0.012
13	1.027	1.102	-0.036	0.014	-0.144	-0.003
14	0	1.713	-0.379	0	-0.713	0.051
15	0.573	1.248	-0.002	0.012	-0.372	0.043
16	0.805	1.113	0.011	0.007	-0.226	0.030
17	0.319	1.714	0.332	-0.326	-0.505	0.332
18	0.967	1.160	-0.009	-0.051	-0.170	0.144
19	1.011	1.066	-0.017	-0.013	-0.085	0.086
20	1.711	1.711	(-0.002)	0	0	0.452
21	1.072	1.072	0.285	0	0	0.320
22	1.010	1.010	0.165	0	0	0.209

Brackets indicate the exact value is zero.

$\tau_{r\theta} = \tau_{\theta z} = u_\theta = 0$

$E/p = 1$ $p_r/p = 0$ $p_z/p = 1$ $d/a = 1\frac{1}{2}$ $\nu = 0$

N	σ_r/p	σ_θ/p	σ_z/p	τ_{zr}/p	Eu_r/ap	Eu_z/ap
1	0.129	0.129	0.085	0	0	0
2	0.062	0.106	0.327	0	-0.053	0
3	-0.053	0.052	0.764	0	-0.052	0
4	-0.070	0.012	0.984	0	-0.018	0
5	-0.040	-0.005	1.035	0	0.010	0
6	-0.016	-0.009	1.034	0	0.024	0
7	-0.003	-0.009	1.025	0	0.028	0
8	-0.013	-0.013	(-0.002)	0	0	0.478
9	0.129	0.129	0.085	0	0	0
10						
11	0.303	-0.115	0.303	0.304	0.081	0.424
12	-0.055	0.024	0.844	0.086	-0.026	0.080
13	-0.072	0.016	0.964	0.003	-0.023	0.003
14	0	-0.183	1.834	0	0.183	-0.081
15	0.127	-0.081	1.128	-0.027	0.121	-0.076
16	0.066	-0.037	1.038	-0.022	0.074	-0.058
17	0.420	-0.200	0.430	-0.426	0.141	-0.697
18	-0.035	-0.005	0.929	-0.171	0.005	-0.316
19	-0.038	0.007	0.979	-0.082	-0.011	-0.188
20	-0.205	-0.205	(-0.003)	0	0	-0.962
21	0.081	0.081	0.419	0	0	-0.551
22	0.056	0.056	0.709	0	0	-0.343

Brackets indicate the exact value is zero.

$\tau_{r\theta} = \tau_{\theta z} = u_\theta = 0$

$E/p = 1$ $p_r/p = 1$ $p_z/p = 1$ $d/a = 1\frac{1}{2}$ $\nu = 0$

N	σ_r/p	σ_θ/p	σ_z/p	τ_{zr}/p	Eu_r/ap	Eu_z/ap
1	1.287	1.287	0.526	0	0	0
2	1.183	1.249	0.626	0	-0.124	0
3	1.022	1.173	0.819	0	-0.173	0
4	0.950	1.108	0.942	0	-0.162	0
5	0.940	1.067	0.991	0	-0.133	0
6	0.950	1.042	1.006	0	-0.106	0
7	0.961	1.028	1.009	0	-0.084	0
8	1.649	1.649	(-0.003)	0	0	0.310
9	1.287	1.287	0.526	0	0	0
10						
11	0.692	1.581	0.694	0.695	-0.411	0.255
12	0.939	1.202	0.862	0.168	-0.214	0.068
13	0.955	1.118	0.929	0.017	-0.167	0.006
14	(-0.001)	1.530	1.455	0	-0.530	-0.030
15	0.701	1.167	1.126	-0.016	-0.251	-0.033
16	0.871	1.076	1.050	-0.015	-0.152	-0.028
17	0.740	1.515	0.761	-0.753	-0.364	-0.365
18	0.932	1.155	0.920	-0.223	-0.165	-0.172
19	0.973	1.067	0.962	-0.095	-0.095	-0.102
20	1.507	1.507	(-0.005)	0	0	-0.510
21	1.153	1.153	0.704	0	0	-0.231
22	1.066	1.066	0.874	0	0	-0.134

Brackets indicate the exact value is zero.

$\tau_{r\theta} = \tau_{\theta z} = u_\theta = 0$

TABLE A 6.5.2 TOTAL STRESSES AND INDUCED DISPLACEMENTS ASSOCIATED WITH TWO IDENTICAL SPHERICAL CAVITIES IN A HOMOGENEOUS ISOTROPIC LINEAR ELASTIC INFINITE MASS WITH UNIFORM FIELD STRESS (Fig. A 6.5.2)

$E/p = 1$ $p_r/p = 1$ $p_z/p = 0$ $d/a = 1\frac{1}{2}$ $\nu = 0.25$

N	σ_r/p	σ_θ/p	σ_z/p	τ_{zr}/p	Eu_r/ap	Eu_z/ap
1	1.307	1.307	0.533	0	0	0
2	1.245	1.245	0.363	0	-0.047	0
3	1.159	1.154	0.068	0	-0.097	0
4	1.067	1.097	-0.051	0	-0.139	0
5	1.003	1.064	-0.053	0	-0.152	0
6	0.975	1.043	-0.034	0	-0.145	0
7	0.967	1.030	-0.019	0	-0.128	0
8	1.998	1.998	(-0.001)	0	0	-0.079
9	1.307	1.307	0.533	0	0	0
10						
11	0.473	1.778	0.476	0.475	-0.559	-0.116
12	1.072	1.195	0.023	0.100	-0.182	0.016
13	1.080	1.105	-0.043	0.017	-0.136	0.008
14	0	1.447	-0.461	0	-0.812	0.057
15	0.548	1.179	-0.002	0.014	-0.439	0.046
16	0.793	1.085	0.014	0.009	-0.267	0.029
17	0.390	1.763	0.400	-0.397	-0.577	0.301
18	1.025	1.165	-0.011	-0.062	-0.171	0.123
19	1.042	1.061	-0.021	-0.016	-0.079	0.072
20	2.082	2.082	(-0.002)	0	0	0.406
21	1.153	1.153	0.347	0	0	0.356
22	1.040	1.040	0.201	0	0	0.241

Brackets indicate the exact value is zero.

$\tau_{r\theta} = \tau_{\theta z} = u_\theta = 0$

$E/p = 1$ $p_r/p = 0$ $p_z/p = 1$ $d/a = 1\frac{1}{2}$ $\nu = 0.25$

N	σ_r/p	σ_θ/p	σ_z/p	τ_{zr}/p	Eu_r/ap	Eu_z/ap
1	-0.002	-0.002	0.004	0	0	0
2	-0.049	0.012	0.268	0	-0.104	0
3	-0.130	0.019	0.751	0	-0.114	0
4	-0.114	0.010	0.992	0	-0.061	0
5	-0.062	0.002	1.044	0	-0.013	0
6	-0.025	-0.002	1.039	0	-0.013	0
7	-0.006	-0.003	1.028	0	0.024	0
8	-0.288	-0.288	(-0.002)	0	0	0.488
9	-0.002	-0.002	0.004	0	0	0
10						
11	0.222	-0.215	0.224	0.224	0.054	0.439
12	-0.127	0.004	0.839	0.070	-0.081	0.070
13	-0.121	0.011	0.971	0.001	-0.070	0.000
14	0	0.076	1.913	0	0.153	-0.098
15	0.152	-0.015	1.128	-0.031	0.127	-0.089
16	0.078	-0.011	1.036	-0.024	0.078	-0.652
17	0.353	-0.244	0.360	-0.358	0.122	-0.761
18	-0.091	-0.008	0.931	-0.160	-0.034	-0.339
19	-0.067	0.007	0.983	-0.079	-0.040	-0.202
20	-0.570	-0.570	(-0.001)	0	0	-1.046
21	0.002	0.002	0.359	0	0	-0.646
22	0.026	0.026	0.674	0	0	-0.409

Brackets indicate the exact value is zero.

$\tau_{r\theta} = \tau_{\theta z} = u_\theta = 0$

$E/p = 1$ $p_r/p = 1$ $p_z/p = 1$ $d/a = 1\frac{1}{2}$ $\nu = 0.25$

N	σ_r/p	σ_θ/p	σ_z/p	τ_{zr}/p	Eu_r/ap	Eu_z/ap
1	1.305	1.305	0.537	0	0	0
2	1.197	1.258	0.631	0	-0.150	0
3	1.029	1.173	0.891	0	-0.211	0
4	0.953	1.107	0.941	0	-0.200	0
5	0.941	1.066	0.990	0	-0.165	0
6	0.950	1.041	1.006	0	-0.132	0
7	0.961	1.027	1.009	0	-0.104	0
8	1.710	1.710	(-0.003)	0	0	0.409
9	1.305	1.305	0.537	0	0	0
10						
11	0.695	1.563	0.700	0.699	-0.505	0.323
12	0.945	1.199	0.862	0.170	-0.263	0.086
13	0.958	1.117	0.928	0.017	-0.206	0.008
14	(-0.001)	1.523	1.452	0	-0.660	-0.041
15	0.700	1.165	1.126	-0.016	-0.313	-0.043
16	0.871	1.075	1.050	-0.015	-0.189	-0.037
17	0.744	1.519	0.760	-0.755	-0.455	-0.460
18	0.934	1.157	0.920	-0.223	-0.205	-0.217
19	0.975	1.068	0.962	-0.095	-0.118	-0.129
20	1.512	1.512	(-0.003)	0	0	-0.640
21	1.155	1.155	0.706	0	0	-0.290
22	1.067	1.067	0.875	0	0	-0.168

Brackets indicate the exact value is zero.

$\tau_{r\theta} = \tau_{\theta z} = u_\theta = 0$

TABLE A 6.5.2 TOTAL STRESSES AND INDUCED DISPLACEMENTS ASSOCIATED WITH TWO IDENTICAL SPHERICAL CAVITIES IN A HOMOGENEOUS ISOTROPIC LINEAR ELASTIC INFINITE MASS WITH UNIFORM FIELD STRESS (Fig. A 6.5.2)

E/p = 1 $p_r/p = 1$ $p_z/p = 0$ d/a = 1½ $\nu = 0.49$

N	σ_r/p	σ_θ/p	σ_z/p	τ_{zr}/p	Eu_r/ap	Eu_z/ap
1	1.523	1.523	0.666	0	0	0
2	1.431	1.392	0.454	0	0.021	0
3	1.283	1.202	0.085	0	-0.021	0
4	1.136	1.097	-0.064	0	-0.092	0
5	1.036	1.051	-0.067	0	-0.133	0
6	0.989	1.030	-0.042	0	-0.141	0
7	0.972	1.019	-0.023	0	-0.132	0
8	2.474	2.474	(-0.019)	0	0	0.137
9	1.523	1.523	0.666	0	0	0
10						
11	0.568	1.898	0.626	0.600	-0.568	0.031
12	1.185	1.220	0.029	0.125	-0.122	0.075
13	1.157	1.110	-0.054	0.021	-0.084	0.016
14	0	1.055	-0.583	0	-0.830	0.055
15	0.512	1.078	-0.003	0.018	-0.477	0.041
16	0.776	1.044	0.018	-0.011	-0.291	0.020
17	0.463	1.827	0.526	-0.501	-0.589	0.156
18	1.111	1.171	-0.013	-0.079	-0.131	0.044
19	1.087	1.062	-0.026	-0.021	-0.045	0.025
20	2.607	2.607	(0.009)	0	0	0.201
21	1.272	1.272	0.436	0	0	0.345
22	1.085	1.085	0.253	0	0	0.252

Brackets indicate the exact value is zero.

$\tau_{r\theta} = \tau_{\theta z} = u_\theta = 0$

E/p = 1 $p_r/p = 0$ $p_z/p = 1$ d/a = 1½ $\nu = 0.49$

N	σ_r/p	σ_θ/p	σ_z/p	τ_{zr}/p	Eu_r/ap	Eu_z/ap
1	-0.197	-0.197	-0.117	0	0	0
2	-0.214	-0.127	0.180	0	-0.190	0
3	-0.244	-0.030	0.733	0	-0.221	0
4	-0.179	0.007	1.004	0	-0.139	0
5	-0.093	0.012	1.057	0	-0.059	0
6	-0.038	0.010	1.048	0	-0.012	0
7	-0.011	0.007	1.033	0	-0.011	0
8	-0.703	-0.703	(-0.003)	0	0	0.386
9	-0.197	-0.197	-0.117	0	0	0
10						
11	0.094	-0.362	0.115	0.106	-0.018	0.363
12	-0.233	-0.025	0.832	0.047	-0.182	0.031
13	-0.194	0.004	0.980	-0.003	-0.154	-0.006
14	0	0.455	2.031	0	0.050	-0.111
15	0.187	0.082	1.129	-0.036	0.108	-0.096
16	0.094	0.028	1.032	-0.026	0.068	-0.066
17	0.255	-0.304	0.269	-0.258	0.050	-0.714
18	-0.174	-0.013	0.934	-0.145	-0.111	-0.307
19	-0.111	0.006	0.989	-0.075	-0.093	-0.183
20	-1.114	-1.114	(0.004)	0	0	-0.973
21	-0.114	-0.114	0.270	0	0	-0.696
22	-0.017	-0.017	0.623	0	0	-0.455

Brackets indicate the exact value is zero.

$\tau_{r\theta} = \tau_{\theta z} = u_\theta = 0$

E/p = 1 $p_r/p = 1$ $p_z/p = 1$ d/a = 1½ $\nu = 0.49$

N	σ_r/p	σ_θ/p	σ_z/p	τ_{zr}/p	Eu_r/ap	Eu_z/ap
1	1.326	1.326	0.549	0	0	0
2	1.217	1.266	0.634	0	-0.169	0
3	1.039	1.172	0.817	0	-0.242	0
4	0.957	1.104	0.940	0	-0.231	0
5	0.943	1.063	0.990	0	-0.192	0
6	0.951	1.040	1.006	0	-0.153	0
7	0.961	1.026	1.009	0	-0.121	0
8	1.771	1.771	(-0.022)	0	0	0.523
9	1.326	1.326	0.549	0	0	0
10						
11	0.661	1.536	0.741	0.705	-0.586	-0.586
12	0.952	1.195	0.861	0.172	-0.304	-0.303
13	0.963	1.114	0.926	0.018	-0.238	-0.238
14	0	1.510	1.448	0	-0.781	-0.055
15	0.699	1.160	1.126	-0.017	-0.369	-0.055
16	0.871	1.073	1.050	-0.016	-0.223	-0.046
17	0.718	1.523	0.795	-0.759	-0.539	-0.558
18	0.936	1.158	0.921	-0.223	-0.241	-0.263
19	0.976	1.068	0.963	-0.096	-0.138	-0.158
20	1.492	1.492	(0.013)	0	0	-0.772
21	1.158	1.158	0.706	0	0	-0.351
22	1.068	1.068	0.875	0	0	-0.203

Brackets indicate the exact value is zero.

$\tau_{r\theta} = \tau_{\theta z} = u_\theta = 0$

TABLE A 6.5.2 TOTAL STRESSES AND INDUCED DISPLACEMENTS ASSOCIATED WITH TWO IDENTICAL SPHERICAL CAVITIES IN A HOMOGENEOUS ISOTROPIC LINEAR ELASTIC INFINITE MASS WITH UNIFORM FIELD STRESS (Fig. A 6.5.2)

E/p = 1 $p_r/p = 1$ $p_z/p = 0$ d/a = 2 ν = 0

N	σ_r/p	σ_θ/p	σ_z/p	τ_{zr}/p	Eu_r/ap	Eu_z/ap
1	1.022	1.022	0.299	0	0	0
2	1.038	1.027	0.221	0	-0.014	0
3	1.053	1.037	0.083	0	-0.037	0
4	1.041	1.041	0	0	-0.062	0
5	1.018	1.038	-0.025	0	-0.076	0
6	0.999	1.032	-0.024	0	-0.080	0
7	0.989	1.026	-0.017	0	-0.077	0
8	1.685	1.685	(-0.007)	0	0	-0.301
9	1.075	1.075	0.341	0	0	-0.157
10	1.022	1.022	0.299	0	0	0
11	0.347	1.700	0.368	0.351	-0.495	-0.223
12	0.973	1.159	0.011	0.070	-0.169	-0.045
13	1.023	1.066	-0.009	0.0[illegible]	-0.093	-0.002
14	0	1.710	-0.397	0	-0.710	0.037
15	0.568	1.245	-0.006	-0.007	-0.368	0.034
16	0.800	1.110	0.014	0.006	-0.219	0.027
17	0.336	1.713	0.325	-0.324	-0.504	0.326
18	0.966	1.159	-0.013	-0.052	-0.168	0.138
19	1.011	1.059	-0.019	-0.014	-0.085	0.081
20	1.718	1.718	(0.003)	0	0	0.449
21	1.071	1.071	0.285	0	0	0.315
22	1.009	1.009	0.164	0	0	0.205

Brackets indicate the exact value is zero.

$\tau_{r\theta} = \tau_{\theta z} = u_\theta = 0$

E/p = 1 $p_r/p = 0$ $p_z/p = 1$ d/a = 2 ν = 0

N	σ_r/p	σ_θ/p	σ_z/p	τ_{zr}/p	Eu_r/ap	Eu_z/ap
1	0.100	0.100	0.469	0	0	0
2	0.057	0.083	0.583	0	-0.042	0
3	-0.015	0.051	0.795	0	-0.051	0
4	-0.045	0.023	0.941	0	-0.034	0
5	-0.039	0.006	1.002	0	-0.013	0
6	-0.024	-0.001	1.018	0	0.003	0
7	-0.012	-0.004	1.018	0	0.012	0
8	-0.141	-0.141	(-0.005)	0	0	0.719
9	0.103	0.103	0.324	0	0	0.289
10	0.100	1.100	0.469	0	0	0
11	0.380	-0.171	0.392	0.381	0.120	0.524
12	-0.038	0.008	0.887	0.136	-0.008	0.153
13	-0.047	0.017	0.952	0.037	-0.024	0.039
14	0	-0.196	1.873	0	0.196	-0.060
15	0.136	-0.088	1.142	-0.014	0.132	-0.057
16	0.075	-0.040	1.046	-0.013	0.081	-0.048
17	0.435	-0.205	0.427	-0.426	0.145	-0.690
18	-0.036	-0.007	0.933	-0.177	0.007	-0.273
19	-0.039	0.006	0.983	-0.081	-0.009	-0.182
20	-0.203	-0.203	(0.002)	0	0	-0.956
21	0.080	0.080	0.420	0	0	-0.546
22	0.055	0.055	0.710	0	0	-0.338

Brackets indicate the exact value is zero.

$\tau_{r\theta} = \tau_{\theta z} = u_\theta = 0$

E/p = 1 $p_r/p = 1$ $p_z/p = 1$ d/a = 2 ν = 0

N	σ_r/p	σ_θ/p	σ_z/p	τ_{zr}/p	Eu_r/ap	Eu_z/ap
1	1.122	1.122	0.768	0	0	0
2	1.095	1.110	0.804	0	-0.055	0
3	1.038	1.089	0.878	0	-0.089	0
4	0.996	1.064	0.941	0	-0.096	0
5	0.979	1.044	0.977	0	-0.089	0
6	0.975	1.031	0.994	0	-0.077	0
7	0.977	1.022	1.001	0	-0.065	0
8	1.544	1.544	(-0.012)	0	0	0.419
9	1.178	1.178	0.665	0	0	0.132
10	1.122	1.122	0.768	0	0	0
11	0.727	1.530	0.760	0.730	-0.374	0.301
12	0.935	1.167	0.898	0.207	-0.177	0.107
13	0.976	1.083	0.943	0.069	-0.117	0.038
14	(0.001)	1.514	1.477	-0.001	-0.514	-0.029
15	0.704	1.157	1.136	-0.006	-0.236	-0.235
16	0.875	1.069	1.054	-0.007	-0.139	-0.210
17	0.771	1.508	0.752	-0.750	-0.359	-0.364
18	0.930	1.152	0.921	-0.223	-0.161	-0.170
19	0.972	1.065	0.964	-0.095	-0.092	-0.100
20	1.514	1.514	(0.005)	0	0	-0.507
21	1.151	1.151	0.705	0	0	-0.230
22	1.064	1.064	0.875	0	0	-0.133

Brackets indicate the exact value is zero.

$\tau_{r\theta} = \tau_{\theta z} = u_\theta = 0$

TABLE A 6.5.2 TOTAL STRESSES AND INDUCED DISPLACEMENTS ASSOCIATED WITH TWO IDENTICAL SPHERICAL CAVITIES IN A HOMOGENEOUS ISOTROPIC LINEAR ELASTIC INFINITE MASS WITH UNIFORM FIELD STRESS (Fig. A 6.5.2).

E/p = 1 $p_r/p = 1$ $p_z/p = 0$ d/a = 2 $\nu = 0.25$

N	σ_r/p	σ_θ/p	σ_z/p	τ_{zr}/p	Eu_r/ap	Eu_z/ap
1	1.078	1.078	0.367	0	0	0
2	1.086	1.079	0.273	0	0.005	0
3	1.101	1.062	0.103	0	-0.010	0
4	1.077	1.048	0	0	-0.044	0
5	1.040	1.038	-0.030	0	-0.070	0
6	1.012	1.029	-0.029	0	-0.082	0
7	0.996	1.022	-0.021	0	-0.084	0
8	2.066	2.066	(0.066)	0	0	-0.242
9	1.165	1.165	0.419	0	0	-0.167
10	1.078	1.078	0.367	0	0	0
11	0.470	1.758	0.364	0.425	-0.656	-0.177
12	1.038	1.169	0.012	0.084	-0.165	-0.012
13	1.063	1.070	-0.011	0.039	-0.081	0.018
14	(-0.002)	1.439	-0.485	0.002	-0.811	0.044
15	0.609	1.148	0.004	0.008	-0.391	0.365
16	0.785	1.082	0.017	0.007	-0.262	0.029
17	0.329	1.744	0.391	-0.394	-0.575	0.294
18	1.022	1.164	-0.012	-0.060	-0.172	0.118
19	1.039	1.061	-0.022	-0.016	-0.081	0.069
20	2.048	2.048	(-0.015)	0	0	0.396
21	1.150	1.150	0.341	0	0	0.348
22	1.039	1.039	0.197	0	0	0.235

Brackets indicate the exact value is zero.

$\tau_{r\theta} = \tau_{\theta z} = u_\theta = 0$

E/p = 1 $p_r/p = 0$ $p_z/p = 1$ d/a = 2 $\nu = 0.25$

N	σ_r/p	σ_θ/p	σ_z/p	τ_{zr}/p	Eu_r/ap	Eu_z/ap
1	0.045	0.045	0.412	0	0	0
2	-0.003	0.046	0.541	0	-0.081	0
3	-0.062	0.030	0.780	0	-0.100	0
4	-0.079	0.016	0.941	0	-0.076	0
5	-0.060	0.007	1.007	0	-0.042	0
6	-0.037	0.003	1.023	0	-0.015	0
7	-0.019	0	1.022	0	0.002	0
8	-0.442	-0.422	(0.072)	0	0	0.746
9	0.016	0.016	0.259	0	0	0.328
10	0.045	0.045	0.412	0	0	0
11	0.357	-0.236	0.241	0.306	0.096	0.550
12	-0.098	-0.001	0.884	0.122	-0.056	0.146
13	-0.085	0.013	0.954	0.031	-0.065	0.030
14	(-0.002)	0.071	1.995	0.002	0.167	-0.071
15	0.162	-0.017	1.143	-0.016	0.141	-0.068
16	0.088	-0.012	1.038	-0.014	0.087	-0.055
17	0.288	-0.267	0.355	-0.358	0.126	-0.753
18	-0.095	-0.008	0.939	-0.158	-0.033	-0.329
19	-0.070	0.008	0.988	-0.077	-0.040	-0.194
20	-0.613	-0.613	(-0.016)	0	0	-1.046
21	-0.001	-0.001	0.354	0	0	-0.645
22	0.026	0.026	0.673	0	0	-0.407

Brackets indicate the exact value is zero.

$\tau_{r\theta} = \tau_{\theta z} = u_\theta = 0$

E/p = 1 $p_r/p = 1$ $p_z/p = 1$ d/a = 2 $\nu = 0.25$

N	σ_r/p	σ_θ/p	σ_z/p	τ_{zr}/p	Eu_r/ap	Eu_z/ap
1	1.124	1.124	0.779	0	0	0
2	1.083	1.126	0.814	0	-0.076	0
3	1.039	1.091	0.883	0	-0.111	0
4	0.999	1.065	0.942	0	-0.120	0
5	0.980	1.045	0.977	0	-0.112	0
6	0.976	1.031	0.994	0	-0.097	0
7	0.977	1.022	1.001	0	-0.083	0
8	1.624	1.624	(0.138)	0	0	0.504
9	1.181	1.181	0.679	0	0	1.161
10	1.124	1.124	0.779	0	0	0
11	0.827	1.522	0.605	0.731	-0.469	0.373
12	0.941	1.168	0.896	0.206	-0.221	0.134
13	0.978	1.083	0.943	0.070	-0.146	0.479
14	(-0.004)	1.510	1.469	0.004	-0.644	-0.027
15	0.702	1.158	1.135	-0.008	-0.298	-0.029
16	0.874	1.070	1.054	-0.007	-0.176	-0.026
17	0.617	1.477	0.747	-0.752	-0.450	-0.459
18	0.927	1.157	0.927	-0.218	-0.205	-0.212
19	0.969	1.069	0.966	-0.093	-0.120	-0.125
20	1.435	1.435	(-0.031)	0	0	-0.650
21	1.150	1.150	0.694	0	0	-0.297
22	1.065	1.065	0.870	0	0	-0.172

Brackets indicate the exact value is zero.

$\tau_{r\theta} = \tau_{\theta z} = u_\theta = 0$

TABLE A 6.5.2 TOTAL STRESSES AND INDUCED DISPLACEMENTS ASSOCIATED WITH TWO IDENTICAL SPHERICAL CAVITIES IN A HOMOGENEOUS ISOTROPIC LINEAR ELASTIC INFINITE MASS WITH UNIFORM FIELD STRESS (Fig. A 6.5.2)

$E/p = 1$ $p_r/p = 1$ $p_z/p = 0$ $d/a = 2$ $\nu = 0.49$

N	σ_r/p	σ_θ/p	σ_z/p	τ_{zr}/p	Eu_r/ap	Eu_z/ap
1	1.162	1.162	0.455	0	0	0
2	1.164	1.149	0.338	0	0.048	0
3	1.170	1.097	0.128	0	0.049	0
4	1.128	1.059	0.001	0	0.006	0
5	1.073	1.037	-0.037	0	-0.039	0
6	1.031	1.024	-0.036	0	-0.066	0
7	1.006	1.016	-0.026	0	-0.077	0
8	2.543	2.543	(0.026)	0	0	-0.020
9	1.296	1.296	0.519	0	0	-0.140
10	1.162	1.162	0.455	0	0	0
11	0.511	1.836	0.535	0.536	-0.576	-0.026
12	1.133	1.148	0.006	0.087	-0.090	0.066
13	1.120	1.077	-0.013	0.049	-0.035	0.055
14	0	1.040	-0.610	-0.001	-0.829	0.045
15	0.499	1.070	-0.010	0.012	-0.480	0.039
16	0.765	1.040	0.021	0.010	-0.289	0.027
17	0.492	1.831	0.501	-0.496	-0.590	0.153
18	1.107	1.169	-0.019	-0.079	-0.133	0.040
19	1.084	1.061	-0.029	-0.021	-0.049	0.023
20	2.619	2.619	(0.001)	0	0	0.201
21	1.269	1.269	0.435	0	0	0.343
22	1.083	1.083	0.251	0	0	0.249

Brackets indicate the exact value is zero.

$\tau_{r\theta} = \tau_{\theta z} = u_\theta = 0$

$E/p = 1$ $p_r/p = 0$ $p_z/p = 1$ $d/a = 2$ $\nu = 0.49$

N	σ_r/p	σ_θ/p	σ_z/p	τ_{zr}/p	Eu_r/ap	Eu_z/ap
1	-0.035	-0.035	0.317	0	0	0
2	-0.080	-0.020	0.469	0	-0.140	0
3	-0.133	-0.004	0.752	0	-0.183	0
4	-0.131	0.006	0.941	0	-0.149	0
5	-0.093	0.009	1.015	0	-0.094	0
6	-0.055	0.008	1.030	0	-0.049	0
7	-0.029	0.006	1.027	0	-0.020	0
8	-0.969	-0.969	(0.008)	0	0	0.658
9	-0.112	-0.112	0.151	0	0	0.341
10	-0.035	-0.035	0.317	0	0	0
11	0.198	-0.328	0.201	0.199	0.024	0.481
12	-0.191	-0.015	0.881	0.101	-0.145	0.098
13	-0.143	0.007	0.956	0.021	-0.139	0.002
14	0	0.465	2.082	0	0.065	-0.083
15	0.203	0.086	1.146	-0.018	0.127	-0.075
16	0.109	0.029	1.033	-0.016	0.082	-0.059
17	0.255	-0.315	0.257	-0.256	0.053	-0.703
18	-0.177	-0.013	0.941	-0.144	-0.109	-0.297
19	-0.133	0.006	0.994	-0.073	-0.091	-0.175
20	-1.124	-1.124	0	0	0	-0.966
21	-0.116	-0.116	0.269	0	0	-0.691
22	-0.017	-0.017	0.623	0	0	-0.451

Brackets indicate the exact value is zero.

$\tau_{r\theta} = \tau_{\theta z} = u_\theta = 0$

$E/p = 1$ $p_r/p = 1$ $p_z/p = 1$ $d/a = 2$ $\nu = 0.49$

N	σ_r/p	σ_θ/p	σ_z/p	τ_{zr}/p	Eu_r/ap	Eu_z/ap
1	1.126	1.126	0.771	0	0	0
2	1.084	1.129	0.807	0	-0.091	0
3	1.037	1.094	0.880	0	-0.134	0
4	0.997	1.066	0.942	0	-0.143	0
5	0.980	1.045	0.977	0	-0.133	0
6	0.976	1.031	0.994	0	-0.115	0
7	0.977	1.022	1.001	0	-0.097	0
8	1.573	1.573	(0.034)	0	0	0.638
9	1.184	1.184	0.669	0	0	0.201
10	1.126	1.126	0.771	0	0	0
11	0.708	1.508	0.735	0.735	-0.552	0.454
12	0.938	1.168	0.899	0.207	-0.263	0.162
13	0.977	1.084	0.943	0.070	-0.174	0.574
14	0	1.505	1.472	-0.001	-0.764	-0.038
15	0.702	1.155	1.136	-0.007	-0.352	-0.037
16	0.874	1.069	1.054	-0.007	-0.208	-0.032
17	0.747	1.516	0.758	-0.752	-0.536	-0.551
18	0.929	1.155	0.921	-0.222	-0.242	-0.257
19	0.971	1.067	0.964	-0.094	-0.140	-0.152
20	1.495	1.495	0	0	0	-0.765
21	1.152	1.152	0.704	0	0	-0.348
22	1.065	1.065	0.874	0	0	-0.202

Brackets indicate the exact value is zero.

$\tau_{r\theta} = \tau_{\theta z} = u_\theta = 0$

TABLE A 6.5.2 TOTAL STRESSES AND INDUCED DISPLACEMENTS ASSOCIATED WITH TWO IDENTICAL SPHERICAL CAVITIES IN A HOMOGENEOUS ISOTROPIC LINEAR ELASTIC INFINITE MASS WITH UNIFORM FIELD STRESS (Fig. A 6.5.2)

$E/p = 1$ $p_r/p = 1$ $p_z/p = 0$ $d/a = 2\frac{1}{2}$ $\nu = 0$

N	σ_r/p	σ_θ/p	σ_z/p	τ_{zr}/p	Eu_r/ap	Eu_z/ap
1	1.000	1.000	0.179	0	0	0
2	1.010	1.004	0.145	0	-0.002	0
3	1.026	1.011	0.077	0	-0.011	0
4	1.030	1.017	0.022	0	-0.026	0
5	1.022	1.019	-0.006	0	-0.039	0
6	1.011	1.019	-0.014	0	-0.047	0
7	1.002	1.017	-0.014	0	-0.051	0
8	1.699	1.699	(-0.006)	0	0	-0.357
9	1.071	1.071	0.304	0	0	-0.221
10	1.009	1.009	0.210	0	0	-0.094
11	0.330	1.706	0.336	0.335	-0.500	-0.253
12	0.968	1.158	-0.001	0.060	-0.167	-0.069
13	1.014	1.060	-0.010	0.025	-0.085	-0.017
14	(-0.001)	1.711	-0.410	0	-0.711	0.027
15	0.565	1.246	-0.011	0.004	-0.368	0.025
16	0.797	1.109	0.013	0.004	-0.218	0.022
17	0.317	1.713	0.326	-0.323	-0.504	0.320
18	0.966	1.158	-0.014	-0.051	-0.168	0.133
19	1.010	1.059	-0.021	-0.014	-0.084	0.078
20	1.713	1.713	0	0	0	0.444
21	1.071	1.071	0.284	0	0	0.311
22	1.009	1.009	0.163	0	0	0.201

Brackets indicate the exact value is zero.

$\tau_{r\theta} = \tau_{\theta z} = u_\theta = 0$

$E/p = 1$ $p_r/p = 0$ $p_z/p = 1$ $d/a = 2\frac{1}{2}$ $\nu = 0$

N	σ_r/p	σ_θ/p	σ_z/p	τ_{zr}/p	Eu_r/ap	Eu_z/ap
1	0.063	0.063	0.698	0	0	0
2	0.044	0.055	0.744	0	-0.228	0
3	0.005	1.039	0.843	0	-0.039	0
4	-0.021	0.023	0.930	0	-0.034	0
5	-0.027	0.011	0.981	0	-0.022	0
6	-0.022	0.004	1.003	0	-0.009	0
7	-0.015	0	1.010	0	0	0
8	-0.183	-0.183	(-0.003)	0	0	0.814
9	0.088	0.088	0.386	0	0	0.396
10	0.072	0.072	0.634	0	0	0.162
11	0.405	-0.193	0.408	0.408	0.136	0.574
12	-0.036	-0.001	0.914	0.156	0.001	0.196
13	-0.040	0.011	0.965	0.059	-0.016	0.074
14	0	-0.204	1.895	0	0.204	-0.043
15	0.139	-0.092	1.152	-0.007	0.139	-0.042
16	0.078	-0.043	1.044	-0.007	0.085	-0.037
17	0.423	-0.208	0.429	-0.427	0.147	-0.683
18	-0.038	-0.008	0.937	-0.171	0.009	-0.301
19	-0.040	0.005	0.987	-0.080	-0.007	-0.175
20	-0.209	-0.209	0	0	0	-0.951
21	0.079	0.079	0.420	0	0	-0.541
22	0.055	0.055	0.711	0	0	-0.334

Brackets indicate the exact value is zero.

$\tau_{r\theta} = \tau_{\theta z} = u_\theta = 0$

$E/p = 1$ $p_r/p = 1$ $p_z/p = 1$ $d/a = 2\frac{1}{2}$ $\nu = 0$

N	σ_r/p	σ_θ/p	σ_z/p	τ_{zr}/p	Eu_r/ap	Eu_z/ap
1	1.063	1.063	0.876	0	0	0
2	1.054	1.059	0.890	0	-0.030	0
3	1.030	1.051	0.921	0	-0.051	0
4	1.009	1.040	0.952	0	-0.060	0
5	0.995	1.030	0.975	0	-0.061	0
6	0.989	1.023	0.989	0	-0.057	0
7	0.987	1.017	0.996	0	-0.050	0
8	1.515	1.515	(-0.009)	0	0	0.457
9	1.159	1.159	0.690	0	0	0.176
10	1.080	1.080	0.843	0	0	0.067
11	0.735	1.514	0.745	0.743	-0.363	0.321
12	0.932	1.157	0.913	0.216	-0.166	0.127
13	0.974	1.071	0.955	0.085	-0.101	0.057
14	(-0.001)	1.508	1.485	0	-0.508	-0.016
15	0.704	1.153	1.141	-0.003	-0.230	-0.017
16	0.876	1.066	1.057	-0.003	-0.133	-0.015
17	0.740	1.505	0.754	-0.750	-0.357	-0.363
18	0.928	1.150	0.923	-0.222	-0.160	-0.167
19	0.971	1.064	0.966	-0.094	-0.091	-0.098
20	1.503	1.503	(-0.001)	0	0	-0.508
21	1.150	1.150	0.704	0	0	-0.230
22	1.064	1.064	0.874	0	0	-0.133

Brackets indicate the exact value is zero.

$\tau_{r\theta} = \tau_{\theta z} = u_\theta = 0$

TABLE A 6.5.2 TOTAL STRESSES AND INDUCED DISPLACEMENTS ASSOCIATED WITH TWO IDENTICAL SPHERICAL CAVITIES IN A HOMOGENEOUS ISOTROPIC LINEAR ELASTIC INFINITE MASS WITH UNIFORM FIELD STRESS (Fig. A 6.5.2)

$E/p = 1$ $p_r/p = 1$ $p_z/p = 0$ $d/a = 2\frac{1}{2}$ $\nu = 0.25$

N	σ_r/p	σ_θ/p	σ_z/p	τ_{zr}/p	Eu_r/ap	Eu_z/ap
1	1.028	1.028	0.217	0	0	0
2	1.037	1.028	0.177	0	0.013	0
3	1.053	1.027	0.094	0	0.010	0
4	1.053	1.024	0.026	0	-0.007	0
5	1.040	1.022	-0.007	0	-0.027	0
6	1.023	1.018	-0.017	0	-0.042	0
7	1.010	1.015	-0.017	0	-0.050	0
8	2.061	2.061	(-0.004)	0	0	-0.295
9	1.154	1.154	0.370	0	0	-0.239
10	1.045	1.045	0.255	0	0	-0.107
11	0.406	1.758	0.407	0.407	-0.569	-0.209
12	1.027	1.163	-0.002	0.073	-0.166	-0.037
13	1.048	1.062	-0.013	0.031	-0.075	-0.004
14	0	1.437	-0.498	0	-0.811	0.032
15	0.536	1.173	-0.014	0.005	-0.438	0.030
16	0.782	1.080	0.015	0.005	-0.261	0.025
17	0.386	1.759	0.396	-0.393	-0.575	0.289
18	1.023	1.162	0.017	-0.062	-0.170	0.112
19	1.040	1.059	-0.025	-0.017	-0.078	0.064
20	2.083	2.083	0	0	0	0.397
21	1.151	1.151	0.345	0	0	0.347
22	1.039	1.039	0.198	0	0	0.233

Brackets indicate the exact value is zero.

$\tau_{r\theta} = \tau_{\theta z} = u_\theta = 0$

$E/p = 1$ $p_r/p = 0$ $p_z/p = 1$ $d/a = 2\frac{1}{2}$ $\nu = 0.25$

N	σ_r/p	σ_θ/p	σ_z/p	τ_{zr}/p	Eu_r/ap	Eu_z/ap
1	0.036	0.036	0.660	0	0	0
2	0.016	0.032	0.713	0	-0.050	0
3	-0.022	0.024	0.827	0	-0.073	0
4	-0.044	0.016	0.926	0	-0.068	0
5	-0.045	0.009	0.982	0	-0.049	0
6	-0.034	0.004	1.006	0	-0.029	0
7	-0.023	0.002	1.013	0	-0.013	0
8	-0.538	-0.538	(-0.002)	0	0	0.869
9	0.007	0.007	0.322	0	0	0.459
10	0.036	0.036	0.589	0	0	0.190
11	0.337	-0.247	0.335	0.336	0.116	0.612
12	-0.095	-0.007	0.914	0.143	-0.041	0.196
13	-0.073	0.009	0.967	0.054	-0.051	0.070
14	0	0.068	1.982	0	0.177	-0.053
15	0.167	-0.020	1.154	-0.008	0.151	-0.051
16	0.094	-0.014	1.042	-0.008	0.095	-0.044
17	0.350	-0.255	0.360	-0.358	0.129	-0.744
18	-0.095	-0.011	0.941	-0.160	-0.029	-0.032
19	-0.069	0.005	0.991	-0.077	-0.035	-0.187
20	-0.579	-0.579	0	0	0	-1.034
21	0	0	0.359	0	0	-0.635
22	0.025	0.025	0.676	0	0	-0.400

Brackets indicate the exact value is zero.

$\tau_{r\theta} = \tau_{\theta z} = u_\theta = 0$

$E/p = 1$ $p_r/p = 1$ $p_z/p = 1$ $d/a = 2\frac{1}{2}$ $\nu = 0.25$

N	σ_r/p	σ_θ/p	σ_z/p	τ_{zr}/p	Eu_r/ap	Eu_z/ap
1	1.064	1.064	0.877	0	0	0
2	1.053	1.060	0.890	0	-0.037	0
3	1.031	1.051	0.921	0	-0.063	0
4	1.009	1.040	0.952	0	-0.075	0
5	0.995	1.030	0.975	0	-0.076	0
6	0.989	1.023	0.988	0	-0.071	0
7	0.987	1.017	0.996	0	-0.063	0
8	1.523	1.523	(-0.006)	0	0	0.574
9	1.161	1.161	0.692	0	0	0.220
10	1.081	1.081	0.844	0	0	0.084
11	0.734	1.511	0.742	0.743	-0.453	0.403
12	0.933	1.156	0.912	0.216	-0.207	0.159
13	0.975	1.071	0.955	0.085	-0.126	0.071
14	(-0.001)	1.505	1.484	0	-0.634	-0.021
15	0.704	1.152	1.141	-0.003	-0.287	-0.021
16	0.875	1.066	1.057	-0.003	-0.166	-0.020
17	0.730	1.503	0.756	-0.751	-0.446	-0.455
18	0.928	1.151	0.923	-0.222	-0.199	-0.210
19	0.971	1.064	0.966	-0.094	-0.113	-0.123
20	1.504	1.504	(-0.001)	0	0	-0.637
21	1.150	1.150	0.703	0	0	-0.289
22	1.064	1.064	0.874	0	0	-0.166

Brackets indicate the exact value is zero.

$\tau_{r\theta} = \tau_{\theta z} = u_\theta = 0$

TABLE A 6.5.2 TOTAL STRESSES AND INDUCED DISPLACEMENTS ASSOCIATED WITH TWO IDENTICAL SPHERICAL CAVITIES IN A HOMOGENEOUS ISOTROPIC LINEAR ELASTIC INFINITE MASS WITH UNIFORM FIELD STRESS (Fig. A 6.5.2)

$E/p = 1$ $p_r/p = 1$ $p_z/p = 0$ $d/a = 2\frac{1}{2}$ $\nu = 0.49$

N	σ_r/p	σ_θ/p	σ_z/p	τ_{zr}/p	Eu_r/ap	Eu_z/ap
1	1.068	1.068	0.273	0	0	0
2	1.065	1.077	0.223	0	0.032	0
3	1.089	1.053	0.118	0	0.048	0
4	1.086	1.037	0.033	0	0.032	0
5	1.065	1.026	-0.009	0	0.004	0
6	1.041	1.018	-0.022	0	-0.022	0
7	1.021	1.013	-0.021	0	-0.039	0
8	2.578	2.578	(0.006)	0	0	-0.088
9	1.275	1.275	0.464	0	0	-0.220
10	1.098	1.098	0.321	0	0	-0.107
11	0.518	1.839	0.508	0.513	-0.584	-0.062
12	1.113	1.174	-0.002	0.092	-0.127	0.043
13	1.096	1.067	-0.016	0.039	-0.039	0.050
14	0	1.033	-0.628	0.001	-0.831	0.035
15	0.493	1.066	-0.017	0.006	-0.485	0.032
16	0.758	1.038	0.019	0.006	-0.293	0.025
17	0.476	1.815	0.483	-0.496	-0.591	0.015
18	1.106	1.169	-0.021	-0.077	-0.135	0.037
19	1.082	1.061	-0.032	-0.021	-0.051	0.020
20	2.610	2.610	(0.005)	0	0	0.196
21	1.267	1.267	0.430	0	0	0.338
22	1.082	1.082	0.248	0	0	0.245

Brackets indicate the exact value is zero.

$\tau_{r\theta} = \tau_{\theta z} = u_\theta = 0$

$E/p = 1$ $p_r/p = 0$ $p_z/p = 1$ $d/a = 2\frac{1}{2}$ $\nu = 0.49$

N	σ_r/p	σ_θ/p	σ_z/p	τ_{zr}/p	Eu_r/ap	Eu_z/ap
1	-0.004	-0.004	0.604	0	0	0
2	-0.030	0.004	0.668	0	-0.091	0
3	-0.064	0.004	0.803	0	-0.132	0
4	-0.079	0.006	0.919	0	-0.127	0
5	-0.071	0.006	0.984	0	-0.098	0
6	-0.052	0.006	1.010	0	-0.066	0
7	-0.034	0.005	1.017	0	-0.039	0
8	-1.065	-1.065	(0.007)	0	0	0.774
9	-0.113	-0.113	0.227	0	0	0.484
10	-0.017	-0.017	0.523	0	0	0.207
11	0.232	-0.324	0.230	0.231	0.043	0.545
12	-0.182	-0.014	0.914	0.125	-0.124	0.147
13	-0.122	-0.007	0.970	0.046	-0.115	0.035
14	0	0.470	2.112	0	0.075	-0.061
15	0.210	0.087	1.158	-0.009	0.140	-0.057
16	0.117	0.029	1.038	-0.009	0.092	-0.048
17	0.255	-0.320	0.254	-0.255	0.057	-0.693
18	-0.179	-0.014	0.945	-0.143	-0.107	-0.287
19	-0.114	0.006	0.998	-0.072	-0.089	-0.166
20	-1.131	-1.131	(0.001)	0	0	-0.959
21	-0.118	-0.118	0.268	0	0	-0.685
22	-0.018	-0.018	0.624	0	0	-0.445

Brackets indicate the exact value is zero.

$\tau_{r\theta} = \tau_{\theta z} = u_\theta = 0$

$E/p = 1$ $p_r/p = 1$ $p_z/p = 1$ $d/a = 2\frac{1}{2}$ $\nu = 0.49$

N	σ_r/p	σ_θ/p	σ_z/p	τ_{zr}/p	Eu_r/ap	Eu_z/ap
1	1.064	1.064	0.877	0	0	0
2	1.034	1.081	0.891	0	-0.059	0
3	1.026	1.058	0.921	0	-0.084	0
4	1.007	1.043	0.952	0	-0.095	0
5	0.995	1.032	0.975	0	-0.094	0
6	0.989	1.024	0.989	0	-0.087	0
7	0.987	1.018	0.996	0	-0.078	0
8	1.513	1.513	(0.014)	0	0	0.686
9	1.161	1.161	0.691	0	0	0.264
10	1.081	1.081	0.844	0	0	0.101
11	0.750	1.515	0.739	0.744	-0.541	0.483
12	0.931	1.159	0.912	0.216	-0.251	0.191
13	0.973	1.074	0.955	0.085	-0.155	0.085
14	(-0.001)	1.503	1.484	0.001	-0.757	-0.026
15	0.703	1.153	1.141	-0.003	-0.347	-0.025
16	0.875	1.067	1.057	-0.003	-0.201	-0.023
17	0.732	1.495	0.737	-0.749	-0.534	-0.544
18	0.926	1.155	0.924	-0.221	-0.242	-0.250
19	0.969	1.067	0.966	-0.093	-0.141	-0.146
20	1.479	1.479	(0.006)	0	0	-0.763
21	1.150	1.150	0.698	0	0	-0.347
22	1.064	1.064	0.873	0	0	-0.200

Brackets indicate the exact value is zero.

$\tau_{r\theta} = \tau_{\theta z} = u_\theta = 0$